COMBINING A ONE-DIMENSIONAL EMPIRICAL AND NETWORK SOLVER WITH COMPUTATIONAL FLUID DYNAMICS TO INVESTIGATE POSSIBLE MODIFICATIONS TO A COMMERCIAL GAS TURBINE COMBUSTOR

by

Johannes Jacobus Gouws

Submitted in partial fulfilment
of the requirements for the degree

MASTER OF ENGINEERING

in the Faculty of Mechanical/Aeronautical Engineering
University of Pretoria
Pretoria

Supervisor: Mr R.M. Morris

January 2007

COMBINING A ONE-DIMENSIONAL EMPIRICAL AND NETWORK SOLVER WITH COMPUTATIONAL FLUID DYNAMICS TO INVESTIGATE POSSIBLE MODIFICATIONS TO A COMMERCIAL GAS TURBINE COMBUSTOR

by

Johannes Jacobus Gouws

Promoter: Mr R.M. Morris

Department: Mechanical and Aeronautical Engineering

Degree: Master of Engineering

SUMMARY

Gas turbine combustion chambers were traditionally designed through trial and error which was unfortunately a time-consuming and expensive process. The development of computers, however, contributed a great deal to the development of combustion chambers, enabling one to model such systems more accurately in less time. Traditionally, preliminary combustor designs were conducted with the use of one-dimensional codes to assist in the prediction of flow distributions and pressure losses across the combustion chamber mainly due to their rapid execution times and ease of use. The results are generally used as boundary conditions in three- dimensional models to predict the internal flow field of the combustor. More recent studies solve the entire flow

i

field from prediffuser to combustor exit. This approach is, however, a computationally expensive procedure and can only be used if adequate computer resources are available.

The purpose of this study is two-fold; (1) to develop a one-dimensional incompressible code, incorporating an empirical-based combustion model, to assist a one-dimensional network solver in predicting flow- and temperature distributions, as well as pressure losses. This is done due to the lack of a combustion model in the network solver that was used. An incompressible solution of flow splits, pressure losses, and temperature distributions is also obtained and compared with the compressible solution obtained by the network solver; (2) to utilise the data, obtained from the network solver, as boundary conditions to a three-dimensional numerical model to investigate possible modifications to the dome wall of a standard T56 combustion chamber. A numerical base case model is validated against experimental exit temperature data, and based upon that comparison, the remaining numerical models are compared with the numerical base case. The effect of the modification on the dome wall temperature is therefore apparent when the modified numerical model is compared with the numerical base case.

A second empirical code was developed to design the geometry of axial straight vane swirlers with different swirl angles. To maintain overall engine efficiency, the pressure loss that was determined from the network analysis, of the base case model, is used during the design of the different swirlers. The pressure loss across the modified combustion chamber will therefore remain similar to that of the original design. Hence, to maintain a constant pressure loss across the modified combustion chambers, the network solver is used to determine how many existing hole features should be closed for the pressure loss to remain similar. The hole features are closed, virtually, in such a manner as not to influence the equivalence ratio in each zone significantly, therefore maintaining combustion performance similar to that of the original design. Although the equivalence ratios in each combustion zone will be more or less unaffected, the addition of a swirler will influence the emission levels obtained from the system due to enhanced air-fuel mixing.

A purely numerical parametric analysis was conducted to investigate the influence of different swirler geometries on the dome wall temperature while maintaining an acceptable exit temperature distribution. The data is compared against the data obtained from an experimentally validated base case model. The investigation concerns the replacement of the existing splash-cooling devices on the dome wall with that of a single swirler. A number of swirler parameters such as blade angle, mass flow rate, and number of blades were varied during the study, investigating its influence on the dome wall temperature distribution.

Results showed that the swirlers with approximately the same mass flow as the existing splash-cooling devices had almost no impact on the dome wall temperatures but maintained the exit temperature profile. An investigation of swirlers with an increased mass flow rate was also done and results showed that these swirlers had a better impact on the dome wall temperatures. However, due to the increased mass flow rate, stable combustion is not guaranteed since the air/fuel ratio in the primary combustion zone was altered.

The conclusion that was drawn from the study, was that by simply adding an axial air swirler might reduce high-temperature gradients on the dome but will not guarantee stable combustion during off-design operating conditions. Therefore, a complete new hole layout design might be necessary to ensure good combustion performance across a wide operating range.

ACKNOWLEDGEMENTS

TABLE OF CONTENTS

NOMENCLATURE

A	=	Area $[\,m^2\,]$
A_r	=	Aole area ratio
A/F	=	Air/fuel ratio
C/H	=	Carbon to hydrogen ratio
C_d	=	Discharge coefficient
C_p	=	Specific heat [kJ/kgK]
C_1	=	Internal convection [W]
C_2	=	Convection to annulus [W]
C_3	=	External convection [W]
D_h	=	Hydraulic diameter [m]
F/A	=	Fuel/air ratio
G_ϕ	=	Tangential momentum flux
G_x	=	Axial momentum flux
I	=	Total number of nodes
J	=	Number of branches associated with a specific node
K	=	Loss coefficient
K_{sw}	=	Swirler blade loss coefficient
$K_{1\text{-}2}$	=	Conduction through liner wall [W]
$K_{2\text{-}3}$	=	Conduction through casing wall [W]
L_u	=	Luminosity factor
L_v	=	Swirler vane length [m]
P	=	Total pressure [Pa]
P_i	=	Total pressure upstream of hole [Pa]
P_w	=	Wetted perimeter [m]
R	=	Radiation [W]
S_N	=	Swirl number
S_v	=	Swirler blade pitch [m]
T	=	Temperature [K]

T_s = Static temperature [K]

$T_{w,ad}$ = Gas temperature at the combustor liner wall [K]

ΔT = Temperature rise [K]

Q = Volume flow rate [m³/s]

V = Velocity [m/s]

V_n = Normal velocity component

V_t = Tangential velocity component

W = Tangential velocity component

k_w = Wall conductivity [W/mK]

l_b = Beam length [m]

k = Conductivity [W/mK]

m = Massflow rate [kg/s]

p_i = Static pressure upstream of hole [Pa]

p_j = Static pressure downstream of hole [Pa]

r_t = Tip radius [m]

r_h = Hub radius [m]

t_w = Liner wall thickness [m]

v_{nj} = Jet velocity component normal to the liner wall

v_j = Resultant jet velocity

x = Distance from cooling slot [m]

Symbols

θ = Jet angle [º]

θ_v = Swirler blades angle [º]

ϕ = Equivalence ratio

ρ = Density [kg/m^3]

η_c = Combustion efficiency

η_f = Film-cooling efficiency

ε_g = Gas emissivity

ε_w = Wall emissivity

σ = Stefan Boltzmann constant $(5.67 \times 10\text{-}8 \left[W/mK^4 \right])$

μ = Viscosity [kg/ms]

α = Mass flow ratio

φ = Mass flow ratio/area ratio

Subscripts

a = Air

an = Annulus

c = Casing

g = Gas

h = Hole / Hub

hub = Hub

L = Combustor liner

mr = Maximum circumferential mean value

max = Maximum

out = Zone outlet

q = Fuel/air ratio by mass

sw = Swirler

w_1 = Inner liner wall

w_2 = Outer liner wall

zone = Recirculation, primary, secondary, dilution zone

ij = Values associated with element e_{ij}

nj = Jet normal to flow direction

PZ = Primary zone

RZ = Recirculation zone

1 = Flame side of liner wall

3 = Combustor inlet

4 = Combustor outlet

03 = Total inlet property

CHAPTER 1 –

INTRODUCTION

1.1   Preamble

Modern gas turbine combustor design and development is typically a combination of using empirical correlations, numerical modelling and extensive component testing. The United States Army Research and Technology Laboratories is one of many organisations who demonstrated in 1975 the ability of using empirical/analytical methods to successfully design and develop a small reverse-flow annular combustor. Prior to 1975, combustion chamber design consisted mainly of expensive and time-consuming trial and error rig tests. Even though the empirical/analytical method provided valuable design guidance, the accuracy of the model was limited by sub-models predicting turbulence, combustion and heat transfer (Mongia *et al.*, 1986).

Due to the ever-increasing computing power, numerical methods such as computational fluid dynamics (CFD) has become a more attractive and alternative approach that could be utilised during the design and development of combustors. Numerical modelling provides the combustor designer with the ability to predict and understand the complex flow process within the combustion chamber early in the design phase prior to expensive rig tests. Experimental rig tests will, however, never be totally eliminated, but with the use of numerical methods, experimental time can be reduced to only a few verification experiments.

Numerical modelling is a very broad term and often interpreted as the use of CFD in combustion simulation. Although very powerful, CFD solutions of combustors are very specialised and time consuming processes. CFD techniques are therefore very seldom used during the initial sizing of a combustor. Initial sizing of combustors are usually done through empirical formulations and when extended to a full CFD simulation, the empirical formulations are used to calculate the boundary conditions for the CFD simulation.

With the recent developments in compressible network solvers, network solvers now have the potential of filling the modelling gap between and analytical design and a full CFD simulation. A network solver has the advantage that it can account accurately for the geometry and therefore flow splits in the combustor, while also accounting for the properties of the combustion process.

The purpose of this project is to use numerical modelling to investigate possible modifications to the dome of a standard Allison T56 combustion chamber due to the formation of cracks in the area. These cracks are believed to be caused by high-temperature gradients, which in some cases may even be augmented by blocked splash-cooling strips on the dome (Figure 1.1). The design of the combustor currently in use is rather old, compared to modern-day combustion systems, but still widely used.

(a)   (b)
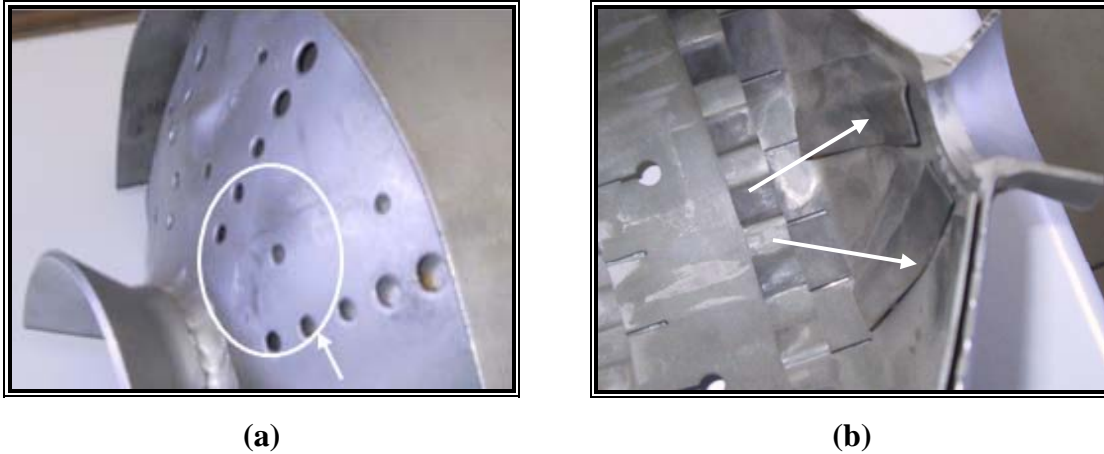
Figure 1.1: Defects on combustor dome; (a) Crack formation on dome wall,

(b) Thermal distortion of the splash cooling devices on the inside of the dome

The thermal characteristics of the combustor will be modeled by combining a one-dimensional analytical model with a commercial network solver, Flownex, to predict flow distributions, pressure losses, and one-dimensional temperature distributions. The data obtained will be used in the CFD analysis to investigate possible modifications to the existing geometry to solve crack formation problems. The numerical model will then also be used to simulate geometrical changes to the combustor and the effect it will have on the simulated thermal gradients. Although experimental exit temperature distributions will be used to validate the numerical data of the base case, the modification analysis will be purely numerical. Thermal stresses will not form part of this project.

1.2   Overview of the T56 gas turbine engine

The T56 engine is a turboprop gas turbine engine used by several air forces worldwide. These engines are used on aircraft such as the Lockheed C-130 Hercules, L-188 Electra, and the P3-Orion, to name a few. The engine is depicted in figure 1.2 and consists of a 14-stage axial compressor, combustion system, and four turbine stages. At take-off the compressor has a pressure ratio of 9.5:1 and delivers 14.515 kg/s of air at an inlet temperature and pressure of approximately 566.15 K and 923 897 Pa to six can-annular throughflow combustion chambers. All of this is achieved at a constant rotational speed of 13 820 rpm.
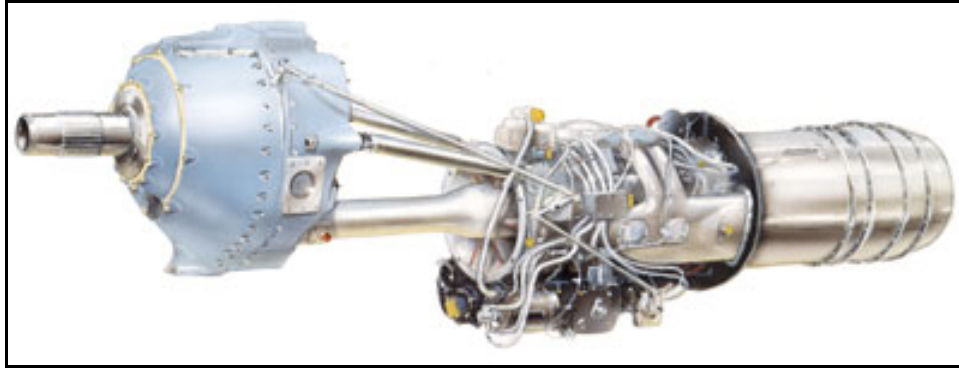
Figure 1.2: The T56 gas turbine engine (www.rolls-royce.com)

The combustion system consists of an inner and outer casing that provides the airflow and mechanical connection between the compressor and turbine. The combustion gases flow into a four-stage axial turbine, providing it with an acceptable temperature distribution that promotes the lifespan of the turbine blades. A single combustor unit is depicted in figure 1.3.
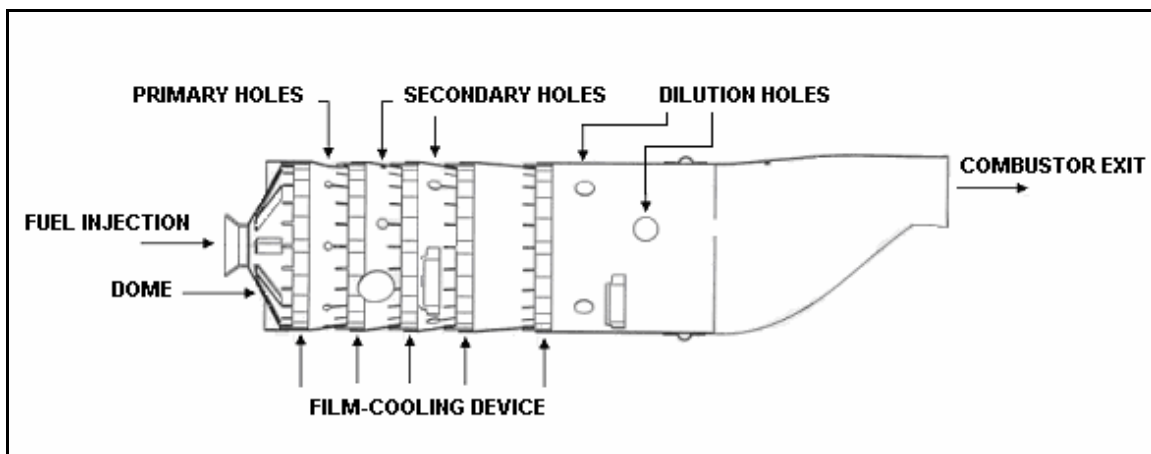
Figure 1.3: Single T56 combustion chamber

The combustion chamber can be divided into three different sections namely; primary, secondary and dilution zones. The importance of each zone will be discussed in the subsequent chapter. The primary zone contains a single hole set comprising of seven air admission holes. The secondary and dilution zone each consists of two hole sets. The first and second hole sets in the secondary zone consists of three and four holes respectively, whereas the first and second sets in the dilution zone comprises of four and two holes

respectively. Use is made of eight splash strips on the dome to impart a swirling motion to the flow within the primary zone and to cool the dome wall. Film-cooling air is admitted through five wiggle strip sets along the combustor liner as well as a number of splash-cooling devices. Typical operating conditions during take-off, and used during this study as the design point, are displayed in table 1.1.

Table 1.1: Operating conditions during take-off

Combustor inlet temperature, T_{03} [K]	566.15
Combustor inlet pressure, P_{03} [Pa]	923 897
Total mass flow rate, m_a [kg/s]	14.154
Air/fuel ratio	50

Since the T56 engine dates back to the 1950s, minor changes have been made to the combustion chamber. Due to stringent regulations to reduce aircraft emission levels, such as NO_x, CO, and smoke, some investigations were conducted on the combustion system to reduce smoke emissions.

Previous work was done by Skidmore (1986) on two different combustion systems, the T56-A-7 (Series II) and T56-A-15 (Series III), to investigate the discrepancy in smoke emission characteristics between the two designs. It was found that the Series III produced approximately 50% more smoke than the Series II engine. It is believed that the reason for this difference might be due to the design of the primary zone, especially the amount of air flow through the first set of circumferential holes. The percentage mass flow rate has decreased from 6.4% for the series II combustor to 3.4% for the series III combustor. Further investigations were underway to determine the influence of the primary zone holes on the smoke emission levels (Skidmore, 1986).

A low-smoke modification has been introduced into the Series III Allison T56 engine combustion system and used by the Royal Australian Air Force (RAAF) in 1990. The modification consisted of enlarging the primary zone holes from 6.4mm to 11mm to increase the strength of the main toroidal vortex, thus improving the mixing of the air and fuel. However, extensive turbine erosion became evident after the modified combustion

system had been employed for two years. After some investigations, it was found that the erosion was caused by hard carbon deposits which were formed in the fuel-rich region inside the dome of the combustion chamber (Skidmore *et al.*, 1995).

The fundamental purpose of a gas turbine combustion chamber is to promote stable and efficient combustion over a wide range of operating conditions while providing an acceptable exit temperature distribution to the turbine vanes. In addition, the combustor should have a low total pressure loss to keep the engine efficiency high, low emission levels that comply with regulations, acceptable liner wall temperatures in order to ensure structural durability and good re-light capabilities over a wide range of air/fuel ratios. Designing such a device to comply with all of the above-mentioned requirements, therefore, becomes a difficult task in which certain compromises have to be made. The following section will discuss related literature and some of the tools that are used during a typical preliminary design phase as well as a few important aspects concerning combustion chamber performance.

1.3   Combustor design methodology

Traditionally, combustor design or modification required a number of experimental rig tests that were unfortunately a very expensive and time-consuming process (Lawson, 1993; Eccles and Priddin, 1999). Alternative methods were therefore needed to conduct preliminary design studies to predict total pressure losses and flow distributions across combustion chambers prior to expensive rig tests. Some of the earliest work was done by Knight and Walker (1953) who conducted analyses to predict component pressure losses that could be used to predict isothermal flow distributions of gas turbine combustion chambers. Losses through swirlers and liner hole features as well as losses due to heat addition and bends were determined. Certain limitations on the accuracy of these analyses were due to uncertainty of compressibility and the mixing of the gas streams, but resulted in pressure loss predictions within 5 percent of measured data. In an attempt to investigate the influence of a number of inlet parameters on the total pressure loss and flow distributions of a combustion chamber, Graves and Gronman (1957) presented all these variables graphically. These graphs were presented in terms of the combustor

reference Mach number, ratio of combustor exit-to-inlet total temperature, fraction of total airflow passing through the liner, ratio of total hole area in the liner wall to the total combustor cross-sectional area, and the ratio of the liner cross-sectional area to total combustor cross-sectional area. The effects of a number of geometries and operating variables were determined analytically from compressible and incompressible flow relations. These curves were, however, developed for tubular combustion chambers with constant annulus and liner cross-sectional area along the combustor axis with flush circular air admission holes. These results could, however, also be used for can-annular and annular combustion chambers with constant annulus air velocities, but with less accuracy.

As the development of computers progressed, it became a viable option for designers to use it as a tool to conduct one-dimensional analysis that is less time-consuming. Samuel (1961) described a one-dimensional analytical method that was based on the actual sequence of processes that the flow experienced as it passed through the combustion system. The method calculated the pressure distribution and mass flow rates throughout a gas turbine combustion system when inlet flow conditions, exit temperatures, and the geometry of the system are known. The method was designed for annular and can-annular systems with any type of liner flow. Joubert and Hattingh (1982) described a similar approach in which the pressure drop and flow splits were calculated for a reverse-flow combustion chamber. The analysis employed the continuity, momentum, and energy equations in a step-wise manner. The combustor model was divided into a number of stations and calculations proceeded from one station to the next by using the results from the previous station as the inputs to the following station. The method proved to be adequate for combustion chamber design.

The one-dimensional approach described above is, however, not extremely versatile. When complex geometries need to be analysed this approach becomes difficult to implement. A one-dimensional network model on the other hand is capable of modelling complicated geometries effectively without difficulty, while maintaining rapid execution. Stuttaford and Rubini (1997) described a network model consisting of a number of

independent sub-flows that are linked together to model a certain process. The process can be modelled by overlaying a network on the system geometry that comprises a number of elements that are linked together by nodes. The elements define the actual feature such as orifice and duct sections in the domain of interest. The elements are then linked together by nodes to form a meaningful overall structure. Semi-empirical formulations are used to describe the flow through elements, while the overall governing equations are solved within the nodes. The governing equations that are employed consist of the continuity equation and pressure-drop flow relations. Pressure drop and flow distributions can be obtained in this way throughout the region of interest. Heat transfer can be included in the strategy, by computing conduction, convection, and radiation effects (Stuttaford, 1997).

A commercially available network solver, FLOWNET (www.flownex.com), was utilised by Hicks and Wilson (1999) to predict general heat transfer to a combustor liner and to investigate the influence of cooling devices on the liner wall. The original network code was developed by a company in South Africa but was adapted for combustor analysis by Cranfield University. A number of semi-empirical sub-models to represent various features relevant to a gas turbine combustor were added to the model. Some of the features included cooling/dilution ports, diffusers, pedestals, and pin-fins. To be able to predict combustion products at various efficiency levels, a gas property model was incorporated as well. The heat transfer analysis included in the FLOWNEX model accounted for conduction, convection, and radiation in the combustor. Combustor film-cooling effects were included in the convection model. The radiation model initially made use of a simple semi-empirical relationship based on a luminosity factor as outlined by Lefebvre (1998). This model proved to be capable of providing quantitive agreement with experimental results. It is important to note that the accuracy and limitations of network models are inherent due to the use of empirical formulations that might not be specifically suited for the problem at hand. Although the network model was capable of predicting general trends it was unable to predict temperatures within an accuracy less than 80 K.

With the use of these empirical/analytical models, a number of advanced technology combustors have been designed over the years. However, even though the models have proved to be useful in the combustor design process, some limitations persist. These models cannot predict local hot spots, exit temperature distributions, flow phenomena inside a combustion chamber, combustor lean-flame stability and ignition characteristics. A need therefore persists for more accurate modelling techniques that could provide the engineer with insight regarding the internal flow in a combustor.

Due to the hostile environment inside a combustion chamber, it is difficult to investigate the internal flow field using experimental measurements. However, numerical methods can be used to model the internal flow field of a combustor. The numerical solution can provide detailed information of all flow properties being modelled across the entire flow field, whereas experimental measurements can only provide flow properties being measured in the region of the flow field where measurements are taken (Hu and Prociw, 1993). CFD has been developed since the early seventies but due to the requirement of specialist knowledge and intensive computer power, these tools have remained in the domain of the specialist numerical scientist. The recent development of relatively inexpensive but powerful computers has, however, led to the use of CFD as an everyday designer's tool. CFD provides the combustor designer with the ability to understand the complex flow process within the combustion chamber early in the design process, and to improve the design if necessary, thus requiring fewer expensive rig tests. Rig tests will, however, never be completely eliminated, but with the use of numerical methods such as CFD, experimental time can be reduced to only a few verification experiments (Eccles and Priddin, 1999; Hornsby and Norster, 1997; McGuirk and Palma, 1993).

As described by Sivaramakrishna *et al.* (2001), the role of CFD in the development of gas turbine combustion chambers has changed remarkably over the last decade and has become a valuable part of an overall integrated design system. After validating these codes with reliable experimental data, it has been utilised for optimisation studies. Such studies include optimisation of combustion chambers for low emission levels and

adequate exit temperature distributions by determining optimum liner hole size and location.

Due to more stringent regulations regarding emission levels and its impact on the environment, it has become a great concern to engine manufacturers and they are responding to the need. The only feasible changes that can be made to combustion chambers to reduce emission levels, are changes to fuel injectors and liner hole patterns and locations. The exhaust gases from a gas turbine engine consist of carbon dioxide, carbon monoxide, water vapour, unburned hydrocarbons, soot, and excess oxygen and nitrogen. Carbon dioxide and water vapour are natural products formed during the combustion process, and the only way to reduce these levels is to add less fuel. Unburned hydrocarbons, soot, and carbon monoxide are, however, a result of inefficient combustion (Sturgess *et al.*, 1992). Hornsby and Norster (1997) utilised CFD to predict emission levels from a can-annular combustor that gave good quantitive results. Others such as Feitelberg and Lacey (1998) and Liedtke et al (2002) utilised CFD to investigate the performance of new low emission combustor designs, such as rich-burn quick-quench lean-burn (RQL) and lean premixed prevapourised (LPP) combustors.

One of the more difficult problems encountered in gas turbine combustion chambers is to achieve an exit temperature profile that is acceptable to the nozzle guide vanes (NGVs). The exit temperature profile is affected by; the fuel injector spray characteristics, jet penetration and mixing, total pressure drop across the liner, as well as the physical dimensions and shape of the combustor liner. When the exit temperature profile for a specific combustion chamber is determined experimentally, the tests are usually done at the maximum pressure because this will be the operating condition with maximum heat release. The temperature that is most important to the turbine blades is the average radial temperature profile. These profiles are obtained by adding together the temperature measurements around each radius and then dividing it by the number of locations at each radius (Lefebvre, 1998). Another important parameter is the maximum spatial temperature that controls the stress and erosion on the inlet guide vanes. The maximum

spatial temperature typically occurs at 50 to 70 percent of the radial position and is normally defined in terms of the pattern factor (Crocker and Smith, 1995).

Snyder *et al.* (2001) and Crocker and Smith (1995) have proved that CFD analysis could be utilised to determine optimum exit temperature distributions by studying the position and size of the dilution holes. Lawson (1993) successfully modelled a high bypass turbofan aircraft engine combustor in an effort to define liner and dilution modifications necessary to create inboard peaked and flat exit temperature profiles. Before modifications were made to the model, it was calibrated first to match existing baseline data, thereby obtaining qualitative results. The computational modelling of combustors has shown to be an effective method to predict exit temperature profiles. The process has also proved to be time- and cost-effective.

The correct evaluation of CFD models is mainly dependent on the specification of boundary conditions. These boundary conditions are generally obtained from experimental data, but due to the complexity of combustion chamber geometries, inappropriate experimental data, and numerical model limitations, simplifications might be necessary when specifying boundary conditions (McGuirk and Palma, 1993; Smiljanovski and Brehm, 1999).

A gas turbine combustor is a very complex combustion device. The challenge in such a device is two-fold, namely (i) the development of models to describe the real-world component geometries and (ii) an accurate description of the coupled interacting physical and chemical phenomena (Tangirala *et al.*, 2000). Traditionally CFD analysis of combustion chambers has been coupled in a weakly manner, with the flow through the air admission holes being derived from one-dimensional empirical correlations and then used as boundary conditions to simulate the internal flow of the combustor (Hu and Prociw, 1993; Lawson, 1993; Fuller and Smith, 1993). In addition to flow distribution predictions, jet angles through liner holes are also predicted through the utilisation of empirical correlations as shown by Lawson (1993). These methods may, however, be deficient in at least two ways. No information regarding velocity profile shapes or

turbulence conditions at the port entry locations is provided (McGuirk and Spencer, 2000). The solution obtained from these simulations is therefore strongly dependent on the accuracy of the description of the boundary conditions. When coupling a CFD model with a one-dimensional model, certain assumptions are made regarding the specification of the boundary conditions of the various liner features. Holdeman *et al.*, (1997) investigated the effect of opposed rows of jets on the mixing with subsonic cross-flow in rectangular ducts. In their analysis, a uniform flow boundary was assumed for the jets and mainstream. The discharge coefficients (C_d) for the holes, which are defined as the ratio between the effective hole area and the geometric hole area, were expected to be less than unity. A discharge coefficient has therefore been assumed to determine the effective hole area across which a uniform flow boundary could be specified.

An alternative and more recent approach is to model a combustion system in a fully coupled manner. This approach consists of modelling the entire flow field from compressor outlet to turbine inlet (Crocker *et al.*, 1999; McGuirk and Spencer, 2001; Malecki *et al.*, 2001; McGuirk and Spencer, 2000; Snyder *et al.*, 2001). Two reasons to implement a fully coupled approach are: (i) flow splits and boundary conditions for the combustor liner are modelled explicitly and no longer need to be approximated; and (ii) liner wall temperatures can be predicted when the flow fields on both sides of the liner walls are modelled in a coupled fashion (Crocker *et al.*, 1999). Although belief in the importance of fully coupled combustor modelling is evidently growing, insufficient computer resources may limit the use of coupled calculations. (McGuirk and Spencer, 2001).

The accuracy of the CFD model depends primarily on the accuracy of the geometry being created and also whether a sufficiently refined grid is used to capture the nature of the flow (Hornsby and Norster, 1997). Constructing an accurate and realistic CFD model and generating an acceptable grid are the most time-consuming and expensive phases of CFD simulations. The two main approaches in generating a grid are either constructing a structured or an unstructured mesh. When generating a mesh on a complex geometry, a structured mesh is more difficult and time-consuming to construct and demand a high

degree of user expertise, but allow clustering of the mesh more efficiently in boundary layer regions. Some geometries can simply not be meshed using a structured approach unless significant simplifications and assumptions are made to the geometrical features. The unstructured approach, on the other hand, offers the ability of generating a grid automatically, and is much easier to learn and use. It also requires fewer simplifications of the CAD model, and grid refinement near local geometric features is easily controlled. The unstructured approach, however, requires additional processing time compared to the structured methodology (Eccles and Priddin,1999; Maleck *et al.*, 2001).

1.4   Need for this study

It is evident from the literature survey that in recent years CFD has become an accepted method to model gas turbine combustion chambers, assisting designers in predicting the internal flow and heat transfer of such systems. The results are, however, dependent on the boundary conditions provided and need to be validated against experimental data. Although recent computer capabilities have increased providing designers the ability to model a combustion system in a fully coupled manner from compressor outlet to turbine inlet, some further computer development is still needed. Modelling a combustion chamber in an uncoupled manner is, therefore, still the preferred method.

Despite the increased progress made in numerical methods, one-dimensional analysis is still used for initial sizing of combustion chambers. Consequently, the data obtained from such an analysis is linked to numerical models, providing the boundary conditions for three-dimensional numerical analysis. One-dimensional network solvers have the capability of modelling complex combustor geometries more effectively, providing simple, fast, and accurate solutions.

The purpose of this study is two-fold; (1) to develop a one-dimensional incompressible code, incorporating an empirical-based combustion model, to assist a one-dimensional network solver in predicting flow- and temperature distributions, as well as pressure losses. This is done due to the lack of a combustion model in the network solver that was used. An incompressible solution of flow splits, pressure losses, and temperature

distributions is also obtained and compared with the compressible solution obtained by the network solver. In this way the abilities of a network solver is compared against a traditional one-dimensional empirical solver; (2) to utilise the data, obtained from the network solver, as boundary conditions for a three-dimensional numerical model to investigate modifications to the dome wall of a standard T56 combustion chamber. A numerical base case model will be validated against experimental exit temperature data, and based upon that comparison, the remaining numerical models will be compared with the numerical base case. The effect of the modification can therefore be seen when the numerical model is compared with the original design.

Seeing that gas temperature will have an effect on the air density, and therefore the flow distributions and pressure loss, the combustion process has to be accounted for when a one-dimensional analysis is conducted. A combustion model was however not available in the network solver, and for this reason, a one-dimensional empirical solver was developed and combined with the network solver to assist in one-dimensional combustion predictions. The one-dimensional code that was created is empirically based and solves for incompressible flow in can- and can-annular type combustion systems. The model, within the one-dimensional code, is divided into stations so that in moving from one station to the next the flow distributions and pressure losses can be determined across the system. In addition, the system model is divided into four zones in which the total air flow in each zone can be calculated. The adiabatic flame temperature is determined from general kerosene temperature rise curves, followed by a one-dimensional heat transfer balance across the combustor liner. These gas temperatures are then used as inputs to the network solver.

In addition to the one-dimensional code, a second empirical code was developed to conduct initial sizing of axial swirlers. The input to this code is however the pressure loss obtained from the network solver. To maintain overall engine performance within the limits established in the engine cycle, the pressure loss had to be maintained similar to that of the original design, for all cases. The pressure loss obtained from the network solver is therefore used within the swirler design code, to generate various geometries

while maintaining a constant pressure loss. The network solver is used to determine virtually how many hole features should be closed to maintain a constant pressure loss for a specific swirler design. The hole features were closed in such a manner as not to influence the equivalence ratio in each combustion zone significantly. Consequently, the various swirler geometries are analyzed using CFD and its influence on the dome wall temperatures is investigated.

1.5   Outline of this study

Chapter 2 provides background information regarding general combustor layouts as well as one-dimensional empirical design methodology. The computational process that was utilised during the one-dimensional empirical code is described along with the correlations that were used.

A discussion of one-dimensional models continues in Chapter 3, elaborating more about network models and the results obtained with such an analysis compared to the empirical model.

Chapter 4 describes the numerical model and the associated boundary conditions that were utilised during the study. A short description of the grid generation and numerical models is provided.

The numerical results obtained during the study are presented in Chapter 5. The original combustion chamber is solved and used as a base case model with its exit temperature distribution validated against experimental data. The base case model was validated against exit temperature distributions obtained experimentally by Skidmore (2004). Six additional models were developed, one with the original combustion chamber with blocked splash-cooling devices and five cases investigating the effect of a swirler on the dome wall temperature and exit temperature distribution.

Finally, Chapter 6 provides a summary of the study, discussing the outcome of the numerical results as well as some recommendations.

CHAPTER 2   UNIVERSITEIT VAN PRETORIA
UNIVERSITY OF PRETORIA
YUNIBESITHI YA PRETORIA
Combustion design principles: 1-D empirical design

CHAPTER 2 –

COMBUSTOR DESIGN PRINCIPLES:

1-D EMPIRICAL DESIGN

2.1 Preamble

The following chapters will discuss the ability of a one-dimensional empirical solver to predict pressure losses, flow distributions and temperature distributions across gas turbine combustor chambers. Such an analysis is essential during the preliminary design phase to reduce costs and development time and has proved to provide comparative results. The empirical correlations utilised in such an analysis to predict flow distributions and temperature distributions are presented in this chapter.

2.2 Basic combustor layout and design

Generally, all combustion arrangements incorporate similar components, such as a perforated liner that is situated within an air casing, diffuser for pressure recovery purposes, and a fuel injector. The basic combustor features are illustrated in figure 2.1.

A combustion chamber consists of a liner which shelters the flame from the approaching air and generates an area where stable combustion can take place with the proper addition of air. The combustion chamber can be divided into three zones, namely primary, secondary and dilution zone. Air is added to the three different zones through various air admission holes in the liner. The purpose of the primary zone is to anchor the flame and to provide adequate amounts of air through the primary holes to sustain the flame. A low

pressure recirculation flow pattern is generally generated in the primary zone due to the impingement of the primary jets on one another which could, in some cases, even be enhanced through the utilisation of an air swirler. The recirculation region ensures that some of the fuel can flow in the upstream direction to mix with the incoming air flow, thus enhancing air/fuel mixing.
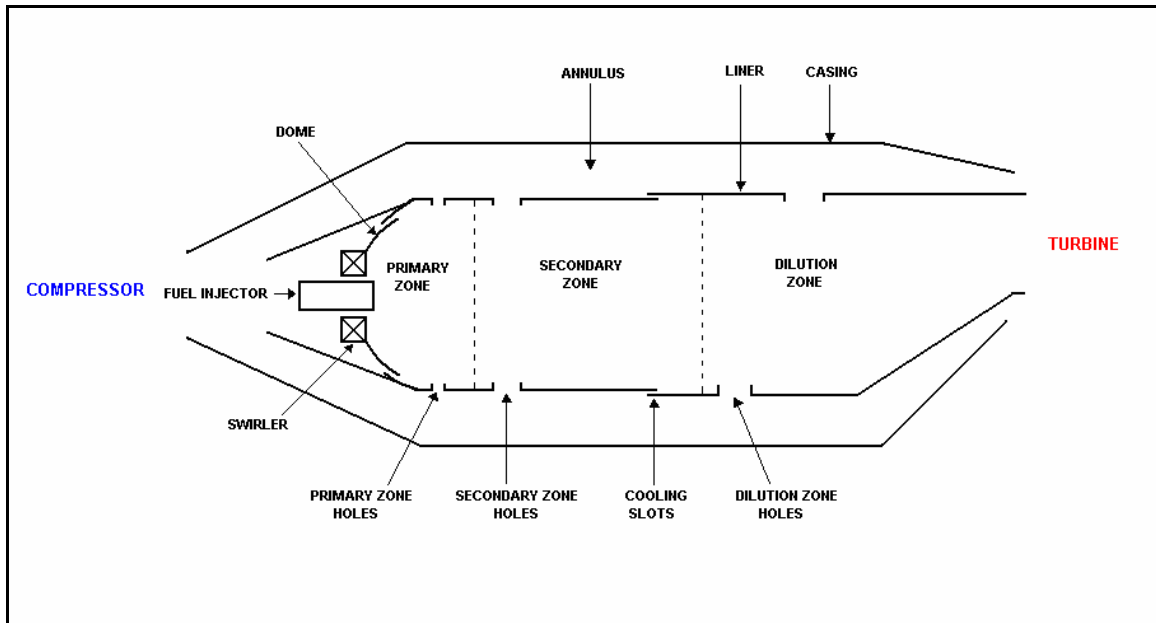
Figure 2.1: Basic combustor features (Mattingly *et al.*, 2002)

The secondary or intermediate zone is downstream of the primary zone and is generally used to provide enough time at a sufficient temperature for carbon monoxide and hydrocarbon burn-out to occur, prior to the dilution zone. The temperatures in this zone should be maintained low enough to avoid dissociation of products in the combustion gases, and high enough to prevent extreme quenching. The secondary zone's penetration and distribution should also be adjusted to improve the temperature distribution approaching the dilution zone.

The function of the dilution zone is to admit the remaining air after combustion and wall-cooling requirements have been met, to provide an exit temperature profile with a mean temperature and temperature distribution that are acceptable to the turbine blades. The exit temperature profile is affected by the fuel injector spray characteristics, jet

penetration and mixing, total pressure drop across the liner, and the physical dimensions and shape of the combustor liner. Experimental tests have shown that a suitable exit temperature profile is dependent on the adequate penetration of the dilution jets into the main stream, coupled with the correct number of jets to form a sufficient localised mixing region. Experience has shown that when a large number of small dilution jets are used, inadequate jet penetration is achieved resulting in a hot core. On the other hand, when a small number of large dilution jets are used, overpenetration is evident, resulting in a cold core (Lefebvre and Norster, 1969).

When the exit temperature profile for a specific combustion chamber is determined experimentally, the tests are usually done at the maximum pressure because this will be the operating condition with maximum heat release. A dimensionless parameter known as the pattern factor can be used as an indication of the quality and uniformity of the exit temperature profile. From an engine performance point of view, the mass-flow-weighted mean temperature (T_4) recorded for all the exit temperatures for a specific liner is of great concern. For the design of the nozzle guide vanes (NGV), due to its fixed position at the exit of the combustion chamber, the maximum recorded temperature should be used in order for the vanes to withstand the temperatures. The pattern factor is normally defined as (Lefebvre, 1998):

$$\text{Pattern factor} = \frac{T_{max} - T_4}{T_4 - T_3} \qquad (2.1)$$

The profile factor on the other hand is also a dimensionless parameter that is used to define the radial temperature profile at the combustion chamber exit. The profile factor is defined as follows (Lefebvre, 1998):

$$\text{Profile factor} = \frac{T_{mr} - T_4}{T_4 - T_3} \qquad (2.2)$$

The parameters used in equation (2.1) and (2.2) are explained in figure 2.2.
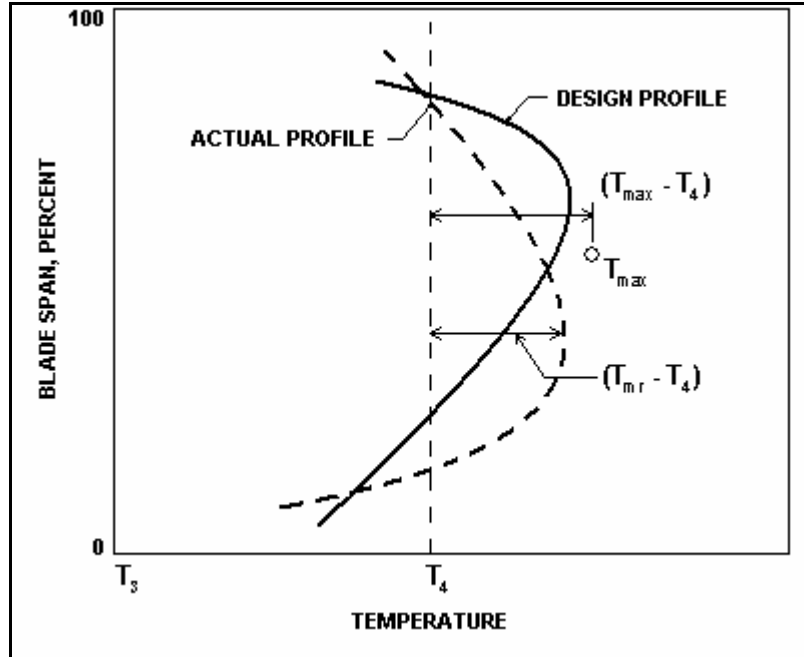
Figure 2.2: Explanation of exit temperature profile parameters (Lefebvre, 1998)

2.3   One-dimensional flow calculations

For an initial one-dimensional design analysis, the mass flow distributions across the various features of the combustion liner can be predicted with analytical and empirical correlations. The flow through specific features is, however, affected by the geometry of the combustor liner in the vicinity of the hole and not only by its size and pressure drop.

The essential correlations for one-dimensional flow and temperature predictions will be discussed in the subsequent section, providing the assumption that the flow is incompressible. The computer code developed to implement these correlations is presented in Appendix D. The basic empirical equation for incompressible flow through liner holes, which is derived from the simple Bernoulli equation combined with the continuity equation, can be expressed as follow:

$$m_h = C_d A_h \left(2\rho \left(P_1 - p_j \right) \right)^{0.5} \tag{2.3}$$

where P_1 =   total pressure upstream of the hole

p_j =   static pressure downstream of the hole

19

m_h = massflow through hole feature

C_d = hole feature discharge coefficient

A_h = total through flow area of specific hole set

ρ = air density

As described by Adkins and Gueroui (1986), the flow on the outside of a combustion chamber is normally parallel to the liner walls, and when the flow passes over a liner hole the air is drawn into it due to the lower static pressure inside the chamber. As the flow is drawn in, it is both deflected and accelerated and also contracts in cross-sectional area. This contraction is so rapid that fluid dynamic forces cause it to continue contracting for some distance after it has passed through the hole. A minimum cross-sectional area is reached at some distance which is known as the vena contracta. The velocity and static pressure are uniform over the cross-section due to no streamwise curvature of the jet. The static pressure will be equal to that of the surrounding gases. The minimum jet area is normally expressed as a fraction of the geometric hole area known as the discharge coefficient (C_d), which is generally in the range of 0.6 for plain flush circular holes. Figure 2.3 is a schematic illustration of this phenomenon.
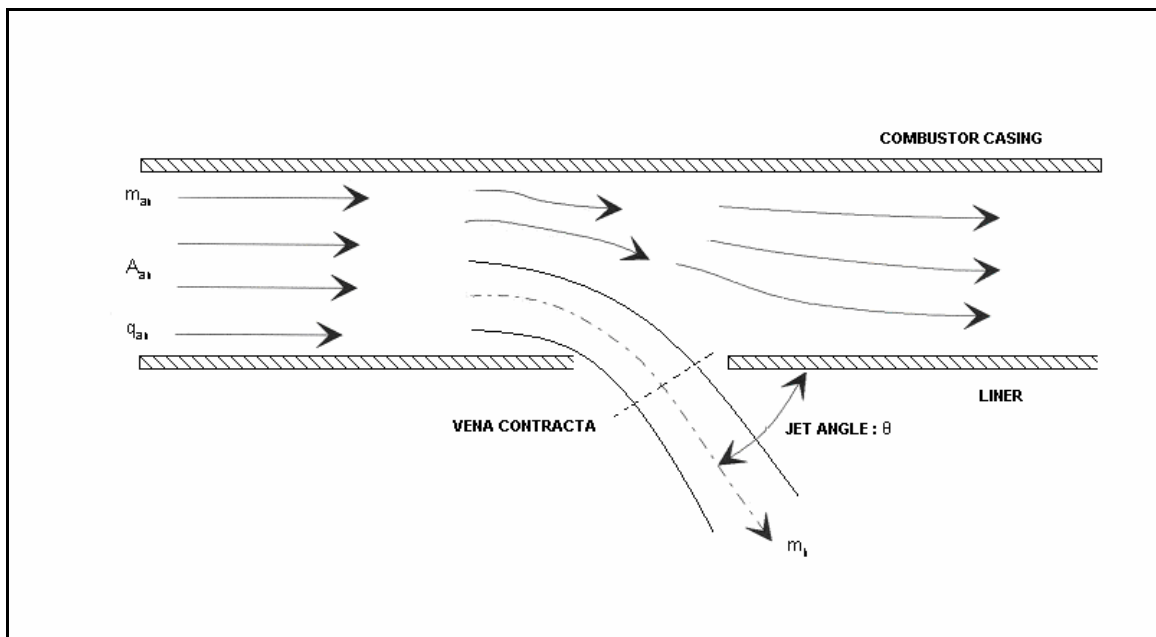
Figure 2.3: Flow through liner hole (Van Niekerk and Morris, 2001)

Correlations, presented by Norster (1980), can be used to predict the discharge coefficient through the various liner hole features. These correlations are, however, only valid for plain and plunged holes. Therefore, initial discharge coefficients of 0.8 can be assumed for the cooling devices that are aligned with the flow, as described by Dodds and Bahr (1990).

The correlations for plain and plunged holes are defined by (Norster, 1980):

Plain holes:

$$C_d = \frac{1.25(K-1)}{\sqrt{\left[4K^2 - K(2-\alpha)^2\right]}} \tag{2.4}$$

Plunged holes:

$$C_d = \frac{1.65(K-1)}{\sqrt{\left[4K^2 - K(2-\alpha)^2\right]}} \tag{2.5}$$

In the above-mentioned equations, the hole loss coefficient, K, and the hole bleed ratio, α, are presented by the following expressions (Norster, 1980):

$$K = 1 + 0.64\left\{2\varphi^2 + \sqrt{\left[4\varphi^4 + 1.56\varphi^2(4\alpha - \alpha^2)\right]}\right\} \tag{2.6}$$

where

Mass flow ratio (bleed ratio): $\qquad \alpha = \dfrac{\dot{m}_h}{\dot{m}_{an}}$ (2.7a)

Hole area ratio: $\qquad A_r = \dfrac{A_{h,geom}}{A_{an}}$ (2.7b)

Mass flow ratio/area ratio: $\qquad \varphi = \dfrac{\alpha}{A_r}$ (2.7c)

The jet flow angle for plain and plunged holes can also be expressed as a function of the loss coefficient, K, respectively (Norster, 1980):

Plain holes:

$$\sin\theta = \frac{1}{1.6C_d}\frac{(K-1)}{K} \qquad\qquad (2.8)$$

Plunged holes:

$$\sin\theta = \frac{1}{1.2C_d}\frac{(K-1)}{K} \qquad\qquad (2.9)$$

With the use of the above-mentioned equations and correlations, the following procedure can be used to predict pressure drop and flow distributions through liner hole features:

- Manipulate equation (2.3) so that it describe the pressure as a function of the mass flow rate
- Guess an initial mass flow rate through all the liner holes
- With the initial guess, use the following procedure to calculate the discharge coefficients (Odgers and Kretchemer, 1980a):

       step 1: Calculate α (mass flow ratio) Eq. 2.7 (a) from initial mass flow

       step 2: Calculate A_r (hole area ratio) Eq. 2.7 (b)

       step 3: Calculate φ Eq. 2.7 (c)

       step 4: Calculate K using Eq. 2.6

       step 5: Insert K into either Eq. 2.4 or Eq. 2.5 to determine the appropriate discharge coefficient

- Calculate the area-weighted pressure drop across the liner
- Adapt individual mass flow distributions by correlating the pressure drop

- Restart iteration with new mass flow distributions until pressure drop converges (assuming that the pressure drop across all the features are the same, therefore ignoring frictional losses)

The prediction of flow distributions is followed by the prediction of the adiabatic flame temperature which is a function of the local air/fuel ratio. To facilitate the prediction, the combustion chamber is divided into a recirculation, primary, secondary and dilution zones in which the airflow can be assumed for each zone. Following usual practice, as described by Kretchmer and Odgers (1978), the flow within the recirculation zone include the sum of all the flow admitted through (a) the swirler, (b) any additional air admitted through the flare, (c) 2/3 of the air admitted through the first row of holes in the primary zone, and (d) 1/3 of the air admitted through the second row of primary holes. None of the air used for film cooling of the primary zone wall is assumed to enter the recirculation. If there is only one row of holes for primary air admission, then half the air admitted is assumed to take part in the recirculation. Skidmore (1986) assumed for the T56 combustion chamber that the primary zone include one third of the air entering through the first hole set. The remaining air flow then forms part of the air flow for the secondary zone. In the same way, the secondary zone include half of the air entering through the third hole set and one third of the air entering through the third cooling device with the remaining air flow becoming part of the dilution zone. The latter assumption was utilised during this study.

Chemical reaction rates are generally controlled by the flame temperature which is usually assumed to be the adiabatic temperature. The adiabatic flame temperature would be the maximum temperature that can be achieved for given reactants because any heat transfer from the reacting substance and/or any incomplete combustion would tend to lower the temperature of the products. The adiabatic temperatures are, however, rarely achieved due to heat losses from the flame by radiation and convection. Nonetheless, the adiabatic flame temperature plays a significant role in determining combustion efficiencies and in heat transfer calculations. However, before the adiabatic flame

temperature can be predicted, some definitions such as stoichiometric air/fuel ratios and equivalence ratios should be discussed.

Complete combustion of hydrocarbon fuels can be achieved with the proper amount of air to completely convert the fuel to carbon dioxide and water vapour. Stoichiometric combustion refers to this complete combustion process. Stoichiometric mixtures contain sufficient oxygen for complete combustion; therefore, operating at stoichiometric air/fuel ratios will release all the latent heat of combustion of the fuel (Lefebvre, 1998). The typical stoichiometric air/fuel ratio used for kerosene is 14.74.

A convenient way of comparing different fuels in terms of their mixing strength is to make use of the equivalence ratio (ϕ). The equivalence ratio is defined as the actual fuel/air ratio divided by the stoichiometric fuel/air ratio. It can also be defined as the stoichiometric air/fuel ratio divided by the actual air/fuel ratio. Therefore, when $\phi = 1$ it denotes a stoichiometric mixture, when $\phi < 1$ it indicates a fuel-lean mixture, while $\phi > 1$ indicates a fuel-rich mixture.

$$\phi = \frac{\left(\text{F/A}\right)_a}{\left(\text{F/A}\right)_s} \quad \text{or} \quad \phi = \frac{\left(\text{A/F}\right)_s}{\left(\text{A/F}\right)_a} \tag{2.10}$$

Where "s" and "a" denote stoichiometric and actual mixtures respectively.

The adiabatic flame temperature is influenced by the fuel/air ratio, inlet temperature and pressure. Since the total amount of air in each of the four combustion zones can be predicted as discussed in the previous paragraph, the air/fuel ratio and hence the equivalence ratio in each zone can be predicted. Temperature rise curves for kerosene, depicted in figure 2.4, can then be utilised to predict the temperature rise (ΔT) for a specific combustion zone. These curves present the undissociated temperature rise due to combustion at a certain inlet temperature and pressure as a function of the equivalence ratio. The adiabatic flame temperature can subsequently be obtained using the expression defined in equation (2.11).
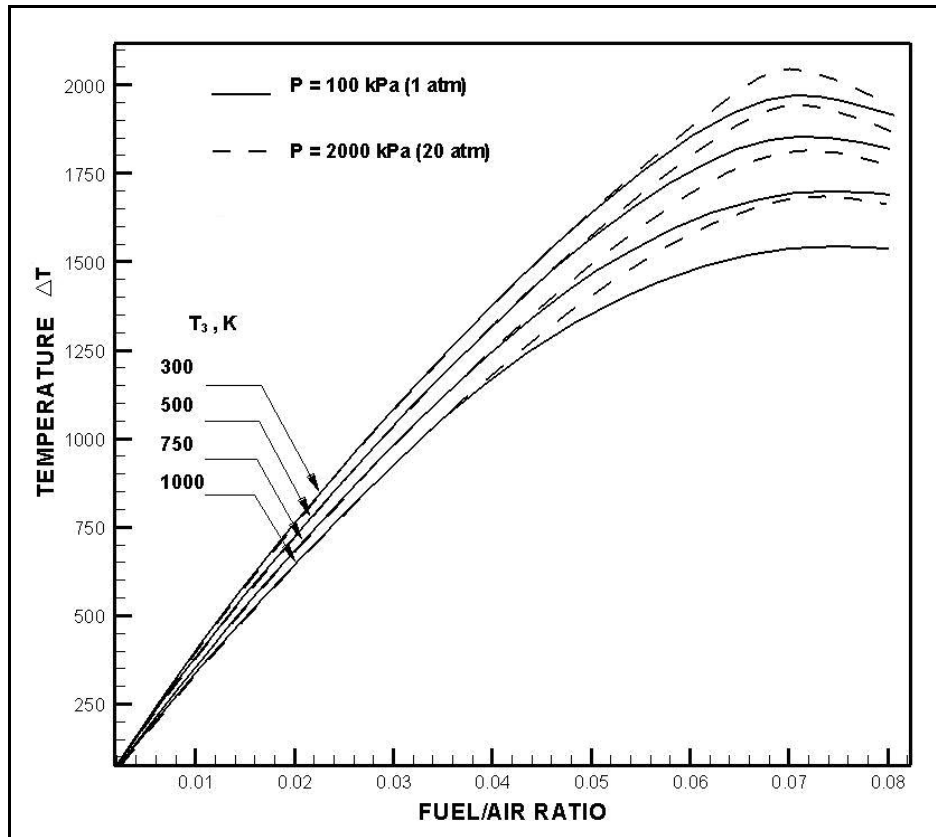
Figure 2.4: Temperature rise curves (Lefebvre, 1998)

$$T_g = T_3 + \Delta T \tag{2.11}$$

With the intention of predicting gas temperatures more accurately, combustion efficiency has to be accounted for. Gosselin *et al.* (1999), as well as Odgers and Kretchemer (1980a), presented empirical correlations for the prediction of combustion efficiency in the re-circulation, primary, secondary, and dilution zone which in turn predicts the mean temperatures in the specific zone. The following correlation is used to predict combustion efficiency in the recirculation zone:

$$\eta_{RZ} = 0.56 + 0.44 \tanh \left[1.548 \times 10^{-3} \left(T_3 + 108 \ln P_3 - 1863 \right) \right] \tag{2.12}$$

where,

T_3	=	inlet temperature [K]
P_3	=	inlet pressure [Pa]

The temperature distribution in the recirculation zone is considered to be linear between T_3 at the inlet of the injector face and T_{RZ} at the end of the recirculation zone. The temperature will vary linearly between T_{RZ} and T_{PZ} for the remainder of the primary zone. Combustion efficiency for the primary zone is presented as follows:

$$\eta_{PZ}=0.71+0.29\tanh\left[1.548\times10^{-3}\left(T_3+108\ln P_3-1863\right)\right]$$ (2.13)

The correlations presented by Gosselin *et al.* (1999) for the secondary and dilution zones indicated lower values of combustion efficiency than that of the primary zone. For this reason, it was assumed that combustion was completed in the primary combustion zone and consequently a combustion efficiency of 90 percent was assumed for the secondary and dilution zones.

Since the combustion efficiencies in the primary zone can be accounted for using equation (2.13), the mean gas temperature in the zone can be predicted. For the maximum temperature in the recirculation zone,

$$T_{out,RZ}=T_3+\eta_{RZ}\Delta T$$ (2.14)

According to Odgers and Kretchemer (1980b), this zone is only partially stirred and this maximum temperature will exist locally only. Therefore, a mean outlet temperature is assumed,

$$T_{out,RZ}=\frac{1}{3}T_3+\frac{2}{3}T_{RZ}$$ (2.15)

The temperatures in the remaining zones can be calculated by assuming a linear temperature distribution as follows:

$$T_{out,zone}=T_3+\eta_{zone}\Delta T_{zone}$$ (2.16)

2.4   Heat transfer process

Peak gas temperatures in the primary zone of a combustion chamber exceed 2000 K. Protection of the combustor liner against these high gas temperatures is of great importance to ensure durability and structural integrity. Combustion chambers are typically fabricated from a nickel- or cobalt-based alloy such as Hastelloy-X or HS188. These high-temperature alloys are good for long-term operations at temperatures of up to 1150 K. At temperatures higher than 1150 K, the strength of these materials decreases to unacceptable levels. At approximately a temperature of 1400 K, rapid oxidation starts occurring and the liner material starts melting at a temperature range between 1500–1750 K. The increasing operating conditions of modern-day gas turbine engines, to improve overall engine efficiency and specific fuel consumption and to reduce emission levels such as NO_x, influence the effective use of film-cooling devices. This leads to the research and development of more advanced cooling devices and materials that can withstand higher temperatures (Dodds and Bahr, 1990; Rizk, 1994; Gosselin *et al.*, 1999).

During the present study, the material utilised on the T56 combustion chamber was analysed with an electron microscope situated at the University of Pretoria, South Africa. The data obtained from the analysis showed close agreement to Hastelloy-X, and for the purpose of the study the material properties of Hastelloy-X were used. The data obtained from the analysis is presented in Appendix A.

A need therefore exists to predict liner wall temperatures prior to more expensive experimental tests, by conducting a one-dimensional heat balance along the liner wall. The heat transfer process consists of three modes of heat transfer, namely convection, radiation, and conduction. The inner liner wall is heated by convection and radiation from the hot combustion gases and cooled on the outside by the annulus air flow through convection and radiation from the outer liner surface to the casing wall. Calculations are conducted for equilibrium conditions where both the internal and external heat fluxes are equal. Heat loss along the liner wall through conduction is assumed to be very small and may be neglected. Figure 2.5 is a schematic illustration of such a heat transfer process.
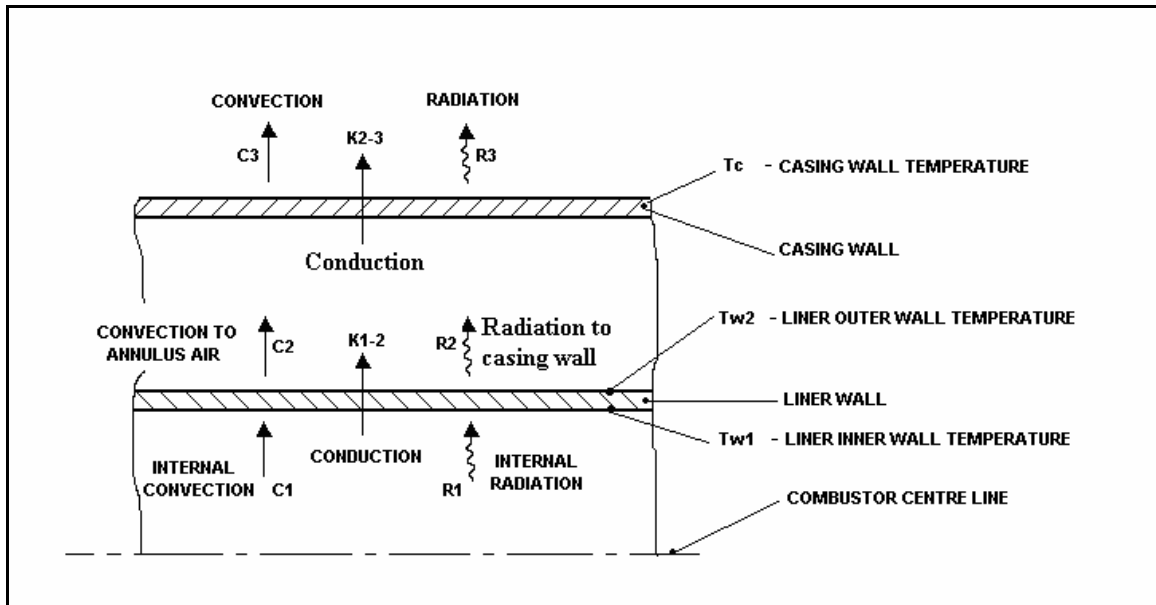
Figure 2.5: Heat transfer process

When steady-state conditions are assumed, the heat flux into a wall segment must equal the heat loss from the same segment. Considering all three heat transfer modes, the steady-state heat transfer process can be described by the following expression where the internal and external liner areas are A_{w1} and A_{w2} respectively.

$$(R_1 + C_1)A_{w1} = (R_2 + C_2)A_{w2} = K_{1-2}A_{wm} \qquad (2.17)$$

where

R_1 = Internal radiation from the hot gas to the liner wall

C_1 = Internal convection of the hot gas to the liner wall

R_2 = External radiation from the outer liner area to the casing internal wall

C_2 = Convection on the external surface of the combustor in the annulus

K_{1-2} = Conduction through the liner wall

A_{w1} = Liner internal heat transfer area

A_{w2} = Liner outer heat transfer area

A_{wm} = Mean liner heat transfer area, $\dfrac{(A_{w1} + A_{w2})}{2}$

Gas radiation can be considered to have two components, namely non-luminous and luminous radiation. Non-luminous radiation originates from certain gases, especially from carbon dioxide and water vapour. Luminous radiation on the other hand, depends on the number and size of the solid particles, mainly soot in the flame. The chemistry and soot formation, atomisation quality, fuel distribution in the combustion zone, and fuel-air mixing are all effected by the pressure which in turn influences the emissivity of luminous gases. Increasing the inlet temperature and liner size, owing to a larger beam length, will noticeably increase the emissivity and radiation. The beam length (l_b) is defined as the radius of gas hemisphere that will radiate to a unit area, at the centre of its base, the same amount as the average radiation from the actual gas mass. Due to the complexity in estimating the luminous emissivity, a luminosity factor (L_u) is introduced into the empirical expression for a non-luminous flame, assuming an isothermal gas temperature T_g which is bounded by walls at a temperature T_w (Lefebvre, 1998; Rizk, 1994; Lienhard and Lienhard, 2003).

The gas emissivity for luminous gases can be predicted as follows:

$$\varepsilon_g = 1 - e^{\left(-290 P_3 L_u (q l_b)^{0.5} T_g^{-1.5}\right)} \tag{2.18}$$

where

$$
\begin{aligned}
P &= \text{gas pressure, kPa} \\
T_g &= \text{gas temperature, K} \\
l_b &= \text{beam length, m} \\
q &= \text{fuel/air ratio by mass}
\end{aligned}
$$

The size and shape of the gas volume determine the beam length (l_b) which can be expressed, for most practical purposes, with sufficient accuracy as follows:

$$l_b = 3.4 \frac{\text{volume}}{\text{surface area}} \tag{2.19}$$

The luminosity factor L_u depends mainly on parameters such as carbon/hydrogen mass ratios and fuel hydrogen content. A number of correlations exist, but the correlation used during the present study, and provided by Lefebvre (1998), is presented as follows:

$$L_u = 7.53 \left(\frac{C}{H} - 5.5 \right)^{0.75}$$

(2.20)

The internal radiation flux (R_1) from the hot gases into a wall segment is calculated from the equation proposed by Lefebvre (1998) as follows:

$$R_1 = 0.5\sigma \left(1 + \varepsilon_w \right) \varepsilon_g T_g^{1.5} \left(T_g^{2.5} - T_{w1}^{2.5} \right)$$

(2.21)

Assuming a heat transfer relation for a straight pipe, internal convection (C_1) between the gas and the liner wall is given by (Rizk, 1994):

$$C_1 = 0.020 \frac{k_g}{D_h^{0.2}} \left(\frac{\dot{m}_g}{A_L \mu_g} \right)^{0.8} \left(T_g - T_{w1} \right)$$

(2.22)

where D_h is defined as the hydraulic diameter,

$$D_h = \frac{4A}{P_w}$$

(2.23)

Some difficulties occur when the latter equation is applied to the primary combustion zone. Due to the flow reversal region in the primary zone, the direction of flow corresponds, to that of the assumed pipe analogy, only in the region adjacent to the wall. Another complication can occur when a swirler is used; the local gas velocity close to the wall will be greater than the downstream component. The question as to whether or not the bulk gas temperature T_g is appropriate for temperature predictions can also be asked. To account for this, the value of the constant in equation (2.22) is reduced from 0.020 to 0.017, for the primary zone calculations as described by Lefebvre (1998). Crocker *et al*. (1999) presented alternative values of 0.046 and 0.04 for calculations in the primary zone

and remainder of the combustion chamber respectively. However, the former results have shown to provide better comparative results during this study.

Although heat conduction through the liner wall is considered insignificant it can be expressed by:

$$K_{1-2} = \frac{k_w}{t_w}\left(T_{w1} - T_{w2}\right)$$

(2.24)

Heat is removed from the combustor liner through radiation to the outer casing and convection to the annulus air. Using typical values of emissivity for both the casing and liner walls, the external radiation (R_2) can be calculated as follows (Lefebvre 1998):

$$R_2 A_w = \frac{\sigma\left(T_{w2}^4 - T_c^4\right)}{\dfrac{\left(1-\varepsilon_w\right)}{\varepsilon_w A_w} + \dfrac{1}{A_w F_{wc}} + \dfrac{\left(1-\varepsilon_c\right)}{\varepsilon_c A_c}}$$

(2.25)

where

A_w = surface area of liner wall

A_c = surface area of casing

F_{wc} = geometric shape factor between liner and casing

The heat transfer due to radiation is relatively small when compared to the external convective heat transfer. Its impact on the heat transfer increases with an increase in liner temperature, but can often be neglected at low temperatures. The geometric shape factor is also assumed to be unity due to radiation across a long annular space. The net radiation heat transfer from the liner then reduces to:

$$R_2 = \frac{\sigma\varepsilon_w\varepsilon_c\left(T_{w2}^4 - T_3^4\right)}{\varepsilon_c + \varepsilon_w\left(1-\varepsilon_c\right)\left(\dfrac{A_w}{A_c}\right)}$$

(2.26)

The correlation for external convection (C_2) is similar to equation (2.22) except that the properties of the annulus air are used and they are based on the hydraulic diameter of the annulus.

$$C_2 = 0.020 \frac{k_a}{D_{an}^{0.2}} \left(\frac{\dot{m}_{an}}{A_{an}\mu_a} \right)^{0.8} \left(T_{w2} - T_3 \right) \tag{2.27}$$

2.5   Film-cooling devices

A film-cooling device provides a protective film of cooling air between the liner wall and the hot combustion gases by injecting the air along the inner surface of the liner. Generally, combustion chambers are designed to incorporate a number of cooling slots along the length of a combustor liner to overcome the gradual destruction of the film due to the turbulent mixing with the combustion gases (Rizk, 1994).

Typical film-cooling devices used on conventional combustion chambers include splash-cooling rings, wiggle strips, stacked rings, machined rings, z-rings, and rolled rings. These devices are spaced at intervals along the axial direction of the combustion liner to provide a film-cooled blanket on the inner surface of the combustor liner. Splash-cooling rings, wiggle strips, stacked rings, and machined rings are fabricated from sheet metal. The splash-cooling device utilises the static pressure drop across the liner to provide the desired film cooling. The air jets impinge on a deflector which is attached to the inner surface of the liner. As the cooling air impinges on the deflector, the air is directed in a direction parallel to the combustor wall, thus forming a uniform film-cooled blanket. If the static pressure drop across the liner is too low, a cooling device that utilises the total pressure drop needs to be used. Wiggle strips and machined rings are examples of cooling devices that utilise the total pressure drop across the liner. The disadvantage of utilising the total pressure drop across the combustor liner is the variation of annulus air velocity due to the availability of the air flow and this may influence the cooling air flow in downstream locations. The wiggle strip configuration employs a corrugated metal strip to form a film-cooling slot and provides a stiff structure. The cooling flow area is very sensitive to variation in material thickness and ring diameter. Due to this it is more

difficult to control the film-cooling air flow through a wiggle strip compared to machined rings. Machined rings can be constructed of a single piece of metal or by welding several rings together. A number of orifices, spaced equally apart, are machined into the ring to provide the required cooling flow. Stacked rings are similar to machined rings but differ in the construction method (Dodds and Bahr, 1990). Typical film-cooling devices are depicted in figure 2.6.
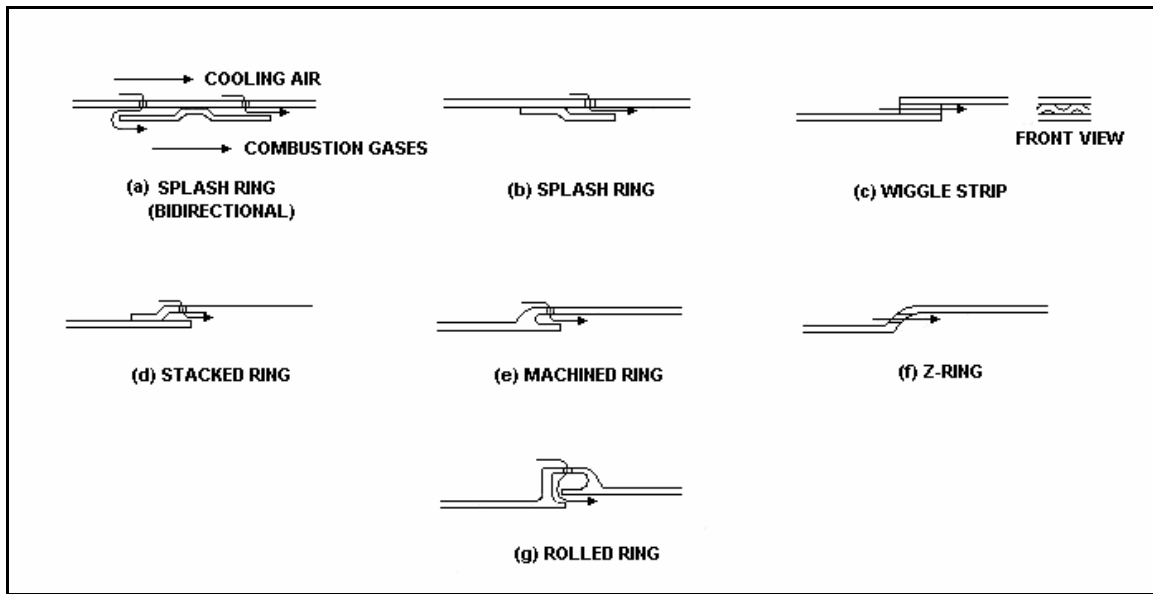
Figure 2.6: Film-cooling devices (Dodds and Bahr, 1990)

Another method of protecting the combustor liner is to apply a ceramic coating to the inside to insulate it from the hot combustion gases. Ceramic tiles are used in industrial gas turbine engines. The heat transfer coefficient on the cool side can be increased by using forced convection or by adding fins on the backside. The latter method has the disadvantage of additional weight and difficulty of manufacturing. An alternative approach is to merely roughen the backside surface, which will increase the convective heat transfer coefficient. However, this will also increase the pressure drop across the combustor liner (Lefebvre, 1998; Dodds and Bahr, 1990).

Ballal and Lefebvre (1986) derived the following expression for film-cooling effectiveness based on turbulent boundary layer models by utilising available experimental data:

$$\eta_f = 1.10 m^{0.65} \left(\frac{\mu_a}{\mu_g} \right)^{0.15} \left(\frac{x}{s} \right)^{-0.2} \left(\frac{t}{s} \right)^{-0.2}$$

(2.28)

where m is defined as the mass velocity ratio $\dfrac{(\rho V)_a}{(\rho V)_g}$, μ is the dynamic viscosity, s is the cooling slot gap, t is the slot thickness, and x is the distance downstream of the slot. The subscripts "a" and "g" denote the air and gas streams respectively. The film-cooling effectiveness is defined as:

$$\eta_f = \frac{T_g - T_{w,ad}}{T_g - T_a}$$

(2.29)

where

T_g =   Predicted gas temperature [K]

T_a =   Cooling air temperature [K]

$T_{w,ad}$ =   Gas temperature at the combustor liner wall [K]

A value close to unity for the effectiveness indicates that the wall temperature ($T_{w,ad}$) approaches that of the cooling air temperature (T_a). Equation (2.28) is valid for values of m ranging between 0.5 and 1.3. For higher values, the first term in equation (2.28) is replaced by a constant equal to 1.28. To illustrate these variables, figure 2.7 depicts a typical film- cooling device schematically.
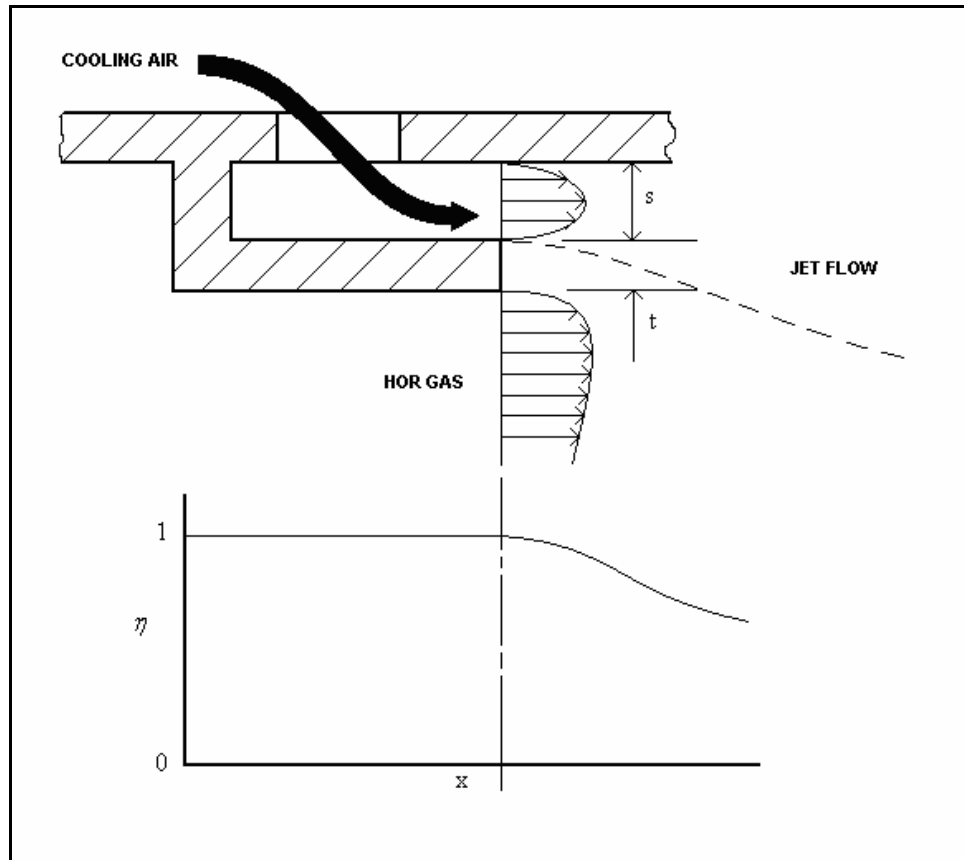
Figure 2.7: Schematic depletion of a film-cooling process

2.6   Swirler design

Turbulent flow in gas turbine combustors, especially in the primary zone, is of great importance to enhance the mixing of the fuel and air resulting in efficient and complete combustion. Recirculating flow is generally achieved when the air flow through the primary jets impinge on one another, forcing some of the air in the upstream direction and some in the downstream direction. In some cases the jet penetration is so poor that additional methods must be utilised to enhance the recirculating flow. One method is to make use of an air swirler. Air is introduced axially into the swirler, which in turn forces the flow to spiral due to the vanes that are positioned at a fixed predetermined angle. Such devices are normally designed using empirical correlations as outlined by Lefebvre (1998). A number of studies have been conducted to determine the effect of a swirler. In addition to the normal axial swirlers, co-swirlers a well as counter-swirlers were investigated by a number of authors, including Guoqiang *et al*. (2004), Gupta and Lewis

(1998), Micklow *et al.* (1993), and Cia *et al.* (2002). These two devices consist of two concentrical swirlers rotating the air flow in the same as well as opposite directions respectively. Parametric studies were performed in some of the cases to investigate the influence of flow splits through the swirler on the size of the recirculation zone and temperature distribution while maintaining a constant equivalence ratio in the combustion zone. These devices were mainly investigated in an attempt to reduce the emission levels. It is highlighted by Guoqiang and Gutmarl (2004) that by increasing the recirculation zone this will enhance the air flow, thus reducing the combustion temperature and hence thermal NO formation. However, local oxygen levels will also increase as the swirl increases, thus promoting NO formation.

According to Micklow *et al.* (1993), the use of an airblast fuel injector will produce a finer fuel spray, and with the use of a swirler thorough mixing can be achieved, thus reducing soot and NO_x emission levels. Also, such a process will result in a flame of low luminosity and soot, which may result in cooler liner wall temperatures.

According to Gupta *et al.* (1984), the induced swirl has an impact on jet growth, flame size, shape, stability and combustion intensity. The amount of swirl that is being induced, can be characterised by the dimensional number known as the swirl number (S_N). For axial swirlers, the swirl number can be expressed as a function of the vane angle and is described by Mattingly *et al.* (2002) as follows:

$$S_N = \frac{G_\phi}{G_x' r_t} \tag{2.30}$$

Where G_ϕ and G_x', are the axial fluxes of tangential and axial momentum respectively.

$$G_\phi = \int_{r_{hub}}^{r_t} (Wr)\rho U (2\pi r)\,dr = (U\tan\theta_v)U2\pi\rho \int_{r_{hub}}^{r_t} r^2\,dr = \frac{2}{3}\pi\rho U^2 \tan\theta_v \left[r_t^3 - r_{hub}^3 \right] \tag{2.31}$$

and

$$G_x^{'} = \int_{r_{hub}}^{r_t} \left(U\right)\rho U\left(2\rho r\right) dr = \left(U\right) 2\pi\rho U \int_{r_{hub}}^{r_t} r dr = \pi\rho U^2 \left[r_t^2 - r_{hub}^2 \right] \tag{2.32}$$

The swirl number is therefore defined as:

$$S_N = \frac{2}{3} \tan\theta_v \left[\frac{1 - \left(\dfrac{r_{hub}}{r_t}\right)^3}{1 - \left(\dfrac{r_{hub}}{r_t}\right)^2} \right] \tag{2.33}$$

Strong swirl is characterised by a swirl number greater than or equal to 0.6 (Lefebvre, 1998; Dodds and Bahr, 1990). The recirculation zone diameter and length increase with an increase in swirl number up to a swirl number of 1.5, thereafter the recirculation zone diameter continues to increase while the length decreases. If a very strong and long recirculation zone is induced, it may entrain some of the relatively cool secondary gases, which may result in stability problems and low combustion efficiency. Due to flow separation at the inlet to the vane passages, sufficient passage length should be provided to allow the flow to reattach to ensure stable flow at the preferred swirl angle. A parameter called the solidity provides an indication to whether or not an appropriate passage length is available. The solidity is defined at the tip of the swirler vanes and should be at least unity if sufficient passage length is desired. The solidity is defined as (Dodds and Bahr, 1990):

$$Solidity = \frac{L_v}{S_v} \tag{2.34}$$

where L_v denotes the swirler vane length and S_v the pitch at the tip.

Lefebvre (1998) describes the mass flow through an axial swirler as a function of the pressure loss across the swirler, liner area, vane angle, and the type of vanes used:

$$\dot{m}_{sw} = \left\{ \frac{2\rho_3 \Delta P_{sw}}{K_{sw}\left[\left(\dfrac{\sec\theta_v}{A_{sw}}\right)^2 - \dfrac{1}{A_L^2}\right]} \right\}^{0.5} \tag{2.35}$$

K_{sw} is the blade loss coefficient which is defined by the type of vanes used, either curved or straight vanes. The value of K_{sw} is 1.3 for straight vanes and 1.15 for curved vanes. Curved vanes will result in a slightly better swirl but is more difficult to manufacture. The flow area of an axial swirler can be calculated as follows:

$$A_{sw} = \frac{\pi}{4}\left[D_{sw}^2 - D_{hub}^2\right] - 0.5n\left(\frac{t_v}{\cos\theta_v}\right)\left(D_{sw} - D_{hub}\right) \tag{2.36}$$

Where, n represents the number of blades, and t_v represents the blade material thickness. Other types of swirlers that are currently used in combustion chambers include radial swirlers, counter-rotating swirlers, and converging swirlers as depicted in figure 2.8 and 2.9. The type of swirler used affects the recirculation zone shape and size. Counter-rotating swirlers with a higher inner swirl number produce a much larger and stronger recirculation zone than with a co-swirling outer swirler, as described by Dodds and Bahr (1990). The swirl angle and flow rate through a swirler can be controlled by using a converging outer swirl cup. Each passage in this arrangement converges from inlet to exit where the flow is measured at the exit.
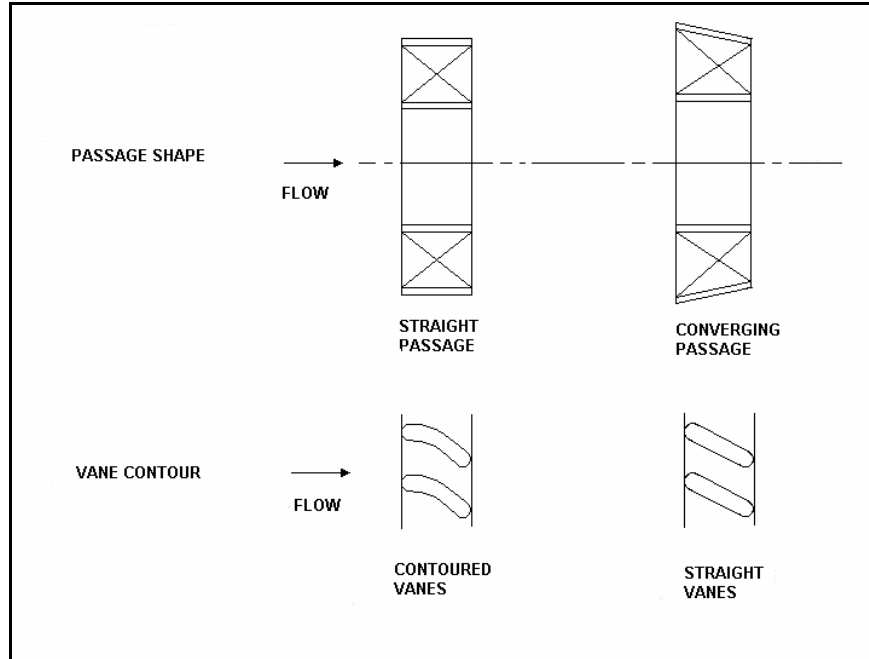
Figure 2.8: Swirler passage shapes and vane types (Dodds and Bahr, 1990)
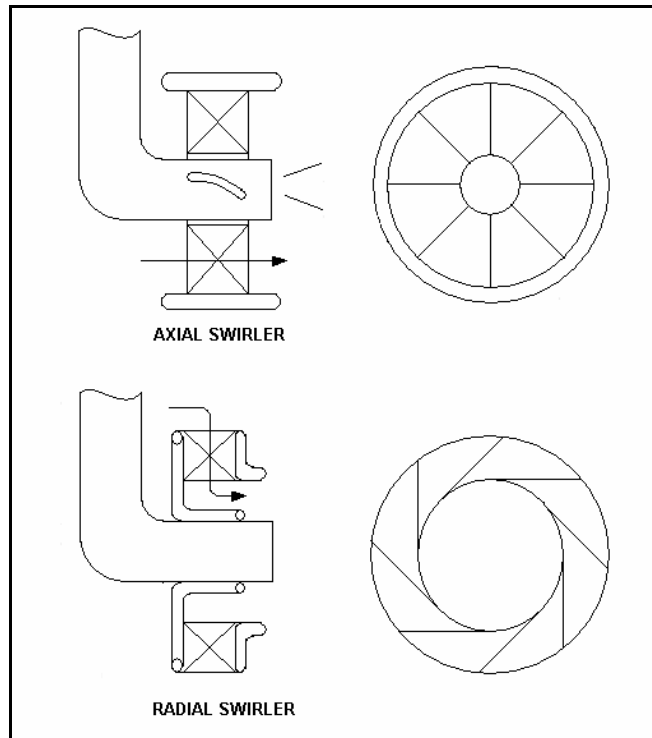
Figure 2.9: Axial and radial swirler (Dodds and Bahr, 1990)

2.7   1-D flow and temperature predictions

By implementing the previous formulations into a computer code, it is possible to predict one-dimensional incompressible flow and temperature predictions across a combustor liner. A computer code was thus generated as part of the study and is presented in Appendix D. With this code it is possible to predict pressure losses across the combustion chamber, flow distributions as well as temperature distributions across a can or can-annular combustion system. The model geometry is divided into a number of stations utilising the formulations described in a step-wise manner at each station.

The data in table 2.1 presents the predicted flow distributions and pressure drop across a single T56 combustor unit along with the discharge coefficients that were used. The discharge coefficients for the plain holes were predicted with equation (2.4) whereas the discharge coefficients for the cooling devices were assumed due to the lack of appropriate correlations. For the splash-cooling devices, a discharge coefficient of 0.6 was assumed and since the wiggle strip devices are aligned into the flow, utilising the total pressure loss, a discharge coefficient of 0.8 was assumed. The data in table 2.1 is described in sequence when moving from the dome, downstream towards the combustor exit. The hole layout of the combustion chamber is depicted in figure 2.10.
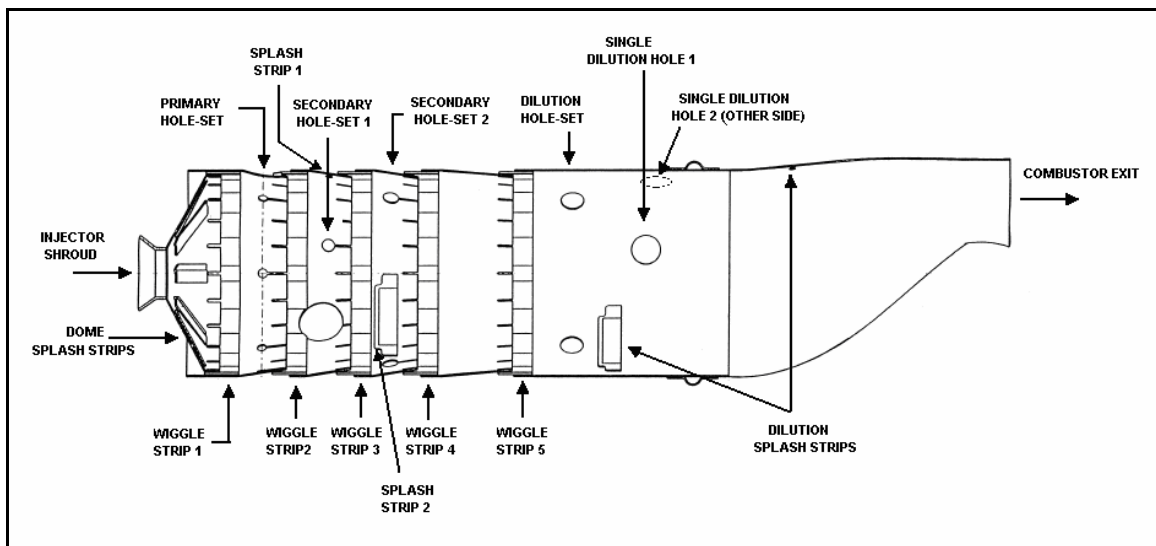
Fig. 2.10: Description of combustor hole layout

Table 2.1: Predicted vs. experimental mass flow distributions

		Predicted	Experimental	Predicted
	Hole type	Mass fraction [%]	Mass fraction [%]	Cd [-]
1	Injector shroud	0.542	0.74	**0.615**
2	Dome splash strips	4.639	6.14	0.6
3	Wiggle strip 1	12.78	15.63	0.8
4	Primary hole-set	3.013	4.82	**0.582**
5	Wiggle strip 2	12.787	10.69	0.8
6	Secondary hole-set 1	2.263	3.51	**0.585**
7	Splash strip 1	0.876	0.19	0.6
8	Wiggle strip 3	12.78	11.07	0.8
9	Secondary hole-set 2	4.702	6.6	**0.586**
10	Splash strips 2	1.751	0.83	0.6
11	Wiggle strip 4	12.774	9.59	0.8
12	Wiggle strip 5	12.761	9.87	0.8
13	Dilution hole-set	9.511	10.8	**0.588**
14	Dilution splash strips	2.608	2.62	0.6
15	Single dilution hole 1	3.833	4.36	**0.597**
16	Single dilution hole 2	2.375	3.27	**0.6**
	Pressure loss	2.16%		

Experimental mass flow distributions were obtained from Van Niekerk and Morris (2001) for a single T56 combustor unit. The data was obtained from isothermal experimental tests at atmospheric conditions. When comparing the predicted mass flow predictions with the experimental mass flow distributions, it can be seen that although there are discrepancies they follow the same trend as shown in figure 2.11. The discrepancy is due to the inappropriate discharge coefficients assumed for some of the hole features during the predictions, especially for the cooling devices.
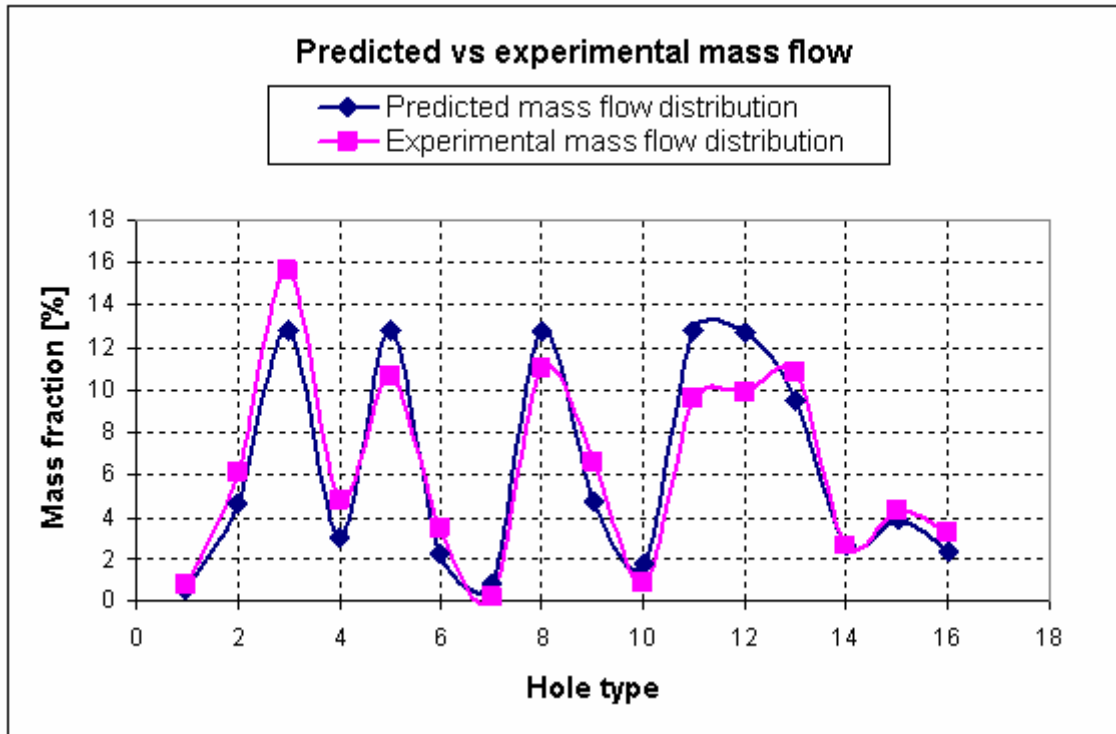
Figure 2.11: Predicted and experimental mass flow comparison

Figure 2.12 depicts the one-dimensional temperature distribution along the combustor liner. The predictions make use of the correlations previously discussed. The effect of the cooling devices is clearly depicted in figure 2.12 by the sudden reduction of wall temperature. Since the effect of the film cooling devices are modelled with film-cooling efficiency, therefore assuming 100 percent efficiency at the point of injection, a sudden drop in temperature is evident. The corresponding liner position of the film-cooling devices is illustrated by the dotted red lines on the temperature graph. The red line in figure 2.12 depicts the predicted gas temperature distribution along the combustor liner while the blue line depicts the average liner temperature distribution.

The drawback of the one-dimensional empirical code is the following:

- The effect of swirler flow cannot be predicted
- The flow is considered to be incompressible
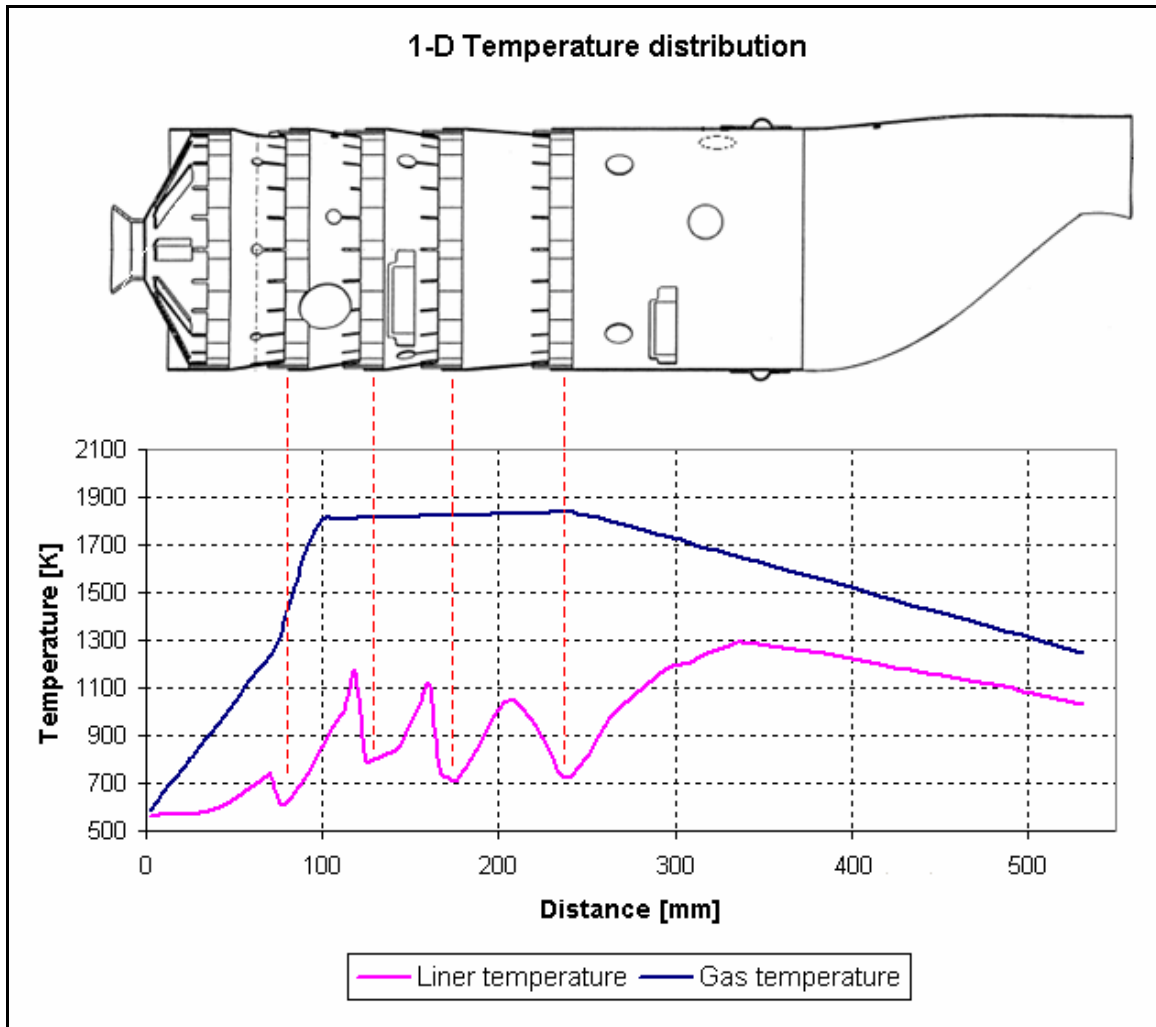
Figure 2.12: One-dimensional temperature distribution along combustor liner

Although the analysis cannot predict the three-dimensional influence of a swirler, the mass flow through a swirler can be predicted. When modifications to a combustor unit are considered, it is important to maintain the same overall pressure loss as this influences the engine performance. A swirler needs to be designed with a similar overall pressure loss, and for this reason accurate pressure drop predictions are important.

2.8   Summary

This chapter started with a general overview of typical gas turbine combustor features followed by a description of the incompressible empirical formulas to predict mass flow distributions and pressure losses across combustor features. These correlations are used

within the one-dimensional program presented in Appendix D. In addition, heat transfer correlations are added to predict combustor liner temperature distributions. Heat transfer is necessary to be included in such flow calculations, since temperature will influence the fluid pressure and density, hence mass flow distributions.

CHAPTER 3 –
1-D NETWORK APPROACH

3.1   Preamble

This chapter describes the network model and its governing equations that were utilised during the study to predict flow distributions and temperature distributions across the combustion chamber. The network approach has the ability to account for incompressible as well as compressible flow effects. These network models have proved to predict flow distributions and pressure losses with reasonable accuracy across combustion chambers, which is the reason why these models are generally used during preliminary design studies.

3.2   1- D network solver

Although combustor design has evolved since the development of numerical methods, it is still a tedious task requiring several numerical iterations, followed by experimental verification. Due to its rapid execution time, one-dimensional models are still preferred during the initial design phase as they are ideal for optimisation studies prior to more expensive and time-consuming three-dimensional analysis. As part of this investigation, a one-dimensional empirical model was developed to predict liner temperatures and flow distributions for the current combustor being considered. This model was described in the previous chapter. However, due to the limitations of using empirical correlations and assuming incompressible flow, it was decided to combine the empirical model with a one-dimensional network solver, FLOWNET. Network models employ the governing equations of mass, momentum and energy and are therefore suitable for both

compressible and incompressible flow, while parameters such as gas temperatures, combustion efficiency and gas emissivity can be obtained from the empirical formulations.

Figure 3.1 illustrates the network layout that was developed for a single combustor liner to solve the isothermal flow distribution through the different features. Due to the symmetry, only half of the combustor was modelled. The squares and circles, shown in more detail for the primary and secondary zone in figure 3.2, denote the nodes and elements respectively. The type of element that was used varied depending on the type of geometrical feature modelled. The gas flow inside the combustion chamber and the air flow in the annulus, were modelled with DG elements (duct with variable area). These elements account for area changes in a duct as well as frictional losses and momentum addition. The geometrical flow features, such as primary, secondary, and dilution holes, as well as film-cooling devices were modelled with RD elements (restrictor with discharge coefficient). These elements are used when the combustor feature has a known discharge coefficient. A swirler, on the other hand, can be modelled with an RL element (restrictor with loss coefficient) which is similar to the RD element but accounts for the pressure drop through the feature contraction as well as accounting for loss coefficients.
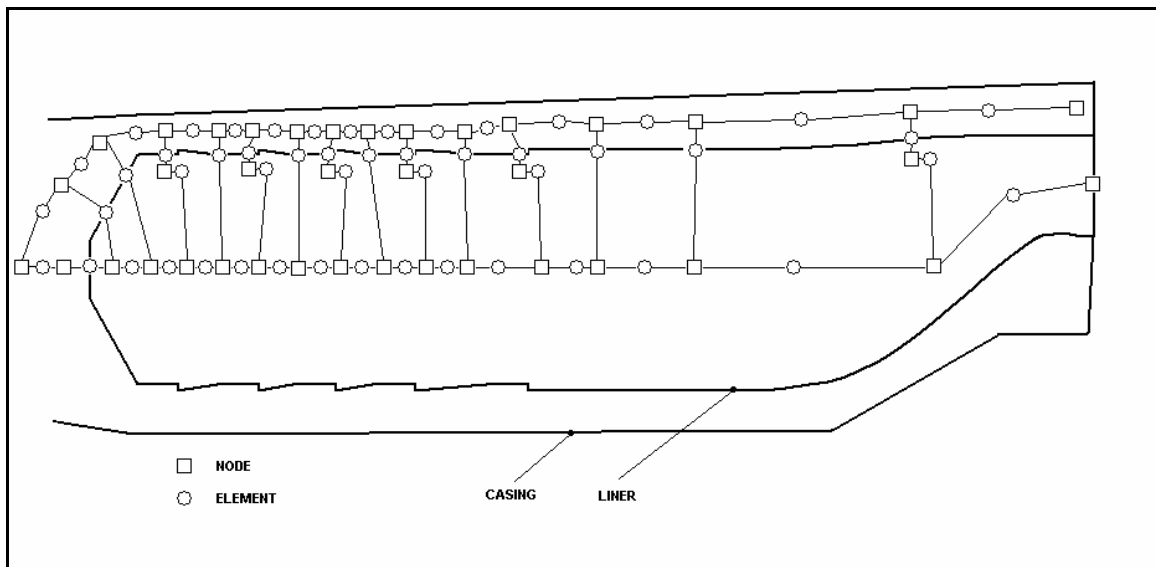
Fig. 3.1: General flow network layout for the combustion chamber
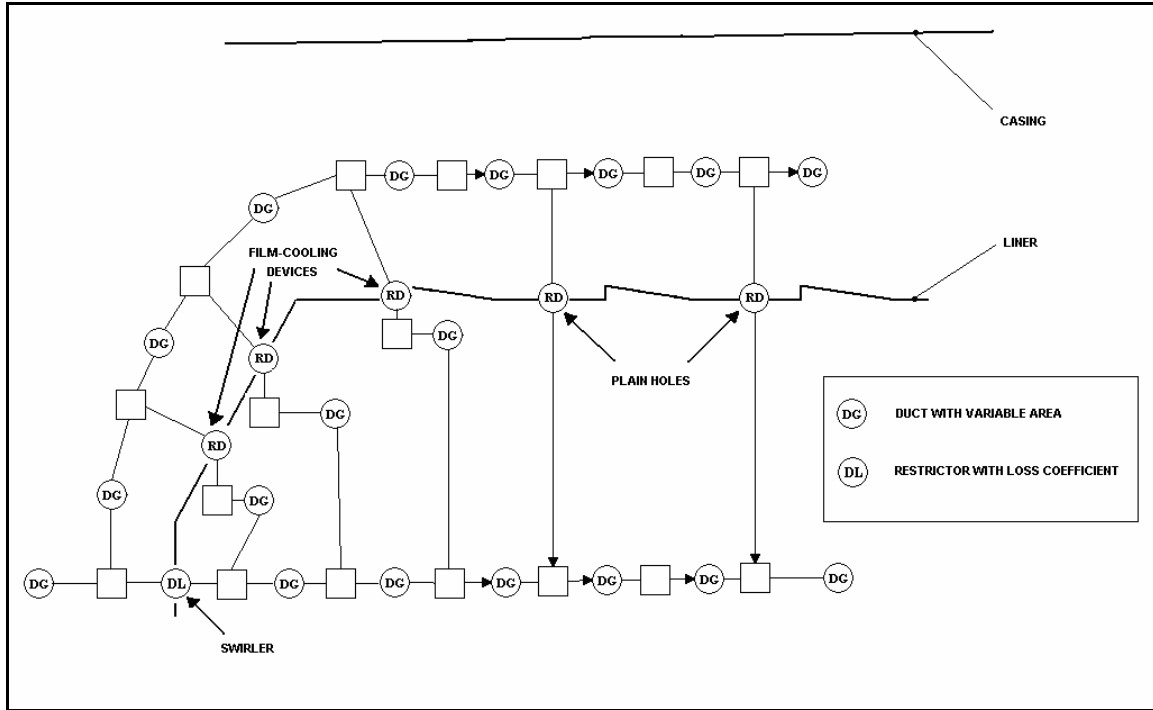
Fig. 3.2: Primary and secondary zone network layout

The initial step in the computational scheme is to assume a pressure at all the nodes and to calculate the corresponding density. The flow rate can then be calculated from the initial pressure and density. Thereafter a correction scheme, presented by Greyvenstein and Laurie (1994), is applied to the pressure, density, and flow rate to satisfy the governing equations. The overall governing equations constitute the continuity equation, which is applied at every node in the network, and the pressure drop-flow relationship which is applied for every element.   The steady-state continuity equation (from the conservation of mass) can be expressed as (Greyvenstein and Laurie, 1994),

$$\sum_{j=1}^{J}\rho_{ij}Q_{ij}s_{ij} = -d_{i} \qquad\qquad i=1,2,....,J \qquad\qquad (3.1)$$

where,

ρ =   density

d_i =   external mass flow into node i

Q =   volume flow rate

s =   is used to relate the flow direction in the network. If s > 0 the flow is in one direction and when s < 0, the flow is in the opposite direction.

The pressure drop-flow relationship in each element is typically defined using the Darcy-Weisbach, Hazen-Williams, Manning or other exponential or empirically determined correlations. The steady-state pressure drop-flow relationship (from the momentum conservation) for any branch element of node i (figure 4.3) can be expressed as (Greyvenstein and Laurie, 1994):

$$\Delta p_{ij} = p_{n_{ij}} - p_i = s_{ij} H_{ij} g_{ij} f_{ij} \tag{3.2}$$

where g_{ij} = $g_{ij}(\rho_{ij})$, which is a function of ρ_{ij},

f_{ij} = $f_{ij}\left(\left|Q_{ij}\right|\right)$, which is a function of Q_{ij}, and

H_{ij} = $Q_{ij}/\left|Q_{ij}\right|$

Note that the mass and energy conservation are applied at the network nodes and momentum conservation is applied across elements.
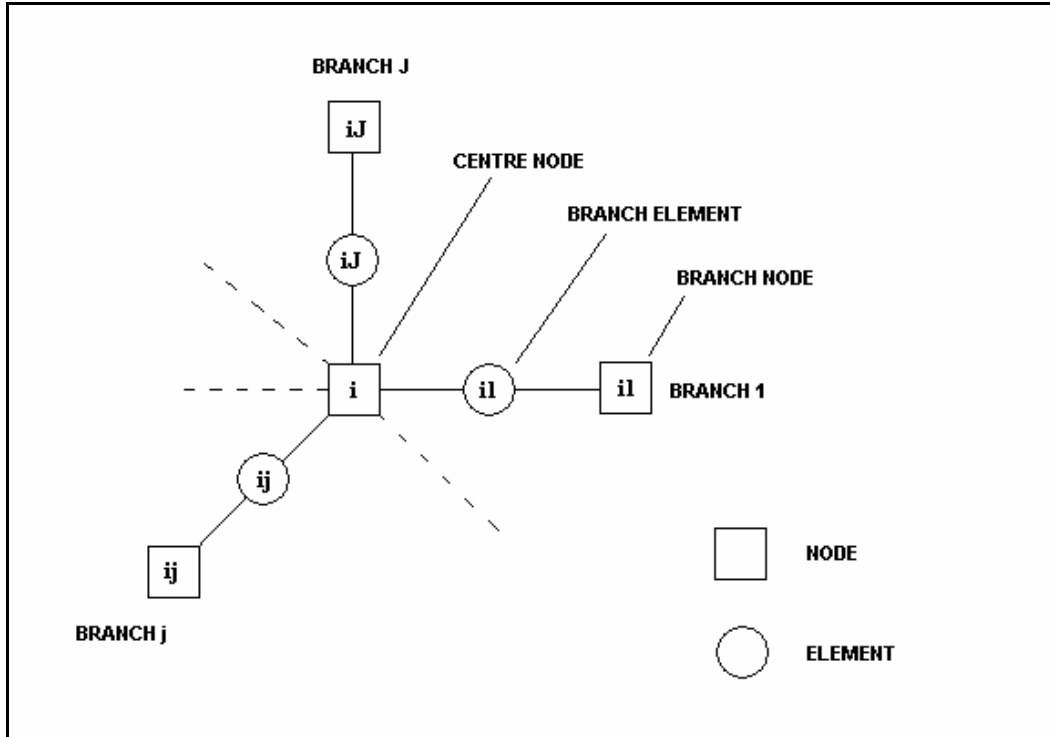
Fig. 3.3: Network arrangement (Greyvenstein and Laurie, 1994)

Heat transfer was modelled with convective, radiative, and conductive heat transfer elements. The heat transfer process is described between two nodes where enthalpy is balanced within each node, thereby satisfying the energy conservation equation. In the absence of a film-cooling device, the heat transfer from the combustion gases to the combustion liner was modelled with convective and radiative elements. These elements are connected to a conductive element which accounts for the conductive heat transfer through the combustor liner. External heat transfer is modelled by the connection of a special heat transfer (HT) element to the conductive element where, for simplicity, a constant heat transfer coefficient for both convection and radiation is specified. Axial conduction along the combustor liner was accounted for with a primitive heat transfer (PCHT) element. Such a process is illustrated in figure 3.4.
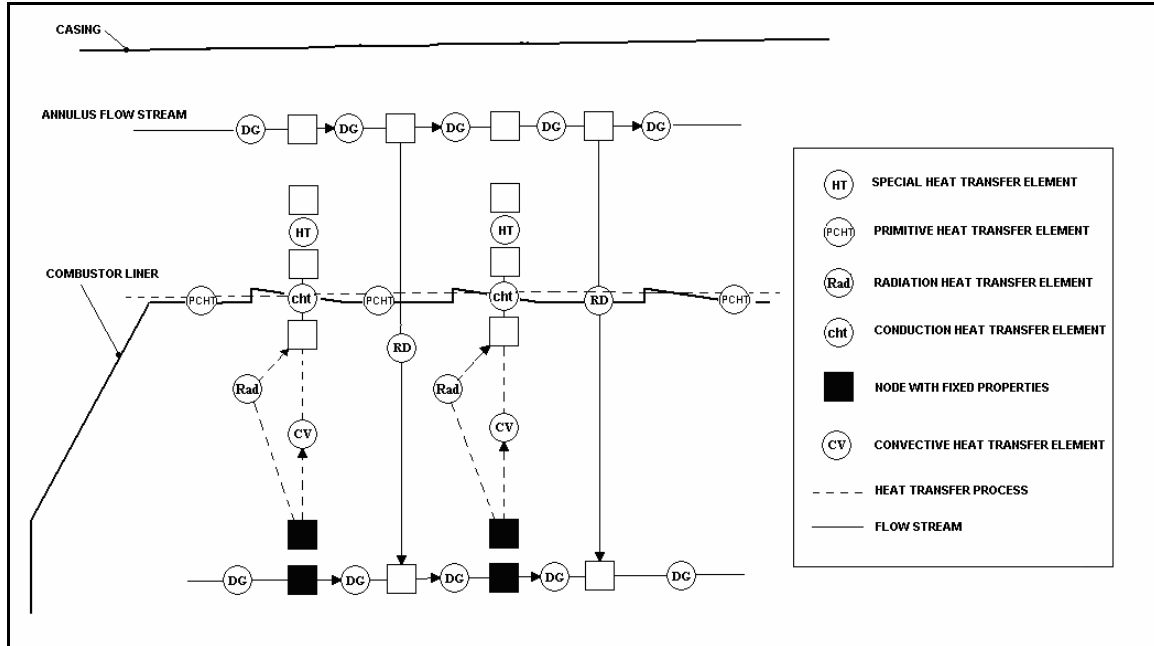
Figure 3.4: Heat transfer process network diagram without a film-cooling device

In figure 3.4, only two heat transfer strings are shown due to the complexity of the model whereas a number of strings are actually used to obtain an adequate resolution. Note in figure 3.4 the heat transfer string, and flow distribution string are not connected due to the use of the (HT) element. An HT element is used in order to apply similar boundary conditions that will compare to its CFD counterpart. The filled nodes denote nodes that have a fixed property assigned to them, in this case, a fixed temperature. Flame temperatures and combustion efficiency were predicted with the use of the empirical correlations presented in the previous chapter.

Modelling of radiation between the combustion gases and the combustor liner, and also between the liner and inner casing was considered. Radiation could not be modelled between the internal flow path and combustion liner due to the limitations of the network model. For this reason, an additional node with fixed temperature, similar to its flow path counterpart, was added to incorporate radiation from the combustion gases to the liner wall (figure 3.4). The radiation element was connected between the additional node and the node connected to the (CHT) element, which describes conduction through the liner

wall. Gas emissivities as well as heat transfer areas were defined within the radiation element.

Modelling the effect of film-cooling air on the combustor liner temperature is generally done with the aid of empirical correlations. These correlations make use of the film-cooling efficiency, as described in the preceding chapter, to predict the temperature increase of the film-cooling air as it flows along the length of the combustor (Lefebvre, 1998; Stuttaford, 1997). However, these correlations are not available in the network model. Therefore, a heat transfer process was utilised from the hot combustion gases to the film-cooling air in a series of heat transfer strings to model the temperature increase of the air as it flows further downstream from the point of injection. It was assumed that the film-cooling air will flow from the point of injection up to the following geometrical feature. Figure 3.5 illustrates the network layout used to define the flow and heat transfer process through a film-cooling device. A cooling device was modelled with RD and DG elements to describe the flow through the cooling orifice and the flow path of the cooling air respectively. For a specific film-cooling heat transfer string, the film-cooling air is heated through convection from the combustion gases – denoted by element 1 in figure 3.5. The heat transfer of the film-cooling air to the combustion liner is thereafter modelled with convection but with a heat transfer area similar to that of the cooling device. This process is depicted by element 2 in figure 3.5. The remaining area with no film-cooling device is heated by convection and radiation from the combustion gases, shown as elements 3 and 4 in figure 3.5.

It was assumed that the influence of the deflector wall on the liner temperature was negligible, due to it being dimensionally very small. In figure 3.5, only a single heat transfer string is shown to describe the heat transfer layout. However, in modelling the film cooling devices, several strings were used to obtain an adequate resolution.
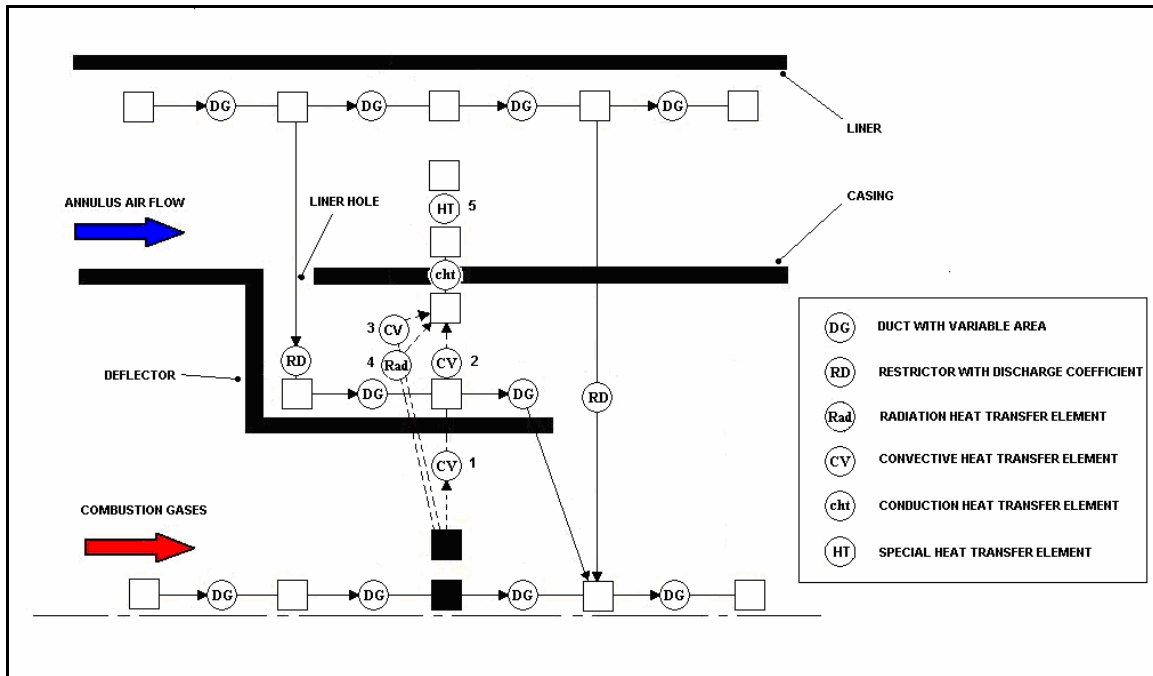
Fig. 3.5: Heat transfer and flow layout for a film-cooling device

Figure 3.6 depicts the dome section of the original combustion chamber (base case), consequently a swirler was not added in this particular model. The initial three heat transfer strings describe the heat transfer to the dome section where no film-cooling devices are present. The remaining heat transfer strings describe the heat transfer process on the dome wall of the combustor when splash-cooling and wiggle strips are present. The wiggle strip on the dome section was modelled with three heat transfer strings whereas the wiggle strips along the remaining combustor wall were modelled with six heat transfer strings individually.
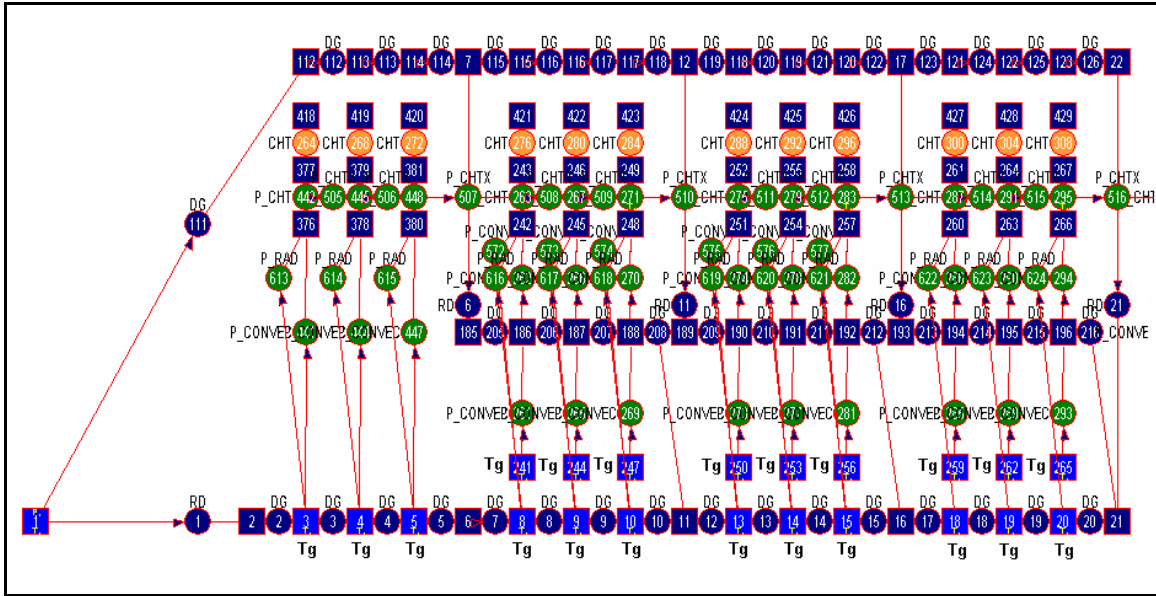
Figure 3.6: Network model of combustor dome section

The green elements in figure 3.6 represent the heat transfer string from the combustion gases to the combustion liner, whereas the dark blue elements represent the flow path along the combustor liner. The nodes, with caption "Tg", depict the fixed gas temperatures calculated using the empirical model.

Figure 3.7 presents the complete network layout of the original combustion chamber (base case). To obtain comparable temperature predictions, four elements were inserted between each hole feature, which in turn resulted in three heat transfer nodes between each feature.

With reference to figure 2.9, the network layout of the T56 combustion chamber is shown in figure 3.8. The final dilution splash-cooling strip, shown in figure 2.9, is however described as dilution splash strips 1 and 2 respectively.

Section 1

Section 3

Section 2
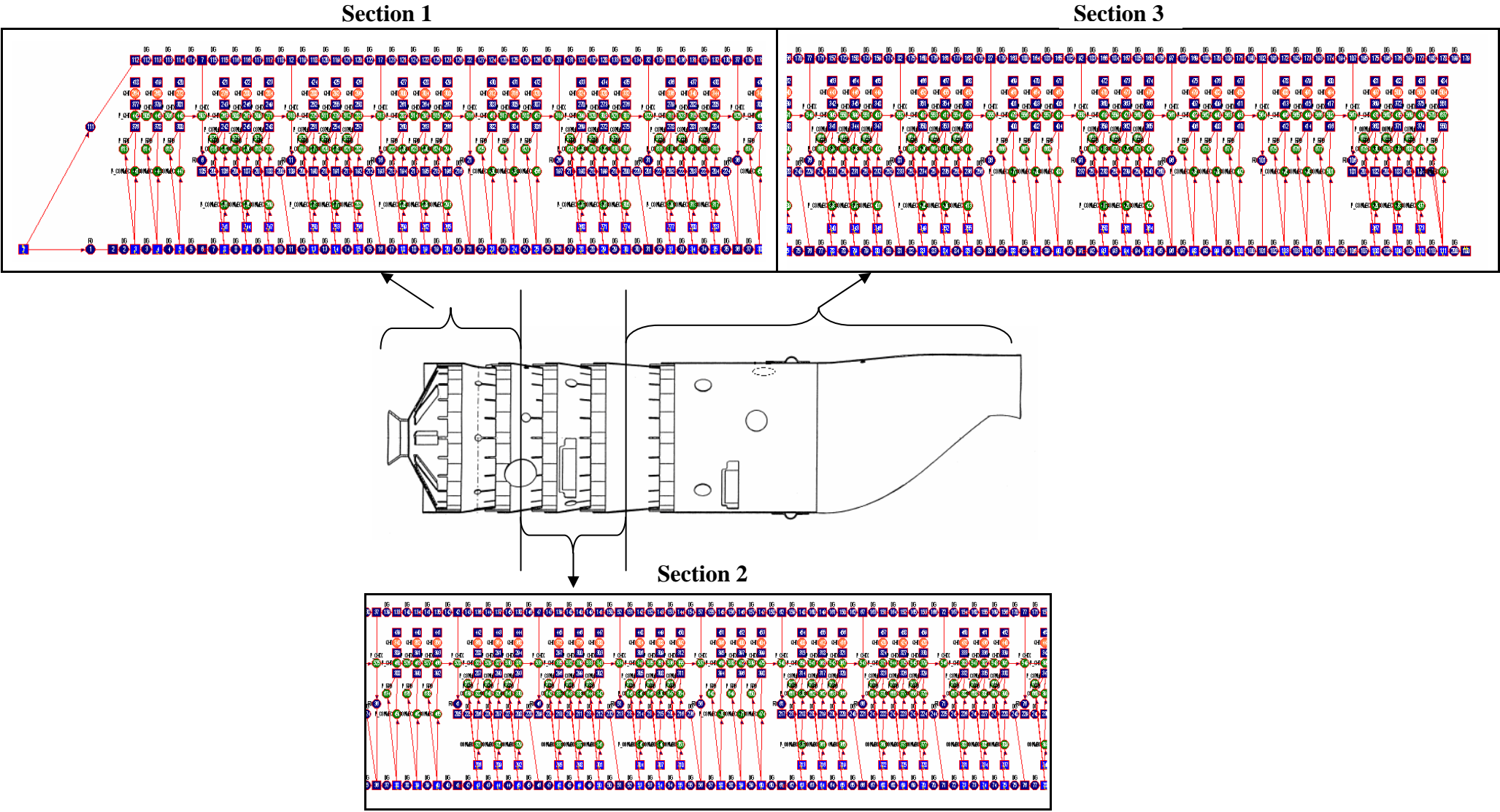
Figure 3.7: Network layout of T56 combustion chamber
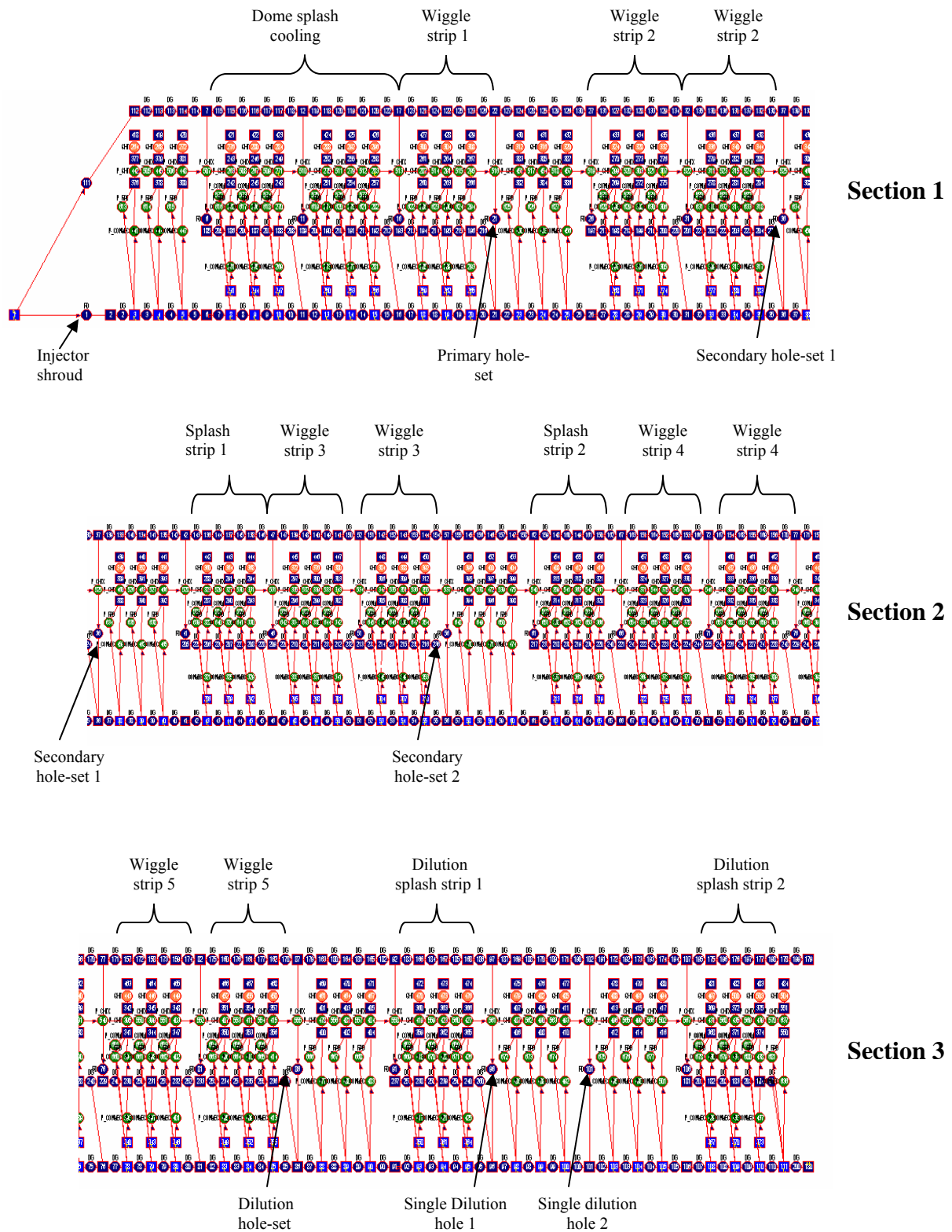
Figure 3.8: Network liner feature description

3.3   Prediction of discharge coefficients and jet angles

An important parameter that influences the mass flow distributions and pressure losses is the discharge coefficient of each of the geometrical features. Correlations presented by Norster (1980) and Adkins and Gueroui (1986) were utilised to predict the discharge coefficients as well as jet angles, through plain and plunged holes, if inadequate experimental data were available. These correlations are presented in the preceding chapter. Jet angles are generally defined as boundary conditions to a numerical model when coupled with a one-dimensional solver. It is, however, difficult to use these correlations in the network model since it is based on a number of parameters that are not available in the network model. An alternative correlation described by Adkins and Gueroui (1986), provides the prediction of the jet angles as a function of the pressure drop across a hole feature. The following formulation can therefore be used, with reference to figure 3.9:
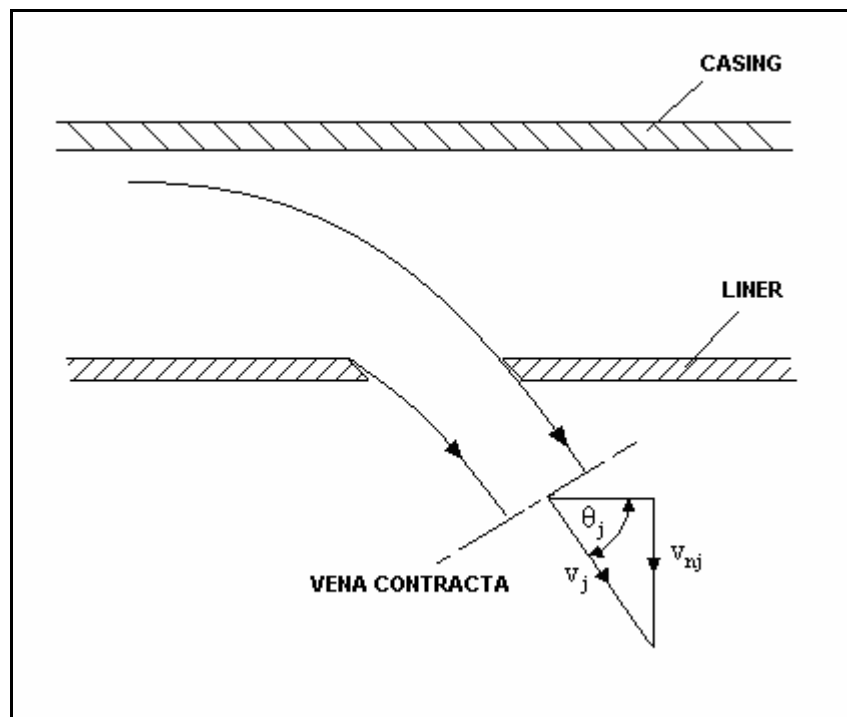
Figure 3.9: Illustration of jet angle

$$\sin\theta_j = v_{nj}/v_j \tag{3.3}$$

where,

v_{nj} =   jet velocity component normal to the liner wall

v_j =   resultant jet velocity

The velocity component normal to the liner can be expressed in terms of the static pressure drop across the hole feature, which in turn can be utilised to predict the jet angle at the vena contracta as shown in equation (3.4).

$$\sin\theta_j = \sqrt{(p_i - p_j)/(P_1 - p_j)} \tag{3.4}$$

3.4   One-dimensional flow and temperature prediction

The data in table 3.1 presents the flow predictions through the various hole features as well as the overall pressure loss that was obtained with the network analysis. The predicted data is compared with the experimental isothermal data, obtained from Van Niekerk and Morris (2001), for a single combustion unit at atmospheric conditions. The data in table 3.1 is described in sequence when moving from the dome, downstream towards the combustor exit, similar to that described in table 2.1.

Table 3.1: Comparison of predicted and experimental flow distributions

		Predicted	Experimental	
	Hole type	**Mass fraction [%]**	**Mass fraction [%]**	**Error %**
1	**Injector shroud**	0.7	--	--
2	**Dome splash strips**	4.63	6.14	24.65
3	**Wiggle strip 1**	12.74	15.63	18.46
4	**Primary hole-set**	3.01	4.82	37.59
5	**Wiggle strip 2**	12.75	10.69	-19.22
6	**Secondary hole-set 1**	2.26	3.51	35.72
7	**Splash strip 1**	0.87	0.19	-359.77
8	**Wiggle strip 3**	12.75	11.07	-15.13
9	**Secondary hole-set 2**	4.69	6.6	28.97
10	**Splash strips 2**	1.75	0.83	-110.55
11	**Wiggle strip 4**	12.75	9.59	-32.9
12	**Wiggle strip 5**	12.75	9.87	-29.15
13	**Dilution hole-set**	9.52	10.8	11.89
14	**Dilution splash strips**	2.62	2.62	-0.11
15	**Single dilution hole 1**	3.84	4.36	11.83
16	**Single dilution hole 2**	2.39	3.27	27.04
	Pressure loss	2.24%		

The prescribed discharge coefficients are the same coefficients as that prescribed in chapter 2. A comparison between the mass flow distributions for the network model (table 3.1) and those obtained in the empirical model (table 2.1) shows a close agreement. The small differences can be attributed to compressibility effects that were accounted for in the network model. Hence, it can be concluded that the flow can be treated as incompressible with reasonable accuracy. However, when comparing the data with the experimental flow distributions some discrepancies are apparent. These discrepancies are mainly due to the difference in predicted and actual discharge coefficients. The discharge coefficients assumed for the cooling devices can significantly influence the predictions, as more than 50 percent of the air supplied is directed through these devices. Furthermore, the discharge coefficients do not only influence the flow predictions but also the overall pressure loss. It is important to maintain the overall pressure loss when considering modifications as this parameter influences the overall engine performance. It is also important to maintain similar equivalence ratios throughout the combustion chamber to ensure that combustion stability is not affected.

Since the importance of predicting accurate discharge coefficients is clear, and the purpose of the present study is to investigate possible modifications to solve practical problems, it was decided to calibrate the network model using the experimental flow distributions. This was done by varying the discharge coefficients in the network solver until the experimental flow distributions for each device were obtained within an error of approximately one percent. Table 3.2 displays the flow distributions and pressure loss predictions that were obtained in this manner.

Table 3.2: Comparison of calibration approach with experimental data

	Hole type	Calibration approach Mass fraction [%]	Experimental Mass fraction [%]	Error %
1	Injector shroud	0.74	--	--
2	Dome splash strips	6.09	6.14	0.81
3	Wiggle strip 1	15.51	15.63	0.79
4	Primary hole-set	4.78	4.82	0.82
5	Wiggle strip 2	10.61	10.69	0.72
6	Secondary hole-set 1	3.48	3.51	0.8
7	Splash strip 1	0.19	0.19	-0.17
8	Wiggle strip 3	10.99	11.07	0.68
9	Secondary hole-set 2	6.55	6.6	0.77
10	Splash strips 2	0.82	0.83	1.53
11	Wiggle strip 4	9.52	9.59	0.77
12	Wiggle strip 5	9.81	9.87	0.63
13	Dilution hole-set	10.73	10.8	0.69
14	Dilution splash strips	2.61	2.62	0.44
15	Single dilution hole 1	4.33	4.36	0.63
16	Single dilution hole 2	3.25	3.27	0.71
	Pressure loss	5.10%		

A comparison between the empirically determined discharge coefficients and that obtained from the calibration method is shown in table 3.3. It is evident that the largest discrepancies between the discharge coefficients occur for the cooling devices. This is due to the assumptions that were made because of the lack of appropriate correlations. The difference in pressure loss is also notable, and it is believed that the larger pressure loss is more representative compared to typical design values. The data obtained from the

network analysis was further utilised as boundary conditions for a refined three-dimensional model of the combustion chamber.

Table 3.3: Comparison of predicted discharge coefficients

Hole type	Assumed Cd	Calibration method Cd
Injector shroud	0.8	0.57
Dome splash strips	0.6	0.532
Wiggle strip 1	0.8	0.655
Primary hole-set	0.583	0.624
Wiggle strip 2	0.8	0.448
Secondary hole-set 1	0.585	0.608
Splash strip 1	0.6	0.087
Wiggle strip 3	0.8	0.464
Secondary hole-set 2	0.586	0.551
Splash strips 2	0.6	0.19
Wiggle strip 4	0.8	0.402
Wiggle strip 5	0.8	0.414
Dilution hole-set	0.588	0.446
Dilution splash strips	0.6	0.4
Single dilution hole 1	0.596	0.452
Single dilution hole 2	0.6	0.549

3.5   1-D temperature predictions

The ability to predict combustor liner temperatures prior to more detailed analysis such as CFD is of great importance to reduce development time and cost. The network approach provides the ability to predict temperature distributions that are comparable to three-dimensional CFD analysis predicting the same basic trend. Even when correlations for film-cooling efficiencies are not available, a network model can model the actual heat transfer between the film-cooling air and combustor liner reasonably well.

Figure 3.10 illustrates the predicted one-dimensional network temperature distribution along the combustor liner. In the dome section of the combustion chamber (distance 0mm ~ 70mm), it is clear that the network model underpredict the wall temperature, since this is the zone with the highest gas temperatures. This is mainly due to the use of the predicted empirical gas temperature. The maximum temperature rise is calculated in each combustion zone through the use of the empirical one-dimensional code and interpolated

between each zone. The temperature for the primary combustion zone will therefore be interpolated between the combustor inlet temperature and the maximum combustion temperature rise in the specific zone. Figure 3.11 depicts the predicted gas temperature.
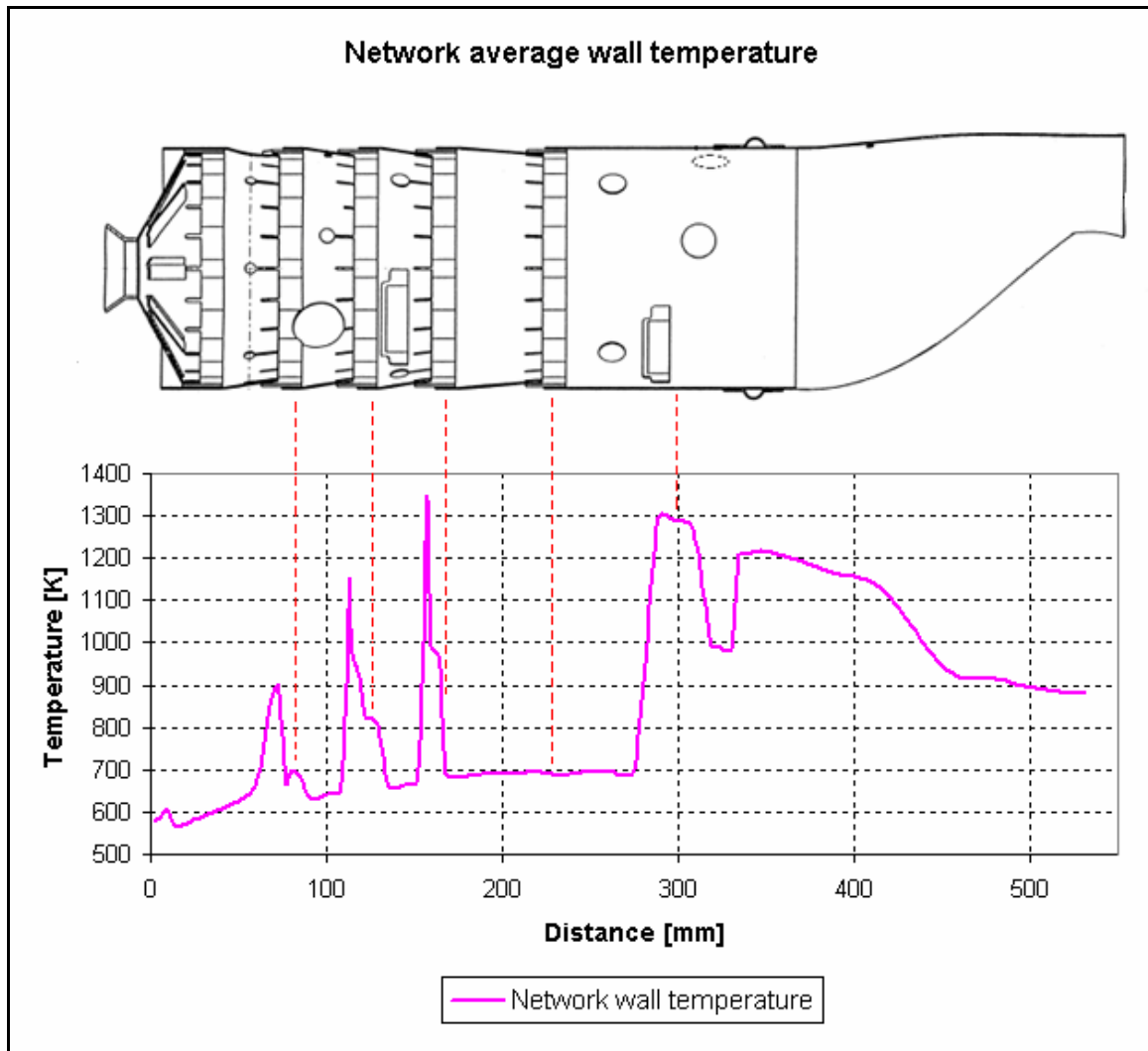
Figure 3.10: Combustor temperature distribution

The gas temperature prediction, presented in figure 3.11, was also used during the temperature predictions in Chapter 2.
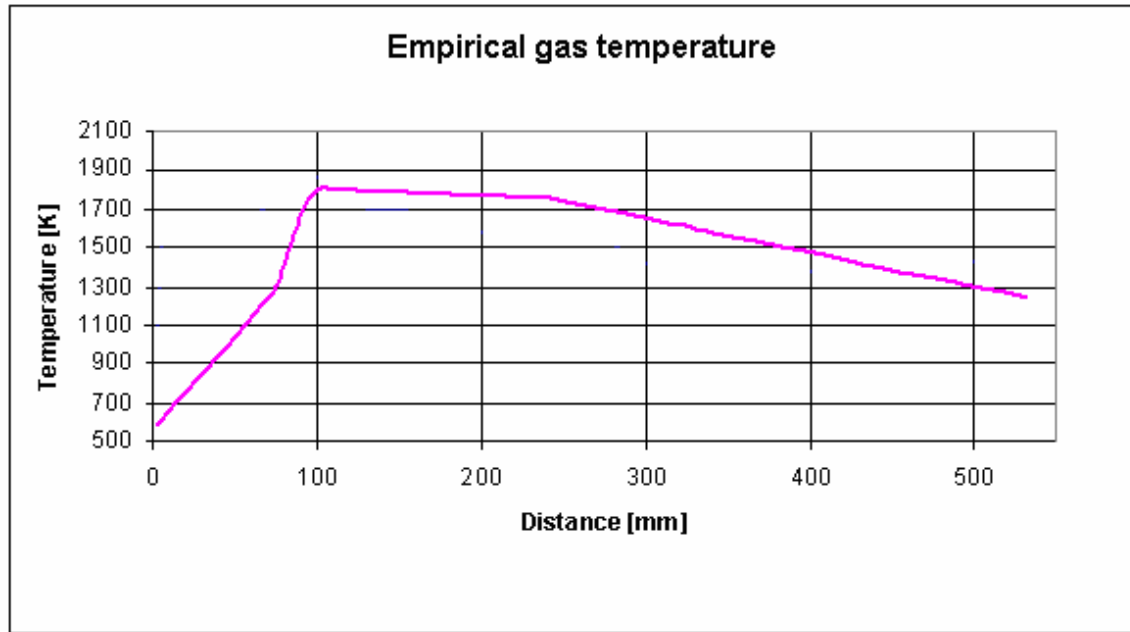
Figure 3.11: Average empirical gas temperature

Comparing the data from figure 2.12 to that of figure 3.10, the trend in temperature distribution along the combustion liner is very similar. The liner temperature predictions in figure 2.11 made use of a film-cooling efficiency to model the effect of film-cooling devices. Conversely, instead of making use of a film-cooling efficiency in figure 3.10, the effect of the cooling device was modelled with a heat transfer process. In this sense, the network approach is more versatile in being able to include any type of cooling device. The network temperature predictions will be compared with CFD predictions in Chapter 5, for validation purposes.

3.6   Empirical swirler design

In addition to the empirical code described in the previous chapter, and the network code described in the present, an empirical swirler code was developed as well. This code is used to design a swirler empirically and to investigate its effect on the dome wall temperatures. For such a design to be conducted, however, an appropriate combustor pressure loss must be obtained. The network solver, along with the empirical code, can consequently be used to obtain an appropriate pressure loss as described in section 3.4.

One of the requirements of a successful swirler design is to deliver the required mass flow rate to the primary zone while at the same time maintaining a strong swirl. The mass flow rate is dependent on the flow area of the swirler, which in turn is dependent on the number of blades and the pressure drop across the device. The inner diameter of the swirler is fixed by the injector diameter, therefore, the only parameter to determine is the swirler outer diameter for specified flow rates and blade angles. Once this has been determined, the corresponding swirl number can be calculated. As previously stated, strong swirl is characterised by a swirl number greater than 0.6.

In the current study, it was decided to investigate five different axial straight vane swirler designs as depicted in figure 3.12. The mass flow distributions and pressure loss obtained from the network results were used and the five cases are presented in table 3.4 The design procedure used can be outlined as:

Step 1:   Define initial parameters such as the injector diameter, solidity at the tip, vane, hub, and outer ring material thickness, percentage pressure drop across the swirler, inlet total temperature and pressure, total mass flow rate per combustor and swirler width. Along with the initial parameters a matrix consisting of percentage mass flow rates through the swirler vs. blade angle can be calculated.

Step 2:   Calculate the flow area of the swirler using equation (2.35)

Step 3:   Determine the swirler blade length with predefined swirler width and blade angle

Step 4:   Guess an initial swirler outer diameter

Step 5:   By defining the solidity at the tip of the swirler, the number of blades can be calculated

Step 6:   Equation (2.36) should be used to calculate the new swirler flow area

Step 7:   Step 5 – 6 is an iterative process adjusting the swirler outer diameter until the swirler flow area calculated in step 2 and step 6 are equal

Sept 8:   The swirl number can now be calculated using equation (2.33)
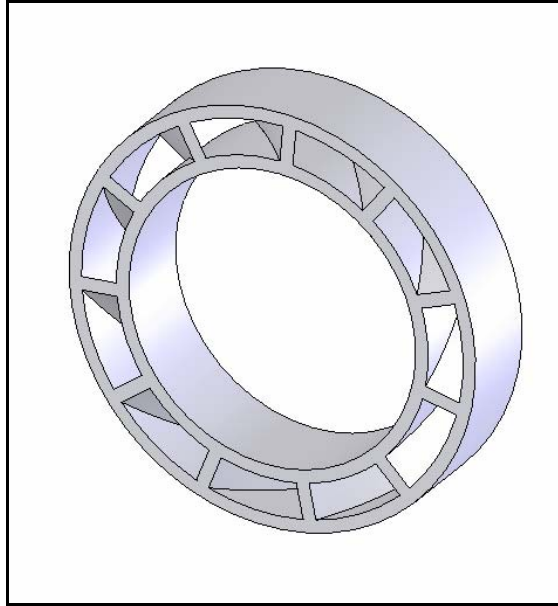
Figure 3.12: Axial straight vane swirler

The computer code written to perform the above procedure as well as the matrix table generated, is presented in Appendix C.

The five cases shown in table 3.4 were subsequently investigated in a three-dimensional numerical model. The influence of the swirler blade angle was investigated in the initial three models while maintaining an airflow rate similar to that of the flow through the splash cooling devices on the original combustion chamber. The subsequent two cases (case 4 and case 5) investigated the effect of increasing the flow rate through the swirler at a fixed blade angle of 40° while maintaining a constant pressure loss of 5.1 percent. More detail regarding the swirler designs are presented in Chapter 5.

Table 3.4: Swirler design cases

	Case 1	Case 2	Case 3	Case 4	Case 5
Pressure loss [%]	5.1	5.1	5.1	5.1	5.1
Flow split [%]	6.097	6.097	6.097	13.85	13.85
Swirler tip diameter [mm]	40.47	40.92	41.85	47.02	47.02
Blade angle [degrees]	33	40	50	40	40
Number of blades	11	10	8	11	11
Swirl number	0.61	0.78	1.1	0.74	0.74

3.7   Summary

The data from the one-dimensional incompressible empirical code, discussed in the previous chapter, was successfully used as inputs to a network solver to predict flow distribution data, pressure losses, and temperature distributions. The distinct advantage of this approach is its rapid execution time while providing good approximations. The results showed that discharge coefficients influenced the one-dimensional flow and pressure drop predictions significantly. Obtaining correlations for the prediction of discharge coefficients for any hole type is, however, a difficult task. The ability of the network solver to predict the general temperature distribution along the combustor liner is also shown, and will be compared with CFD data in the subsequent chapters.

CHAPTER 4 –

NUMERICAL MODEL

4.1   Preamble

Due to the development of computer resources over the past few years, computational fluid dynamics has become one of the primary tools to investigate the complex flow field phenomena inside a gas turbine combustion chamber. These analyses are needed to predict the influence of certain flow parameters on the exit temperature distribution and wall temperatures. This chapter describes the numerical models and boundary conditions that were utilised during the study.

4.2   Turbulence models

The equations governing the flow in a gas turbine combustion chamber are the transport equations for mass, momentum, and energy. The main discussion in this section will be turbulence and therefore only the former two transport equations will be described. Turbulence can be described in short as unsteady flow with velocities and flow properties varying in a random and chaotic way, with various length scales. The transport equation for mass, assuming steady-state conditions, can be written as follows:

$$\frac{\partial \overline{\rho}\,\overline{u}_j}{\partial x_j} = 0 \tag{4.1}$$

The transport equations for momentum can be represented as:

$$\frac{\partial}{\partial t}\left(\rho u_i\right) + \frac{\partial}{\partial x_j}\left(\rho u_i u_j\right) = -\frac{\partial p}{\partial x_i} + \frac{\partial}{\partial x_j}\left(\mu\left(\frac{\partial u_j}{\partial x_i} + \frac{\partial u_i}{\partial x_j}\right)\right) + \rho g_i + F_i \qquad (4.2)$$

The transport equation for momentum is also known as the Navier-Stokes equations. The final term (F_i) is a source term defining the effect of body forces.

The above equations can be applied to laminar as well as turbulent flows. To solve turbulence directly from the above equations will however be a difficult task. To solve all length scales directly from the time-dependent Navier-Stokes equations are beyond current-day computer capabilities and is therefore dependent on future computer hardware development.

In the meantime, adequate information about the turbulence process can be supplied when utilising the time-averaged properties of the flow.

As an example, figure 4.1 depicts typical measured velocities in turbulent flow. To obtain mean properties of the flow, the velocity, u(t), can be decomposed into a mean value $\overline{u}$, and the fluctuating component u'(t).
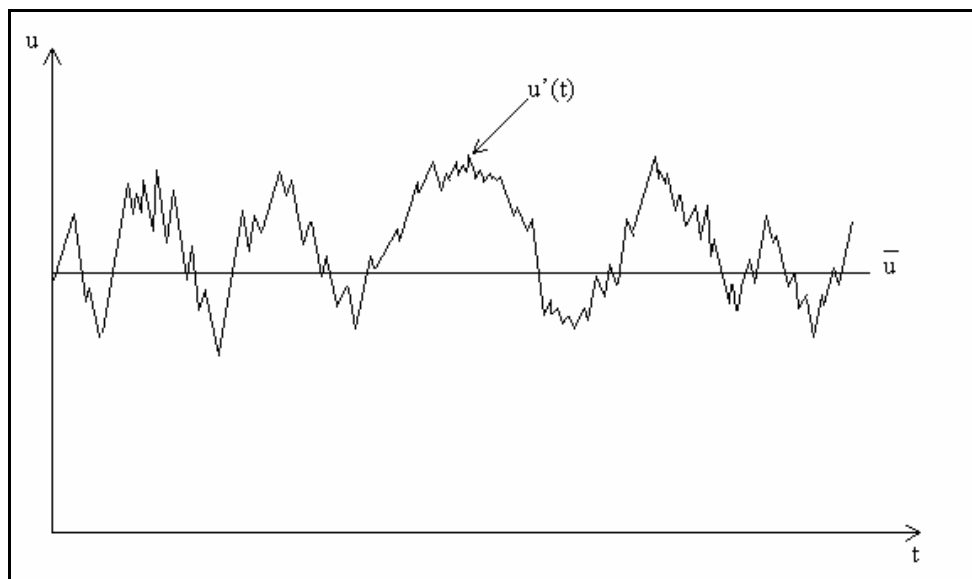
Figure 4.1: Typical point velocity measurement in turbulent flow

$$u = \overline{u} + u(t)^{'} \tag{4.3}$$

Replacing u_i in equation (4.2) with equation (4.3) yields the following expression known as the Reynolds average navier-stokes equations (RANS).

$$\frac{\partial}{\partial t}\left(\rho\, \overline{u}_i\right) + \frac{\partial}{\partial x_j}\left(\rho\, \overline{u}_j\, \overline{u}_i + \rho\, \overline{u_j^{'} u_i^{'}}\right) = -\frac{\partial \rho}{\partial x_i} + \frac{\partial}{\partial x_j}\left(\mu\left(\frac{\partial \overline{u}_j}{\partial x_i} + \frac{\partial \overline{u}_i}{\partial x_j}\right)\right) + \rho g_i + \overline{F}_i \tag{4.4}$$

Comparing equation (4.2) and equation (4.4), it is clear that an additional term has been added to the navier-stokes equation which introduces additional turbulence stresses termed the Reynolds stresses. This term can be described as follows when the Boussinesq hypothesis of μ_t is assumed:

$$-\rho\, \overline{u_i^{'} u_j^{'}} = \mu_t\left(\frac{\partial \overline{u}_i}{\partial x_j} + \frac{\partial \overline{u}_j}{\partial x_i}\right) - \frac{2}{3}\rho \delta_{ij} k \tag{4.5}$$

where the turbulent viscosity, μ_t, is defined using the turbulent kinetic energy, k, and its dissipation rate, ε, as follows:

$$\mu_t = C_\mu \rho \frac{k^2}{\varepsilon} \tag{4.6}$$

In order to obtain adequate information about the turbulence process but without the need to predict every eddy in the flow, the RANS equations represent transport equations for the mean flow quantities only, with all the scales of the turbulence being modelled. The approach of permitting a solution for only the mean flow variables greatly reduces the computational effort. The turbulence models which are derived from RANS equations include the standard k-ε model, RNG k-ε model, realizable k-ε model, standard k-ω model, shear-stress transport (SST) k-ω model, and the Reynolds stress model (RSM).

One of the basic turbulence models is the standard k-ε model. This k-ε model is one of the most widely used and validated models and presents excellent performance for many industrial relevant flows. As the name states, it is a two-equation model, one for k and

one for ε which define the velocity and length scales respectively and are valid for fully turbulent flows. The model, however, performs poorly in certain cases such as unconfined flows, flows with large extra strains such as swirling flow, rotating flows, and in fully developed flows in non-circular ducts (Biswas *et al.*, 1997; Versteeg and Malalasekera, 1995). McGuirk and Palma (1993) showed that although the standard k-ε model did have some difficulty to predict the vortices created by the primary jets, acceptable results in other regions of the combustor and the correct prediction of the main features of the combustor flow were possible. Due to the poor performance of the model in some cases, improvements were made to the standard k-ε model to enhance its ability to predict swirling flow in some cases. The renormalisation group (RNG) k-ε model and realizable k-ε model are two variants of the standard k-ε model. The RNG k-ε model has more accuracy with low Reynolds number flows compared to the standard k-ε model and also has enhanced accuracy for swirling flows. A relatively recent development is the realizable k-ε model which differs from the standard k-ε model in two ways:

- The model contains a new formulation for the turbulent viscosity
- A new transport equation for the dissipation rate, ε, has been derived

An advantage of the realizable k-ε model is to provide improved performance of flows involving rotation, boundary layers under strong adverse pressure gradients, separation, and recirculation (Shih *et al.*, 1995).

It should be noted that the above-mentioned models assume μ_t to be isotropic which may lead to inaccurate flow predictions. The transport equations for k and ε respectively are given by:

$$\frac{\partial}{\partial t}(\rho k) + \frac{\partial}{\partial x_i}\left(\rho \overline{u}_i\, k\right) = \frac{\partial}{\partial x_i}\left[\left(\mu + \frac{\mu_t}{\sigma_k}\right)\frac{\partial k}{\partial x_i}\right] + G_k - \rho\varepsilon \qquad (4.7)$$

$$\frac{\partial}{\partial t}(\rho\varepsilon) + \frac{\partial}{\partial x_i}\left(\rho \overline{u}_i\, \varepsilon\right) = \frac{\partial}{\partial x_i}\left[\left(\mu + \frac{\mu_t}{\sigma_\varepsilon}\right)\frac{\partial\varepsilon}{\partial x_i}\right] + C_{1\varepsilon}\frac{\varepsilon}{k}G_k - C_{2\varepsilon}\rho\frac{\varepsilon^2}{k} \qquad (4.8)$$

where G_k is the generation of k:

$$G_k = -\rho \, \overline{u_i' u_j'} \, \frac{\partial u_j}{\partial x_i} \qquad (4.9)$$

The equations contain five constants; $C_\mu, \sigma_k, \sigma_\varepsilon, C_{1\varepsilon}, C_{2\varepsilon}$. The values of these constants were determined by comprehensive data fitting for a wide range of turbulent flows and recommended values are as follows:

$$C_\mu = 0.09, \ \sigma_k = 1, \ \sigma_\varepsilon = 1.3, \ C_{1\varepsilon} = 1.44, \ C_{2\varepsilon} = 1.92 \qquad (4.10)$$

4.3   Combustion model

In addition to turbulence modelling, numerical models to predict the combustion process should also be considered. Combustion is a process in which fuel reacts with an oxidant to form products of combustion. The products are not usually formed within a single chemical reaction but within a series of elementary reactions. When accounting for combustion through a numerical model, the transport equations must be solved for each species in addition to the flow equations. The flow field is in turn affected by changes in temperature and density due to the species. This results in a large number of partial differential equations (PDEs) to be solved if numerous chemical reactions are to be considered. Models that consider so many reactions require a huge amount of computer resources, so simple models that incorporate only a few reactions are often preferred in numerical combustion procedures used in CFD. The simplest procedure is the simple chemical reaction system (SCRS). Other modelling approaches to solve turbulent combustion include the Eddy break-up and laminar flamelet models (Versteeg and Malalasekera, 1995).

When the SCRS approach is used with the assumption of a one-step, infinitely fast chemical reaction, a mixture fraction method can be used to determine species concentrations. A non-dimensional variable f, called the mixture fraction, can be defined. If the local value of f is 0, the mixture at a point contains only oxidant and if f

equals 1 it contains only fuel. Fluctuating temperatures in the SCRS approach are often accounted for by incorporating a probability density function (PDF) to calculate mean properties. In the PDF method, the average value of scalar variables are obtained by weighting the instantaneous value with a probability density function for mixture fraction f. The two probability functions that give rise to the best results are the Gaussian and β- functions (Baron *et al.*, 1994; Versteeg and Malalasekera, 1995; Smiljanovski *et al.*, 1999; Hoerzer *et al.*, 2002).

A second combustion model is the Eddy break-up model where the rate of consumption of fuel is specified as a function of local flow properties. The mixing-controlled rate of reactions is expressed in terms of the turbulence time scale $\dfrac{k}{\varepsilon}$, where k is the turbulent kinetric energy and ε is the rate of dissipation of k. The model considers the dissipation rates of fuel, oxygen and products, and takes the slowest rate as the reaction rate of fuel. The Eddy break-up model results in rather good predictions and is simple to implement but is dependent on the turbulence model used. The combustion model will therefore be limited if the turbulence model fails to make accurate flow predictions (Versteeg and Malalasekera, 1995).

Another combustion modelling approach is the laminar flamelet model. The model allows the addition of experimental information to describe the relationship between the mixture fraction, mass fraction and temperature. The data is acquired from measurements in a laminar diffusion flame. A transport equation for the mixture fraction is solved and the species mass fraction is deduced from laminar flamelet relationships (Versteeg and Malalasekera, 1995).

The SCRS combustion model that was utilised during the current study shares the basic assumption, similar to other turbulent combustion models, that the instantaneous scalar values such as species concentration, temperature, and density are related to a conserved scalar such as the mixture fraction. The average scalar values are often obtained by integrating the product of the scalar profile and the probability density function (PDF)

over a mixture fraction space combined with an equilibrium non-adiabatic chemistry model. A β-function was assumed for the PDF.

The mixture fraction (f) of an element can be obtained as follows:

$$f = \frac{Z_i - Z_{i,o}}{Z_{i,f} - Z_{i,o}}$$

(4.11)

where Z_i denotes the elemental mass fraction of element i. The subscripts "o" and "f" denote the oxidiser and fuel stream inlets respectively. With the assumption of chemical equilibrium all thermo-chemical scalars, such as temperature, density, and species fraction, are related to the mixture fraction.

The probability density function P(f), describes the temporal fluctuation of f in turbulent flow. Mean scalar values, depending on f , can then be calculated as follows (Yun *et al.*, 2005).

$$\overline{\phi} = \int_{0}^{1} P(f)\phi_i(f)\mathrm{d}f$$

(4.12)

where $\overline{\phi}$ is the average scalar variable.

Since the shape of the PDF is unknown, it can be modelled as a mathematical function by assuming its shape. The shape of the function depends exclusively on the mean mixture fraction $\overline{f}$ and its variance $\overline{f'^2}$.

The β-function describing the shape of the PDF is given as follows (Yun *et al.*, 2005):

$$P(f) = \frac{f^{\alpha-1}(1-f)^{\beta-1}}{\int_0^1 f^{\alpha-1}(1-f)^{\beta-1}\,df} \tag{4.13}$$

where

$$\alpha = \bar{f}\left[\frac{\bar{f}\left(1-\bar{f}\right)}{\overline{f'^2}} - 1\right] \tag{4.14}$$

and

$$\beta = \left(1-\bar{f}\right)\left[\frac{\bar{f}\left(1-\bar{f}\right)}{\overline{f'^2}} - 1\right] \tag{4.15}$$

The assumed PDF, P(f), can therefore be computed as a function of $\bar{f}$ and $\overline{f'^2}$ and used as a weighting function to determine mean values of density, temperature, and species mass fraction.

A simple one-step non-premixed reaction scheme was utilised during the study, assuming an infinitely fast reaction. Five basic species were considered in calculating the PDF look-up tables on the properties of the mixture as a function of density, temperature, and mass fraction of the species. The five species were; Jet A(g), O_2, N_2, CO_2, H_2O. The one-step reaction scheme is presented as:

$$C_xH_y + \left(x+\frac{y}{4}\right)(O_2 + nN_2) \rightarrow xCO_2 + \frac{y}{2}H_2O + n\left(x+\frac{y}{2}\right)N_2 \tag{4.16}$$
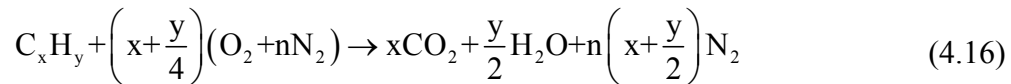
4.4   Fuel spray model

The fuel distribution used in the numerical model corresponds to the experimental measurements obtained by Van Niekerk and Morris (2001). The fuel spray was modelled as a discrete second phase and the droplets were tracked in a Lagrangian framework. The interaction of the fuel spray with the gaseous mixture, i.e. the exchange of mass, momentum and energy between the phases, was taken into account through the particle-source-in-cell method. The spray cone was modelled as six discrete cones covering the total included angle of 110º of the real spray. The spray angle of 110º corresponds with the dual-stage pressure atomisers operating at maximum flow pressure. Equal amounts of fuel are injected through each of the cones and circumferentially the spray was discretised into 36 injection points for each cone. The fuel spray data is presented in tables 4.1 and 4.2 respectively. The fuel that was used during the study was kerosene ($C_{12}H_{24}$).

The experimentally determined drop size data that was presented was adapted for the air/fuel ratio considered. Table 4.1 shows the 12 discretised sizes used in the CFD model.

Table 4.1: Discretised fuel spray data

Size #	Mean droplet size in group [micron]	Volume fraction	Massflow [kg/s]	Droplet size [mm]
1	6.87	0.00226	1.78604E-05	0.00687
2	9.31	0.0058	4.58365E-05	0.00931
3	13.4	0.01669	0.000131899	0.0134
4	18.95	0.03867	0.000305603	0.01895
5	25.7	0.06937	0.000548221	0.0257
6	34.84	0.1066	0.000842444	0.03484
7	47.25	0.14285	0.001128922	0.04725
8	68	0.17171	0.001356998	0.068
9	96.16	0.17766	0.00140402	0.09616
10	130.4	0.14406	0.001138484	0.1304
11	176.8	0.08984	0.000709992	0.1768
12	239.7	0.03448	0.00027249	0.2397

Each cone consisted of equal amounts of fuel. Table 4.2 presents the boundary conditions for each cone angle when the fuel spray was modelled.

Table 4.2: Fuel cone angles

Cone #	Inlet velocity magnitude, [m/s]	Half angle [degrees]	Fuel flow rate [kg/s]	Drop size range [micron]
1	30	5	0.00790277	6.87 - 239.70
2	30	15	0.00790277	6.87 - 239.71
3	30	25	0.00790277	6.87 - 239.72
4	30	35	0.00790277	6.87 - 239.73
5	30	45	0.00790277	6.87 - 239.74
6	30	55	0.00790277	6.87 - 239.75

4.5   Grid generation

Generally, it is found that approximately two-thirds of the calendar time spent on a CFD prediction is undertaken on preparing the geometry and obtaining an acceptable grid (Sivaramakrishna *et al.*, 2001).

For the present combustion chamber and the models being investigated, a single mesh consisted of approximately 100,000 hexahedral and 900,000 tetrahedral cells respectively. Several grid sizes, ranging between 500,000 and 1,500,000 computational cells were solved to verify solution independency on the mesh size. A typical mesh, depicted upstream of the dome section in figures 4.2 and 4.3, therefore contained approximately 1,000,000 cells. An unstructured hybrid mesh was used with primarily hexahedral cells within the core section and film-cooling devices whereas tetrahedral cells were used close to the walls. The splash-cooling devices on the dome are modelled as faces adjacent to the wall with a slot height of approximately 2 mm. The swirler inlets were modelled as faces where unit directional vectors were defined. The normal component (V_n) at the swirler inlet surface is computed by the relation:

$$V_n = \cos\theta_v \qquad\qquad (4.17)$$

whereas, the tangential (swirling) component V_t, at the swirl plane is computed by the relation:

$$V_t = \sin\theta_v \qquad\qquad (4.18)$$
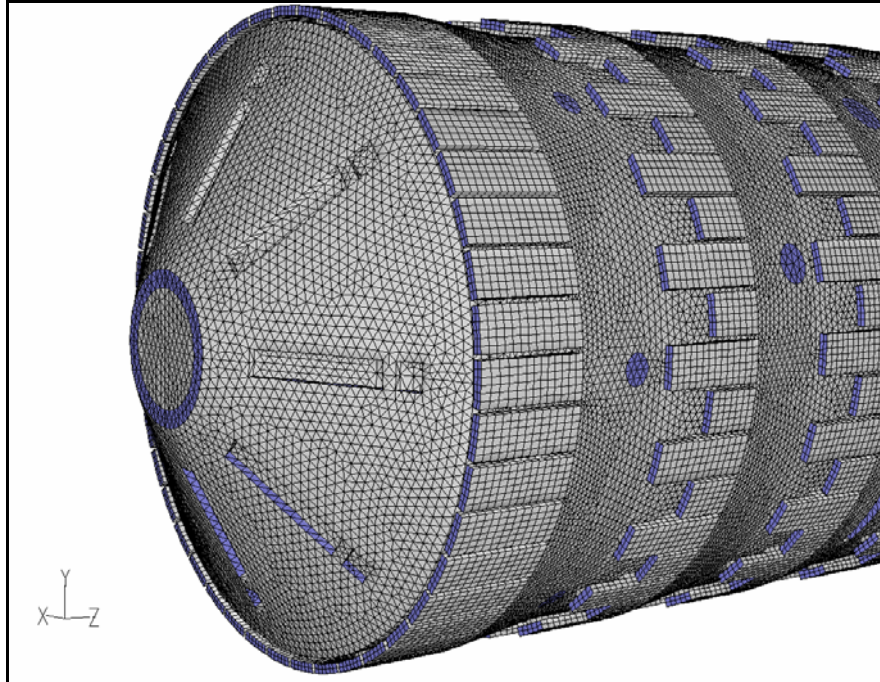
Figure 4.2: Grid on outer wall of T56 combustor
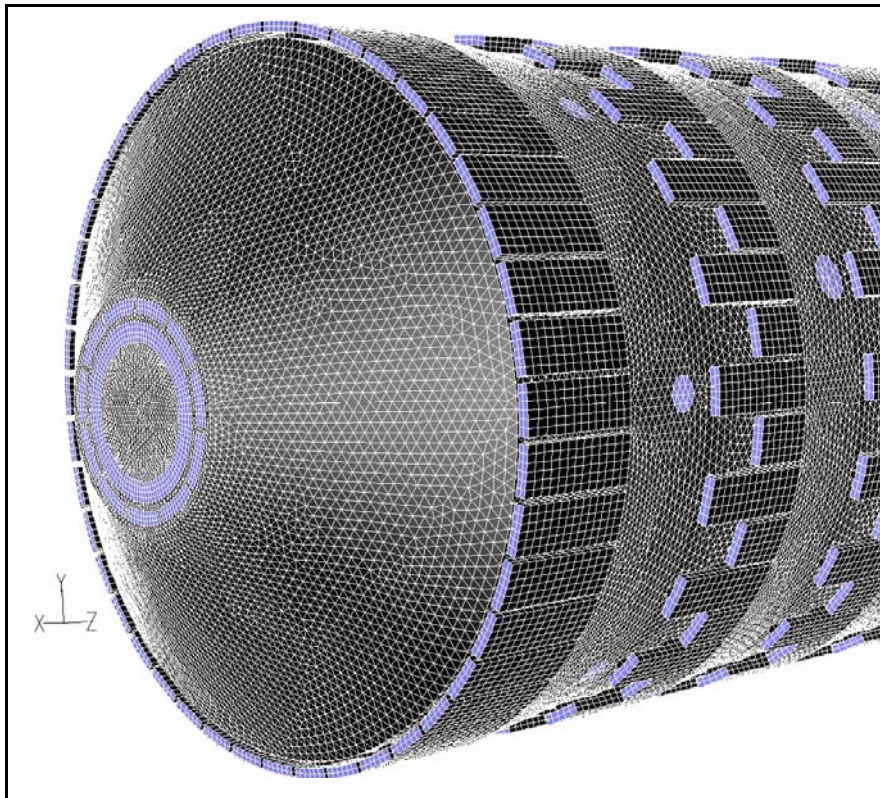
Figure 4.3: Grid on dome with modification of swirler

4.6 Boundary conditions

The boundary conditions utilised within the CFD models were obtained from the one-dimensional models discussed in the previous chapters. The boundary conditions primarily constitute the air and fuel inlets. The air inlet boundaries were prescribed with a uniform mass flow rate along with an inlet temperature, presented in table 1.1. The mass flow rates were obtained from the network results presented in table 3.2 and jet angles calculated using equation 3.3. Table 4.3 provides a summary for the base case input parameters at the various inlets. On the outlet plane, a pressure boundary condition was used. On the outside of the liner wall, a constant heat transfer coefficient of 288 $\frac{W}{m^2 K}$ was prescribed, calculated from the average Reynolds number within the annulus.

The effect of radiation was investigated by using the P-1 radiation model, which is a non-equilibrium diffusion type model, and the variation of the mixture absorption coefficient was taken into account using the weighted-sum-of-gray-gases model. However, radiation was not modelled on all models since it is computationally expensive. The grid independence study and radiation effects on the liner wall temperature are described in Appendix B.1 and Appendix B.2 respectively.

The data in table 4.3 is described in sequence when moving from the dome, downstream towards the combustor exit for the base case. The data presents the mass flow splits through the various hole features as well as the directional vectors that was defined for the plain holes. The hole layout of the combustion chamber is depicted in figure 4.4.
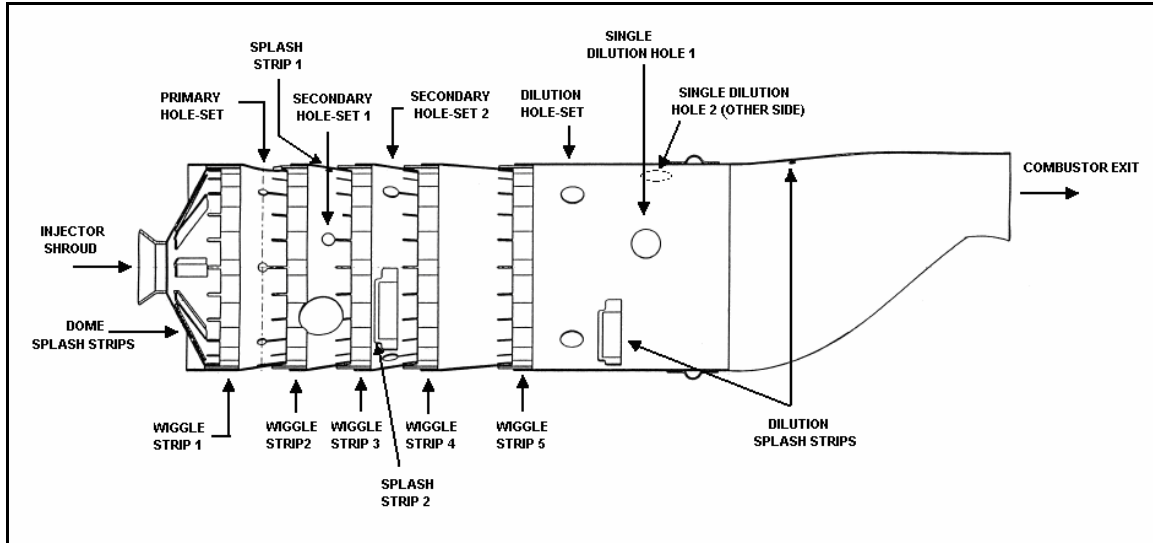
Figure 4.4: Description of combustor hole layout

Table 4.3: Base case boundary conditions

Fluent Inlet designation	Flow splits [%]	Flow splits [kg/s] 2.37642	Splits to individual holes [kg/s]	Directional vector components x	y	z	Hydraulic diameter [mm]
Injector	**0.7448178**	0.0177	0.0177	normal to inlet boundary			7.4
shell swirl 1			0.08551	normal to inlet boundary			2.4
shell swirl 2			0.05938	normal to inlet boundary			3.72
shell swirl 1+2	**6.0969862**	0.14489					
wigg 1 bottom			0.18428	normal to inlet boundary			3.27
wigg 1 top			0.18428	normal to inlet boundary			3.27
wigg 1 total	**15.509043**	0.36856					
shell2 hole 1			0.016245714	0.63474	-0.73253	0.245984	
shell2 hole 2			0.016245714	0.969274	0	0.245984	
shell2 hole 3			0.016245714	0.63474	0.732528	0.245984	
shell2 hole 4			0.016245714	0.137943	0.959408	0.245984	
shell2 hole 5			0.016245714	-0.63474	0.732528	0.245984	
shell2 hole 6			0.016245714	-0.96927	0	0.245984	
shell2 hole 7			0.016245714	-0.63474	-0.73253	0.245984	
shell 2 hole total	**4.7853494**	0.11372					6.828
wigg 2 bottom			0.12605	normal to inlet boundary			3.27
wigg 2 top			0.12604	normal to inlet boundary			3.27
wigg 2 total	**10.607973**	0.25209					
shell3 splash	**0.1880981**	0.00447	0.00447	normal to inlet boundary			3.63
shell 3 hole 1			0.027606667	0.93863	-0.27561	0.2074	
shell 3 hole 2			0.027606667	-0.13922	0.968299	0.2074	
shell 3 hole 3			0.027606667	-0.93863	-0.27561	0.2074	
shell 3 hole total	**3.4850742**	0.08282					9.02
wigg 3 bottom			0.13055	normal to inlet boundary			3.27
wigg 3 top			0.13055	normal to inlet boundary			3.27
wigg 3 total	**10.987115**	0.2611					
shell4 hole 1			0.0389175	0.647886	-0.7477	0.145567	
shell4 hole 2			0.0389175	0.410991	0.899943	0.145567	
shell4 hole 3			0.0389175	-0.41099	0.899943	0.145567	
shell4 hole 4			0.0389175	-0.64789	-0.7477	0.145567	
shell 4 hole total	**6.5506097**	0.15567					11.254
shell 4 splash 1			0.00977	normal to inlet boundary			3.63
shell 4 splash 2			0.00977	normal to inlet boundary			3.63
shell 4 splash total	**0.8222452**	0.01954					
wigg 4 bottom			0.1131	normal to inlet boundary			3.27

wigg 4 top			0.11311	normal to inlet boundary			3.27
wigg 4 total	**9.5189403**	**0.22621**					
wigg 5 bottom			0.11649	normal to inlet boundary			3.27
wigg 5 top			0.11649	normal to inlet boundary			3.27
wigg 5 total	**9.8038226**	**0.23298**					
dilute hole 1			0.063725	0.70639	-0.70639	0.045014	
dilute hole 2			0.063725	0.70639	0.70639	0.045014	
dilute hole 3			0.063725	-0.70639	0.70639	0.045014	
dilute hole 4			0.063725	-0.70639	-0.70639	0.045014	
dilute hole total	**10.726218**	**0.2549**					16
dilute hole 5	4.3321467	0.10295	0.10295	0.972876	-0.2307	0.017103	20.2
dilute hole 6	3.2435344	0.07708	0.07708	-0.46946	-0.88293	0.007156	15.86
dilute splash	**1.7315963**	**0.04115**	0.04115	normal to inlet boundary			3.63
trans splash	**0.8664293**	**0.02059**	0.02059	normal to inlet boundary			3.63
	100	2.37642	2.37642				

A number of models were generated during the study. The initial two models are of the original combustion chamber and one where a single set of splash-cooling devices are blocked on the dome. Another five models were generated to conduct a parametric study of the swirler and to investigate its influence on dome temperatures and exit temperature distributions. The boundary conditions for all the models are presented in Appendix E.

4.7   Summary

The accuracy of CFD models depends mainly on the boundary conditions specified as well as a sufficiently refined grid in areas of high gradients. To maintain adequate processing time, the grid size was kept to a realistic size while obtaining good resolution. A model size of 1,000,000 cells was therefore utilised throughout the study. Present-day computer power is, however, on the increase which may results in more available computer resources meaning that finer grids may be utilised in future studies.

CHAPTER 5 –

NUMERICAL STUDY

5.1   Preamble

The literature survey has shown that CFD can be used to conduct analyses in combustion chambers successfully. These analyses are, however, dependent on the physical models used, as well as the grid size and grid quality which were described in the previous chapter.

Numerically, five test cases with different swirler designs were investigated. Two additional cases are investigated showing the original combustion chamber with and without blocked splash-cooling devices, serving as the base cases. From the results, an evaluation was made on the dome wall temperatures as well as the exit temperature profile. The different test cases are discussed and possible reasons for insufficient dome cooling are also provided. A direct comparison is also made between the experimental and numerical exit temperature distributions.

5.2   Experimental data

Measured exit temperatures and isothermal flow distributions were obtained from Skidmore (2004) and Van Niekerk and Morris (2001). Skidmore (2004) obtained experimental exit temperature distributions at an overall air/fuel ratio of 49.75. Five readings were taken in the radial direction and measured every 3.15° along the 60° exit plane of a single T56 combustion chamber. The flow distribution data, from Van Niekerk and Morris (2001), were obtained at atmospheric conditions. For the purpose of the study,

it was assumed that the flow distributions at atmospheric inlet conditions and operating inlet conditions were similar.

It was assumed that the measured temperature was the static temperature, since it was not clear whether or not total or static temperature was measured. When the expression for the total exit temperature is used (Eq. 5.1), it can be calculated that the dynamic term only imposes a difference of approximately 4 K when an average exit velocity of 90 m/s is used.

$$T_0 = T_s + \frac{V^2}{2C_p} \qquad\qquad (5.1)$$

5.3   Numerical test cases

Initially, the original combustion chamber was modelled to provide a base model against which the other models can be compared. In addition, a numerical model was generated describing the original combustor showing the effect of a blocked splash- cooling device on the dome temperature as well as on the exit temperature profile.

For all the numerical test cases, the pressure drop across the combustion chamber was maintained similar to the original combustion chamber so as not to compromise overall engine performance. All the test cases investigated the influence of replacing the existing splash-cooling devices with an axial swirler to evaluate its influence on the dome wall temperatures and exit temperature profile. The initial three cases all had exactly the same mass flow distributions as the original combustion chamber. The swirlers utilised for these test cases had a mass flow distribution of 6.1 percent which is equivalent to the total splash-cooling device flow distribution. However, the difference between the initial three test cases was the number of blades and the blade angle used for each swirler, which in turn influenced the swirl number and increased the swirler diameter. The inner (hub) diameter of each swirler was fixed at 32.4 mm due to the fuel injector size.

The remaining two cases investigated an increase in swirler mass flow rate from 6.1 percent to 13.85 percent while maintaining a constant pressure loss of 5.1 percent, which

was determined from the network analysis in the previous chapter. To maintain a constant pressure loss, 50 percent of the film-cooling air through the first wiggle strip device for case 4 and the final dilution hole for case 5 was blocked in the numerical model. It should, however, be noted that the increased mass flow rate in the primary zone will influence the equivalence ratio, which in turn may influence the combustion stability and performance. Table 3.4 presented the swirler parameters for the five numerical test cases.

5.4   Numerical analysis of base case

Figure 5.1 depicts the original combustion chamber, at the operating conditions specified in table 1.1, with dome wall temperature and exit temperature distribution. The numerical exit temperature distribution was validated against that obtained experimentally by Skidmore (2004) and is within an error of less than 10 percent.
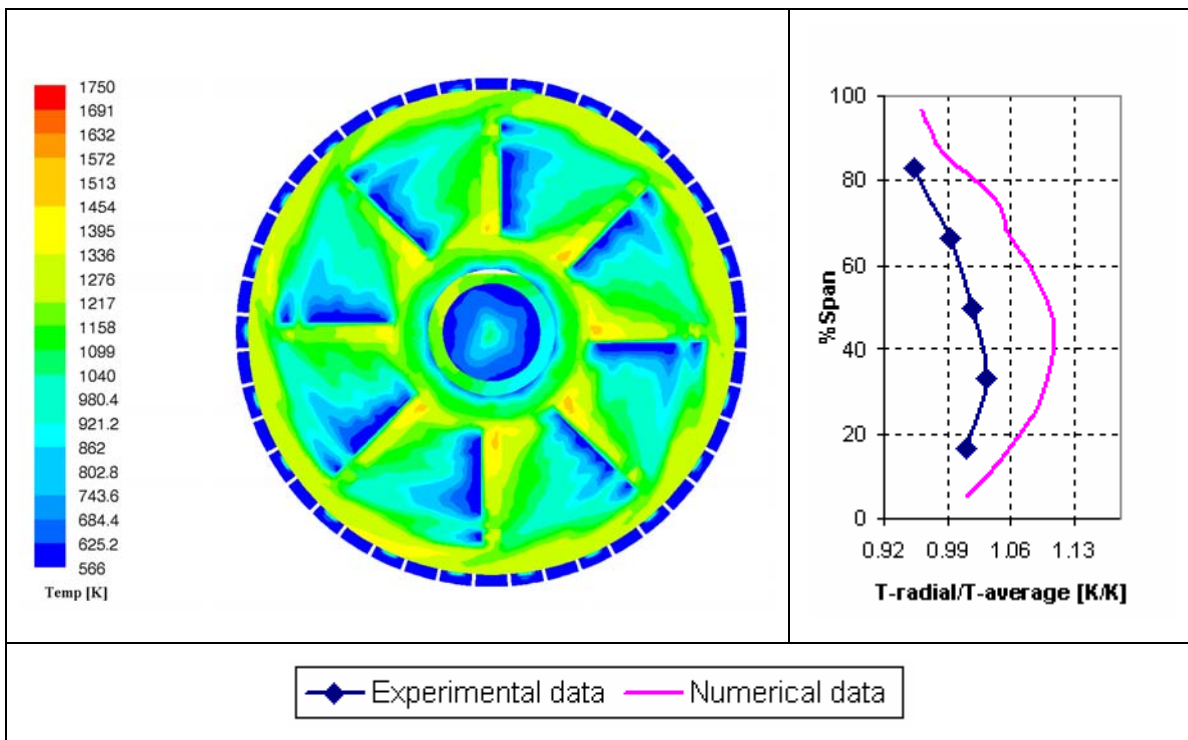
Figure 5.1: Dome wall temperature and exit temperature distribution of original combustor (base case)

As discussed in section 2.4, the maximum allowable temperature for Hastelloy-X is approximately 1150 K. From figure 5.1, it seems that the average dome wall temperature

is within that temperature range, except for a few hot spots. These hot spots are at a temperature of approximately 1500 K, inducing high-temperature gradients. These gradients might result in excessive thermal stresses leading to possible crack formations.

It is believed that blocked cooling devices might contribute to the formation of cracks and therefore an additional analysis was conducted on the original combustion chamber investigating the effect of a single blocked splash-cooling device on the dome wall. The results are depicted in figure 5.2. It is apparent that a significant change can be seen in the temperature distribution on the dome. A high-temperature section is visible on the outer section of the dome inducing a high-temperature gradient between the inner and outer dome surface. Alternatively, the exit temperature distribution had an insignificant change due to the blocked cooling device although the air/fuel ratio in the primary zone has decreased.
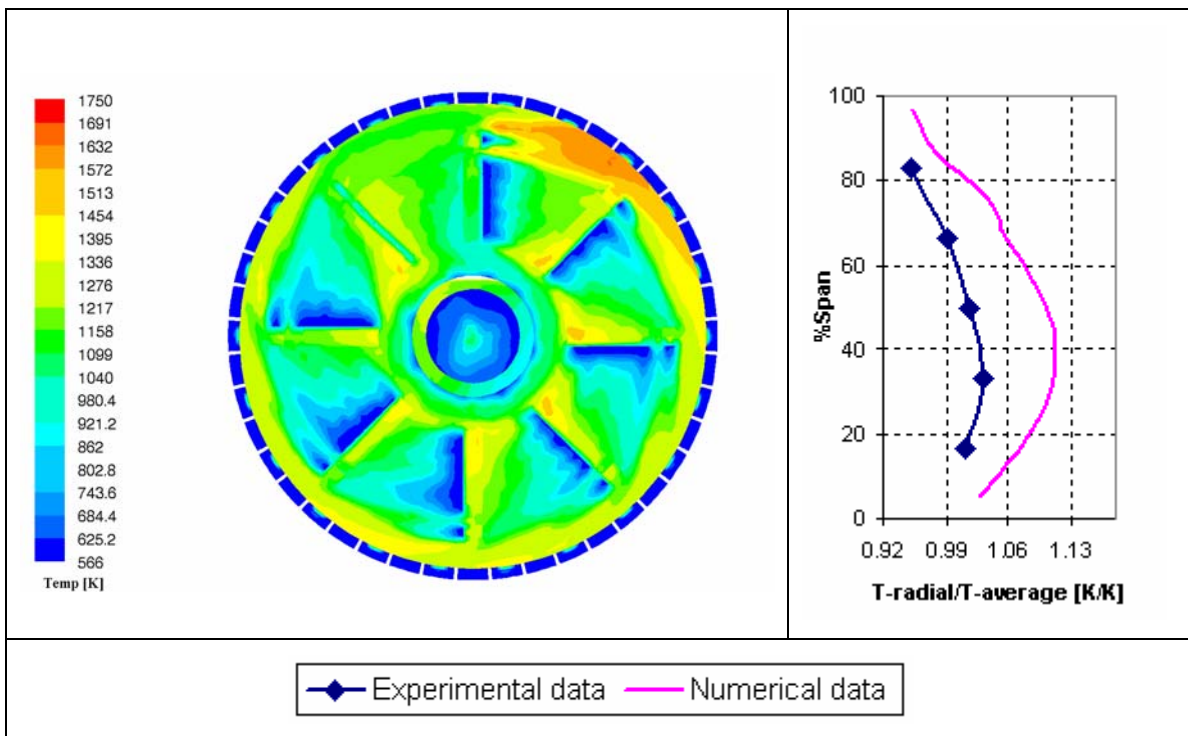
Figure 5.2: Dome wall temperature and exit temperature distribution of original combustor with blocked splash-cooling strips

Comparing figure 5.2 to figure 1.1, it is clear that the area in which cracks are found is comparable to that of the area where high-temperature gradients persist.

In addition to the high dome wall temperatures due to the blocked splash-cooling device, the pressure loss across the combustion chamber will also increase, and consequently may influence overall engine performance and air-fuel mixing in the primary zone.

5.5   Numerical analysis of swirler

Five swirler modifications, presented in table 3.4, are analysed using CFD. Since there is a lack of experimental data for these analyses, the data will be compared with the base case model described in the previous section. The existing splash-cooling devices were replaced with an axial swirler with a similar air flow distribution as the splash-cooling devices. For each case, the number of swirler blades, angle, and consequently outer diameter varied.

Figure 5.3 illustrates the dome wall temperature and exit temperature profile of case 1. The swirler of case 1 consists of 11 blades positioned at an angle of 33° to the axis of the combustor. Although the temperature is relatively uniform across most of the dome wall, it remains too high and may have an effect on the durability of the combustor liner. The area surrounding the swirler is at a lower temperature, as expected, which may give rise to crack formation due to the temperature gradient between the inside and outside dome wall. Also, since the air mass flow rate into the primary combustion zone remained similar to that of the base case, an insignificant change in the exit temperature profile is evident.
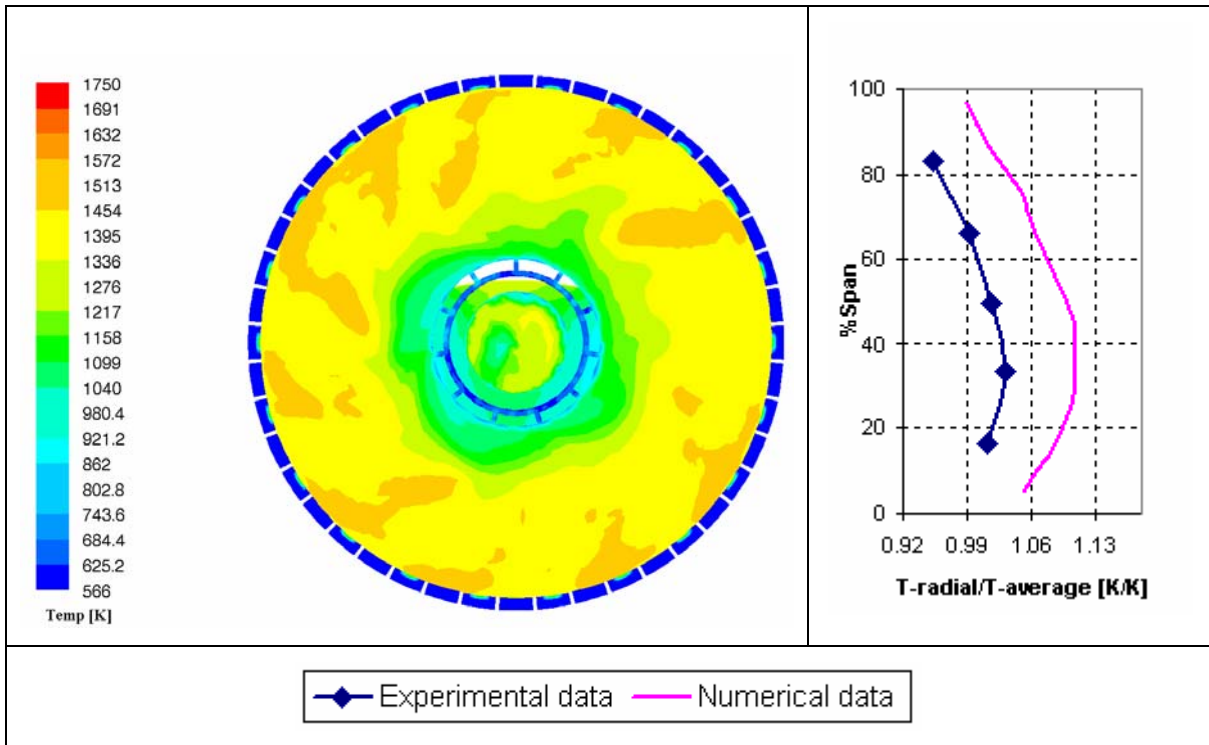
Figure 5.3: Dome wall temperature and exit temperature distribution of case 1

Figure 5.4 illustrates the dome wall temperature and exit temperature distribution for case 2. This swirler is designed to deliver a similar air flow distribution as the splash-cooling devices in the base case, consisting of 10 blades positioned at a swirl angle of 40°. Comparing figure 5.4 and figure 5.3, the effect of increasing the swirler blade angle can clearly be seen. As the swirl angle increases, the cooling effect on the dome will increase as well, due to improved impingement of the air on the dome wall. The temperature contours show clearly that high temperatures still persist on most of the outer surface inducing high temperature gradients between the inside and outside dome wall.
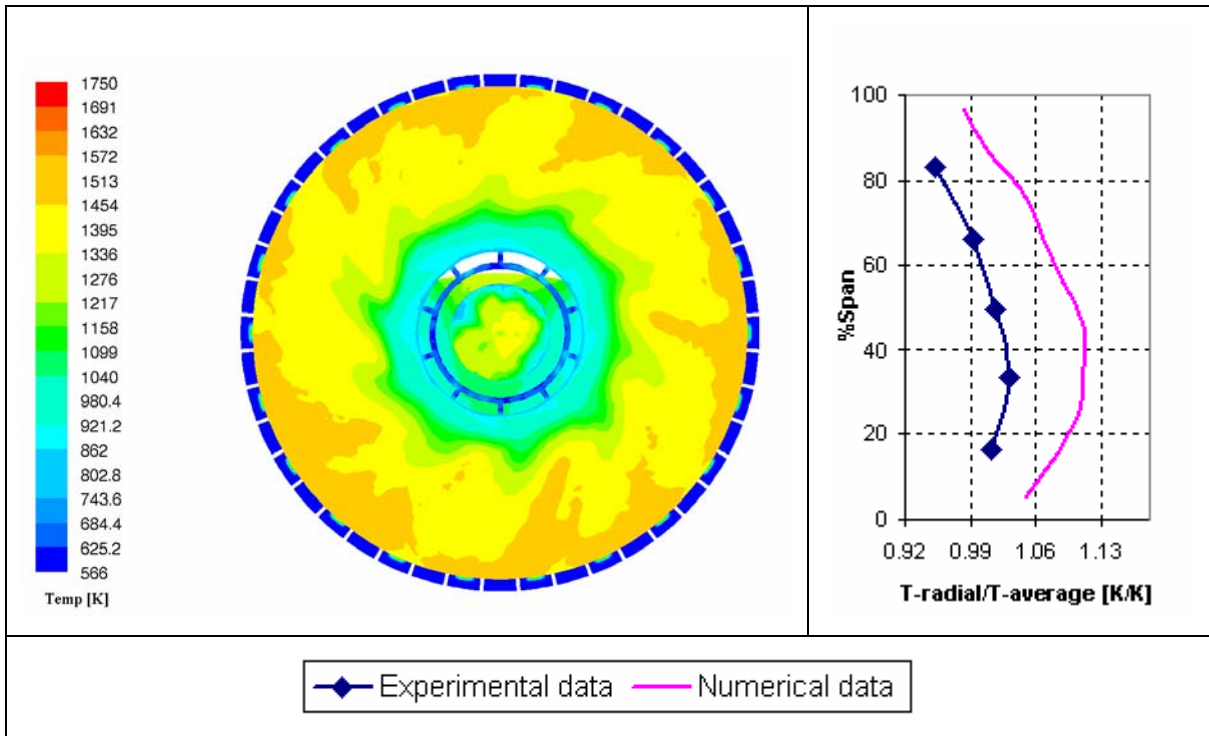
Figure 5.4: Dome wall temperature and exit temperature distribution of case 2

Finally, figure 5.5 depicts the dome wall temperature and exit temperature distribution for case 3. The concept makes use of an axial swirler with eight blades positioned at 50º to the combustor axis, once more, maintaining a similar air mass flow distribution as the splash-cooling devices on the dome of the base case. A distinct difference can be seen when comparing the temperature distribution on the dome wall to the previous two cases. An improvement in temperature distribution is evident due to the larger swirl angles but the penetration of the cooling air is still not adequate to cool the outer dome wall section. Crack formation might therefore still be a problem.
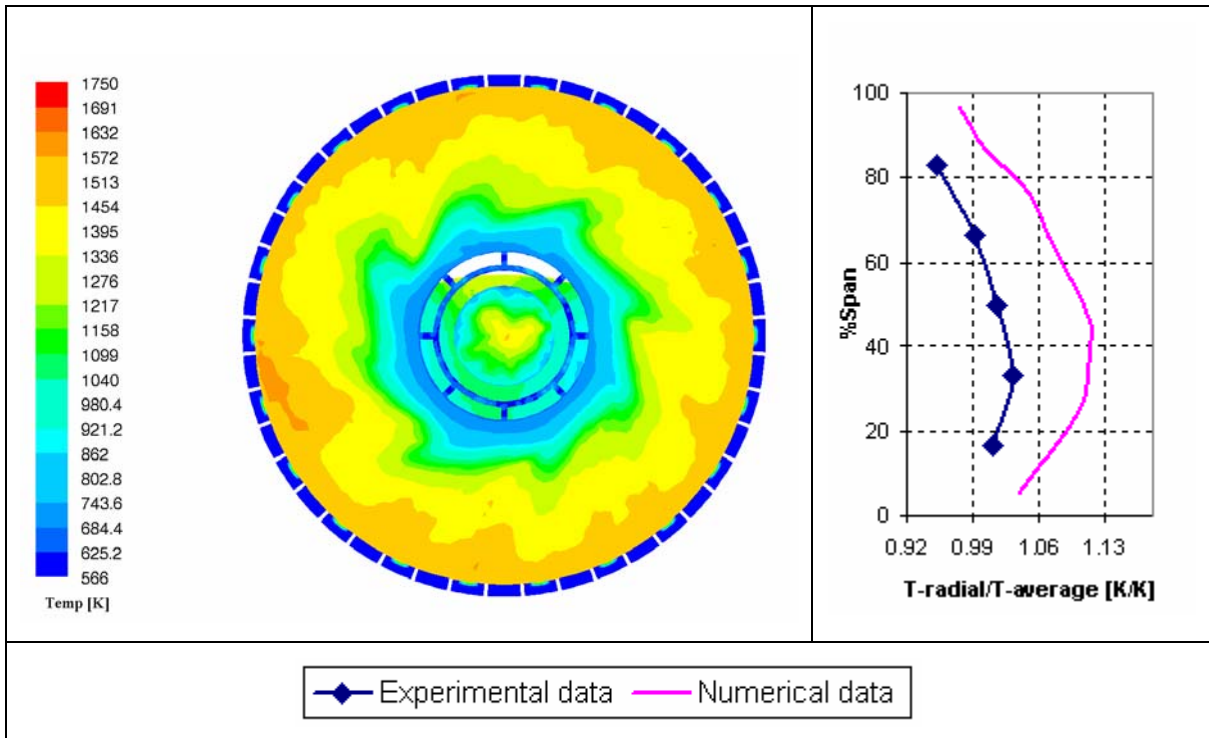
Figure 5.5: Dome wall temperature and exit temperature distribution of case 3

According to the three case studies, the swirler has two significant effects on the combustor. Firstly, the temperature distribution has improved as the swirler blade angle increased and secondly, the swirl number is enhanced therefore improving air fuel mixing within the primary zone. The swirl number of case 3 is approximately 1.1 determined from the one-dimensional swirler analysis. If a swirl angle higher than that of case 3 is used, a larger swirl number will be induced consequently indicating stronger swirl. According to Dodds and Bahr (1990), if a very strong and long recirculation zone is induced it may entrain some of the relatively cool secondary gases, which may result in stability problems and low combustion efficiency. Considering a maximum swirl number of 1.1 from case 3, increasing the swirl angle will therefore induce a stronger swirl. It is, however, evident from the initial three cases that the temperature distribution improves as the swirl angle increases. However, the air does not penetrate far enough along the dome wall due to the lack of momentum, resulting in high temperature regions on the outer dome surface (the hot spot on the dome wall, evident in figure 5.5, is due to a too coarse grid which might be resolved by refining the mesh in that area). For this reason, two additional cases were evaluated with a fixed swirler blade angle of 40° and double the

mass flow rate of the previous three cases. The effect of increased swirler mass flow rate on the dome wall temperature distribution is investigated in case 4 and case 5.

Figure 5.6 illustrates the dome wall temperature and exit temperature distribution of case 4. The swirler utilised in this test case consisted of 11 blades positioned at 40° to the combustor axis, and has an air mass flow distribution of 13.85 percent compared to the 6.1 percent of the previous cases. To maintain a combustor pressure loss of 5.1 percent while increasing the swirler air mass flow rate, 50 percent of the first wiggle strip features were closed in the numerical model. The dome wall temperature has improved significantly due to the increase of swirler mass flow rate as compared with case 2 with similar swirler blade angle. Some hot spots still persist, however, on the outer edge of the dome wall. Comparing the exit temperature profiles, the profile in case 4 has significantly changed. Using the assumptions of flow distributions into each combustion zone, described in section 2.3, the equivalence ratio for the primary zone in the base case can roughly be calculated as 3 whereas the equivalence ratio for primary zone in cases 4 and 5 is reduced to approximately 1.8 due to the additional airflow through the swirler. Owing to the fact that the equivalence ratio in the primary combustion zone for both case 4 and case 5 is closer to unity, more latent heat is released giving rise to a higher exit temperature distribution.
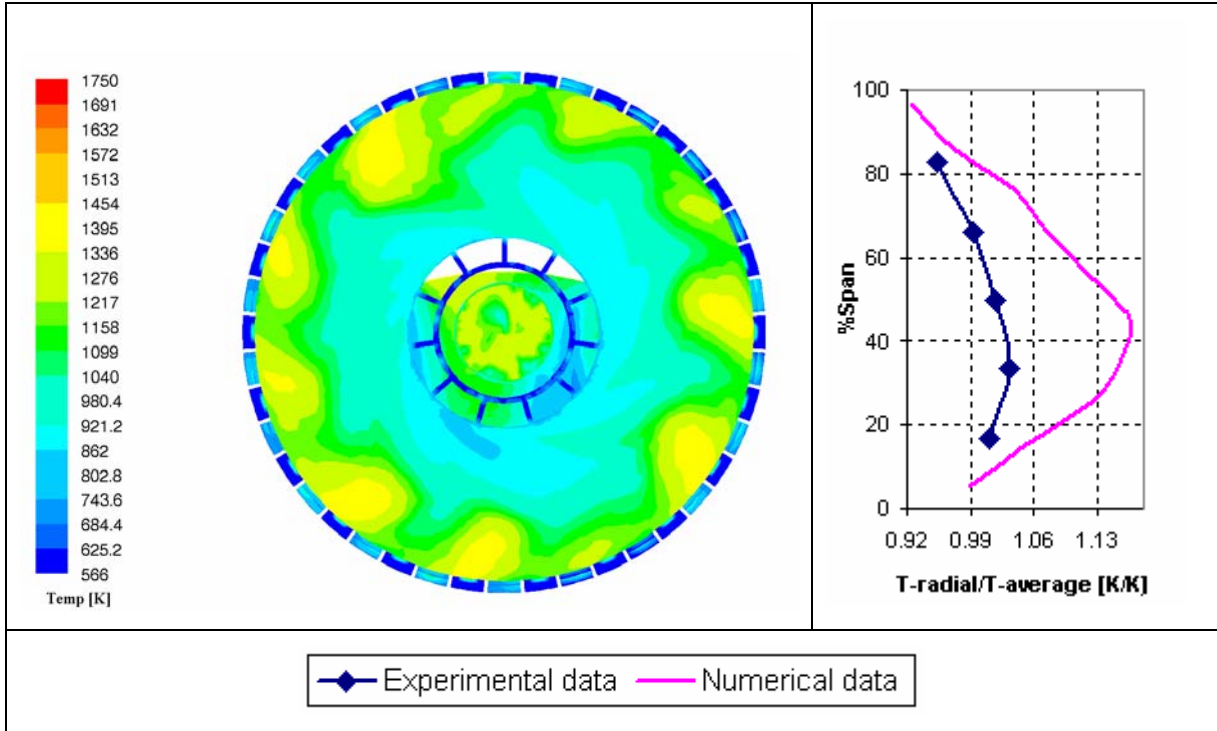
Figure 5.6: Dome wall temperature and exit temperature distribution of case 4

Figure 5.7 illustrates the dome wall temperature and exit temperature distribution for case 5. This case is similar to case 4 but investigates whether the hot spots on the outer dome surface were due to the reduced film-cooling air. Once again, to facilitate a constant pressure drop of 5.1 percent some hole features needed to be closed numerically, therefore the final dilution hole was closed for this case. It was expected that a reduction in dilution air flow will influence the exit temperature distribution, but was not under consideration during this investigation. Under consideration was to determine whether the hot spots on the outer dome area were due to the reduced film-cooling air.

From figure 5.7, it is evident that the addition of 100 percent of the total film-cooling air does not improve the dome wall temperature. The hot spots on the dome outside wall might therefore be due to the recirculation air introducing some of the hot gases into that area. Reducing the dilution air has, however, increased the maximum exit temperature dramatically.
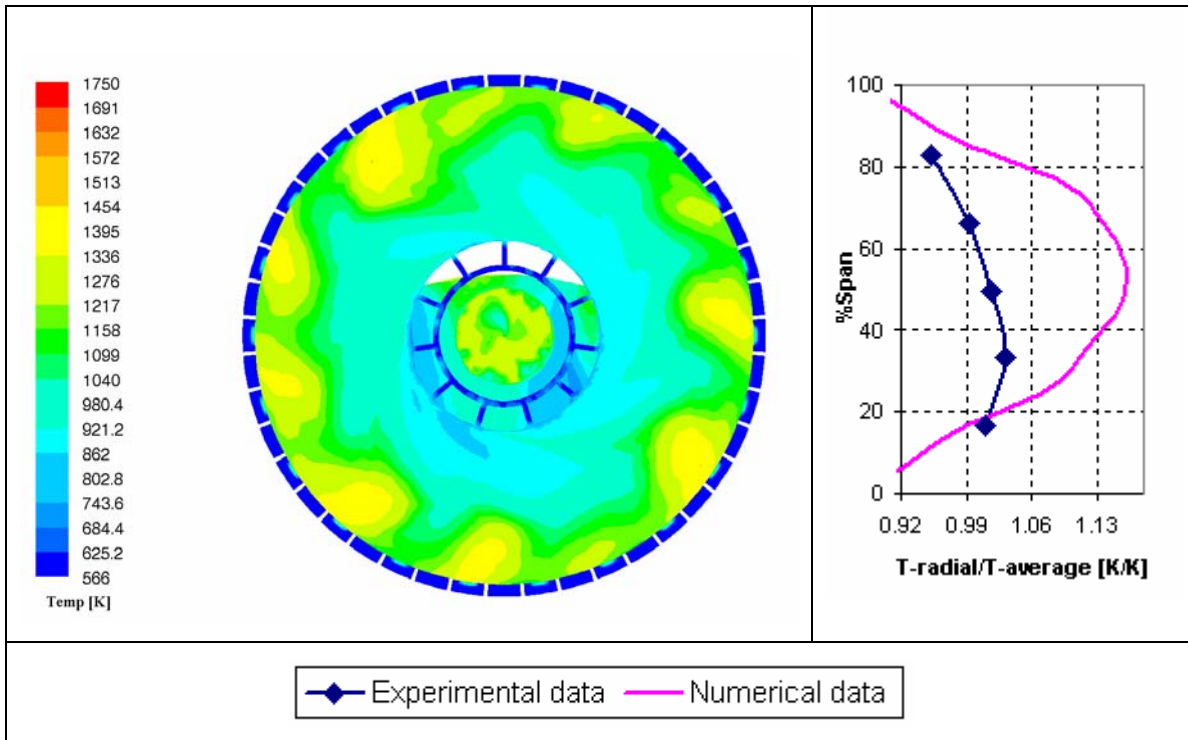
Figure 5.7: Dome wall temperature and exit temperature distribution of case 5

Table 5.1 depicts the pattern and profile factors for each case. Base case 2 in the table presents the base case model with a single blocked splash-cooling device. Case 1 correlates well with the experimental determined profile factor. Since all the models are compared relative to the base case, case 3 is the most satisfactory with respect to profile factor. When comparing the pattern factors, however, case 4 corresponds closest to the base case data.

Table 5.1: Profile and pattern factors

	Experimental data	Base case	Base case 2	Case 1	Case 2	Case 3	Case 4	Case 5
Profile factor	0.0523	0.083	0.086	0.059	0.065	0.072	0.15	0.152
Pattern Factor	0.115	0.366	0.373	0.306	0.277	0.264	0.32	0.41

Figure 5.8 compares all the numerical exit temperature profiles. Notice that the data from the initial three cases is comparatively good relative to the base case due to the mass flow distributions that were maintained similar. Although the reduced dilution air played a significant role in the maximum temperature of case 5, an increase in mass flow distribution through the swirler results in an increase in the maximum temperature for case 4 and consequently also influenced case 5.
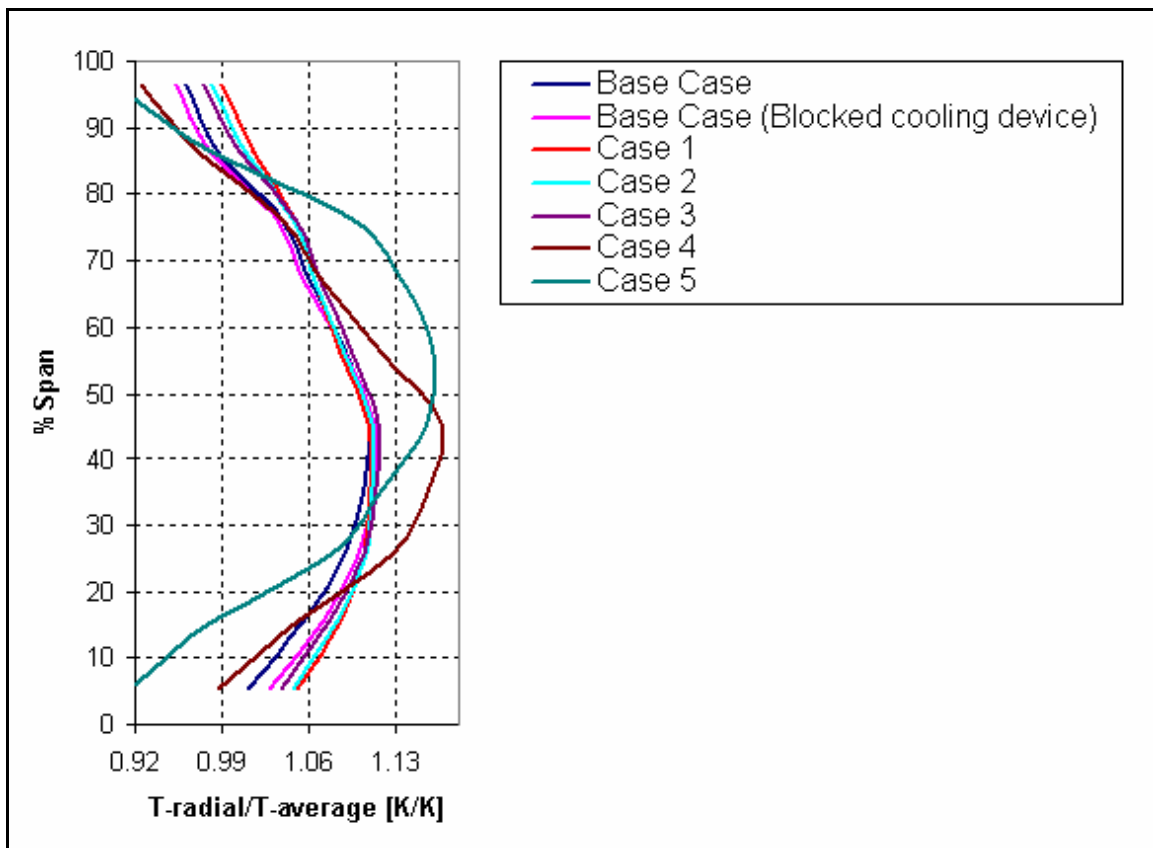
Figure 5.8: Exit temperature profiles of all numerical models

Figure 5.9 and figure 5.10 depict the numerical and experimental exit temperature distributions respectively. Figure 5.9 (a) and (b) depict the exit temperature distribution of the base case and the base case with blocked splash-cooling devices respectively. When comparing these two figures it is evident that the blocked cooling devices have an insignificant influence on the exit temperature distribution but will certainly influence the pressure loss across the combustion chamber. The reduction in cooling air will, however,

influence the equivalence ratio in the primary/secondary zone therefore influencing combustion performance.
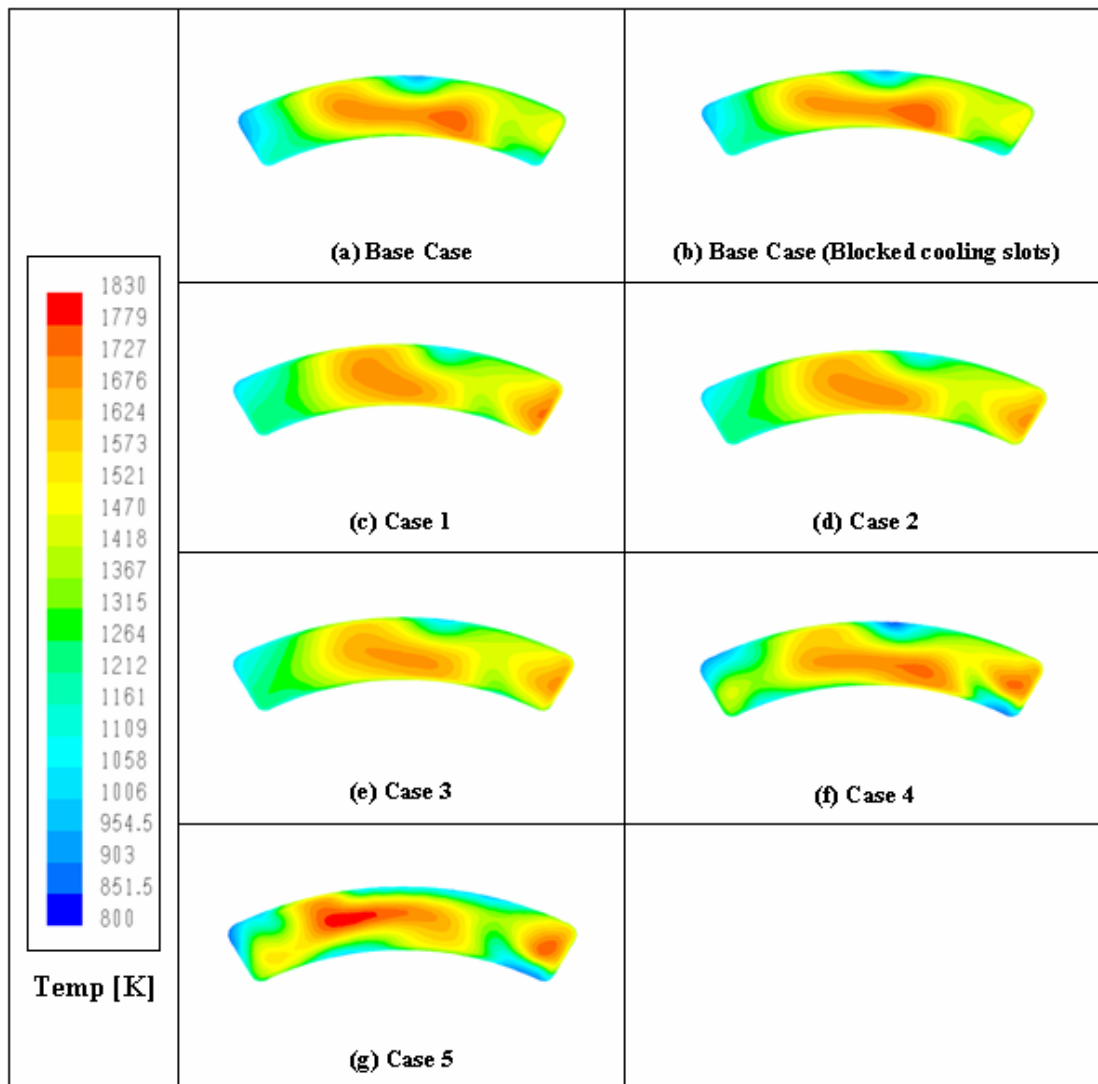
Figure 5.9: Exit temperature distribution of all numerical models
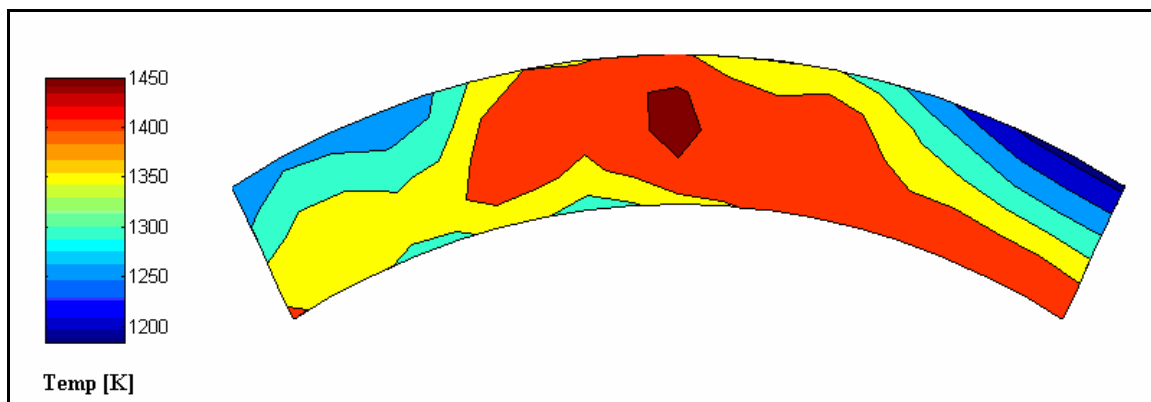
Figure 5.10: Experimental exit temperature distribution

When comparing figure 5.9 (a) and figure 5.10, it is evident that the two figures show the same trend in exit temperature distribution although the maximum temperature differs by as much as 200 K. The discrepancies may be due to the numerical model used, such as the turbulence model, fuel spray and combustion model. The turbulence model may not describe the recirculation effectively in critical areas whereas the fuel droplet size in the spray model will influence evaporation and hence heat release from the fuel. In addition, in the current combustion model only five species were considered with an assumed β PDF function. Nonetheless, with the assumptions that were made comparative results were obtained.

Figures 5.9 (c) to (e) represents the temperature distributions of case 1 to 3. The boundary conditions of these three cases were exactly the same with the only difference being the outer diameter in the swirler, number of blades used, and the angle of the blades. The reason for the evaluation of these three cases was to determine the influence of the blade angle on the exit temperature distribution and dome wall temperature while maintaining a constant swirler mass flow rate similar to the existing splash-cooling devices. It is apparent that since the mass flow rate through the swirlers remained constant, the blade angles had essentially no effect on the exit temperature distribution when comparing the three cases. However, when comparing the three cases to the base case (figure 5.9 (a)) the effect of a swirler on the temperature distribution is clearly depicted. It is interesting to note that the central hot core of figure 5.9 (a) has shifted to the left and that a hot region appears on the right.

Figure 5.9(f), depicts case 4 where the mass flow rate through the swirler was increased from 6.1 percent to approximately 13.85 percent. As mentioned earlier, the flow rate through the first wiggle strip device was reduced by 50 percent in order to maintain a pressure loss of 5.1 percent and to accommodate for the increase in swirler mass flow rate. Comparing case 4 to the previous three cases the exit temperature has changed but the maximum temperature remains at approximately 45 percent of the radial span. An increase in swirler mass flow rate therefore has a significant effect on the exit temperature distribution.

A similar case was conducted with case 5 but with the exception of reducing the flow rate through the first wiggle strip device, the final dilution hole was also blocked to accommodate for the increased swirler mass flow rate and to maintain a constant pressure loss of 5.1 percent. Due to the final dilution hole that was blocked, the exit temperature increased considerably. Note that in both cases 4 and 5 the equivalence ratio in the primary combustion zone was altered, compared with the initial three cases, which may influence combustion stability.

Figure 5.11 depicts, on the center plane, the velocity vectors of the internal flow of the original combustion chamber (base case). Due to the weak recirculation zone, the air in the core of the combustion chamber passes through the primary combustion zone without taking part in the recirculation zone. The recirculation zone is weak and is situated too far downstream from the dome.
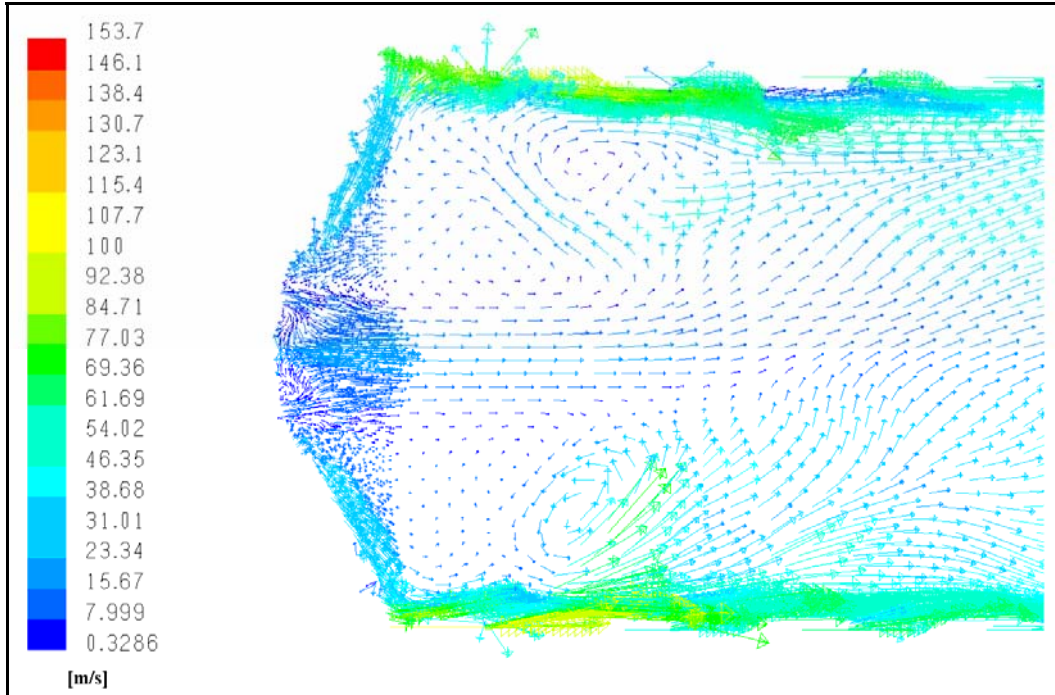
Figure 5.11: Velocity vectors of base case depicted on the center plane

Figure 5.12 depicts path lines of particles being released from the injector shroud. This figure verifies the statement from the previous figure that most of the core flow does not take part in a recirculating flow. A swirling motion is, however, only initiated after the primary combustion zone due to the position of the primary holes.
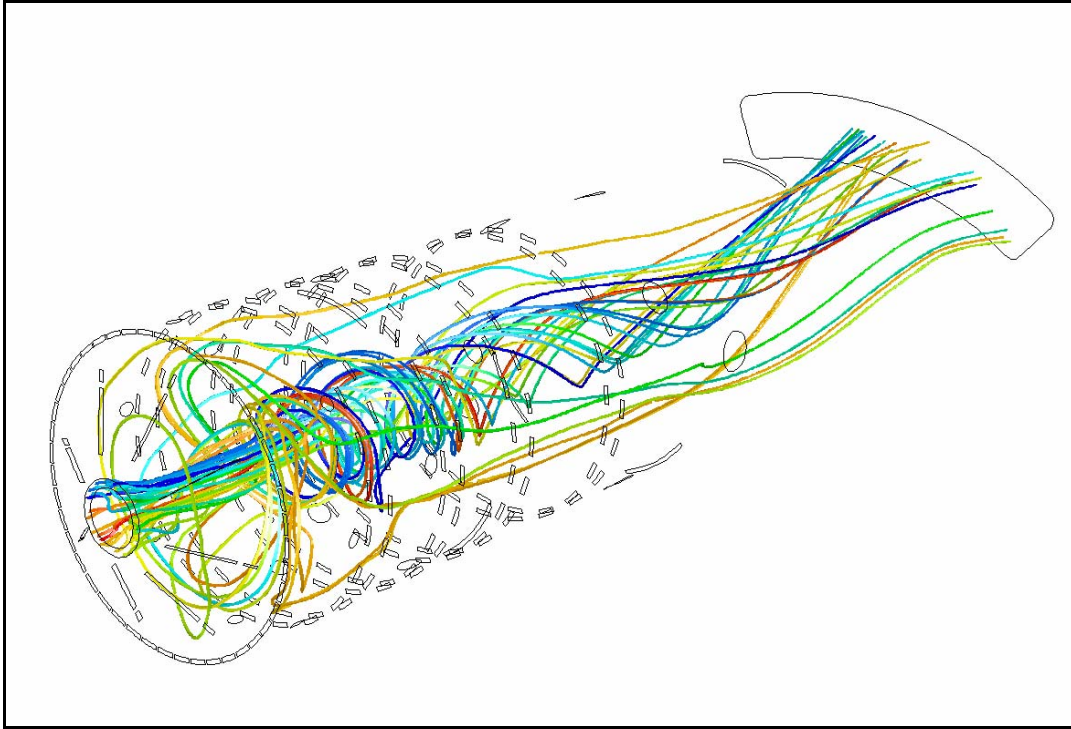
Figure 5.12: Particle track of particles released from injector shroud – Base case

Figure 5.13 depicts, on the center plane, the velocity vectors of the internal flow field of case 2. It is apparent that the recirculation zone has increased with the use of a swirler compared to the base case. Two recirculation zones are, however, present, instead of an ideal single recirculation zone. The core flow is, however, more active in the recirculation zone than in the previous case.

It appears that the inner recirculation zone is generated due to the swirler whereas the second recirculation zone is induced due to the primary air.
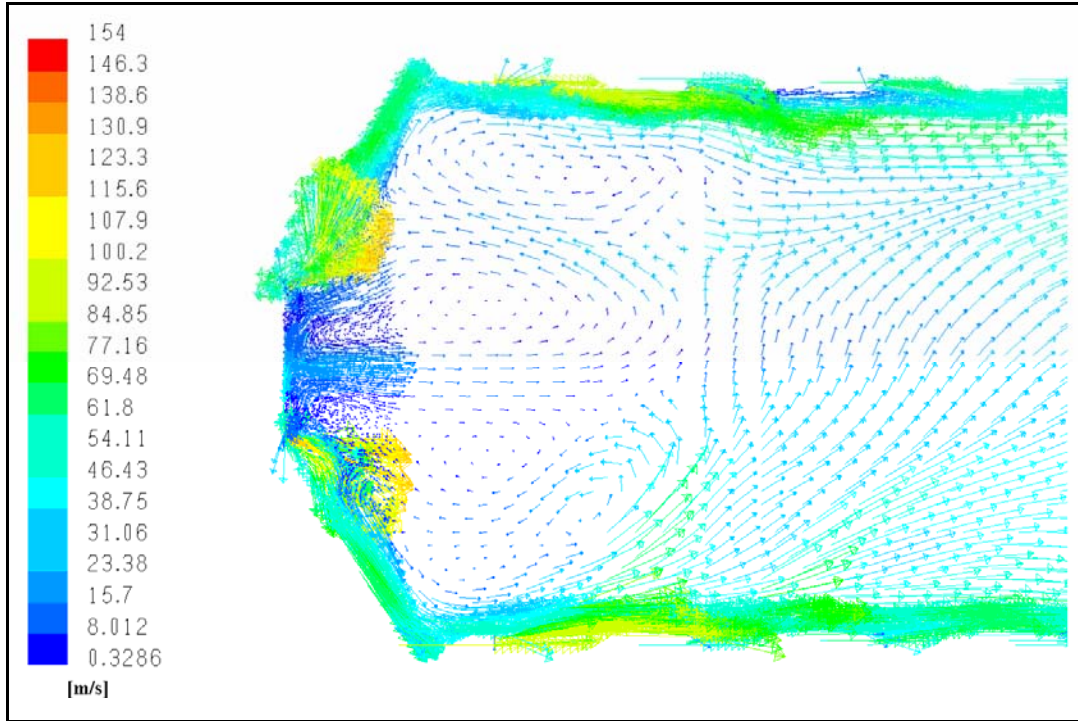
Figure 5.13: Velocity vectors of case 2 depicted on the center plane

Figure 5.14 depicts case 2 with particle path lines for particles being released from the same position as the base case. In case 2, the particles flow outwards around the re-circulation zone due to the larger swirl angle. This may be due to the low pressure induced by the swirler. Air-fuel mixing is therefore enhanced by increasing the residence time.
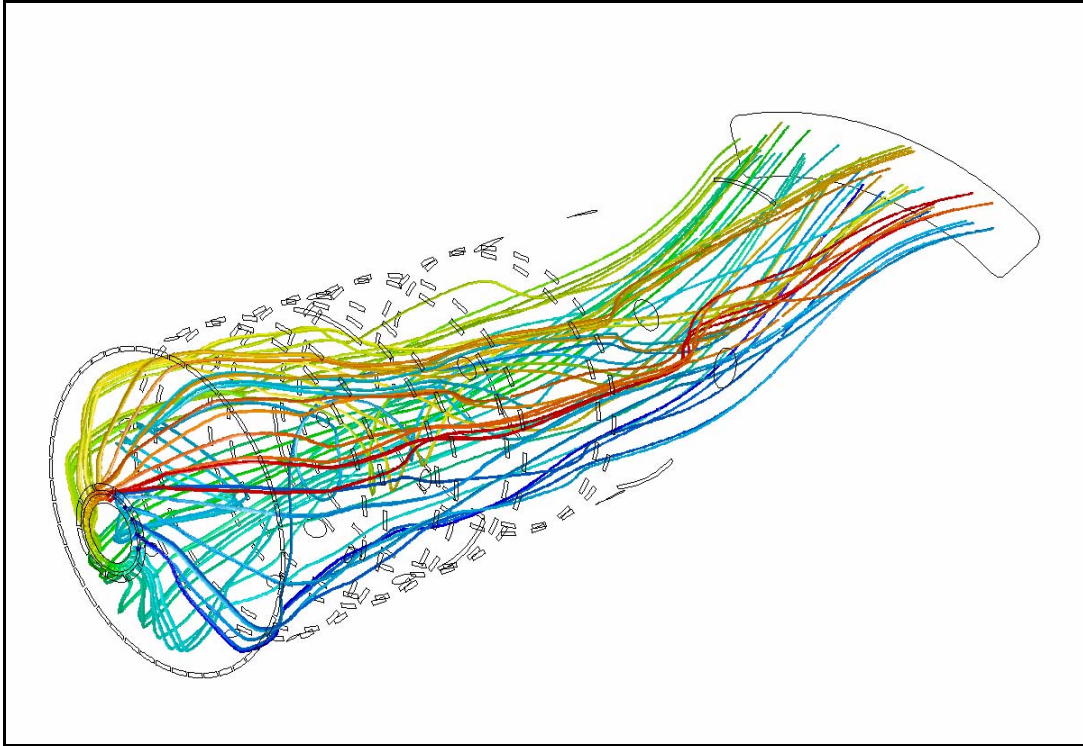
Figure 5.14: Particle track of particles released from injector shroud – Case 2

Figure 5.15 depicts, on the center plane, the velocity vectors for the internal flow field for case 4. Two re-circulation zones exist once again but it seems that the recirculation zone has increased in length. Figure 5.16 depicts the particle path lines of case 4. The flow field appears to be similar to the flow of case 2.
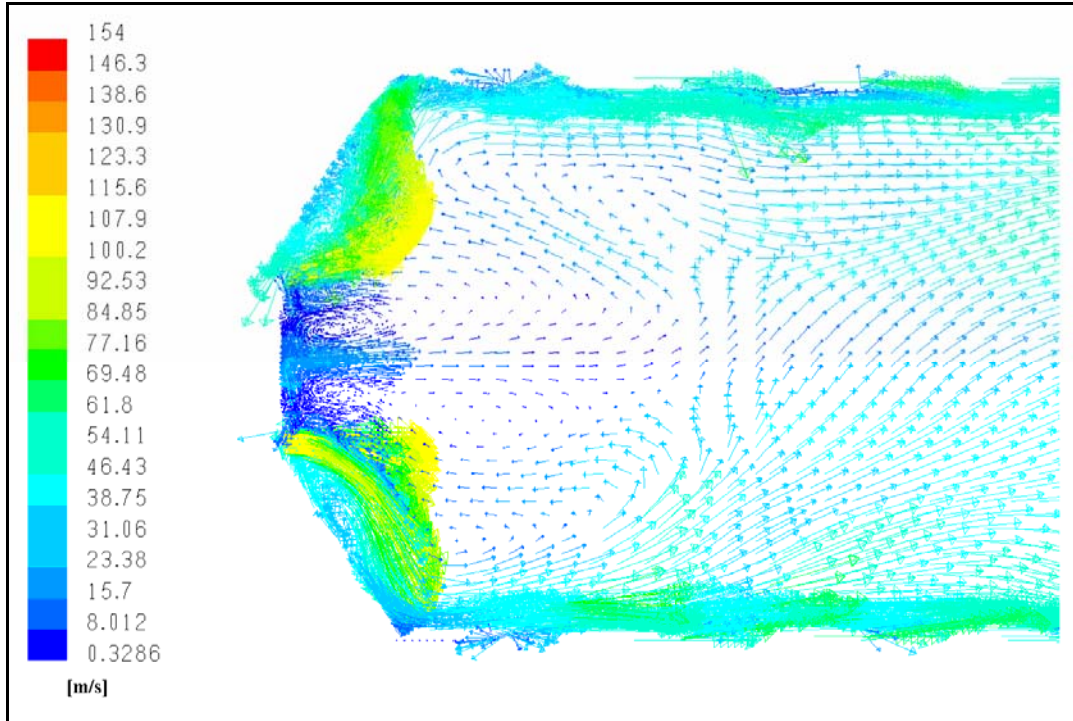
Figure 5.15: Velocity vectors of case 4 depicted on the center plane
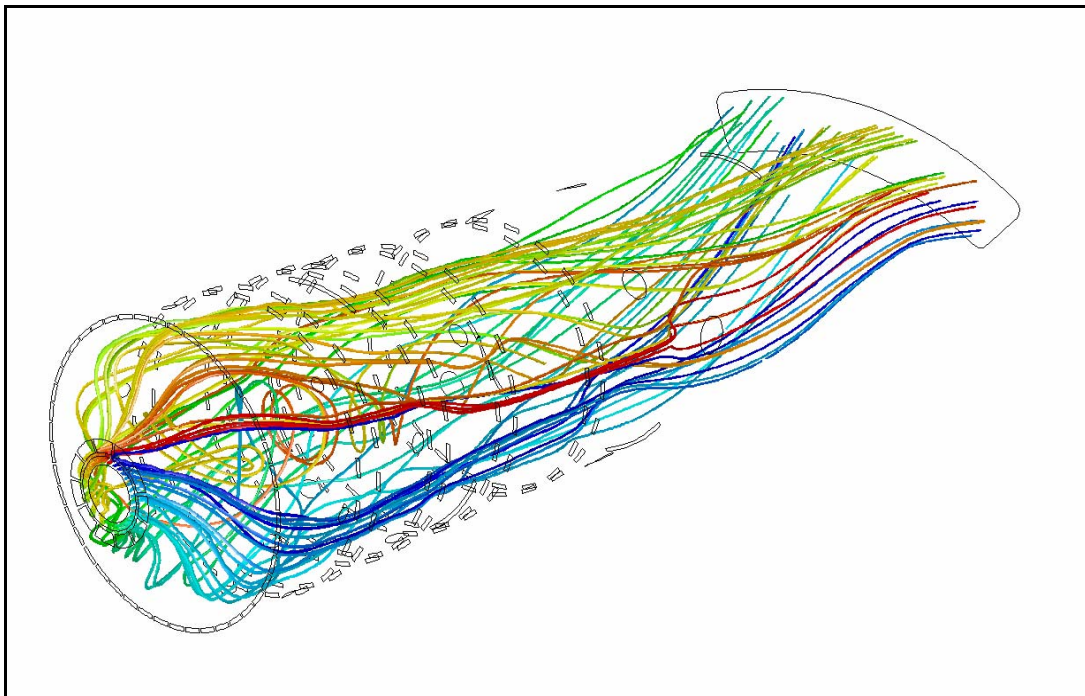
Figure 5.16: Particle track of particles released from injector shroud – Case 4

The following three figures depict the internal temperature contours of the base case, case 2 and case 4 respectively. Due to the core flow that does not participate in the re-circulating flow, the fuel injection is a long and narrow injection compared to the following two cases. Due to the lack of a proper recirculation zone, that is evident from the long fuel injection spray, some of the combustion gases persist near the liner dome wall.
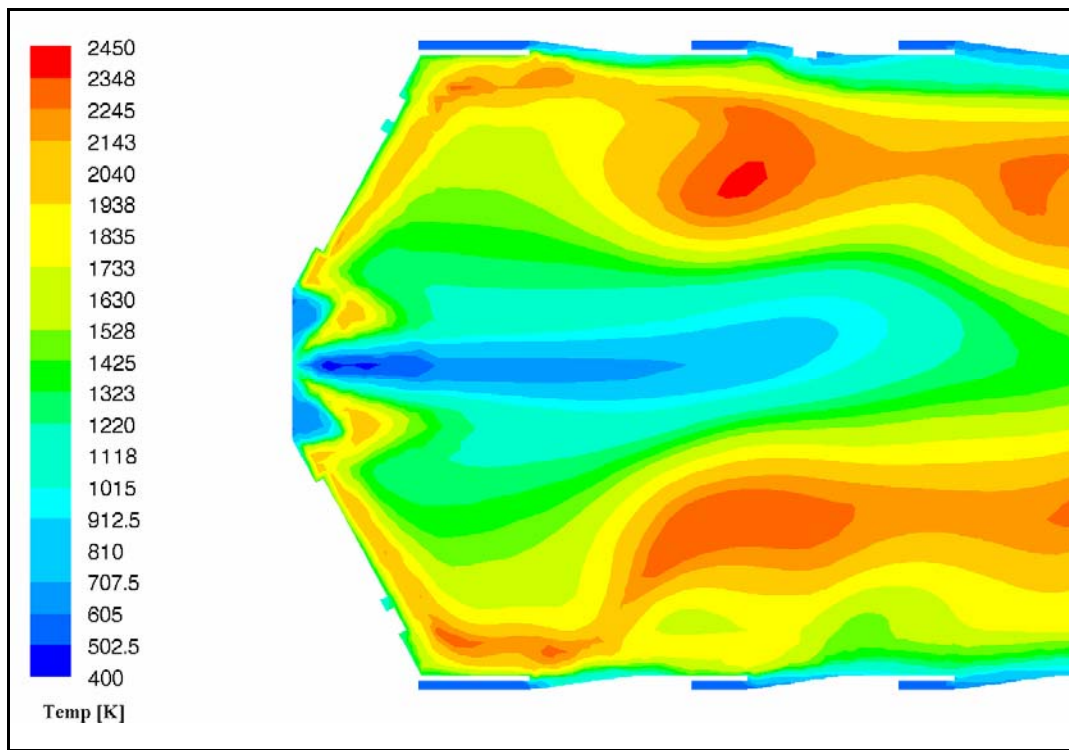
Figure 5.17: Internal gas temperature contour depicted on the center plane of base case

The fuel injection for case 2 and 4 does not penetrate as deep as the base case due to the recirculation flow that is being induced by the swirler. Evidently, the effect of the swirler mass flow rate can be seen in figures 5.18 and 5.19. The addition of swirler air mass flow rate (case 4) increased the momentum and consequently improved the penetration of the cooling air along the combustor liner.
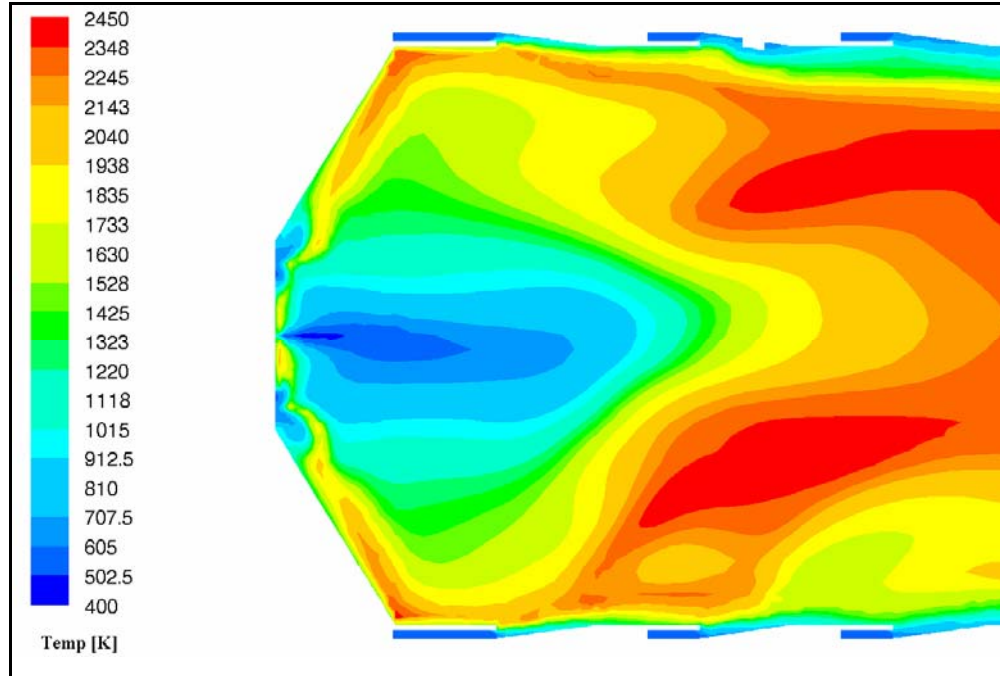
Figure 5.18: Internal gas temperature contour depicted on the center plane

of case 2
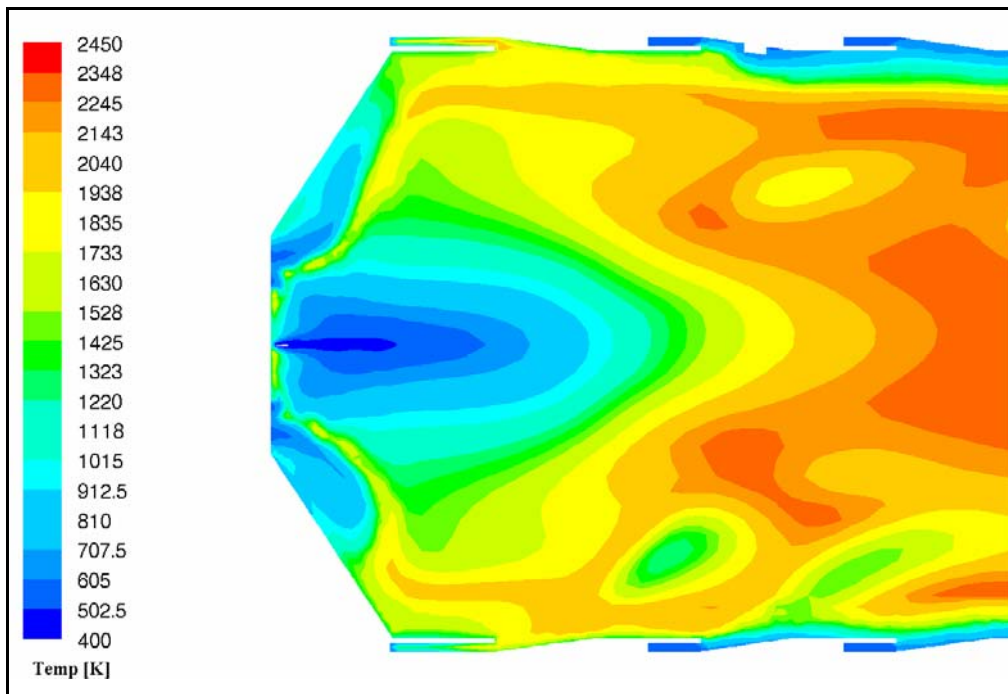
Figure 5.19: Internal gas temperature contour depicted on the center plane

of case 4

5.6   Predicted wall temperatures

The average combustor wall temperature that was obtained from CFD analysis is compared with the predicted one-dimensional network results. Figure 5.20 and figure 5.22 depict the average wall temperatures along the combustor liner. Figure 5.20 represents a comparison between average CFD wall predicted data and network wall temperature data. In this case, the network wall temperatures were obtained from empirically predicted gas temperatures shown in figure 3.10. It is evident that the two graphs show similar trends. Due to the gas temperature that was underpredicted in the primary zone the wall temperature in the dome section is underpredicted as well. The underprediction of the empirical gas temperature is discussed in section 3.6.
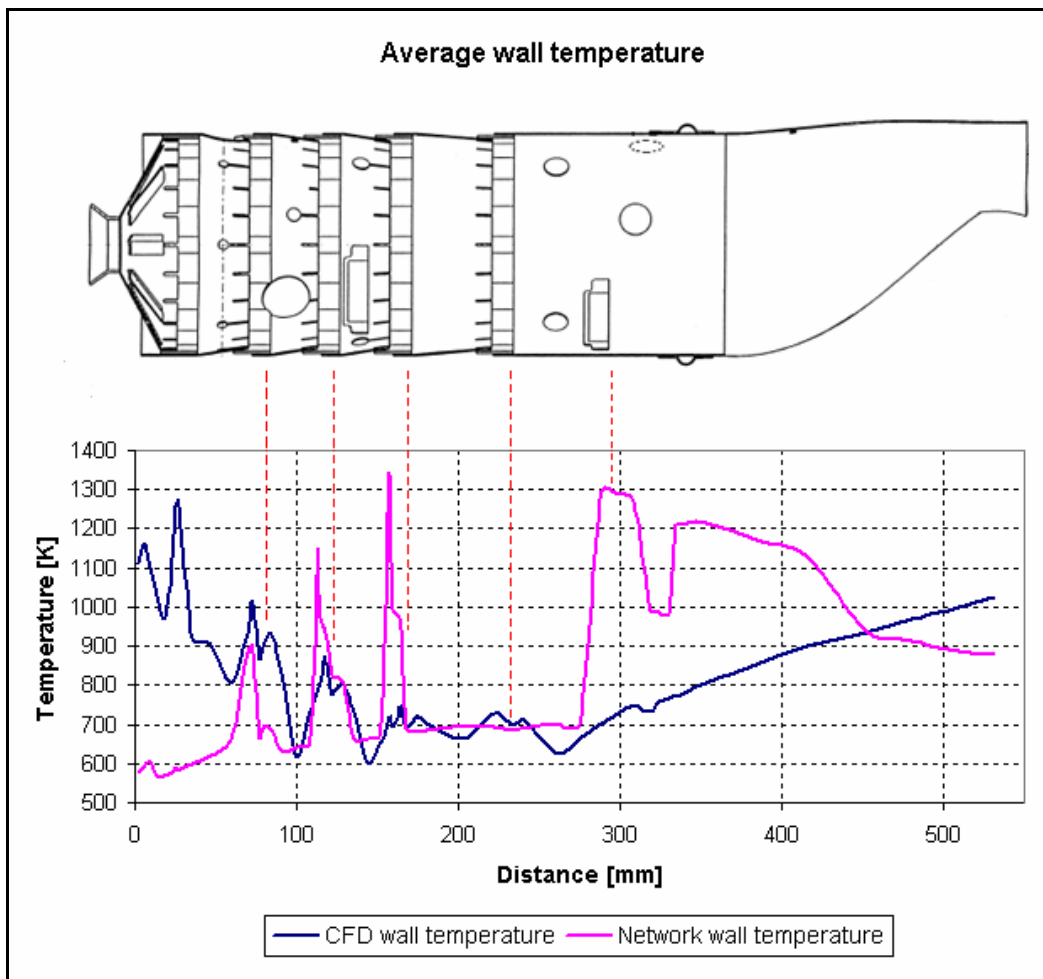
Figure 5.20: Network vs CFD-predicted average wall temperature using the empirical gas temperature predictions

The network temperature predictions shown in figure 5.22 were, however, predicted using the average CFD gas temperatures. The average CFD gas temperature was obtained from the base case CFD model by determining the average gas temperature on various cross sectional planes. The position of these planes was associated with the position of the nodes in the network model that represents the combustor's central axis.

The average CFD gas temperature is compared with the empirical gas temperature, presented earlier in figure 3.10, and is depicted in figure 5.21.
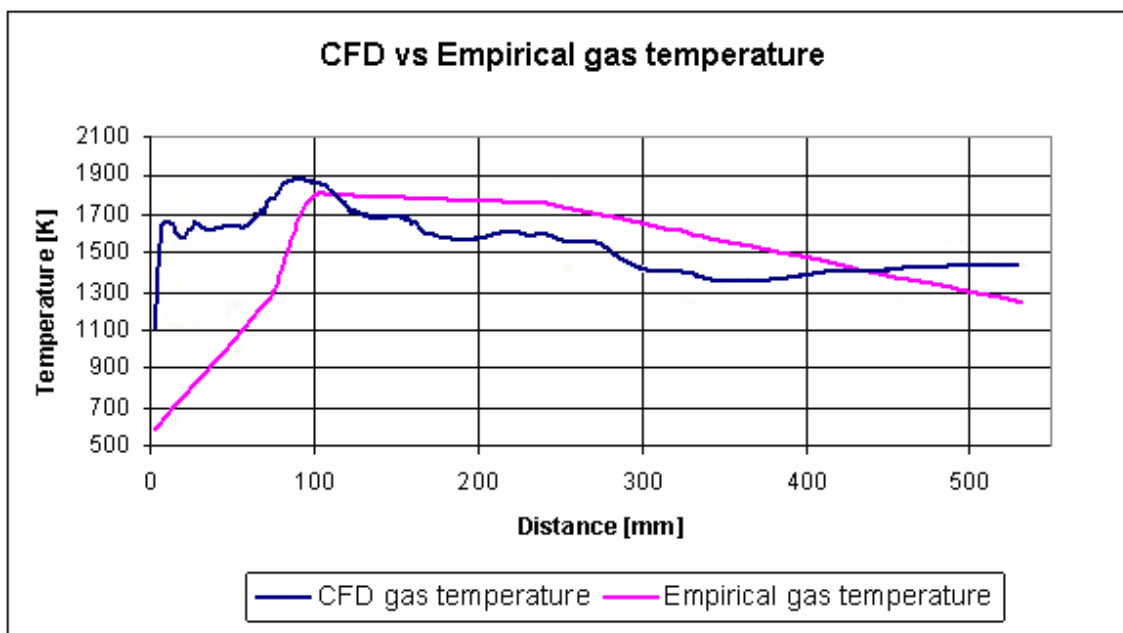
Figure 5.21: Average CFD and empirical gas temperatures

From the comparison of gas temperatures, it is apparent that the temperature predictions in figure 5.22 will be different when compared to the predictions of figure 5.20, but will consequently have a closer resemblance to the CFD results. Figure 5.22 therefore illustrates the ability of the network solver to predict comparative CFD results.
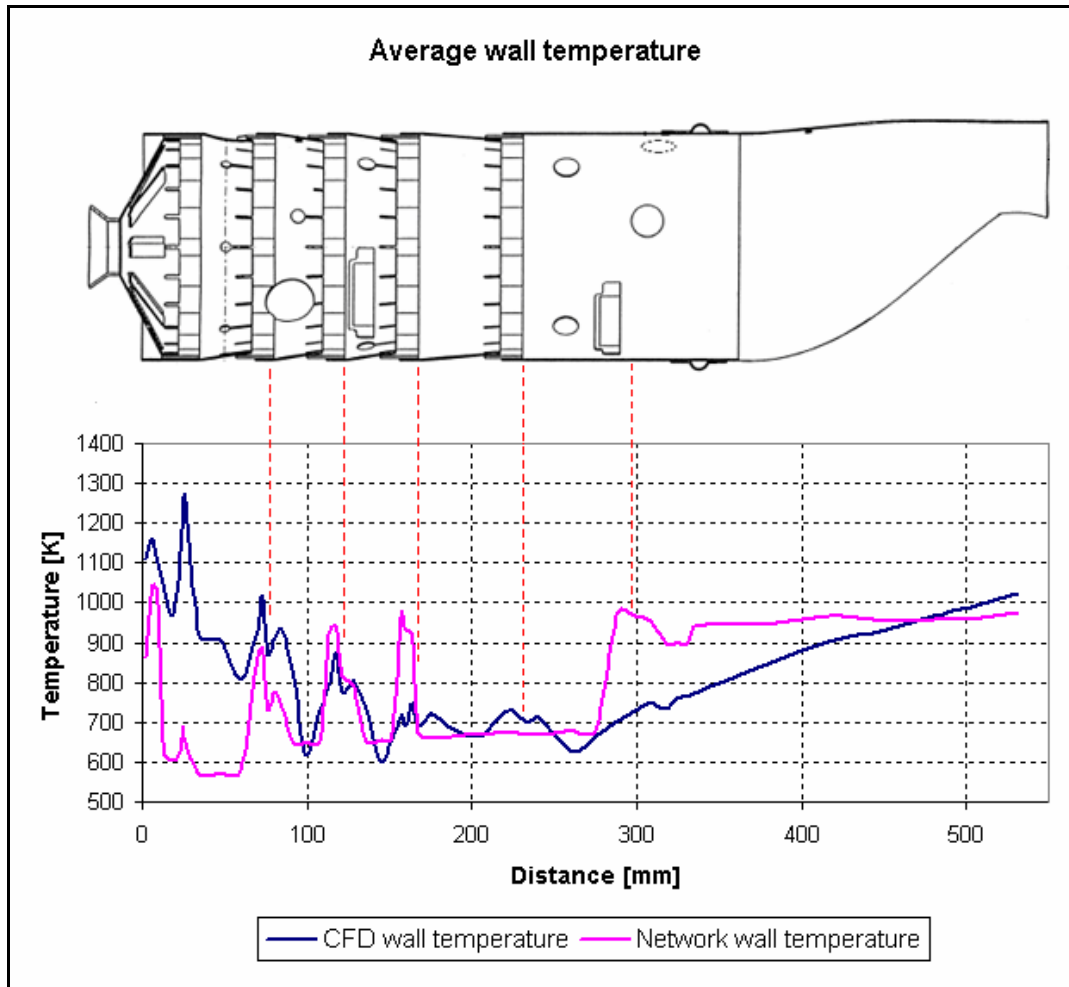
Figure 5.22: Network vs CFD-predicted average temperature using the numerically predicted gas temperatures

In figure 5.20 and figure 5.22 at a distance of approximately 300mm, the network analysis has overpredicted the wall temperature. This can be ascribed to the fact that the CFD analysis accounts for the local cooling effect of the hole features along the combustor wall whereas the network model did not account for such effects. To incorporate such effects into the network analysis a typical film-cooling efficiency needs to be included into all hole features. Such data is, however, not available and for the purposes of this study the results obtained were comparatively good describing the same trend for the temperatures.

5.7   Summary

The effect of swirler blade angle and mass flow rate on the dome wall temperature was investigated through the use of a parametric study. The results showed that the addition of a swirler with a similar flow distribution as the original splash-cooling devices, will not result in a more uniform dome wall temperature. When the mass flow rate through the swirler was, however, increased, the possibility of a more uniform dome wall temperature increased. Case 4 resulted in adequate cooling although hot spots still remained on the outer dome surface. The initial three tests cases showed that increasing the swirler blade angle resulted in an improved dome wall temperature distribution. A swirler with 13.85 percent and higher swirl angle in the range of 45° - 50° might therefore improve the temperature distribution even more. However, due to the fact that a leaner fuel/air ratio is present in the primary combustion zone, some stability problems may exist. For this reason, before any swirler as described above can be used, a complete redesign of the combustor hole sets will be needed.

CHAPTER 6 –

SUMMARY, CONCLUSION AND

RECOMMENDATIONS

6.1   Summary

The purpose of this study was two-fold; (1) to develop a one-dimensional incompressible code, incorporating an empirical combustion model, in conjunction with a network solver to predict flow distributions, pressure losses, and temperatures across a standard T56 combustion chamber; (2) to use the data obtained form the one-dimensional analysis as boundary conditions to investigate possible modifications to a T56 combustion chamber, by replacing the existing dome cooling devices with an axial swirler. The results are compared against an experimental validated numerical base case model.

The network model accounted for compressibility effects and made modelling complex geometries much simpler. Due to a lack of empirical correlations in the network model to model combustion, the model was used in conjunction with the empirical model to obtain gas temperatures and gas emissivities. The method that was used in the network model to predict the effect of film-cooling devices proved to be sufficient when compared with the numerical data. With the network approach, the effect of a film-cooling device can, however, be modelled sufficiently without the use of empirical models.

Although the network model had to be calibrated with experimental flow distribution data, critical data such as pressure losses across the combustion chamber was obtained.

The pressure loss was used during the modifications analysis in order to design the swirler geometries while maintaining overall engine performance. Nonetheless, the one-dimensional analysis proved to predict sufficient flow distributions. The effect of a swirler on the dome wall temperature can, however, not be predicted with the use of a one-dimensional model since the model can only predict the mass flow rate and pressure loss across a specific device. However, an empirical code was developed and used to design the swirler geometry with a specified mass flow rate and pressure loss as inputs.

The investigation was conducted with the use of three-dimensional CFD analysis. The original combustion chamber was analysed and used as a base case model. The numerical exit temperature distribution of this model was within 10 percent of experimental data.

Since the purpose of the study was to investigate the effect of a swirler on the dome wall temperatures by combining a one-dimensional empirical and network solver, no experimental data was available. Therefore, the original combustion chamber was analysed and validated against experimental data that could be used as a model against which the test cases can be compared with. Using a swirler with the same mass flow distribution as the splash-cooling strips, did not offer a sufficient temperature distribution. Doubling the flow rate through the swirler did, however, have a greater impact on the wall temperature. Although temperature gradients still persist with the use of a swirler, lower wall temperatures are apparent which may reduce possible crack formation are apparent.

6.2   Conclusion and contributions

The following conclusions were made during this study;

- The ability of the one-dimensional empirical code to predict flow distributions, pressure losses and temperature distributions proved to compare well with network predictions. The conclusion was made that compressibility had an insignificant effect on these predictions. It was also concluded that the discharge coefficients play a great role in determining pressure losses.

- The one-dimensional network solver predicted basically the same trend of temperature distribution compared to the network solver. The drawback of the empirical code is that it makes use of a film-cooling efficiency correlation to predict the cooling effect on the liner wall. Nonetheless, adequate initial data can be obtained from such an analysis. The network model, on the other hand, used a heat transfer process to model the cooling effect, since no empirical data was available on the swirler. Yet, comparative temperature distributions were obtained compared to CFD data.

- Numerical modelling of the original combustion chamber showed that a poor re-circulation zone exists. This may result in inadequate air-fuel mixing and therefore a loss in combustion efficiency and a possibility of high smoke emissions.

- The original combustion chamber dome wall temperature seems as if the average temperature is below 1150 K, except for minor hot spots on the outer surface. These hot spots will cause high temperature gradients on the dome wall, which may contribute to the formation of cracks. A second numerical analysis proves that in a case where a splash-cooling device might become blocked, the problem may be aggravated due to higher-temperature gradients between the outer and inner surface.

- Particle tracking has shown that the recirculation flow in the primary combustion zone has improved when a swirler is used. The recirculation zone will improve combustion efficiency and might even result in lower emission levels, such as soot and CO_2, due to the increased residence time in the region.

- The initial three swirler cases utilised approximately the same mass flow rate as the splash-cooling devices on the dome. The influence of these swirlers on the dome wall temperature did not prove to be an adequate solution, since high temperatures still persisted on the outer wall area. The temperature distribution

improved, however, as the swirler blade angle increased. In all three cases, the average exit temperature profile stayed virtually unchanged, since the equivalence ratio in the primary combustion zone was not changed greatly. A drawback of these three cases is the physical size of these devices. Due to the small amount of air that it passes (6.1 percent), the dimensions are very small and will therefore be difficult to manufacture.

- Two additional swirler cases were investigated as well. These cases utilised an increased mass flow rate, approximately double that of the previous three cases, while maintaining a similar pressure loss of 5.1 percent. The dome wall temperature distribution improved significantly, due to the increased momentum, but resulted in higher average exit temperature distributions. The reason for it being that the equivalence ratio in the primary combustion zone has been reduced, thus releasing more latent heat. The swirlers used in case 4 and case 5 utilised 11 blades positioned at a 40º angle relative to the combustor axis. The dome wall temperature may, however, be improved even more if a larger blade angle is used.

- The addition of a swirler with the same mass flow distribution as the splash-cooling devices does not result in a more uniform dome wall temperature. In order for it to be accomplished, a swirler with more than double the mass flow rate should be used in order for the cooling air to penetrate to the outer dome surface. The drawback of doubling the swirler mass flow rate is that the equivalence ratio in the primary zone decreases which may result in stability problems at off-design operating conditions. Also, NO_x emission levels might increase due to the primary combustion zone being more fuel lean and therefore operating at conditions closer to the stoichiometric air/fuel ratio. The swirler does, however, enhance the recirculation flow in the primary combustion zone compared with the original combustion chamber. An enhanced recirculation zone will ensure more efficient mixing of the fuel and air which may result in increased combustion efficiency.

From the above discussion, it is evident that by simply replacing the existing splash-cooling devices with an axial air swirler will not result in an adequate solution. When the swirler mass flow rate was increased to attempt to lower the temperature distribution on the dome wall, the equivalence ratio in the primary combustion zone was altered. Due to the change, stable combustion at other operating conditions cannot be guaranteed since these analyses were only conducted at a single operating condition.

To incorporate the swirlers of case 4 and case 5 into the combustion chamber, the primary zone airflow should be reduced to maintain the pressure loss. An investigation should also be conducted to ensure combustion performance at other operating conditions.

6.3   Recommendations for future work

Recommendations for future work, related to this study, can be summarised as follow:

- Investigation to improve the equivalence ratio in the primary combustion zone by re-designing the size and location of the primary jets. Also, investigating the influence of reduced film-cooling air along the combustor liner.

- Include radiation in all the numerical models and describe the external heat transfer coefficient and material conductivity in a user-define-function (UDF). Constant values were used during this study.

- Increase swirler blade angle to 45º or 50º with mass flow distribution of 13.85 percent and investigate dome wall temperature with improved design.

- Experimental verification of the dome wall temperatures as well as the swirler designs should be conducted.

- The effect of emission levels for each swirler should be investigated.

- The data utilised for each element in the network model should be generated in a more generic way since the data had to be inserted individually for every element, making it a time-consuming task.

REFERENCES

Adkins, R.C. and Gueroui, D., 1986, "An Improved Method for Accurate Prediction of Mass Flows Through Combustor Liner Holes", Journal of Engineering for Gas Turbine and Power, Vol. 108, pp 491-497

Ballal, D.R. and Lefebvre, A.H., 1986, "A Proposed Method for Calculating Film-cooled Wall Temperatures in Gas Turbine Combustion Chambers", ASME Paper No. 72-WA/HT-24

Baron, F., Kanniche, M. and Mechitoua, N., 1994, "Influence of Inlet Conditions on Flow and Combustion Characteristics of a Model Annular Combustor, ASME Paper No. 94-GT-281

Biswas, D., Kawano, K., Iwasaki, H. and Ishizuka, M., 1997, "Three-Dimensional Computation of Gas Turbine Combustors and the Validation Studies of Turbulence and Combustion Models", ASME Paper No. 97-GT-362

Cia, J., Jeng, S.M. and Tacina, R., 2002, "Multi-Swirler Aerodynamics: Comparison of Different Configurations", AMSE Paper No, GT-2002-30464

Crocker, D.S. and Smith, C.E., 1995, "Numerical Investigation of Enhanced Dilution Zone Mixing in a Reverse Flow Gas Turbine Combustor", Journal of Engineering for Gas Turbine and Power, Vol. 177, pp 272-281

Crocker, D.S., Nickolaus, D. and Smith, C.E., 1999, "CFD Modeling of a Gas Turbine Combustor from Compressor Exit to Turbine Inlet", Journal of Engineering for Gas Turbine and Power, Vol. 121, pp. 89-95

Dodds, W.J., and Bahr, D.W., 1990, "Combustion System Design", in A.M. Mellor, ed., "Design of Modern Gas Turbine Combustors", pp 343-476, Academic Press, San Deigo

Eccles, N.C. and Priddin, C.H., 1999," Accelerated Combustion Design using CFD", ISABE Paper No. 99-7094

Feitelberg, A.S. and Lacey, M.A., 1998, " The GE Rich-Quench-Lean Gas Turbine Combustor, Journal of Engineering for Gas Turbine and Power, Vol 120, pp. 502-508

Fuller, E.J. and Smith, C.E., 1993, "Integrated CFD Modeling of Gas Turbine Combustors", AIAA, A93-50008

Gosselin, P., De Champlain, A., Kretschmer, D., 1999," Prediction of Wall Heat Transfer for a Gas Turbine Combustor", Journal of Power and Energy, Vol. 213, pp. 169-180

Graves, C.C. and Gronman, J.S., 1957, "Theoretical Analysis for Tubular Turbojet Combustors with Constant Annulus and Liner Cross-Sectional Areas", NACA Report 1373

Greyvenstein, G.P. and Laurie, D.P., 1994, "A Segregated CFD Approach to Pipe Network Analysis", International Journal for Numerical Methods in Engineering, Vol. 37, p3685 − 3705

Guoqiang, L. and Gutmarl, E.J., 2004, "Effects of Swirler Configuration on Flow Structures and Combustion Characteristics", ASME Paper No. GT2004-53674

Gupta, A.K. and Lewis, M.J., 1998, "Effect of Swirl on Combustion Characteristics in Premixed Flames", Transactions of the ASME, Vol. 120, July, pp. 488-494

Gupta, A.K., Lilley, D.G. and Syred, N., 1984, "Swirl Flow − (Energy and engineering science series)", Abacus Press

Hicks, R.A. and Wilson, C.W., 1999, "Comparison between measured and predicted wall temperatures in gas turbine combustors", ASME Paper No. 99-GT-59

Hoertzer, K., Haswlbacher, H., Griffiths, A.J., Syred, N. and Fraser, T.A., 2002, "CFD-Analysis of the Combustion in the Primary Stage of a Two-Stage Combustion Chamber", ASME Paper No. GT-2002-30610

Holdeman, J.D., Liscinsky, D.S. and Bain, D.B., 1997, "Mixing of Multiple Jets with a Confined Subsonic Crossflow Part II – Opposed Rows of Orifices in Rectangular Ducts", ASME Paper No. 97-GT-439

Hornsby, C., and Norster, E.R., 1997, "Application of CFD to DLN Combustors", ASME Paper No. 97-GT-371

Hu, T., and Prociw, L.A., 1993,"Recent CFD Applications in Small Gas Turbine Combustion Systems Development", Proc. 81st Symp. Propulsion and Energetic Panel on Fuel and Combustion Technology for Advanced Aircraft Engines, AGARD Conference, Rome, Italy

Joubert, F.M. and Hattingh, H.V., 1982, "Rekenaar-Modellering van 'n Annulere Teenvloei-verbrandingsruim vir Gasturbienenjins", Journal of Aeronautical Society, Vol. 3, pp 44-50

Knight, H.A. and Walker, R.B., 1953, "The Component Pressure Losses in Combustion Chambers" Aeronautical Research Council R and M 2987, England

Kretschmer, D., and Odgers, J., 1978, "A Simple Method for the Prediction of Wall Temperatures in Gas Turbines", ASME Paper No. 78-GT-90

Lawson, R.J., 1993, "Computational Modeling of an Aircraft Engine Combustor to Achieve Target Exit Temperature Profiles", ASME Paper No. 93-GT-164

Lefebvre, A.H., 1998, "Gas Turbine Combustion" 2nd Edition, Taylor & Francis

Lefebvre, A.H. and Norster, E.R., 1969, "The Design of Tubular Gas Turbine Combustion Chambers for Optimum Mixing Performance", Proceedings of the Institution of Mechanical Engineers, Vol. 183, pp. 150-155

Liedtke, O., Schulz, A., and Wittig, S., 2002, "Design Study of a Lean Premixed Prevaporozed Counter Flow Combustor for a Micro Gas Turbine", ASME Paper No. GT-2002-30074

Lienhard IV, J.H. and Lienhard V, J.H., 2003, "The heat transfer textbook – third edition", Phlogiston Press, Cambridge Massachusetts

Malecki, R.E., Rhie, C.M., McKinney, R.G., Quyang, H., Colet, M.B., and Madabhushi, R.K., 2001, "Application of an Advanced CFD-Based analysis system to the PW6000 Combustor to Optimize Exit Temperature Distribution – Part 1: Description and Validation of the Analysis Tool", ASME Paper No. 2001-GT-0062

Mattingly, J.D., Heiser, W.H., Pratt, D.T., 2002, "Aircraft Engine Design Second Edition", AIAA Education Series

McGuirk, J.J. and Palma, J.M.L.M., 1993, "The Flow Inside a Model Gas Turbine Combustor: Calculations", Journal of Engineering for Gas Turbines and Power, Vol. 115, pp 594-602

McGuirk, J.J. and Spencer, A., 2000, "Coupled and Uncoupled CFD Prediction of the Characteristics of Jets from Combustor Air Admission Ports", ASME Paper 2000-GT-0125

McGuirk, J.J. and Spencer, A., 2001, "Coupled and Uncoupled CFD Predictions of the Characteristics of Jets from Combustor Air Admission Ports", Journal of Engineering for Gas Turbine and Power, Vol. 123, pp 327-332

Micklow, G.J., Roychoudhury, S., Nguyen, H.L. and Cline, M.C., 1993, "Emission Reduction by Varying the Swirler Airflow Splits in Advanced Turbine Combustors", Journal of Engineering for Gas Turbines and Power, Vol. 115, pp 563-569

Mongia, H.C., Reynolds, R.S., and Srinivasan, R., 1986, "Multidimensional Gas Turbine Combustor Modeling: Application and Limitations", AIAA Journal, Vol. 24, pp 890-904

Norster, E.R., 1980, "Combustor Aerodynamics", in Northern Research and Engineering Corporation, "The Design and Development of Gas Turbine Combustors", Woburn, Massachusetts, Volume 1

Odgers, J. and Kretschmer, D., 1980a "Performance evaluation and the Prediction of Pollutant Formation", in Northern Research and Engineering Corporation, "The Design and Development of Gas Turbine Combustors", Woburn, Massachusetts, USA, Volume 2

Odgers, J. and Kretschmer, D., 1980b, "Basic Design Method – Can Combustors", in Northern Research and Engineering Corporation, "The Design and Development of Gas Turbine Combustors", Woburn, Massachusetts, USA, Volume 2

Rizk, N.K., 1994, "A Quasi-3D Calculation Method for Gas Turbine Combustor Liner Wall Cooling Techniques", ASME Paper No. 94-GT-316

Samuel, B.P., 1961, "A Jet Engine Combustor Design Analysis Suitable for Electronic Computers", ASME Paper No. 61-WA-305

Shih, T.H., Liou, W.W., Shabbir, Yang, Z. and Zhu, J., 1995, "A New k-ε Eddy Viscosity Model for High Reynolds Number Turbulent Flows - Model Development and Validation", Computers Fluids, Volume 24, pp.227-238,

Sivaramakrishna, G., Muthuveerappan, N., Vankataraman, S., Sampathkumaran, T.K., 2001, "CFD Modeling of Aero Gas Turbine Combustors", ASME Paper No. 2001-GT-0063

Skidmore, F.W., 1986, "Smoke Emission Tests on Series II and Series III Allison T56 Turboprop Engines", ARL Aero-Prop-TM-438

Skidmore, F.W., Bennett, J.M., and Glenny, D.E., 1995, "An Investigation into Hard Carbon Formation in a Modified Gas Turbine Combustor", ISABE 95-7116

Skidmore, F.W., 2004, Private Communication, Brisbane Australia

Smiljanovski, V. and Brehm N., 1999, "CFD Liquid Spray Combustion of a Single Annular Gas Turbine Combustor", ASME Paper No. 99-GT-300

Snyder, T.S., Stewart, J.F., Stoner, M.D., McKinney, R.G., 2001, "Application of an Advanced CFD-Based Analysis System to the PW6000 Combustor to Optimize Exit Temperature Distribution – Part II: Comparison of Predictions to Full Annular Rig Test Data", ASME Paper 2001-GT-0064

Sturgess, G.J., Sloan, D.G., Lesmerises, A.L., Heneghan, S.P., and Ballal D.R., 1992 "Design and Development of a Research Combustor for Lean Blow-out Series", Journal of Engineering for Gas Turbine and Power, Vol. 114, pp. 13-19

Stuttaford, P.J. and Rubini, P.A., 1997, "Preliminary gas turbine combustor design using a network Approach", Journal of Engineering for Gas Turbine and Power, Vol. 119, pp. 547-552

Stuttaford, P.J., 1997, "Preliminary Gas Turbine Combustor Design Using a Network Approach", PhD Thesis, Cranfield University

Tangirala, V.E., Tolpadi, A.K., Danis, AL, M. and Mongia, H.,2000, "Parametric Modeling Approach to Gas Turbine Combustor Design", ASME Paper No. 2000-GT-129

Van Niekerk, J.E. and Morris, R.M., 2001, "T56 Isothermal tests and CFD predictions", PTE/01/003/1

Versteeg, H.K. and Malalasekera, W., 1995, "An Introduction to Computational Fluid Dynamics – The Finite Volume Method", Prentice Hall

Yun, S., Lightstone, M.F. and Thomson, M.J., 2005, "An Evaluation of Beta PDF Integration using the Density-weighted PDF and the un-weighted PDF", International Journal of Thermal Sciences, Vol. 44, pp 421-428

APPENDIX A -

Material Properties

A1.   Material properties of Hastelloy-X

Figure A.1 and table A.1 depicts the results obtained from the electron microscope at the University of Pretoria in South Africa. Table A.2 present the typical composition of the material respectively. After comparing the data with various compositions, Hastelloy-X proved to have the closest agreement with the experimental data. For this reason it was concluded that the combustion chamber was manufactured from Hastelloy-X. The material properties for the material, and used during the study, are presented in table A.3. Although some of the properties were a function of the temperature, mean values were used during the study
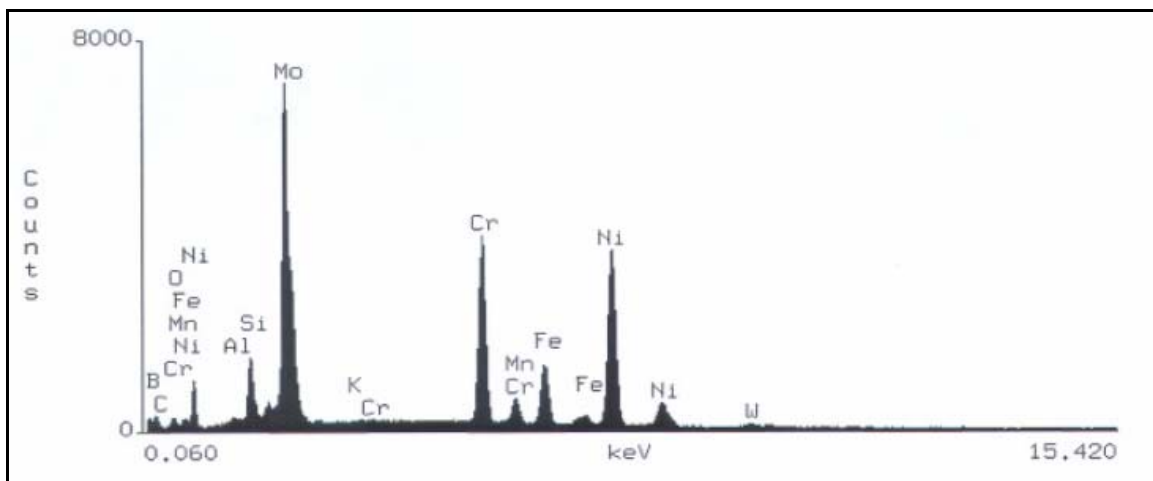
Figure A.1: Electron microscope results of Hastelloy-X

Table A1: Experimental composition of material

Element	k-ratio	ZAF	Atom %	Element	Wt % Err.	
	(calc.)			Wt %	(3-Sigma)	
Al-K	0.001	4.91	1.6	0.7	+ / -	0.2
Si-K	0.002	3.34	1.4	0.7	+ / -	0.1
Cr-K	0.216	0.98	23.6	21.2	+ / -	0.4
Mn-K	0.007	0.99	0.7	0.7	+ / -	0.2
Fe-K	0.18	1.02	19	18.4	+ / -	0.5
Ni-K	0.434	1.1	47.1	47.9	+ / -	0.8
Mo-K	0.071	1.16	5	8.2	+ / -	2
Co-K	0.012	1.11	1.3	1.3	+ / -	0.2
W-M	0.004	2.32	0.3	0.9	+ / -	0.4
Total			100	100		

Table A.2: Typical material composition

Elements	Min [%]	Max[%]
Molybdenum	8	10
Chromium	20.5	23
Iron	17	20
Tingsten	0.2	1
Cobalt	0.5	2.5
Carbon	0.05	0.015
Silicon	--	1
Manganese	--	1
Boron	--	0.01
Phosphorus	--	0.04
Sulfur	--	0.03
Nickel	Remainder	

Table A.3: Material properties

Density [kg/m3]	8820
Thermal conductivity [W/m.K]	16.9
External emissivity	465
Spesific heat Cp [J/kg.K]	465

APPENDIX B –

Grid independence study

B.1   Grid independence study

A study was conducted on three different mesh sizes consisting of 500 000, 1000 000, and 1500 000 cells to determine grid independency. Figure B.1 depicts the numerical exit temperature distribution obtained from each mesh size, and compares it to the experimental exit temperature distribution obtained by Skidmore (2004). From the study close agreement between the three cases are evident. Nonetheless, the results obtained from 1000 000 cells shows closest agreement with experimental data. Due to the availability of computer recourses and to keep the computational time relatively low, it was considered that a 1000 000 cells result in comparatively good results and consequently having grid independence.
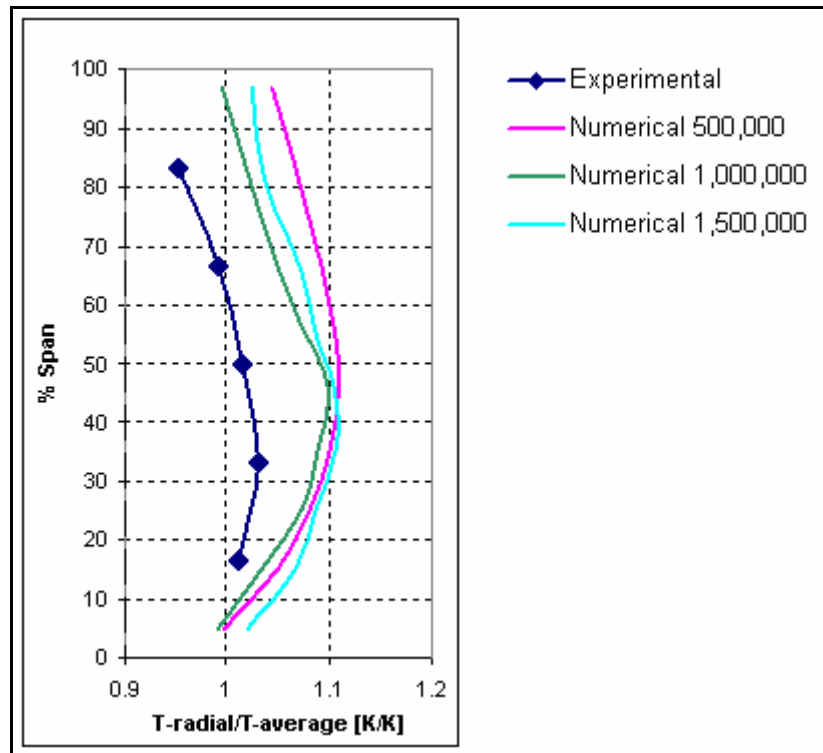
Figure B.1: Grid independency study

B.2   Effect of radiation on the liner wall temperatures

Radiation was modeled using the P-1 radiation model, which is a non-equilibrium diffusion type model, and the variation of the mixture's absorption coefficient was taken into account using the Weighted-Sum-of-Gray-Gases model. The effect of radiation was

investigated only on the base case model and compared with a similar model without radiation. Figure B.2.depicts the average liner wall temperature along the combustor liner with and without radiation and figure B.3 depict the effect of radiation on the exit temperature profile.

The effect of radiation on the liner wall temperature was found to be a maximum of 10% on the dilution zone area and not more than 2% on the average exit temperature distribution.
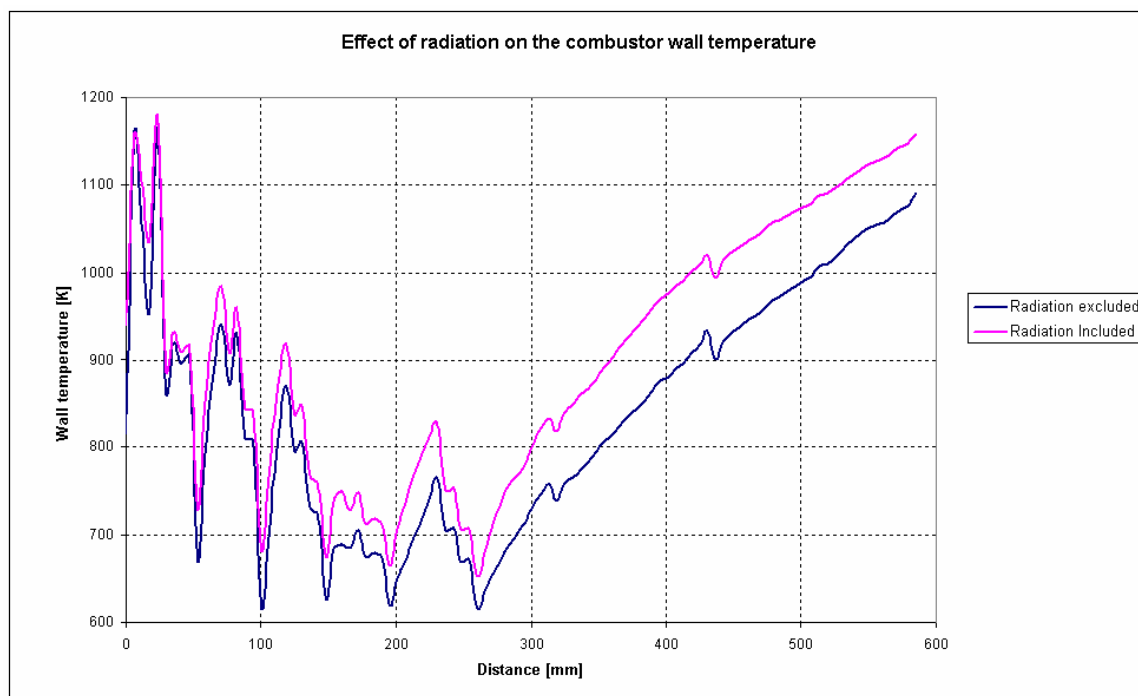
Figure B.2: Effect of radiation on the combustor average axial wall temperature
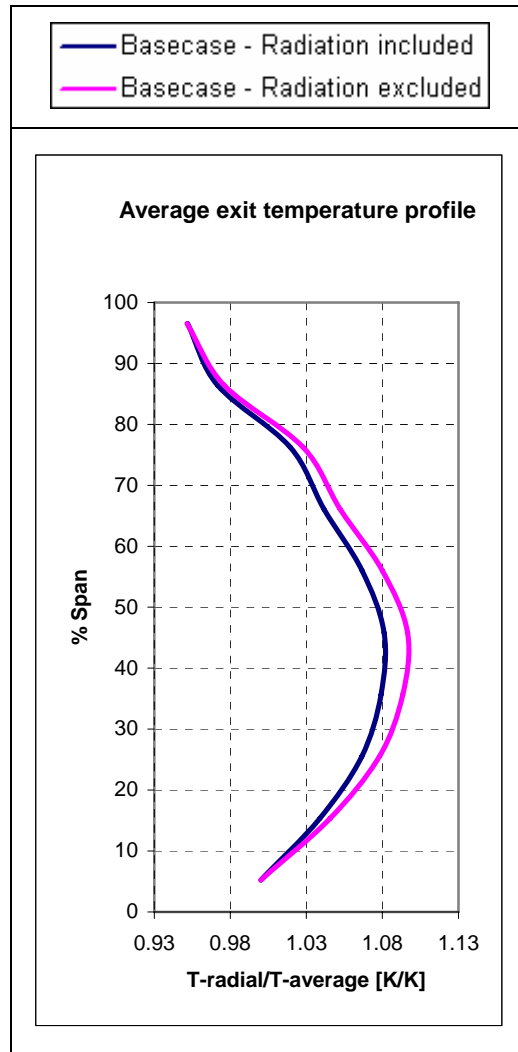
Figure B.3: Effect of radiation on the average outlet temperature distribution

APPENDIX C –

Empirical swirler design program

C.1   Empirical swirler design code

-- **Inputs** --

THETA=[30 31 32 33 34 35 36 37 38 39 40 45 50 55];	**[Swirler blade angles [degrees]]**
massf=[5 6 7 8 9 10 11 12 13.67 14 15 16];	**[Percentage mass flow rate through swirler [%]]**
[q r]=size(THETA);	
[s t]=size(massf);	
P=923897;	**[Combustor inlet pressure [Pa]]**
T=566.15;	
R=287;	**[Gas constant]**
dP=5.1;	**[Percentage pressure drop over combustor]**
Psw=P*(dP/100);	**[Swirler pressure loss [Pa]]**
Ksw=1.3;	**[Blade loss coefficient]**
L=0.1403;	**[Average combustor diameter [m]]**
AL=(pi*L^2)/4;	**[Average combustor flow are [m^2]]**
ma=2.37642;	**[Combustor total flow rate [kg/s]]**
Injector_diam=0.0324;	**[Fuel injector diameter [m]]**
Hub_and_Ring_th=0.0015;	**[Swirler hub and outer ring material thickness [m]]**
Vane_th=0.001;	**[Swirler vane material thickness [m]]**
Dhub=Injector_diam+(2*Hub_and_Ring_th);	
Solidity=1;	
Swirler_width=0.01;	**[Swirler width [m]]**
rho=P/(R*T);	**[Density [kg/m^3]]**

CALCULATIONS

```
ntel =0
for i=1:r
   ntel=ntel+1
   for j=1:t
      m=massf(j);                          [Percentage swirler mass flow rate]
      msw=ma*(m/100);                      [Swirler mas flow rate [kg/s]]
      theta(i)=THETA(i)*(pi/180);          [Swirler blade angle [radiant]]

   Calculate initial swirler flow area
```

```
      Asw=sqrt((msw^2*Ksw*(sec(theta(i))^2))/((2*rho*Psw)+((msw^2*Ksw)/AL^2)));
```

```
      Lv=Swirler_width/cos(theta(i));              [Swirler blade length]

      Dsw=0.02;                                     [Initial swirler blade tip diameter [m]]
      ASW=1;                                        [Initial swirler area]
      converg=1;
```

[Determine the number of swirler blades, from which the swirler blade tip diameter will be calculated]:

```
while abs(converg) > 0.00000001

        Number of swirler blades
        n=round((pi*Dsw)/(Lv/Solidity));

         Swirler flow area
        ASW=(pi/4)*(Dsw^2-Dhub^2)-0.5*n*(Vane_th/cos(theta(i)))*(Dsw-Dhub);

        converg=Asw-ASW;
        Dsw=Dsw+0.0000001;
     end
```

[Calculate swirl number and swirler loss coefficient]:

```
    DSW(i,j)=Dsw;
    N(i,j)=n;

        Swirl number
    SN(i,j)=(2/3)*((1-(Dhub/DSW(i,j))^3)/(1-(Dhub/DSW(i,j))^2))*tan(theta(i));

    Sw_area(i,j)=ASW;

     Loss coeff
    Loss_coeff(i,j)=(Sw_area(i,j)^2)*(Ksw*(((sec(theta(i))^2)/(Sw_area(i,j)^2)))-1/AL^2); [Loss coeff.]
```

[Calculate hydraulic diameter of single swirler opening]:

```
        Blade half thickness
        B_half_thick=(Vane_th/cos(theta(i)))/2;

        Blade height
        Blade_height=(Dsw-Dhub)/2;

        Inner arc length of single opening
        half_blade_angle=(B_half_thick/(Dhub/2))*2;
        arc_angle=(((2*pi)/n)-half_blade_angle);
        inner_arc_length=(Dhub/2)*arc_angle;

        Outer arc length of single opening
        Half_Blade_Angle=(B_half_thick/(Dsw/2))*2;
        Arc_Angle=(((2*pi)/n)-Half_Blade_Angle);
        Outer_Arc_length=(Dsw/2)*Arc_Angle;

        Calculate wettet perimiter
        P=(2*Blade_height)+(inner_arc_length+Outer_Arc_length);

        Calculate hydroulic diameter
        Hd(i,j)=(4*(ASW/n))/P;
   end
end
```

[Write output file]

```
THeta='Vane Angle:   ';
Massflow='m_sw [%]';
dswirler='D_sw [mm]';
number_of_vanes='N_vanes';
Swirl_n='SN';
W='Swirler Width [mm]:  ';
S_area='Asw [m^2]';
Loss='Loss Coeff';
Hyd='Hydr_D [mm]';
Design_data='******** Design data  *******';
Pressure='Total Pressure [Pa]       ';
Temp='Temperature [K]          ';
dp='Pressure drop [%]         ';
massflow='Total Massflow [kg/s]     ';
Injector_d='Injector diameter [mm]    ';
Blade_th='Blade thickness [mm]      ';
Sol='Solidity at tip          ';
Hub_ring='Hub & Ring thickness [mm]  ';
Swirler_w='Swirler width [mm]        ';
final=('****************************************');

fid=fopen('Swirler Data.txt','w');

fprintf(fid,'%6s\n',Design_data);
fprintf(fid,'\n');
fprintf(fid,'%6s',Pressure);
fprintf(fid,'%2.0f\n',P);
fprintf(fid,'%6s',Temp);
fprintf(fid,'%2.2f\n',T);
fprintf(fid,'%6s',dp);
fprintf(fid,'%2.3f\n',dP);
fprintf(fid,'%6s',massflow);
fprintf(fid,'%2.3f\n',ma);
fprintf(fid,'%6s',Injector_d);
fprintf(fid,'%2.3f\n',Injector_diam*1000);
fprintf(fid,'%6s',Blade_th);
fprintf(fid,'%2.3f\n',Vane_th*1000);
fprintf(fid,'%6s',Sol);
fprintf(fid,'%2.2f\n',Solidity);
fprintf(fid,'%6s',Hub_ring);
fprintf(fid,'%2.3f\n',Hub_and_Ring_th*1000);
fprintf(fid,'%6s',Swirler_w);
fprintf(fid,'%2.3f\n',Swirler_width*1000);
fprintf(fid,'%6s\n',final);
fprintf(fid,'\n');

for i=1:r;

  th=THETA(i);

  fprintf(fid,'%18s',THeta);
  fprintf(fid,'%1.1f\n',th);
  fprintf(fid,'%18s',W);
  fprintf(fid,'%1.2f',Swirler_width*1000);
```

```
    fprintf(fid,'\n');
    fprintf(fid,'\n');
    fprintf(fid,'%s',Massflow);
    fprintf(fid,'%13s',dswirler);
    fprintf(fid,'%12s',number_of_vanes);
    fprintf(fid,'%8s',Swirl_n);
    fprintf(fid,'%16s',S_area);
    fprintf(fid,'%14s',Loss);
    fprintf(fid,'%13s\n',Hyd);

    for j=1:t;

        M=massf(j);
        D=DSW(i,j);
        NUM=N(i,j);
        Sn=SN(i,j);
        Loss_C=Loss_coeff(i,j);
        Area=Sw_area(i,j);
        HD=Hd(i,j);

        fprintf(fid,'%7.3f',M);
        fprintf(fid,'%15.2f',D*1000);
        fprintf(fid,'%9.0f',NUM);
        fprintf(fid,'%11.2f',Sn);
        fprintf(fid,'%15.8f',Area);
        fprintf(fid,'%11.2f',Loss_C);
        fprintf(fid,'%14.5f\n',HD*1000);
    end

    fprintf(fid,'\n');
    fprintf(fid,'\n');

end
fclose(fid);
```

C.2   Swirler lookup tables (Program output)

(These specific tables were used to design the swirlers of case 4 & 5)

```
********   Design data   *******

Total Pressure [Pa]        0
Temperature [K]            566.15
Pressure drop [%]          5.100
Total Massflow [kg/s]      2.376
Injector diameter [mm]     32.400
Blade thickness [mm]       1.000
Solidity at tip            1.00
Hub & Ring thickness [mm]  1.500
Swirler width [mm]         10.000
*******************************************
```

```
   Vane Angle:   30.0
Swirler Width [mm]:  10.00
```

m_sw [%]	D_sw [mm]	N_vanes	SN	Asw [m^2]	Loss Coeff	Hydr_D [mm]
5.000	39.47	11	0.55	0.00021369	1.73	3.35678
6.000	40.23	11	0.54	0.00025641	1.73	3.86495
7.000	40.98	11	0.54	0.00029914	1.73	4.33699
8.000	41.71	11	0.53	0.00034186	1.73	4.77782
9.000	42.49	12	0.53	0.00038458	1.73	5.09273
10.000	43.20	12	0.53	0.00042728	1.73	5.46449
11.000	43.89	12	0.52	0.00046999	1.73	5.81505
12.000	44.57	12	0.52	0.00051268	1.73	6.14679
13.670	45.69	12	0.52	0.00058395	1.73	6.66431
14.000	45.91	12	0.51	0.00059803	1.73	6.76174
15.000	46.65	13	0.51	0.00064070	1.73	6.85171
16.000	47.30	13	0.51	0.00068335	1.73	7.11037

```
   Vane Angle:   31.0
Swirler Width [mm]:  10.00
```

m_sw [%]	D_sw [mm]	N_vanes	SN	Asw [m^2]	Loss Coeff	Hydr_D [mm]
5.000	39.52	11	0.57	0.00021589	1.77	3.38658
6.000	40.29	11	0.57	0.00025906	1.77	3.89789
7.000	41.04	11	0.56	0.00030223	1.77	4.37267
8.000	41.77	11	0.56	0.00034539	1.77	4.81572
9.000	42.50	11	0.55	0.00038855	1.77	5.23127
10.000	43.28	12	0.55	0.00043170	1.77	5.50427
11.000	43.98	12	0.54	0.00047484	1.77	5.85615
12.000	44.67	12	0.54	0.00051797	1.77	6.18907
13.670	45.79	12	0.54	0.00058999	1.77	6.70839
14.000	46.01	12	0.53	0.00060421	1.77	6.80613
15.000	46.77	13	0.53	0.00064732	1.77	6.89434
16.000	47.42	13	0.53	0.00069041	1.77	7.15372

```
   Vane Angle:   32.0
Swirler Width [mm]:  10.00
```

m_sw [%]	D_sw [mm]	N_vanes	SN	Asw [m^2]	Loss Coeff	Hydr_D [mm]
5.000	39.57	11	0.59	0.00021821	1.81	3.41779
6.000	40.34	11	0.59	0.00026185	1.81	3.93243
7.000	41.10	11	0.58	0.00030548	1.81	4.40993
8.000	41.84	11	0.58	0.00034911	1.81	4.85539
9.000	42.57	11	0.57	0.00039273	1.81	5.27301
10.000	43.36	12	0.57	0.00043634	1.81	5.54576
11.000	44.07	12	0.57	0.00047995	1.81	5.89906
12.000	44.77	12	0.56	0.00052355	1.81	6.23329
13.670	45.90	12	0.56	0.00059633	1.81	6.75439
14.000	46.12	12	0.56	0.00061071	1.81	6.85250
15.000	46.78	12	0.55	0.00065428	1.81	7.14082
16.000	47.54	13	0.55	0.00069784	1.81	7.19892

Vane Angle: 33.0
Swirler Width [mm]: 10.00

m_sw [%]	D_sw [mm]	N_vanes	SN	Asw [m^2]	Loss Coeff	Hydr_D [mm]
5.000	39.57	10	0.62	0.00022065	1.85	3.48342
6.000	40.40	11	0.61	0.00026478	1.85	3.96854
7.000	41.17	11	0.61	0.00030889	1.85	4.44889
8.000	41.92	11	0.60	0.00035301	1.85	4.89686
9.000	42.65	11	0.60	0.00039712	1.85	5.31660
10.000	43.38	11	0.59	0.00044122	1.85	5.71163
11.000	44.17	12	0.59	0.00048531	1.85	5.94388
12.000	44.87	12	0.58	0.00052940	1.85	6.27936
13.670	46.02	12	0.58	0.00060300	1.85	6.80239
14.000	46.24	12	0.58	0.00061754	1.85	6.90083
15.000	46.91	12	0.57	0.00066160	1.85	7.19014
16.000	47.67	13	0.57	0.00070564	1.85	7.24605

Vane Angle: 34.0
Swirler Width [mm]: 10.00

m_sw [%]	D_sw [mm]	N_vanes	SN	Asw [m^2]	Loss Coeff	Hydr_D [mm]
5.000	39.62	10	0.64	0.00022322	1.89	3.51848
6.000	40.46	11	0.63	0.00026786	1.89	4.00633
7.000	41.24	11	0.63	0.00031249	1.89	4.48968
8.000	41.99	11	0.62	0.00035711	1.89	4.94019
9.000	42.74	11	0.62	0.00040173	1.89	5.36214
10.000	43.47	11	0.61	0.00044635	1.89	5.75912
11.000	44.27	12	0.61	0.00049096	1.89	5.99065
12.000	44.98	12	0.61	0.00053555	1.89	6.32746
13.670	46.14	12	0.60	0.00061001	1.89	6.85246
14.000	46.36	12	0.60	0.00062472	1.89	6.95120
15.000	47.04	12	0.59	0.00066929	1.89	7.24154
16.000	47.70	12	0.59	0.00071384	1.89	7.51933

Vane Angle: 35.0
Swirler Width [mm]: 10.00

m_sw [%]	D_sw [mm]	N_vanes	SN	Asw [m^2]	Loss Coeff	Hydr_D [mm]
5.000	39.67	10	0.66	0.00022591	1.94	3.55523
6.000	40.47	10	0.66	0.00027108	1.94	4.09772
7.000	41.31	11	0.65	0.00031626	1.94	4.53227
8.000	42.08	11	0.65	0.00036142	1.94	4.98547
9.000	42.83	11	0.64	0.00040658	1.94	5.40972
10.000	43.57	11	0.64	0.00045174	1.94	5.80871
11.000	44.29	11	0.63	0.00049688	1.94	6.18540
12.000	45.10	12	0.63	0.00054201	1.94	6.37757
13.670	46.27	12	0.62	0.00061737	1.94	6.90454
14.000	46.49	12	0.62	0.00063225	1.94	7.00368
15.000	47.17	12	0.62	0.00067736	1.94	7.29507
16.000	47.84	12	0.61	0.00072246	1.94	7.57384

Vane Angle: 36.0
Swirler Width [mm]: 10.00

m_sw [%]	D_sw [mm]	N_vanes	SN	Asw [m^2]	Loss Coeff	Hydr_D [mm]
5.000	39.73	10	0.69	0.00022874	1.99	3.59359
6.000	40.53	10	0.68	0.00027448	1.99	4.14032
7.000	41.38	11	0.68	0.00032022	1.99	4.57679
8.000	42.16	11	0.67	0.00036595	1.99	5.03270
9.000	42.92	11	0.66	0.00041167	1.99	5.45932
10.000	43.67	11	0.66	0.00045739	1.99	5.86041
11.000	44.40	11	0.66	0.00050310	1.99	6.23895
12.000	45.12	11	0.65	0.00054880	1.98	6.59755
13.670	46.40	12	0.64	0.00062510	1.98	6.95884
14.000	46.63	12	0.64	0.00064017	1.98	7.05834
15.000	47.32	12	0.64	0.00068585	1.98	7.35080
16.000	47.99	12	0.64	0.00073151	1.98	7.63057

```
    Vane Angle:   37.0
Swirler Width [mm]:  10.00

m_sw [%]      D_sw [mm]  N_vanes      SN     Asw [m^2]   Loss Coeff  Hydr_D [mm]
   5.000        39.79       10       0.71   0.00023172      2.04       3.63388
   6.000        40.60       10       0.71   0.00027805      2.04       4.18486
   7.000        41.40       10       0.70   0.00032438      2.04       4.69710
   8.000        42.25       11       0.69   0.00037071      2.04       5.08201
   9.000        43.02       11       0.69   0.00041703      2.04       5.51113
  10.000        43.78       11       0.68   0.00046334      2.04       5.91432
  11.000        44.52       11       0.68   0.00050964      2.04       6.29478
  12.000        45.25       11       0.67   0.00055594      2.04       6.65515
  13.670        46.54       12       0.67   0.00063323      2.04       7.01536
  14.000        46.77       12       0.67   0.00064850      2.04       7.11527
  15.000        47.47       12       0.66   0.00069476      2.04       7.40879
  16.000        48.15       12       0.66   0.00074102      2.04       7.68961


    Vane Angle:   38.0
Swirler Width [mm]:  10.00

m_sw [%]      D_sw [mm]  N_vanes      SN     Asw [m^2]   Loss Coeff  Hydr_D [mm]
   5.000        39.85       10       0.74   0.00023484      2.09       3.67591
   6.000        40.68       10       0.73   0.00028180      2.09       4.23139
   7.000        41.48       10       0.73   0.00032876      2.09       4.74750
   8.000        42.27       10       0.72   0.00037571      2.09       5.22951
   9.000        43.13       11       0.71   0.00042265      2.09       5.56513
  10.000        43.89       11       0.71   0.00046959      2.09       5.97058
  11.000        44.64       11       0.70   0.00051652      2.09       6.35302
  12.000        45.38       11       0.70   0.00056344      2.09       6.71511
  13.670        46.69       12       0.69   0.00064177      2.09       7.07420
  14.000        46.92       12       0.69   0.00065724      2.09       7.17449
  15.000        47.63       12       0.69   0.00070413      2.09       7.46915
  16.000        48.32       12       0.68   0.00075100      2.09       7.75101


    Vane Angle:   39.0
Swirler Width [mm]:  10.00

m_sw [%]      D_sw [mm]  N_vanes      SN     Asw [m^2]   Loss Coeff  Hydr_D [mm]
   5.000        39.92       10       0.76   0.00023813      2.15       3.72000
   6.000        40.75       10       0.76   0.00028574      2.15       4.28011
   7.000        41.57       10       0.75   0.00033335      2.15       4.80009
   8.000        42.37       10       0.75   0.00038096      2.15       5.28553
   9.000        43.24       11       0.74   0.00042856      2.15       5.62147
  10.000        44.01       11       0.73   0.00047615      2.15       6.02918
  11.000        44.77       11       0.73   0.00052374      2.15       6.41365
  12.000        45.52       11       0.72   0.00057131      2.15       6.77756
  13.670        46.73       11       0.72   0.00065074      2.15       7.34553
  14.000        46.97       11       0.71   0.00066643      2.15       7.45248
  15.000        47.79       12       0.71   0.00071397      2.15       7.53193
  16.000        48.49       12       0.71   0.00076151      2.15       7.81492


    Vane Angle:   40.0
Swirler Width [mm]:  10.00

m_sw [%]      D_sw [mm]  N_vanes      SN     Asw [m^2]   Loss Coeff  Hydr_D [mm]
   5.000        39.99       10       0.79   0.00024157      2.22       3.76604
   6.000        40.83       10       0.78   0.00028988      2.21       4.33099
   7.000        41.66       10       0.78   0.00033818      2.21       4.85509
   8.000        42.47       10       0.77   0.00038648      2.21       5.34406
   9.000        43.27       10       0.77   0.00043477      2.21       5.80244
  10.000        44.14       11       0.76   0.00048305      2.21       6.09025
  11.000        44.91       11       0.75   0.00053133      2.21       6.47682
  12.000        45.66       11       0.75   0.00057959      2.21       6.84261
  13.670        46.89       11       0.74   0.00066017      2.21       7.41331
  14.000        47.13       11       0.74   0.00067609      2.21       7.52078
  15.000        47.97       12       0.73   0.00072432      2.21       7.59723
  16.000        48.67       12       0.73   0.00077254      2.21       7.88132
```

```
     Vane Angle:   45.0
Swirler Width [mm]:  10.00

m_sw [%]      D_sw [mm]    N_vanes      SN      Asw [m^2]    Loss Coeff   Hydr_D [mm]
   5.000        40.33         9        0.94     0.00026171      2.60        4.07653
   6.000        41.23         9        0.93     0.00031405      2.60        4.69055
   7.000        42.12         9        0.92     0.00036637      2.60        5.26089
   8.000        43.07        10        0.91     0.00041869      2.60        5.67745
   9.000        43.93        10        0.91     0.00047101      2.60        6.15276
  10.000        44.76        10        0.90     0.00052331      2.60        6.59932
  11.000        45.58        10        0.89     0.00057561      2.60        7.02071
  12.000        46.38        10        0.89     0.00062790      2.60        7.41988
  13.670        47.82        11        0.88     0.00071520      2.60        7.79599
  14.000        48.08        11        0.87     0.00073244      2.60        7.90616
  15.000        48.84        11        0.87     0.00078469      2.60        8.23004
  16.000        49.59        11        0.86     0.00083694      2.60        8.54005


     Vane Angle:   50.0
Swirler Width [mm]:  10.00

m_sw [%]      D_sw [mm]    N_vanes      SN      Asw [m^2]    Loss Coeff   Hydr_D [mm]
   5.000        40.77         8        1.12     0.00028790      3.15        4.47438
   6.000        41.75         8        1.10     0.00034547      3.15        5.15000
   7.000        42.81         9        1.09     0.00040303      3.15        5.66972
   8.000        43.75         9        1.08     0.00046059      3.15        6.22840
   9.000        44.67         9        1.07     0.00051814      3.15        6.75122
  10.000        45.57         9        1.06     0.00057568      3.14        7.24291
  11.000        46.45         9        1.06     0.00063321      3.14        7.70734
  12.000        47.46        10        1.05     0.00069073      3.14        7.89994
  13.670        48.87        10        1.04     0.00078676      3.14        8.54403
  14.000        49.14        10        1.03     0.00080573      3.14        8.66528
  15.000        49.97        10        1.03     0.00086322      3.14        9.02196
  16.000        50.77        10        1.02     0.00092068      3.14        9.36355


     Vane Angle:   55.0
Swirler Width [mm]:  10.00

m_sw [%]      D_sw [mm]    N_vanes      SN      Asw [m^2]    Loss Coeff   Hydr_D [mm]
   5.000        41.35         7        1.33     0.00032264      3.95        4.99421
   6.000        42.54         8        1.31     0.00038715      3.95        5.65067
   7.000        43.60         8        1.30     0.00045166      3.95        6.31909
   8.000        44.64         8        1.29     0.00051617      3.95        6.94158
   9.000        45.64         8        1.27     0.00058066      3.95        7.52459
  10.000        46.63         8        1.26     0.00064514      3.95        8.07331
  11.000        47.75         9        1.25     0.00070962      3.95        8.32420
  12.000        48.70         9        1.24     0.00077408      3.95        8.78348
  13.670        50.24         9        1.23     0.00088170      3.95        9.50056
  14.000        50.54         9        1.23     0.00090296      3.95        9.63570
  15.000        51.43         9        1.22     0.00096738      3.95       10.03330
  16.000        52.30         9        1.21     0.00103178      3.95       10.41446
```

APPENDIX D –

Incompressible 1-D code

D.1   1-D empirical program

The one dimensional empirical program utilise empirical correlations throughout. The incompressible pressure drop flow relationships, discussed in Chapter 2, were used to predict pressure losses and flow distributions.

The one-dimensional incompressible code was coded in Matlab 6 and consists of a number of functions which will be described in the subdequent section. The initial section consists of an INPUT function where the primary inputs to the program are defined. The following function called FLOWCHECK is a function that combines the input function and the remaining functions. The remaining functions are FLOWSPLITS, COMBUSTION, ELEMENTS, and HEAT TRANSFER. The function called FLOWSPITS performs the flowsplit and pressure loss predictions and the function, COMBUSTION, calculates the gas temperature at each node along the combustor axis. Combustion efficiency can be accounted for during these calculations. ELEMENTS calculate the relevant properties at each of the nodes that will be used during the HEAT TRANSFER calculations. HEAT TRANSFER predicts the heat transfer along the combustion liner at each node. The following diagram depicts the logic behind the program.
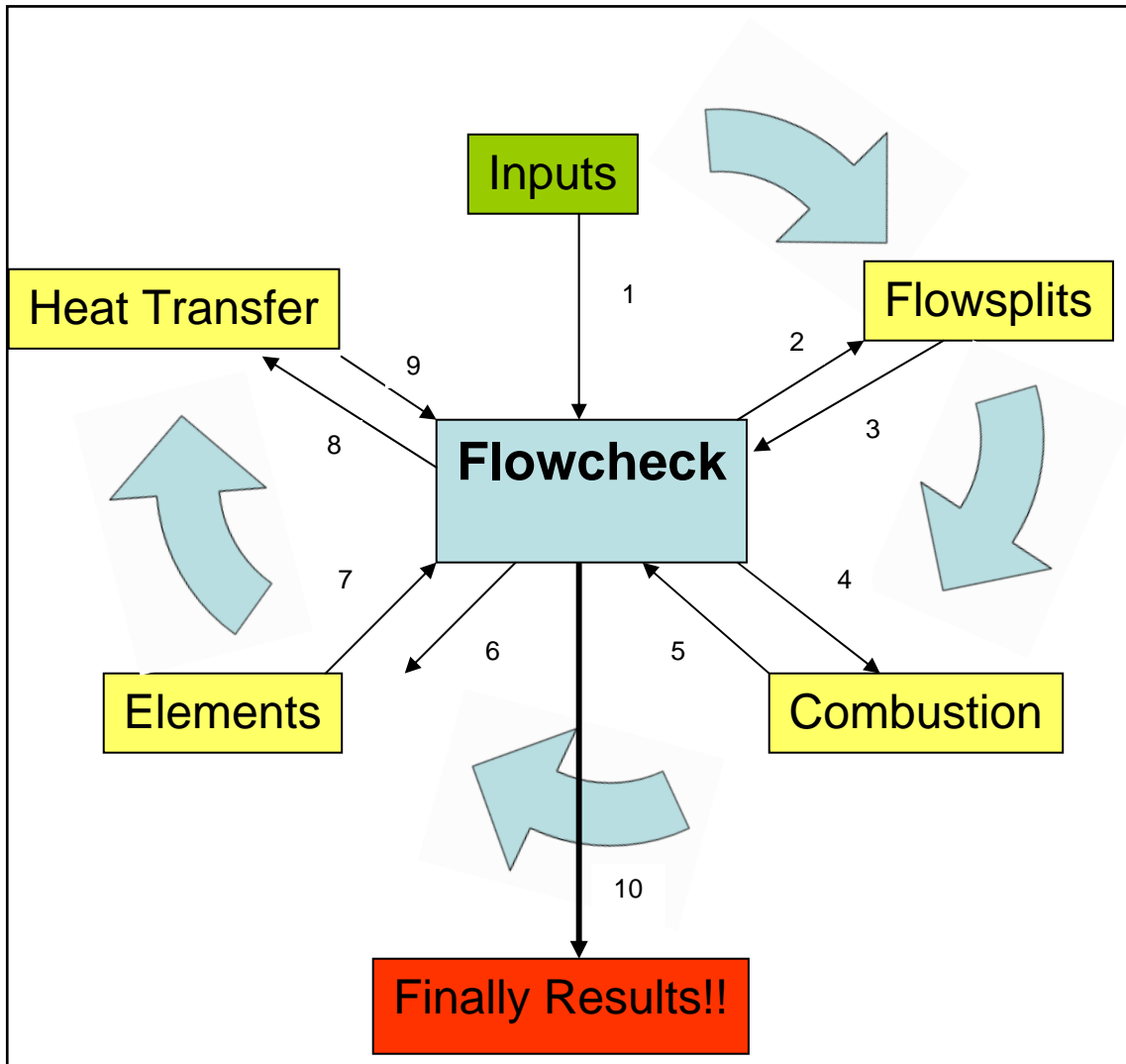
Diagram A.1: Calculation sequence of one-dimensional empirical model

The numbering in the diagram describes the sequence in which calculations are done.

D.2   INPUTS

This file is used to define the inputs to the program

Define function:
----
function[R,Zones,Nodes,Com,T3,P3,ma,S_A_F,Overall_A_F,Rz_boundary,Pz_boundary,Sz_boundary,Total_comb_length,Hole_type,Number_of_holes,...

Hole_diameter,Hole_Position,Discharge_Coeff,cooling_slot_height,slot_height,Rz_flow,Pz_flow,Sz_flow,Dz_flow,Liner_Diameter,...

Casing_outer_Diameter,Casing_inner_Diameter,Casing_Diameter,Amb_temp,eLi,eLo,eCi,eCo,sigma,k_L,k_C,t_L,t_C,Radiation_Model,bb,nn,...

d,s,Nb,nCans,CFD,s_d,steek,qq,Num_elements,DSw_out,DSw_in,BladeTh,NBlades,Theta,K_sw,h0,Outside_conv,Outside_rad,mm,qm]=INPUTS(ii);

General inputs:

R=287.5;   **[Gas constant]**
Zones=4;   **[Number of combustion zones]**
Nodes=25;   **[Number of nodes in each zone]**

Select combustor type:

Com=2   **[Com = 2; Tubular combustor**
                                                       Com = 1; Can-annular combustor]

if Com==1
  nCans=1;
elseif Com ==2
  nCans=6;   **[Define number of combustion chambers in**
                                                        can-annular combustion system]

end

Inlet conditions:

T3=566.15;%Temperature in K   **[Combustor inlet temperature [K]]**
P3=923897;%Pressure in Pa   **[Combustor inlet pressure [Pa]]**
ma=14.25859/nCans;%Total massflow [kg/s]   **[Total flow rate of combustion system [kg/s]]**
S_A_F=14.7;%Stoichiometric air/fuel ratio   **[Stoichiometric air-fuel ratio]**
Overall_A_F=49.75;%Overall air/fuel   **[Operating air-fuel ratio]**
Rz_boundary=75; %[mm] rel to dome   **[Re-circulation zone boundary [mm]]**
Pz_boundary = 95;%[mm] rel to dome   **[Primary zone boundary [mm]]**
Sz_boundary = 245;%[mm] rel to dome   **[Secondary zone boundary [mm]]**
Total_comb_length = 548.5;%[mm] rel to dome   **[Total combustor length [mm]]**

Hole layout:

   [Two options: 1, calculate flow splits(mm=1) or 2, specify flow splits (mm=2)]

```
if mm==2
    [Define individual mass flow rates through hole sets [kg/s]:
    -------------------------------------------------------------------------------------
    qm=[0.0176925 0.085480296 0.059362303 0.3687117 0.1137038 0.1260885 0.1260885
        0.0828009 0.0044821 0.13057065 0.13057065 0.155694 0.0195797 0.11311405 0.11311405
        0.11641665 0.11641665 0.254772 0.04118814 0.1028524 0.0771393 0.02059407];
    -------------------------------------------------------------------------------------
else
    qm=0;
end
```

Define hole type:

```
Hole_type=[1 3 3 4 1 4 4 1 3 4 4 1 3 4 4 4 4 1 3 1 1 3];
```
        1=Plain holes
        2=Plunged holes
        3=Splash cooling device
        4=Wiggle strip
        5=Machined ring
        6=Swirler

Define number of holes in each hole set:

```
Number_of_holes=[1 32 8 44 7 22 22 3 4 22 22 4 8 22 22 22 22 4 8 1 1 4];
```

Define hole diameters of each hole set [mm]:

```
%If holetype == 6 , Hole_diameter = flow area of swirler
Hole_diameter=[7.46 3 5 9 11 9 9 9.02 4.8 9 9 11.254 4.8 9 9 9 9 16 4.8 2 1 4.8]
```

Note: Not DIAMETER of Wiggle strip, but slot width

Define hole set position [mm]:

```
Hole_Position=[0 11.889 22.626 27.5 67.23 74.5 86.5 113.2 113.5 119.2 131.2 156.4 158.5 165.5 177.5
               231.5 242.5 283 314.5 334.4 334.97 434.5];
```

Define hole discharge coefficient – if value is 0, discharge coefficient will be calculated (Set only 0 for Plain and Plunged Holes!!) :

```
Discharge_Coeff =[0.569 0.532 0.532 0.655 0.624 0.448 0.448 0.609 0.087 0.465 0.465 0.552 0.191
                  0.403 0.403 0.416 0.417 0.451 0.406 0.461 0.561 0.418];
```

Define cooling slot height [mm]:

```
cooling_slot_height=[2 2 2 2 2 2 2 2 2 2 2 2 2 2 2];
slot_height=[0 2 2 2 0 2 2 0 2 2 2 0 2 2 2 2 2 0 2 0 0 2];
```
    [cooling_slot_height and slot_height are the same, except for the matrix size]

Define air mass fraction into each zone:

```
%Fraction of Massflow into zone
Rz_flow=[1 1 1 0    0   0 0 0 0 0    0    0   0 0 0 0 0 0 0 0 0 0];          [Recirculation zone]
Pz_flow=[0 0 0 0.333 0.5 0 0 0 0 0    0    0   0 0 0 0 0 0 0 0 0 0];          [Primary zone]
Sz_flow=[0 0 0 0.666 0.5 1 1 1 1 0.333 0.333 0.5 1 0 0 0 0 0 0 0 0 0];        [Secondary zone]
Dz_flow=[0 0 0 0     0 0 0 0 0 0.666 0.666 0.5 0 1 1 1 1 1 1 1 1 1];          [Dilution zone]


[r s]=size(Hole_type);
Nb=s;                                                                         [Number of hole sets]
```

Define liner diameter at each hole set position [mm]:

```
Liner_Diameter=[34 75 75 142 138 142 142 138 138 142 142 138 138 142 142 142 142 138 138 138
               138 138];
```

Define casing diameter at each hole set position [mm]:

```
if Com ==1                                                                   [Tubular combustor]
    Casing_Diameter=[191.3287  191.3287 191.3287 191.3287  191.3287  191.3287  191.3287  191.3287
                    191.3287  191.3287  191.3287  191.3287  191.3287  191.3287  191.3287  191.3287
                    191.3287  191.3287  191.3287  191.3287  191.3287 191.3287 ];
    Casing_outer_Diameter=493*(zeros(1,Nb));
    Casing_inner_Diameter=153*(zeros(1,Nb));

  elseif Com ==2                                                             [Can-annular
                                                                             combustor]

    Casing_Diameter=zeros(1,Nb);
    Casing_outer_Diameter=493*(ones(1,Nb)); %Casing outer diameter at hole
    Casing_inner_Diameter=153*(ones(1,Nb)); %Casing inner diameter at hole

  end
```

Swirler data:

```
DSw_out=23.09;                                                              [Swirler outer diameter
                                                                             [mm]]

DSw_in=13.4;                                                                [Swirler inner diameter
                                                                             [mm]]

BladeTh=1;                                                                  [Blade thickness [mm]]
NBlades=12;                                                                 [Number of blades]
Theta=50;                                                                   [Blade angle]
K_sw=1.3;                                                                   [Blade loss coeff.]
```

Heat transfer:

```
Amb_temp=25;                                                               [Ambient temp [ºC]]
eLi=0.4;                                                                    [Liner inner emisivity]
eLo=0.8;                                                                    [Liner outer emisivity]
eCi=0.8;                                                                    [Casing inner emisivity]
eCo=0.8;                                                                    [Casing outer emisivity]
```

sigma=5.67e-8;   **[Stefan-Boltzmann constant]**

k_L=16.9;   **[Liner wall conductivity]**
k_C=16.9;   **[Casing wall conductivity]**

t_L=1;   **[Liner wall thickness [mm]]**

t_C=1;   **[Casing wall thickness [mm]]**

[Radiation Model (1- Simple, 2-Accurate, 3-Off)]
Radiation_Model = 2;

[Outside Convection (1- Default convection on, 2- Define outside heat transfer coeff, 3- Outside convection off)]
Outside_conv = 3; %1- Default convection on , 2- Define outside heat transfer coeff , 3- Outside convection off

[Outside radiation (1-Outside radiation on, 2- Outside radiation off)]
Outside_rad = 2; % 1- Outside Radiation on , 2- Outside Radiation off

```
if Outside_conv ==2
    h0=input('Define casing outside heat transfer coefficeint : ');
else
    h0=0;
end
```

Properties:

[Turn on/off Film cooling (1-on, 2-off)]
bb=1;

[Account for combustion efficiency (1-on, 2-off)]
nn=1;%input('Do you want to incorp. combustion eff ? (Y/N)-(1/2) ');

Network Solver:

[Print network data file (1-yes, 2-no)]
qq=1; %Do you want to print the network data file? (Y/N)-(1/2)

[Define number of elements between nodes (matrix size same as Nb)]
Num_elements=[4 4 4 4 4 4 4 4 4 4 4 4 4 4 4 4 4 4 4 4 5];

****

D.3   FLOWCHECK

Function:

```
[R,Zones,Nodes,Com,T3,P3,ma,S_A_F,Overall_A_F,Rz_boundary,Pz_boundary,Sz_boundary,Total_com
b_length,Hole_type,Number_of_holes,Hole_diameter,Hole_Position,Discharge_Coeff,cooling_slot_height,
slot_height,Rz_flow,Pz_flow,Sz_flow,Dz_flow,Liner_Diameter,Casing_outer_Diameter,Casing_inner_Dia
meter,Casing_Diameter,Amb_temp,eLi,eLo,eCi,eCo,sigma,k_L,k_C,t_L,t_C,Radiation_Model,bb,nn,d,s,N
b,nCans,CFD,s_d,steek,qq,Num_elements,DSw_out,DSw_in,BladeTh,NBlades,Theta,K_sw,h0,Outside_co
nv,Outside_rad,mm,qm]=INPUTS(ii);
```

Convert data to [m]:

```
Rz_boundary=Rz_boundary/1000;
Pz_boundary=Pz_boundary/1000;
Sz_boundary=Sz_boundary/1000;
Total_comb_length=Total_comb_length/1000;
t_L=t_L/1000;
t_C=t_C/1000;
```

Calculate total number of nodes in computational domain:

```
Number_of_nodes=(Zones*Nodes);%-(Zones-1);
```

Convert ambient temperature from ºC to K:

```
Tamb=Amb_temp + 273.15; %Ambient temp in [K]
```

Determine how many hole features are cooling slots:

```
Number_of_cooling_slots=0;
   for i=1:Nb
     Holetype=Hole_type(i);
     if Holetype == 3 %Splash Cooling
        Number_of_cooling_slots = Number_of_cooling_slots + 1;
     end
     if Holetype == 4 % Wiggle Strip
        Number_of_cooling_slots = Number_of_cooling_slots + 1;
     end
     if Holetype == 5 % Machined Ring
        Number_of_cooling_slots = Number_of_cooling_slots + 1;
     end
   end

if Number_of_cooling_slots == 0
   bb=2;
end
```

Calculate annulus air flow area and effective casing diameter for can-annular combustor:

```
if Com == 2

    for i=1:Nb
      Aflow=((0.25*pi)*(Casing_outer_Diameter(i)^2 - Casing_inner_Diameter(i)^2) –
             (nCans*0.25*pi*(Liner_Diameter(i)^2)))/nCans;
      Casing_Diameter(i)=sqrt((4/pi)*Aflow + Liner_Diameter(i)^2);
    end

  end
```

Calculate zone lengths:

```
  for i=1:Zones
    if i==1
      Length_zone(i)=Rz_boundary;
    end
    if i==2
      Length_zone(i)=Pz_boundary-Rz_boundary;
    end;
    if i==3
      Length_zone(i)=Sz_boundary-Pz_boundary;
    end
    if i==4
      Length_zone(i)=Total_comb_length-Sz_boundary;
    end
  end

  for i=1:Zones
    if i==1
      Length(i)=Length_zone(i);
    else
      Length(i)=Length(i-1)+Length_zone(i);
    end
  end
```

Initial conditions for solver:

```
  T_annulus=(ones(1,Number_of_nodes)*T3);        [Initial Annulus air temperature [K]]
  T_GAS=(ones(1,Number_of_nodes)*T3);            [Initial Gas temperature [K]]
  dp_hot=0;                                       [Initial Hot losses]
```

LOOP CALCULATIONS START

```
Number_of_iter=1000;
ntel=0;
Converg=10;

while (Converg > 1e-6) & (ntel < Number_of_iter)
  ntel=ntel+1
```

```
for i=1:Number_of_nodes
    rho_annulus(i)=P3/(R*T_annulus(i));          [Annulus air density [kg/m^3]]
    rho_gas(i)=P3/(R*T_GAS(i));                  [Gas density [kg/m^3]]
end
```

Define function for "Flowsplit" subroutine:

```
Pressure_drop,Flowsplits,jetangle,X,U_ref,rho_hole,element_th,Tgx,q_ref,Dref,rho_ref,A_L]=Flowsplit
(Number_of_cooling_slots,Hole_type,Number_of_holes,Hole_diameter,NBlades,BladeTh,K_sw,Theta,Nb,
R,ma,P3,T3,Com,DSw_out,DSw_in,Hole_Position,Nodes,T_annulus,Number_of_nodes,Length,rho_annul
us,rho_gas,dp_hot,Zones,Casing_Diameter,Liner_Diameter,t_L,Discharge_Coeff,slot_height,nCans,Casing
_outer_Diameter,Casing_inner_Diameter,mm,qm);
```

Define function for "Combustion subroutine":

```
[Tgas,Air_fuel_node,Length,Air_fuel,Equivalence_Ratio,Casing_D,Liner_D,Airflow,Airflow_node,Airflo
w_zone,eta_Rz,eta_Pz,eta_Sz,eta_Dz,theta,EI_CO,EI_HC,eta_comb,Nox,NOx,Comb_eff]=Combustion(T
3,P3,Nb,ma,x,y,Hole_Position,Massflow,Overall_A_F,S_A_F,Total_comb_length,Pz_boundary,Rz_bound
ary,Sz_boundary,nn,Casing_Diameter,Liner_Diameter,Number_of_nodes,Nodes,X,Zones,Length,Hole_typ
e,Rz_flow,Pz_flow,Sz_flow,Dz_flow,Pressure_drop,element_th,nCans,A_ref,Dref);
```

Calculate fuel flow and fuel-air ratio at each computational node:

```
    Fuel_flow=(ma/Overall_A_F);

    for i=1:Number_of_nodes
        FAR(i)=1/Air_fuel_node(i);
    end
```

Calculate annulus air and gas properties as a function of temperature:

```
    for i=1:Number_of_nodes

        Ta=T_annulus(i)-273;
        Tg=T_GAS(i)-273;
        k_a(i)=(2.4186e-2)+((7.8957e-5)*Ta)-((3.7873e-8)*Ta^2)+((1.6685e-11)*Ta^3);
        k_g(i)=(2.4186e-2)+((7.8957e-5)*Tg)-((3.7873e-8)*Tg^2)+((1.6685e-11)*Tg^3);

        mu_a(i)=(1.733e-5)+((4.5543e-8)*Ta)-((2.2106e-11)*Ta^2)+((7.7219e-15)*Ta^3);
        mu_g(i)=(1.733e-5)+((4.5543e-8)*Tg)-((2.2106e-11)*Tg^2)+((7.7219e-15)*Tg^3);

        Cp_an(i)=1002.106 + (0.089329*Ta) + ((2.332e-4)*Ta^2) - ((1.2831e-7)*Ta^3);
        Cp_gas(i)=1002.106 + (0.089329*Tg) + ((2.332e-4)*Tg^2) - ((1.2831e-7)*Tg^3);

        Gamma_air(i)=Cp_an(i)/(Cp_an(i)-R);


        Pr_air(i)=(Cp_an(i)*mu_a(i))/k_a(i);
        Pr_gas(i)=(Cp_gas(i)*mu_g(i))/k_g(i);
    end
```

Define function for "Elements:

[Momflux,T_GAS,m_annulus,Hyd_D,dp_hot,Reo,Rei,d_AL,d_ACi,ALi,ALo,Aci,Aco,m_internal,Pattern_
Factor,M_inner,Local_AF,Y_max]=Elements(Zones,Length,Tgas,X,Number_of_nodes,Rz_boundary,Pz_b
oundary,Sz_boundary,Total_comb_length,Massflow,ma,Hole_Position,Nb,Fuel_flow,Airflow_node,Casin
g_D,Liner_D,t_L,t_C,P3,R,T3,U_ref,mu_a,mu_g,element_th,Nodes,Tgx,nCans,q_ref,Pressure_drop,Dref,
Overall_A_F,Liner_Diameter,rho_hole_gas,rho_annulus,V_jet,Cd,Hole_diameter,Com,Number_of_holes);

Define function for "Heat_transfer ":

[Liner_temp,Casing_temp,New_Tannulus,old_Tannulus,eta_filmcooling,J,distance_downstream_slot,e_g,
Average_haLo]=Heat_transfer(Zones,Nodes,Number_of_nodes,ma,Overall_A_F,T_GAS,R,Liner_D,Casin
g_D,element_th,x,y,Hole_type,Massflow,Number_of_cooling_slots,cooling_slot_height,mu_a,Pz_boundar
y,k_g,T_annulus,sigma,k_L,k_C,t_L,t_C,Airflow_node,Nb,X,mu_g,k_a,Hyd_D,m_annulus,d_AL,d_ACi,T
3,Cp_an,bb,Reo,Rei,Pr_air,Pr_gas,Fuel_flow,FAR,P3,Hole_Position,Tamb,ALi,ALo,Aci,Aco,eLi,eLo,eCi,
eCo,Total_comb_length,Radiation_Model,m_internal,Liner_Diameter,nCans,M_inner,Local_AF,h0,Outsid
e_conv,Outside_rad);

Check for convergence:

Converg=norm((New_Tannulus-old_Tannulus)/New_Tannulus);

   T_annulus=New_Tannulus;

end   **[End Loop calculations]**

Define function for "netw ":
----
if qq == 1

  [element_length]=netw(Num_elements,Nb,Hole_Position,Total_comb_length,Number_of_nodes,X,Line
  r_D,Casing_D,T_GAS,Liner_temp,t_C,t_L,e_g,slot_height);
end

Calculates individual cooling mass flow rates:

Cooling_massflow=0;

for i=1:Nb
  Holetype=Hole_type(i);

  if Holetype == 3
    Cooling_massflow=Cooling_massflow+Massflow(i);
  elseif Holetype == 4
    Cooling_massflow=Cooling_massflow+Massflow(i);
  elseif Holetype == 5
    Cooling_massflow=Cooling_massflow+Massflow(i);
  end
end

Per_cooling_massflow=(Cooling_massflow/ma)*100;   **[Total % cooling flow]**

WRITE OUTPUT DATA FILES

```
if Com == 2
    Comtype = 'Combustor type : Can - Annular';
elseif Com == 1
    Comtype = 'Combustor type : Tubular     ';
end

if Radiation_Model==1
    Radm='Simple';
elseif Radiation_Model ==2
    Radm='Accurate';
elseif Radiation_Model == 3
    Radm='Off';
end

if bb==1
    Cooling='Film Cooled Liner';
elseif bb==2
    Cooling='Uncooled Liner';
end

nCann='Number of cans:              ';
HoleType='Hole type    ';
NHoles='nHoles';
DHole='HDiam [mm]';
Hpos='XPos [mm]';
MF='m/can [kg/s]';
mf='mdot [%]';
Disch='Cd';
Jet='Vjet [m/s]';
Mom='J';
Jangle='Jet ang';
ymax='Y_max [mm]';


Inp=' *********  INPUTS *********     ';
InletP='Inlet Pressure [Pa]           ';
InletT='Inlet Temperature [K]           ';
Mass='Total Massflow [kg/s]           ';
MC='Total massflow per Can [kg/s]    ';
Rz='Rz boundary (rel to dome) [mm]    ';
Pz='Pz boundary (rel to dome) [mm]   ';
Sz='Sz boundary (rel to dome) [mm]   ';
TL='Total Combustor Length [mm]      ';
Inh='**** HEAT TRANSFER INPUTS ****   ';
Lcmodel='Radiation Model              ';
Frmodel='Flame radiation modes          ';
AmbT='Ambient Temperature [C]          ';
Lie='Liner inner emissivity        ';
Loe='Liner outer emissivity         ';
Cie='Casing inner emissivity         ';
Coe='Casing outer emissivity         ';
```

142

```
Lthe='Liner thermal conductivuty [W/mK] ';
Cthe='Casing thermal conductivity [W/mK]';
Ld='Liner wall thickness [mm]          ';
CD='Casing wall thickness [mm]       ';
AF='Overall Air/Fuel Ratio           ';
SAF='Stoichoimetric Air/Fuel Ratio     ';
Resu='******** RESULTS ********       ';
pres='Pressure Loss [Pa]              ';
Persp='Pressure Loss [%]              ';
PF='Pattern Factor                ';
th='Theta (*10^6)                ';
ALiner='Flametube flow area [m^2]       ';
Ref_A='Reference Area (Aref)          ';
AL_Aref='(Flametube flow area)/(Ref Area)';
Ref_D='Reference Diameter (Dref)       ';
Ref_p='Reference density             ';
Ref_u='Reference Velocity (Uref)       ';
Ref_q='Reference velocity head (qref)    ';
CO='EI_CO [g CO/kg fuel]            ';
HC='EI_HC [g HC/kg fuel]            ';
Nox_L=['EI_NOx(Lefebvre Model) [g/kg fuel]'];
Nox_O=['EI_NOx(Odgers Model) [g/kg fuel]  '];
Combeff='Combustion efficiency (figure 2.2)';
eCom='Emission Comb. efficiency [%]     ';
Coolingflow='Total amount of cooling air [%]   ';
%************** Zone Data ******************
Airflowrz='Mass flow rate in Rz per Can [kg/s]';
Airflowpz='Mass flow rate in Pz per Can [kg/s]';
Airflowsz='Mass flow rate in Sz per Can [kg/s]';
Airflowdz='Mass flow rate in Dz per Can [kg/s]';
airflowrz='Percentage of total flow in Rz [%] ';
airflowpz='Percentage of total flow in Pz [%] ';
airflowsz='Percentage of total flow in Sz [%] ';
airflowdz='Percentage of total flow in Dz [%] ';
Rz_phi='Rz equivalence ratio            ';
Pz_phi='Pz equavalence ratio            ';
Sz_phi='Sz equavalence ratio            ';
Dz_phi='Dz equavalence ratio             ';
Rz_eff='Rz combustion efficiency [%]      ';
Pz_eff='Pz combustion efficiency [%]      ';
Sz_eff='Sz combustion efficiency [%]      ';
Dz_eff='Dz combustion efficiency [%]      ';
hLocoeff='Average Backside h_coeff         ';
Rz_frac='Rz_f';
Pz_frac='Pz_f';
Sz_frac='Sz_f';
Dz_frac='Dz_f';
%%%%%%%%%%%%%%%%%% FLOW %%%%%%%%%%%%%%%%%%%%%%
linerd='[Liner_D]';
casingd='[Casing_D]';
x_distance='[X (mm)]';
int_flow_area='[Int_A]';
an_flow_area='[AA] ';
Per='[P]';
Hydrou='[Hyd_D]';
Gasemm='[eg]';
```

```
Gas_temp='[Tg(C)]';
Linertemp='[Liner temp [K]]';


AnnulusM='Mannulus';
Liner='LinerD';

if Com==2
    lod='LOD [mm]';
    cid='CID [mm]';
    cod='COD [mm]';
 elseif Com ==1
    lod='LOD [mm]';
    cd='COD [mm]';
 end
%***************************GENDATA.TXT***************************
fid=fopen('Gendata.txt','w');
fprintf(fid,'%s\n',Comtype);
fprintf(fid,'\n');
fprintf(fid,'%s ',nCann);
fprintf(fid,'%6.1f\n ',nCans)
fprintf(fid,'\n');

%**********INPUTS*********
fprintf(fid,'%s\n',Inp);
fprintf(fid,'%s',InletP);
fprintf(fid,'%6.2f\n',P3);
fprintf(fid,'%s',InletT);
fprintf(fid,'%6.2f\n',T3);
fprintf(fid,'%s',Mass);
fprintf(fid,'%6.3f\n',ma*nCans);
if Com ==2
    fprintf(fid,'%s',MC);
    fprintf(fid,'%6.3f\n',ma);
end
fprintf(fid,'%s',AF);
fprintf(fid,'%6.3f\n',Overall_A_F);
fprintf(fid,'%s',SAF);
fprintf(fid,'%6.3f\n',S_A_F);
fprintf(fid,'%s',Rz);
fprintf(fid,'%6.3f\n',Rz_boundary*1000);
fprintf(fid,'%s',Pz);
fprintf(fid,'%6.3f\n',Pz_boundary*1000);
fprintf(fid,'%s',Sz);
fprintf(fid,'%6.3f\n',Sz_boundary*1000);
fprintf(fid,'%s',TL);
fprintf(fid,'%6.3f\n',Total_comb_length*1000);
fprintf(fid,'\n');

%******* HEAT TRANSFER *******
fprintf(fid,'%s\n',Inh);
fprintf(fid,'%s',Lcmodel);
fprintf(fid,'%6s\n',Radm);
fprintf(fid,'%s',Frmodel);
fprintf(fid,'%6s\n',Cooling);
fprintf(fid,'%s',AmbT);
```

144

```
fprintf(fid,'%6.1f\n',Tamb-273.15);
fprintf(fid,'%s',Lie);
fprintf(fid,'%6.2f\n',eLi);
fprintf(fid,'%s',Loe);
fprintf(fid,'%6.2f\n',eLo);
fprintf(fid,'%s',Cie);
fprintf(fid,'%6.2f\n',eCi);
fprintf(fid,'%s',Coe);
fprintf(fid,'%6.2f\n',eCo);
fprintf(fid,'%s',Lthe);
fprintf(fid,'%6.2f\n',k_L);
fprintf(fid,'%s',Cthe);
fprintf(fid,'%6.2f\n',k_C);
fprintf(fid,'%s',Ld);
fprintf(fid,'%6.2f\n',t_L*1000);
fprintf(fid,'%s',CD);
fprintf(fid,'%6.2f\n',t_C*1000);
fprintf(fid,'\n');

  %**********RESULTS***********
fprintf(fid,'%s\n',Resu);
fprintf(fid,'%s',pres);
fprintf(fid,'%6.3f\n',Pressure_drop);
fprintf(fid,'%s',Persp);
fprintf(fid,'%6.3f\n',Pressure_Loss);
fprintf(fid,'%s',PF);
fprintf(fid,'%6.3f\n',Pattern_Factor);
fprintf(fid,'%s',th);
fprintf(fid,'%6.3f\n',theta);
fprintf(fid,'%s',ALiner);
fprintf(fid,'%6.3f\n',A_L);
fprintf(fid,'%s',Ref_A);
fprintf(fid,'%6.2f\n',A_ref);
fprintf(fid,'%s',AL_Aref);
fprintf(fid,'%6.3f\n',A_L/A_ref);
fprintf(fid,'%s',Ref_D);
fprintf(fid,'%6.3f\n',Dref);
fprintf(fid,'%s',Ref_p);
fprintf(fid,'%6.3f\n',rho_ref);
fprintf(fid,'%s',Ref_u);
fprintf(fid,'%6.3f\n',U_ref);
fprintf(fid,'%s',Ref_q);
fprintf(fid,'%6.3f\n',q_ref);
fprintf(fid,'%s',CO);
fprintf(fid,'%6.3f\n',EI_CO);
fprintf(fid,'%s',HC);
fprintf(fid,'%6.3f\n',EI_HC);
fprintf(fid,'%s',Nox_L);
fprintf(fid,'%6.3f\n',Nox);
fprintf(fid,'%s',Nox_O);
fprintf(fid,'%6.3f\n',NOx);
fprintf(fid,'%s',Combeff);
fprintf(fid,'%6.3f\n',Comb_eff);
fprintf(fid,'%s',eCom);
fprintf(fid,'%6.3f\n',eta_comb);
fprintf(fid,'%s',Coolingflow);
```

```
fprintf(fid,'%6.3f\n',Per_cooling_massflow);
fprintf(fid,'%s',hLocoeff);
fprintf(fid,'%6.3f\n',Average_haLo);

fprintf(fid,'\n');
fclose(fid);

%*********************** HOLEDATA 1/2.TXT***********************
fid=fopen('Holedata1_2.txt','w');
fprintf(fid,'%s',HoleType);
    fprintf(fid,'%14s',Hpos);
    fprintf(fid,'%8s',NHoles);
    fprintf(fid,'%13s',DHole);
    fprintf(fid,'%13s',MF);
    fprintf(fid,'%13s',mf);
    fprintf(fid,'%8s',Disch);
    fprintf(fid,'%15s',Jet);
    fprintf(fid,'\n');


for i=1:Nb

   split=Flowsplits(i);
   massf=Massflow(i);
   hpos=Hole_Position(i);
   hdiam=Hole_diameter(i);
   nHoles=Number_of_holes(i);
   Holetype = Hole_type(i);
   vjet=V_jet(i);
   Coeff=Cd(i);

   if Holetype == 1
      Htype='Plain        ';
   end
   if Holetype== 2
      Htype ='Plunged       ';
   end
   if Holetype == 3
      Htype = 'Splash Cooling ';
   end
   if Holetype ==4
      Htype='Wiggle Strip   ';
   end
   if Holetype ==5
      Htype='Machined Ring  ';
   end
   if Holetype==6
      Htype = 'Swirler       ';
   end

   fprintf(fid,'%s',Htype);
   fprintf(fid,'%10.1f',hpos);
   fprintf(fid,'%11.1f',nHoles);
   fprintf(fid,'%11.2f',hdiam);
   fprintf(fid,'%13.5f',massf);
   fprintf(fid,'%14.3f',split);
```

```
      fprintf(fid,'%11.3f',Coeff);
      fprintf(fid,'%11.3f',vjet);

      fprintf(fid,'\n');
 end
fclose(fid);

%%%%%%%%%% Holedata 2/2 %%%%%%%%%%%%
fid=fopen('Holedata2_2.txt','w');
 fprintf(fid,'%s',HoleType);

      fprintf(fid,'%7s',Mom);
      fprintf(fid,'%12s',Jangle);
      fprintf(fid,'%13s',ymax);

      if Com ==2
         fprintf(fid,'%11s',lod);
         fprintf(fid,'%11s',cid);
         fprintf(fid,'%12s',cod);
      elseif Com==1
         fprintf(fid,'%11s',lod);
         fprintf(fid,'%12s',cd);
      end

      fprintf(fid,'%6s',Rz_frac);
      fprintf(fid,'%7s',Pz_frac);
      fprintf(fid,'%7s',Sz_frac);
      fprintf(fid,'%7s',Dz_frac);

 fprintf(fid,'\n');


 for i=1:Nb
    if Com==2

       LOD= Liner_Diameter(i);
       CID=Casing_inner_Diameter(i);
       COD=Casing_outer_Diameter(i);
    elseif Com==1
       LOD= Liner_Diameter(i);
       CD=Casing_Diameter(i);

    end

    Holetype = Hole_type(i);

    momflux=Momflux(i);
    jangle=jetangle(i);
    yMax=Y_max(i);
    rz_flow=Rz_flow(i);
    pz_flow=Pz_flow(i);
    sz_flow=Sz_flow(i);
    dz_flow=Dz_flow(i);

    if Holetype == 1
       Htype='Plain       ';
```

```
        end
        if Holetype== 2
            Htype ='Plunged       ';
        end
        if Holetype == 3
            Htype = 'Splash Cooling';
        end
        if Holetype ==4
            Htype='Wiggle Strip  ';
        end
        if Holetype ==5
            Htype='Machined Ring ';
        end
        if Holetype==6
            Htype = 'Swirler       ';
        end

        fprintf(fid,'%s',Htype);

        fprintf(fid,'%7.3f',momflux);
        fprintf(fid,'%11.3f',jangle);
        fprintf(fid,'%11.3f',yMax);


        if Com ==2
        fprintf(fid,'%10.2f',LOD);
        fprintf(fid,'%12.2f',CID);
        fprintf(fid,'%12.2f',COD);
        elseif Com ==1
            fprintf(fid,'%10.2f',LOD);
            fprintf(fid,'%12.2f',CD);
        end

        fprintf(fid,'%8.2f',rz_flow);
        fprintf(fid,'%7.2f',pz_flow);
        fprintf(fid,'%7.2f',sz_flow);
        fprintf(fid,'%7.2f',dz_flow);

        fprintf(fid,'\n');
    end
fclose(fid);



%****************** ZONE Data ********************8
fid =fopen('Zone_Data.txt','w');
  fprintf(fid,'%s',Airflowrz);
  fprintf(fid,'%6.3f',Airflow_zone(1));
  fprintf(fid,'\n');
  fprintf(fid,'%s',Airflowpz);
  fprintf(fid,'%6.3f',Airflow_zone(2));
  fprintf(fid,'\n');
  fprintf(fid,'%s',Airflowsz);
  fprintf(fid,'%6.3f',Airflow_zone(3));
  fprintf(fid,'\n');
  fprintf(fid,'%s',Airflowdz);
```

```
fprintf(fid,'%6.3f',Airflow_zone(4));
fprintf(fid,'\n');
fprintf(fid,'\n');
fprintf(fid,'%s',airflowrz);
fprintf(fid,'%6.3f',(Airflow_zone(1)/ma)*100);
fprintf(fid,'\n');
fprintf(fid,'%s',airflowpz);
fprintf(fid,'%6.3f',(Airflow_zone(2)/ma)*100);
fprintf(fid,'\n');
fprintf(fid,'%s',airflowsz);
fprintf(fid,'%6.3f',(Airflow_zone(3)/ma)*100);
fprintf(fid,'\n');
fprintf(fid,'%s',airflowdz);
fprintf(fid,'%6.3f',(Airflow_zone(4)/ma)*100);
fprintf(fid,'\n');
fprintf(fid,'\n');
fprintf(fid,'%s',Rz_phi);
fprintf(fid,'%6.3f',Equivalence_Ratio(1));
fprintf(fid,'\n');
fprintf(fid,'%s',Pz_phi);
fprintf(fid,'%6.3f',Equivalence_Ratio(2));
fprintf(fid,'\n');
fprintf(fid,'%s',Sz_phi);
fprintf(fid,'%6.3f',Equivalence_Ratio(3));
fprintf(fid,'\n');
fprintf(fid,'%s',Dz_phi);
fprintf(fid,'%6.3f',Equivalence_Ratio(4));
fprintf(fid,'\n');
fprintf(fid,'\n');
fprintf(fid,'%s',Rz_eff);
fprintf(fid,'%6.3f',eta_Rz*100);
fprintf(fid,'\n');
fprintf(fid,'%s',Pz_eff);
fprintf(fid,'%6.3f',eta_Pz*100);
fprintf(fid,'\n');
fprintf(fid,'%s',Sz_eff);
fprintf(fid,'%6.3f',eta_Sz*100);
fprintf(fid,'\n');
fprintf(fid,'%s',Dz_eff);
fprintf(fid,'%6.3f',eta_Dz*100);
fprintf(fid,'\n');

fclose(fid);

%%%%%%%%%%%% FLOW %%%%%%%%%%%%%%%

fid=fopen('Flow.txt','w');
fprintf(fid,'%s',linerd);
fprintf(fid,'%12s',casingd);
fprintf(fid,'%8s',x_distance);
fprintf(fid,'%10s',int_flow_area);
fprintf(fid,'%10s',an_flow_area);
fprintf(fid,'%8s',Per);
fprintf(fid,'%10s',Hydrou);
fprintf(fid,'%10s',Gas_temp);
fprintf(fid,'%6s',Gasemm);
```

```
    fprintf(fid,'%20s',Linertemp);

  fprintf(fid,'\n');

 for i=1:Number_of_nodes
    LD=Liner_D(i);
    Cas=Casing_D(i);
    xdis=X(i);
    I_flow=(pi*Liner_D(i)^2)/4;
    an_flow=(pi/4)*(Casing_D(i)^2-Liner_D(i)^2);
    perim=pi*(Casing_D(i)+Liner_D(i));
    Hydroulic_D=(4*an_flow)/perim;
    Gas_emm=e_g(i);
    GasTemp=T_GAS(i)-273.15;
    Liner_T=Liner_temp(i)-273.15;


    fprintf(fid,'%6.3f',LD);
    fprintf(fid,'%12.3f',Cas);
    fprintf(fid,'%10.4f',xdis*1000);
    fprintf(fid,'%10.4f',I_flow);
    fprintf(fid,'%10.3f',an_flow);
    fprintf(fid,'%10.3f',perim);
    fprintf(fid,'%8.3f',Hydroulic_D);
    fprintf(fid,'%10.3f',GasTemp);
    fprintf(fid,'%10.4f',Gas_emm);
    fprintf(fid,'%10.3f',Liner_T);

    fprintf(fid,'\n');
 end
 fclose(fid);
```

****

D.4   FLOWSPLITS

Define function for "netw ":

```
function[rho_hole_gas,V_jet,A_ref,Pressure_Loss,RefPressure_Loss,Cd,Massflow,Pressure_drop,Flowspli
ts,jetangle,X,U_ref,rho_hole,element_th,Tgx,q_ref,Dref,rho_ref,A_L]=Flowsplit(Number_of_cooling_slots
,Hole_type,Number_of_holes,Hole_diameter,NBlades,BladeTh,K_sw,Theta,Nb,R,ma,P3,T3,Com,DSw_ou
t,DSw_in,Hole_Position,Nodes,T_annulus,Number_of_nodes,Length,rho_annulus,rho_gas,dp_hot,Zones,C
asing_Diameter,Liner_Diameter,t_L,Discharge_Coeff,slot_height,nCans,Casing_outer_Diameter,Casing_i
nner_Diameter,mm,qm);
```

Convert units from mm to m:

```
Hole_Position=Hole_Position/1000;
Hole_diameter=Hole_diameter/1000;
Liner_Diameter=Liner_Diameter/1000;
Casing_Diameter=Casing_Diameter/1000;
slot_height=slot_height/1000;
Casing_inner_Diameter=Casing_inner_Diameter/1000;
```

```
Casing_outer_Diameter=Casing_outer_Diameter/1000;
DSw_out=DSw_out/1000;
DSw_in=DSw_in/1000;
BladeTh=BladeTh/1000;
```

Define end node at each zone:

```
Tgx=zeros(1,Zones+1);
Tgx(1)=Hole_Position(1);
Tgx(2:Zones+1)=Length(1:Zones);
```

Calculate position of each computational node:

```
X=zeros(1,Number_of_nodes);

for i=1:Zones
    if i==1
        dx=(Tgx(i+1)-Tgx(i))/(Nodes-1);
        for j=2:(i*Nodes)
            X(1)=Tgx(1);
            X(j)=X(j-1)+dx;
        end
    end

    if i == 2
        dx=(Tgx(i+1)-Tgx(i))/Nodes;
        for j=(i-1)*(Nodes)+1 : (i*Nodes)
            X(j)=X(j-1)+dx;
        end
    end

    if i == 3
        dx=(Tgx(i+1)-Tgx(i))/Nodes;
        for j=(i-1)*(Nodes)+1 : (i*Nodes)
            X(j)=X(j-1)+dx;
        end
    end

    if i == 4
        dx=(Tgx(i+1)-Tgx(i))/Nodes;
        for j=(i-1)*(Nodes)+1 : (i*Nodes)
            X(j)=X(j-1)+dx;
        end
    end
end
```

Generate density matrix for each computational node:

```
rho_nodes=zeros(1,Number_of_nodes);
```

Calculate distance between node- defining elements:

```
element_th=zeros(1,Number_of_nodes);
for i=1:Number_of_nodes-1
    element_th(i)=X(i+1)-X(i);
    element_th(Number_of_nodes) = element_th(Number_of_nodes -1);
end
```

Define air and gas density at each hole set:

```
for j=1:Nb
    for i=1:Number_of_nodes

        if (j <= Nb)

            if (X(i) <= Hole_Position(j)+(element_th(i))) & (X(i) >= Hole_Position(j)-(element_th(i)))
                rho_hole(j)=rho_annulus(i);
                 rho_hole_gas(j)=rho_gas(i);

            end
        end
    end
end


rho_ref=P3/(R*T3);                                          [Reference density]
```

```
Qmass=ma;                                                   [Total mass flow rate]
```

Define comnustor type and calculate reference data for selected combustor type:

```
Liner_Diam=sum(Liner_Diameter)/Nb;%Average Liner diameter

Dref=0;
A_ref=0;
  for i=1:Nb

    if Com ==1 %Tubular
        AreaAnnulus(i) = ((pi*0.25)*((Casing_Diameter(i)^2)-(Liner_Diameter(i)^2)));
        Dref=Dref+Casing_Diameter(i);
        A_ref=A_ref+0.25*pi*Casing_Diameter(i)^2;
    elseif Com ==2 % Can-annular
         AreaAnnulus(i)= (((0.25*pi)*(Casing_outer_Diameter(i)^2-Casing_inner_Diameter(i)^2)) -
((0.25*pi*Liner_Diameter(i)^2)*nCans))/nCans;
         Dref=Dref+(Casing_outer_Diameter(i)-Casing_inner_Diameter(i))/2;
         A_ref=A_ref+0.25*pi*(Casing_outer_Diameter(i)^2-Casing_inner_Diameter(i)^2);
     end

   end
A_L=(pi*(Liner_Diam^2)*0.25);
A_ref=A_ref/Nb;
Dref=Dref/Nb;
rho_ref=P3/(R*T3);
U_ref=Qmass/(rho_ref*A_ref);
q_ref=0.5*rho_ref*(U_ref^2);
```

Calculate total hole area:

```
AreaTotal = 0.0;
ntel = 0;

convergence=1000;
```

[Initial pressure drop]
```
for i = 1:Nb;
  tmp_dP(i)=0;
  dp(i)=0;
```

[Initial mass flow rate]
```
  if mm==1                              [mm=1, calculate specific mass flow rates]
    qm(i)=(Qmass/(Nb));
    dqm(i)=0;
  end
```

[Calculate total hole area]
```
  Holetype=Hole_type(i);

  if Holetype==6;
    Harea(i)=Hole_diameter(i)*1000;
  end

  if Holetype==4 %Wiggle strip
    Wiggle_width=Hole_diameter(i);
    Harea(i)=(Wiggle_width*slot_height(i))*Number_of_holes(i);
  end

  if (Holetype ~= 4) & (Holetype ~= 6)
    Harea(i) = pi/4*(Hole_diameter(i)^2)*Number_of_holes(i);
  end
 AreaTotal = AreaTotal + Harea(i);
end

ntel=0;
```

CALCULATE PRESSURE LOSSES IF MASS FLOW SPLITS ARE DEFINE (mm=2)

```
if mm==2
  dP_aver = 0;
  ntel = ntel + 1;
  Qmpass = Qmass;

for i=1:Nb;
  Holetype=Hole_type(i);
```

Calculate pressure loss and flow rates for specific holes:

```
        if Holetype == 1;                                                    [Plain Holes]


  Beta(i) = qm(i)/Qmpass;
        Alpha(i) = Harea(i)/(AreaAnnulus(i));
  Qmpass=(Qmpass-qm(i));
  if Discharge_Coeff(i) == 0
    Mu(i) = Beta(i)/Alpha(i);
    K(i) = 1 + 0.64*((2*(Mu(i)^2))+((4*(Mu(i)^4))+(1.56*(Mu(i)^2)*((4*Beta(i))-(Beta(i)^2)))))^0.5;
    Cd(i) =(K(i)-1)/(0.8*((4*(K(i)^2))-(K(i)*(2-Beta(i))^2)))^0.5;
    jetangle(i)=asin((1/(1.6*Cd(i)))*((K(i)-1)/K(i)))*(180/pi);
  elseif Discharge_Coeff(i) ~= 0
    Mu(i) = Beta(i)/Alpha(i);
    K(i) = 1 + 0.64*((2*(Mu(i)^2))+((4*(Mu(i)^4))+(1.56*(Mu(i)^2)*((4*Beta(i))-(Beta(i)^2)))))^0.5;
    Cd(i)=Discharge_Coeff(i);
    jetangle(i)=asin((1/(1.6*Cd(i)))*((K(i)-1)/K(i)))*(180/pi);
  end

  tmp_dP(i)=dp(i);

  dp(i) = (((qm(i)/(Cd(i)*Harea(i)))^2)/(2*rho_hole(i)))+dp_hot ;
  dP_aver = (dP_aver + dp(i)*qm(i));
        end
```

```
        if Holetype == 2;                                                    [Plunged Holes]


    Beta(i) = qm(i)/Qmpass;
        Alpha(i) = Harea(i)/(AreaAnnulus(i));
  Qmpass=(Qmpass-qm(i));
  if Discharge_Coeff(i) == 0
    Mu(i) = Beta(i)/Alpha(i);
    K(i) = 1 + 0.36*((2*(Mu(i)^2))+((4*(Mu(i)^4))+(2.77*((4*Beta(i))-(Beta(i)^2)))))^0.5;
    Cd(i) =(K(i)-1)/(0.6*((4*(K(i)^2))-(K(i)*(2-Beta(i))^2)))^0.5;
    jetangle(i)=asin((1/(1.2*Cd(i)))*((K(i)-1)/K(i)))*(180/pi);
  elseif Discharge_Coeff(i) ~= 0;
    Mu(i) = Beta(i)/Alpha(i);
    K(i) = 1 + 0.36*((2*(Mu(i)^2))+((4*(Mu(i)^4))+(2.77*((4*Beta(i))-(Beta(i)^2)))))^0.5;
    Cd(i)=Discharge_Coeff(i);
    jetangle(i)=asin((1/(1.2*Cd(i)))*((K(i)-1)/K(i)))*(180/pi);
  end

  tmp_dP(i)=dp(i);

  dp(i) = (((qm(i)/(Cd(i)*Harea(i)))^2)/(2*rho_hole(i)))+dp_hot;
```

```
    dP_aver = (dP_aver + dp(i)*qm(i));

        end
```

```
        if Holetype == 3;                                          [Splash Cooling device]
    Cd(i) =  Discharge_Coeff(i);
    jetangle(i)=0;
    tmp_dP(i)=dp(i);

    dp(i) = (((qm(i)/(Cd(i)*Harea(i)))^2)/(2*rho_hole(i)))+dp_hot;
    dP_aver = (dP_aver + dp(i)*qm(i));
        end

        if Holetype == 4 ;%Wiggle strip
    Cd(i) =  Discharge_Coeff(i);
    jetangle(i)=0;

    tmp_dP(i)=dp(i);

    dp(i) = (((qm(i)/(Cd(i)*Harea(i)))^2)/(2*rho_hole(i)))+dp_hot;

    dP_aver = (dP_aver + dp(i)*qm(i));
  end
```

```
        if Holetype ==5;                                          [Machined Rings]
    Cd(i)=Discharge_Coeff(i);
    jetangle(i)=0;

    tmp_dP(i)=dp(i);

        dp(i) = (((qm(i)/(Cd(i)*Harea(i)))^2)/(2*rho_hole(i)))+dp_hot;

        dP_aver = (dP_aver + dp(i)*qm(i));


        end
```

```
        if Holetype ==6;                                          [Swirler]

    Swirl_angle=Theta*(pi/180);
    jetangle(i)=0;

    tmp_dP(i)=dp(i);

    K=K_sw*(((sec(Swirl_angle)/Harea(i))^2)-(1/(A_L^2)));
    tmp_dP(i)=dp(i);
    dp(i)=((qm(i)^2)*K/(2*rho_hole(i)))+dp_hot; %Lefebvre 1998 swirler formula
        dP_aver=dP_aver+(dp(i)*qm(i));

        end

end
```

Check for convergence:

---

dP_aver = dP_aver/Qmass;

  convergence=0.0;
  for i = 1:Nb;
          convergence = convergence + abs(tmp_dP(i) - dp(i));
  end

end %   **[end for mm]**

CALCULATE PRESSURE LOSSES AND MASS FLOW SPLITS (mm=1)

---

if mm==1
  while (convergence > 0.0001) & (ntel < 1000);

     dP_aver = 0;
     ntel = ntel + 1;
     Qmpass = Qmass;

for i=1:Nb;
  Holetype=Hole_type(i);

Calculate pressure loss and flow rates for specific holes :

---

        if Holetype == 1;   **[Plain Holes]**

  Beta(i) = qm(i)/Qmpass;
        Alpha(i) = Harea(i)/(AreaAnnulus(i));
  Qmpass=(Qmpass-qm(i));
  if Discharge_Coeff(i) == 0
    Mu(i) = Beta(i)/Alpha(i);
    K(i) = 1 + 0.64*((2*(Mu(i)^2))+((4*(Mu(i)^4))+(1.56*(Mu(i)^2)*((4*Beta(i))-(Beta(i)^2))))^0.5);
    Cd(i) =(K(i)-1)/(0.8*((4*(K(i)^2))-(K(i)*(2-Beta(i))^2))^0.5);
    jetangle(i)=asin((1/(1.6*Cd(i)))*((K(i)-1)/K(i)))*(180/pi);
  elseif Discharge_Coeff(i) ~= 0
    Mu(i) = Beta(i)/Alpha(i);
    K(i) = 1 + 0.64*((2*(Mu(i)^2))+((4*(Mu(i)^4))+(1.56*(Mu(i)^2)*((4*Beta(i))-(Beta(i)^2))))^0.5);
    Cd(i)=Discharge_Coeff(i);
    jetangle(i)=asin((1/(1.6*Cd(i)))*((K(i)-1)/K(i)))*(180/pi);
  end

  tmp_dP(i)=dp(i);

  dp(i) = (((qm(i)/(Cd(i)*Harea(i)))^2)/(2*rho_hole(i)))+dp_hot ;
  dP_aver = (dP_aver + dp(i)*qm(i));
        end

---

if Holetype == 2;   **[Plunged Holes]**

```
    Beta(i) = qm(i)/Qmpass;
        Alpha(i) = Harea(i)/(AreaAnnulus(i));
    Qmpass=(Qmpass-qm(i));
    if Discharge_Coeff(i) == 0
       Mu(i) = Beta(i)/Alpha(i);
       K(i) = 1 + 0.36*((2*(Mu(i)^2))+((4*(Mu(i)^4))+(2.77*((4*Beta(i))-(Beta(i)^2)))))^0.5;
       Cd(i) =(K(i)-1)/(0.6*((4*(K(i)^2))-(K(i)*(2-Beta(i))^2))^0.5);
       jetangle(i)=asin((1/(1.2*Cd(i)))*((K(i)-1)/K(i)))*(180/pi);
    elseif Discharge_Coeff(i) ~= 0;
       Mu(i) = Beta(i)/Alpha(i);
       K(i) = 1 + 0.36*((2*(Mu(i)^2))+((4*(Mu(i)^4))+(2.77*((4*Beta(i))-(Beta(i)^2)))))^0.5;
       Cd(i)=Discharge_Coeff(i);
       jetangle(i)=asin((1/(1.2*Cd(i)))*((K(i)-1)/K(i)))*(180/pi);
    end

    tmp_dP(i)=dp(i);

    dp(i) = (((qm(i)/(Cd(i)*Harea(i)))^2)/(2*rho_hole(i)))+dp_hot;

    dP_aver = (dP_aver + dp(i)*qm(i));

end
```

----

if Holetype == 3;   **[Splash Cooling]**

```
    Cd(i) =  Discharge_Coeff(i);
    jetangle(i)=0;
    tmp_dP(i)=dp(i);

    dp(i) = (((qm(i)/(Cd(i)*Harea(i)))^2)/(2*rho_hole(i)))+dp_hot;
    dP_aver = (dP_aver + dp(i)*qm(i));
        end

        if Holetype == 4 ;%Wiggle strip
    Cd(i) =  Discharge_Coeff(i);
    jetangle(i)=0;

    tmp_dP(i)=dp(i);

    dp(i) = (((qm(i)/(Cd(i)*Harea(i)))^2)/(2*rho_hole(i)))+dp_hot;

    dP_aver = (dP_aver + dp(i)*qm(i));
  end
```

```
if Holetype ==5;                                          [Machined Ring]
    Cd(i)=Discharge_Coeff(i);
    jetangle(i)=0;

    tmp_dP(i)=dp(i);

        dp(i) = (((qm(i)/(Cd(i)*Harea(i)))^2)/(2*rho_hole(i)))+dp_hot;

        dP_aver = (dP_aver + dp(i)*qm(i));

   end
```

```
if Holetype ==6;                                          [Swirler]


    Swirl_angle=Theta*(pi/180);
    jetangle(i)=0;

    tmp_dP(i)=dp(i);

    K=K_sw*(((sec(Swirl_angle)/Harea(i))^2)-(1/(A_L^2)));
    tmp_dP(i)=dp(i);
    dp(i)=((qm(i)^2)*K/(2*rho_hole(i)))+dp_hot; %Lefebvre 1998 swirler formula
        dP_aver=dP_aver+(dp(i)*qm(i));

end

end
```

Adapt mass flow rate and check for convergence:

```
dP_aver = dP_aver/Qmass;
        Qnew = 0;

        for i = 1:Nb;
    dqm(i) = qm(i)*dP_aver/dp(i);
    Qnew = Qnew + dqm(i);
        end

        for i = 1:Nb;
        Qm_new = dqm(i)*(Qmass/Qnew)-qm(i);
        qm(i) = qm(i)+(1/Nb)*Qm_new;
  %qm(i)=qm(i)+Qm_new;
        end

  convergence=0.0;
  for i = 1:Nb;
         convergence = convergence + abs(tmp_dP(i) - dp(i));
        end

end %end while loop
end %                                                     [end mm]
```

Define jet velocity:

```
Massflow=qm;

for i=1:Nb
  Holetype=Hole_type(i);


  if Holetype ~= 4 & Holetype ~= 6
    V_jet(i)=Massflow(i)/(((0.25*pi)*(Hole_diameter(i)^2))*rho_hole(i)*Number_of_holes(i));
  end

  if Holetype == 4
    V_jet(i)=(Massflow(i)/(Number_of_holes(i)))/((Hole_diameter(i)*slot_height(i))*rho_hole(i));
  end

  if Holetype==6
    V_jet(i)=Massflow(i)/(Hole_diameter(i)*1000*Number_of_holes(i)*rho_hole(i));
  end
end
```

Calculate reference Mach number:

```
Cp_air=1002.106 + (0.089328*(T3-273.15))+ (2.332e-4*((T3-273.15)^2))-(1.2831e-7*((T3-273.15)^3));
Gamma_air=Cp_air/(Cp_air - R);
sonic_vel=sqrt(Gamma_air*R*T3);
Ref_Mach=U_ref/sonic_vel;
```

Outputs to Flowcheck:

```
Pressure_drop=dP_aver;
jetangle=jetangle;
Flowsplits=(Massflow/ma)*100;
Cd=Cd;
Pressure_Loss=(Pressure_drop/P3)*100;
RefPressure_Loss=Pressure_drop/q_ref;
```

D.5   COMBUSTION

Define function foe "combustion":

---
function[Tgas,Air_fuel_node,Length,Air_fuel,Equivalence_Ratio,Casing_D,Liner_D,Airflow,Airflow_node,Airflow_zone,eta_Rz,eta_Pz,eta_Sz,eta_Dz,theta,EI_CO,EI_HC,eta_comb,Nox,NOx,Comb_eff]=Combustion(T3,P3,Nb,ma,x,y,Hole_Position,Massflow,Overall_A_F,S_A_F,Total_comb_length,Pz_boundary,Rz_boundary,Sz_boundary,nn,Casing_Diameter,Liner_Diameter,Number_of_nodes,Nodes,X,Zones,Length,Hole_type,Rz_flow,Pz_flow,Sz_flow,Dz_flow,Pressure_drop,element_th,nCans,A_ref,Dref);

Convert dimensions from mm to m:

Hole_Position=Hole_Position/1000;
Liner_Diameter=Liner_Diameter/1000;
Casing_Diameter=Casing_Diameter/1000;

Display warning message:

---
if P3 < 100000
        disp('Inlet Pressure cannot be less than 10 kPa, is going to set P3=100000')
        P3 = 100000;
 end

Calculate fuel flow:

Fuel_flow=(ma/Overall_A_F);

Define air mass flow in each segment:

Airflow_zone=zeros(1,Zones);

for i=1:Zones
   for j=1:Nb
     if i==1
        Airflow_zone(i)=Airflow_zone(i)+(Rz_flow(j)*Massflow(j));
     end

     if i==2
        Airflow_zone(i)=Airflow_zone(i)+(Pz_flow(j)*Massflow(j));
     end

     if i==3
        Airflow_zone(i)=Airflow_zone(i)+(Sz_flow(j)*Massflow(j));
     end

     if i==4
        Airflow_zone(i)=Airflow_zone(i)+(Dz_flow(j)*Massflow(j));
     end
   end
end

160

Define air flow in each zone:

```
Airflow=zeros(1,Zones);
for i=1:Zones
   if i==1
      Airflow(i)=Airflow_zone(i);
   end

   if i==2
      Airflow(i)=Airflow(i-1)+Airflow_zone(i);
   end

   if i==3
      Airflow(i)=Airflow(i-1)+Airflow_zone(i);
   end

   if i==4
      Airflow(i)=Airflow(i-1)+Airflow_zone(i);
   end
end
```

Define air flow at each computational node:

```
for j=1:Zones
   for i=1:Number_of_nodes
      if j==1
         if (X(i) <= Rz_boundary)
            Airflow_node(i)=Airflow(j);
         end
      end
      if j==2
         if (X(i) > Rz_boundary) & (X(i) <= Pz_boundary+0.0000001)
            Airflow_node(i)=Airflow(j);
         end
      end
      if j==3
         if (X(i) > Pz_boundary) & (X(i) <= Sz_boundary+0.0000001)
            Airflow_node(i)=Airflow(j);
         end
      end
      if j==4
         if (X(i) > Sz_boundary) & (X(i) <= Total_comb_length+0.0000001)
            Airflow_node(i) = Airflow(j);
         end
      end
   end
end
```

Air/Fuel ratio at each computational node:

```
for i=1:Number_of_nodes
   Air_fuel_node(i)=Airflow_node(i)/Fuel_flow;
end
```

Air/Fuel ratio in each zone:

```
for i=1:Zones

   if i==1
      Air_fuel(i)=Airflow(i)/Fuel_flow;
   end
   if i==2
      Air_fuel(i)=Airflow(i)/Fuel_flow;
   end
   if i==3
      Air_fuel(i)=Airflow(i)/Fuel_flow;
   end
   if i==4
      Air_fuel(i)=Airflow(i)/Fuel_flow;
   end
end
```

Equivalence ratio in each zone:

```
for i=1:Zones
        Equivalence_Ratio(i)=(S_A_F)/(Air_fuel(i));
end
```

Determine casing and liner diameter at each computational node:

```
Liner_D=zeros(1,Number_of_nodes);
Casing_D=zeros(1,Number_of_nodes);

Liner_D(Number_of_nodes)=Liner_Diameter(Nb);
Casing_D(Number_of_nodes)=Casing_Diameter(Nb);

for j=1:Nb
   for i=1:Number_of_nodes

        Liner_D(1)=Liner_Diameter(1);
        Casing_D(1)=Casing_Diameter(1);

      if (Hole_Position(j) < X(i))
         Liner_D(i)=Liner_Diameter(j);
         Casing_D(i)=Casing_Diameter(j);
      end

    if j < 2
      if Liner_Diameter(j) ~= Liner_Diameter(j+1)
         if abs(Hole_Position(j+1) - Hole_Position(j)) < 0.000001
            Liner_D(i)=(Liner_Diameter(j+1)+Liner_Diameter(j))/2;
```

```
        elseif (X(i) > Hole_Position(j)) & (X(i) <= Hole_Position(j+1))
            if Liner_Diameter(j) > Liner_Diameter(j+1)
                Liner_D(i)=Liner_Diameter(j) - X(i)*((Liner_Diameter(j+1)-
Liner_Diameter(j))/(Hole_Position(j+1)-Hole_Position(j)));
            elseif Liner_Diameter(j) < Liner_Diameter(j+1)
                Liner_D(i)=Liner_Diameter(j) + X(i)*((Liner_Diameter(j+1)-
Liner_Diameter(j))/(Hole_Position(j+1)-Hole_Position(j)));
            end
        end

    end


    if Casing_Diameter(j) ~= Casing_Diameter(j+1)
        if abs(Hole_Position(j+1) - Hole_Position(j)) < 0.000001
            Casing_D(i)=(Casing_Diameter(j+1)+Casing_Diameter(j))/2;
        elseif (X(i) > Hole_Position(j)) & (X(i) < Hole_Position(j+1))
            if Casing_Diameter(j) > Casing_Diameter(j+1)
                Casing_D(i)=Casing_Diameter(j) - X(i)*((Liner_Diameter(j+1)-
Liner_Diameter(j))/(Hole_Position(j+1)-Hole_Position(j)));
            elseif Casing_Diameter(j) < Casing_Diameter(j+1)
                Casing_D(i)=Casing_Diameter(j) + X(i)*((Liner_Diameter(j+1)-
Liner_Diameter(j))/(Hole_Position(j+1)-Hole_Position(j)));
            end
        end

    end

end
end
```

Calculate averge liner diameter in each zone:

```
Sz_number=0;
Dz_number=0;
Pz_number=0;
Pz_Liner_diameter=0;
Sz_Liner_diameter=0;
Dz_Liner_diameter=0;
for i=1:Number_of_nodes
  if (X(i) <= Pz_boundary)
     Pz_number=Pz_number+1;
     Pz_Liner_diameter=Pz_Liner_diameter + Liner_D(i);
  end

  if (X(i) <= Sz_boundary) & (X(i) > Pz_boundary)
     Sz_number=Sz_number+1;
     Sz_Liner_diameter=Sz_Liner_diameter+Liner_D(i);
  end

  if (X(i) > Sz_boundary) & (X(i) <= Total_comb_length)
     Dz_number=Dz_number+1;
     Dz_Liner_diameter=Dz_Liner_diameter+Liner_D(i);
```

```
   end
end


Average_Pz_diam=Pz_Liner_diameter/Pz_number;
Average_Sz_diam=Sz_Liner_diameter/Sz_number;
Average_Dz_diam=Dz_Liner_diameter/Dz_number;
```

LOOK-UP TABLES FOR ADIABATIC TEMPERATURE

```
Pressure=[10000 30000 100000 300000 1000000 3000000];%Pa
Tref=[200 400 600 800 1000];%K
phi=[0.02 0.03 0.04 0.05 0.06 0.07 0.08 0.1 0.15 0.2 0.3 0.4 0.5 0.6 0.7 0.8 0.9 1 1.1 1.2 1.3 1.4 1.5];

for i=1:6
   if P3==Pressure(i)
      P1=Pressure(i);
      P2=0;
   elseif (P3 > Pressure(i)) & (P3 < Pressure(i+1))
      P1=Pressure(i);
      P2=Pressure(i+1);
   end
end

for j=1:5
   if T3 == Tref(j)
      a=j;
      T1=Tref(j);
   elseif (T3 > Tref(j)) & (T3 < Tref(j+1))
      a=j;
      T1=Tref(j);
      T2=Tref(j+1);
   end
end

if P1==Pressure(1)
%Temp rise for Pressure(1)
dT1=[60 88 116 145 174 201 229 288 421 549 794 1017 1226 1450 1608 1766 1894 1968 1973 1922 1853 1779 1713;
    57 85.5 114 141.5 169 196 223 278 407 527 758 978 1183 1365 1534 1674 1778 1820 1843 1815 1758 1690 1623;
    54 81 108 134 160 185.5 211 261 384 501 723 934 1126 1301 1452 1570 1651 1696 1708 1693 1656 1595 1531;
    51 76.5 102 127 152 176 200 250 365 478 695 896 1074 1232 1362 1454 1515 1552 1569 1567 1538 1490 1436;
    48 72 96 120 144 167.5 191 235 348 458 664 862 1030 1150 1255 1328 1379 1412 1428 1430 1418 1372 1327];


   if T3 == Tref(a)
      DT1=dT1(a,:);
   elseif (T3 > Tref(a)) & (T3 < Tref(a+1))
      DT1=(dT1(a,:)-dT1(a+1,:))*((T3-T2)/(T1-T2))+dT1(a+1,:);
   end


end
```

```
if P1==Pressure(2)
%Temp rise for Pressure(2)
dT1=[60 88 116 145 174 201.5 229 288 421 549 794 1017 1235 1432 1614 1774 1911 1993 1998 1936 1861 1784 1715;
    57 85.5 114 141.5 169 196 223 278 407 527 758 978 1184 1370 1540 1687 1805 1871 1882 1840 1773 1702 1629;
    54 81 108 134 160 185.5 211 261 384 501 723 934 1126 1309 1465 1596 1684 1738 1756 1732 1678 1612 1543;
    51 76.5 102 127 152 176 200 250 365 478 695 896 1077 1244 1382 1488 1562 1608 1622 1609 1573 1518 1455;
    48 72 96 120 144 167.5 191 235 348 458 664 862 1022 1169 1285 1373 1433 1468 1484 1481 1453 1414 1360];

  if T3 == Tref(a)
     DT1=dT1(a,:);
  elseif (T3 > Tref(a)) & (T3 < Tref(a+1))
     DT1=(dT1(a,:)-dT1(a+1,:))*((T3-T2)/(T1-T2))+dT1(a+1,:);
  end


end


if P1==Pressure(3)
%Temp rise for Pressure(3)
dT1=[60 88 116 145 174 201.5 229 288 421 549 794 1017 1234 1432 1614 1784 1930 2025 2012 1944 1868 1789 1713;
    57 85.5 114 141.5 169 196 223 278 407 527 758 978 1183 1374 1548 1700 1830 1912 1911 1855 1785 1707 1633;
    54 81 108 134 160 185.5 211 261 384 501 723 934 1126 1310 1472 1610 1723 1789 1802 1762 1695 1625 1552;
    51 76.5 102 127 152 176 200 250 365 478 695 896 1083 1251 1399 1520 1602 1660.0 1678 1652 1603 1540 1471;
    48 72 96 120 144 167.5 191 235 348 458 664 862 1030 1189 1319 1419 1489 1530 1550 1538 1502 1449 1387];

  if T3 == Tref(a)
     DT1=dT1(a,:);
  elseif (T3 > Tref(a)) & (T3 < Tref(a+1))
     DT1=(dT1(a,:)-dT1(a+1,:))*((T3-T2)/(T1-T2))+dT1(a+1,:);
  end


end


if P1==Pressure(4)
%Temp rise for Pressure(4)
dT1=[60 88 116 145 174 201.5 229 288 421 549 794 1017 1239 1438 1609 1789 1940 2043 2025 1942 1868 1790 1720;
    57 85.5 114 141.5 169 196 223 278 407 527 758 978 1139 1373 1550 1710 1850 1940 1930 1861 1787 1709 1640;
    54 81 108 134 160 185.5 211 261 384 501 723 934 1145 1323 1484 1639 1750 1820 1838 1769 1705 1630 1550;
    51 76.5 102 127 152 176 200 250 365 478 695 896 1085 1252 1409 1590 1640 1707 1718 1672 1618 1550 1480;
    48 72 96 120 144 167.5 191 235 348 458 664 862 1033 1192 1345 1450 1530 1580 1611 1579 1529 1469 1399];

  if T3 == Tref(a)
     DT1=dT1(a,:);
  elseif (T3 > Tref(a)) & (T3 < Tref(a+1))
     DT1=(dT1(a,:)-dT1(a+1,:))*((T3-T2)/(T1-T2))+dT1(a+1,:);
  end


end


if P1==Pressure(5)
%Temp rise for Pressure(5)
dT1=[60 88 116 145 174 201.5 229 288 421 549 794 1017 1239 1433 1615 1789 1949 2059 2030 1949 1869 1789 1710;
    57 85.5 114 141.5 169 196 223 278 407 527 758 978 1185 1377 1552 1718 1861 1968 1944 1870 1790 1711 1635;
    54 81 108 134 160 185.5 211 261 384 501 723 934 1129 1313 1482 1630 1770 1859 1853 1779 1710 1630 1552;
    51 76 102 127 152 176 200 250 365 478 695 896 1089 1257 1420 1560 1673 1749 1753 1705 1640 1555 1480;
    48 72 96 120 144 167.5 191 235 348 458 664 862 1033 1200 1350 1475 1560 1635 1649 1613 1550 1479 1407];
```

```
    if T3 == Tref(a)
       DT1=dT1(a,:);
   elseif (T3 > Tref(a)) & (T3 < Tref(a+1))
       DT1=(dT1(a,:)-dT1(a+1,:))*((T3-T2)/(T1-T2))+dT1(a+1,:);
   end

end

if P1==Pressure(6)
%Temp rise for Pressure(6)
dT1=[60 88 116 145 174 201.5 229 288 421 549 794 1017 1230 1430 1617 1790 1950 2079 2039 1950 1869 1790 1715;
    57 85.5 114 141.5 169 196 223 278 407 527 758 978 1180 1375 1552 1720 1872 1989 1951 1870 1790 1711 1639;
    54 81 108 134 160 185.5 211 261 384 501 723 934 1130 1315 1489 1649 1789 1887 1870 1795 1715 1637 1550;
    51 76.5 102 127 152 176 200 250 365 478 695 896 1083 1260 1421 1520 1700 1785 1780 1717 1640 1561 1485;
    48 72 96 120 144 167.5 191 235 348 458 664 862 1035 1205 1359 1498 1605 1675 1685 1635 1563 1489 1410];

    if T3 == Tref(a)
       DT1=dT1(a,:);
   elseif (T3 > Tref(a)) & (T3 < Tref(a+1))
       DT1=(dT1(a,:)-dT1(a+1,:))*((T3-T2)/(T1-T2))+dT1(a+1,:);
   end

end



if P2==Pressure(1)
%Temp rise for Pressure(1)
dT2=[60 88 116 145 174 201 229 288 421 549 794 1017 1226 1450 1608 1766 1894 1968 1973 1922 1853 1779 1713;
    57 85.5 114 141.5 169 196 223 278 407 527 758 978 1183 1365 1534 1674 1778 1820 1843 1815 1758 1690 1623;
    54 81 108 134 160 185.5 211 261 384 501 723 934 1126 1301 1452 1570 1651 1696 1708 1693 1656 1595 1531;
    51 76.5 102 127 152 176 200 250 365 478 695 896 1074 1232 1362 1454 1515 1552 1569 1567 1538 1490 1436;
    48 72 96 120 144 167.5 191 235 348 458 664 862 1030 1150 1255 1328 1379 1412 1428 1430 1418 1372 1327];

    if T3 == Tref(a)
       DT2=dT2(a,:);
   elseif (T3 > Tref(a)) & (T3 < Tref(a+1))
       DT2=(dT2(a,:)-dT2(a+1,:))*((T3-T2)/(T1-T2))+dT2(a+1,:);
   end

end

if P2==Pressure(2)
%Temp rise for Pressure(2)
dT2=[60 88 116 145 174 201.5 229 288 421 549 794 1017 1235 1432 1614 1774 1911 1993 1998 1936 1861 1784 1715;
    57 85.5 114 141.5 169 196 223 278 407 527 758 978 1184 1370 1540 1687 1805 1871 1882 1840 1773 1702 1629;
    54 81 108 134 160 185.5 211 261 384 501 723 934 1126 1309 1465 1596 1684 1738 1756 1732 1678 1612 1543;
    51 76.5 102 127 152 176 200 250 365 478 695 896 1077 1244 1382 1488 1562 1608 1622 1609 1573 1518 1455;
    48 72 96 120 144 167.5 191 235 348 458 664 862 1022 1169 1285 1373 1433 1468 1484 1481 1453 1414 1360];

    if T3 == Tref(a)
       DT2=dT2(a,:);
   elseif (T3 > Tref(a)) & (T3 < Tref(a+1))
       DT2=(dT2(a,:)-dT2(a+1,:))*((T3-T2)/(T1-T2))+dT2(a+1,:);
   end

end
```

```
if P2==Pressure(3)
%Temp rise for Pressure(3)
dT2=[60 88 116 145 174 201.5 229 288 421 549 794 1017 1234 1432 1614 1784 1930 2025 2012 1944 1868 1789 1713;
    57 85.5 114 141.5 169 196 223 278 407 527 758 978 1183 1374 1548 1700 1830 1912 1911 1855 1785 1707 1633;
    54 81 108 134 160 185.5 211 261 384 501 723 934 1126 1310 1472 1610 1723 1789 1802 1762 1695 1625 1552;
    51 76.5 102 127 152 176 200 250 365 478 695 896 1083 1251 1399 1520 1602 1660.0 1678 1652 1603 1540 1471;
    48 72 96 120 144 167.5 191 235 348 458 664 862 1030 1189 1319 1419 1489 1530 1550 1538 1502 1449 1387];

    if T3 == Tref(a)
        DT2=dT2(a,:);
    elseif (T3 > Tref(a)) & (T3 < Tref(a+1))
        DT2=(dT2(a,:)-dT2(a+1,:))*((T3-T2)/(T1-T2))+dT2(a+1,:);
    end

end


if P2==Pressure(4)
%Temp rise for Pressure(4)
dT2=[60 88 116 145 174 201.5 229 288 421 549 794 1017 1239 1438 1609 1789 1940 2043 2025 1942 1868 1790 1720;
    57 85.5 114 141.5 169 196 223 278 407 527 758 978 1139 1373 1550 1710 1850 1940 1930 1861 1787 1709 1640;
    54 81 108 134 160 185.5 211 261 384 501 723 934 1145 1323 1484 1639 1750 1820 1838 1769 1705 1630 1550;
    51 76.5 102 127 152 176 200 250 365 478 695 896 1085 1252 1409 1590 1640 1707 1718 1672 1618 1550 1480;
    48 72 96 120 144 167.5 191 235 348 458 664 862 1033 1192 1345 1450 1530 1580 1611 1579 1529 1469 1399];

    if T3 == Tref(a)
        DT2=dT2(a,:);
    elseif (T3 > Tref(a)) & (T3 < Tref(a+1))
        DT2=(dT2(a,:)-dT2(a+1,:))*((T3-T2)/(T1-T2))+dT2(a+1,:);
    end

end


if P2==Pressure(5)
%Temp rise for Pressure(5)
dT2=[60 88 116 145 174 201.5 229 288 421 549 794 1017 1239 1433 1615 1789 1949 2059 2030 1949 1869 1789 1710;
    57 85.5 114 141.5 169 196 223 278 407 527 758 978 1185 1377 1552 1718 1861 1968 1944 1870 1790 1711 1635;
    54 81 108 134 160 185.5 211 261 384 501 723 934 1129 1313 1482 1630 1770 1859 1853 1779 1710 1630 1552;
    51 76 102 127 152 176 200 250 365 478 695 896 1089 1257 1420 1560 1673 1749 1753 1705 1640 1555 1480;
    48 72 96 120 144 167.5 191 235 348 458 664 862 1033 1200 1350 1475 1560 1635 1649 1613 1550 1479 1407];

    if T3 == Tref(a)
        DT2=dT2(a,:);
    elseif (T3 > Tref(a)) & (T3 < Tref(a+1))
        DT2=(dT2(a,:)-dT2(a+1,:))*((T3-T2)/(T1-T2))+dT2(a+1,:);
    end

end


if P2==Pressure(6)
%Temp rise for Pressure(6)
dT2=[60 88 116 145 174 201.5 229 288 421 549 794 1017 1230 1430 1617 1790 1950 2079 2039 1950 1869 1790 1715;
    57 85.5 114 141.5 169 196 223 278 407 527 758 978 1180 1375 1552 1720 1872 1989 1951 1870 1790 1711 1639;
    54 81 108 134 160 185.5 211 261 384 501 723 934 1130 1315 1489 1649 1789 1887 1870 1795 1715 1637 1550;
    51 76.5 102 127 152 176 200 250 365 478 695 896 1083 1260 1421 1520 1700 1785 1780 1717 1640 1561 1485;
    48 72 96 120 144 167.5 191 235 348 458 664 862 1035 1205 1359 1498 1605 1675 1685 1635 1563 1489 1410];
```

```
  if T3 == Tref(a)
     DT2=dT2(a,:);
  elseif (T3 > Tref(a)) & (T3 < Tref(a+1))
     DT2=(dT2(a,:)-dT2(a+1,:))*((T3-T2)/(T1-T2))+dT2(a+1,:);
  end

end

for i=1:6
  if P3==Pressure(i)
     dT=DT1;

  elseif (P3 > Pressure(i)) & (P3 < Pressure(i+1))
     dp_dT1=DT1;
     dp_dT2=DT2;

     dT=(dp_dT1-dp_dT2)*((P3-P2)/(P1-P2))+dp_dT2;
  end
end

for i=1:Zones
  if Equivalence_Ratio(i) <= 1.5
     Delta_T(i)=interp1(phi,dT,Equivalence_Ratio(i));
  else
     Delta_T(i)=interp1(phi,dT,Equivalence_Ratio(i),'nearest','extrap');
  end
end

 Delta_Ts = interp1(phi,dT,1); %temperature rise stiochiometric gas temperature
```

Calculation of Combustion efficiency :

```
if nn==1;                                                    [Combustion eff. On]

    for i=1:Zones

        [Re-circulation zone]
        eta_Rz=0.56+0.44*tanh(1.5475e-3*(T3+(108*log(P3))-1863));

        [Primary zone]
        eta_Pz=0.71+0.29*tanh(1.5475e-3*(T3+(108*log(P3))-1863));

        if i==1
           Trz=T3+eta_Rz*Delta_T(i);
           Tg(i)=((1/3)*T3)+((2/3)*Trz);
        end

        if i==2
           Tg(i)=T3+eta_Pz*Delta_T(i);
        end
```

```
if i==3

    Volume_Pz=((pi*Average_Pz_diam)/4)*(Pz_boundary);
      if Equivalence_Ratio(i) <= 1 %Air rich

        y=Equivalence_Ratio(i);
        n=(2*y^2)/Equivalence_Ratio(i-1);
        zeta300=(Fuel_flow/((Volume_Pz)*(P3^n)));
        term=y^-1.205;
        zeta=zeta300*(10^(-3.054*term))*(T3^(1.2327*term));
        %term1=(0.911*log10(zeta)) + (4.56*n) +(Equivalence_Ratio(i-1)/log10(Volume_Pz)) +
(558/T3);%Prediction of wall heat transfer for a gas turbine conbustor
        Dstar=0.736-0.0173*(P3/Pressure_drop);
         %term1=0.911*log10(zeta)+(8.02*Equivalence_Ratio(i))-1.097 + Dstar;% NREC
        term1=0.991*log10(zeta)+(4.56*n)-(1.1*Equivalence_Ratio(i))-1.097+Dstar;%A Simple
Method for the Prediction of Wall Temperatures in Gas Turbines

        term2=10^term1;
        eta_Sz=1/(10^term2);
         eta_Sz=0.9; %Approximate

        Tg(i)=T3+eta_Sz*Delta_T(i);
      elseif Equivalence_Ratio(i) > 1
        eta_Sz = 1/Equivalence_Ratio(i);

         Tg(i)=T3+eta_Sz*Delta_T(i);
      end
    end

    if i==4

        Volume_Sz=((pi*Average_Sz_diam)/4)*(Sz_boundary - Pz_boundary);
        if Equivalence_Ratio(i) <= 1 %Air rich

        y=Equivalence_Ratio(i);
        n=(2*y^2)/Equivalence_Ratio(i-1);
        zeta300=(Fuel_flow/((Volume_Sz)*(P3^n)));
        term=y^-1.205;
        zeta=zeta300*(10^(-3.054*term))*(T3^(1.2327*term));
%          term1=(0.911*log10(zeta)) + (4.56*n) +(Equivalence_Ratio(i-1)/log10(Volume_Sz)) +
                (558/T3);
%          term2=10^term1;

        Dstar=0.736-0.0173*(P3/Pressure_drop);
        term1=0.991*log10(zeta)+(4.56*n)-(1.1*Equivalence_Ratio(i))-1.097+Dstar;%A Simple
Method for the Prediction of Wall Temperatures in Gas Turbines
        %term1=0.911*log10(zeta)+(8.02*Equivalence_Ratio(i))-1.097 + Dstar; % NREC
        %term1=(0.911*log10(zeta)) + (4.56*n) +(Equivalence_Ratio(i-1)/log10(Volume_Pz)) +
                (558/T3);%Prediction of wall heat transfer for a gas turbine conbustor
        term2=10^term1;
        eta_Dz=1/(10^term2);
        eta_Dz=0.9; %Approximate

        Tg(i)=T3+eta_Dz*Delta_T(i);

      elseif Equivalence_Ratio(i) > 1
```

```
            y=1;
            n=(2*y^2)/Equivalence_Ratio(i-1);
            zeta300=(Fuel_flow/(Volume_Sz*(P3^n)));
            term=y^-1.205;
            zeta=zeta300*(10^(-3.054*term))*(T3^(1.2327*term));
            Dstar=0.736-0.0173*(P3/Pressure_drop);
            %term1=0.911*log10(zeta)+(8.02/Equivalence_Ratio(i))-1.097 + Dstar; %NREC
            term1=0.991*log10(zeta)+(4.56*n)-(1.1/Equivalence_Ratio(i))-1.097+Dstar;%A Simple
Method for the Prediction of Wall Temperatures in Gas Turbines
            %%term1=(0.911*log10(zeta)) + (4.56*n) +(Equivalence_Ratio(i-1)/log10(Volume_Pz)) +
(558/T3);%Prediction of wall heat transfer for a gas turbine conbustor
            term2=10^term1;
            eta_Dz=1/(10^term2);
          Tg(i)=T3+eta_Dz*Delta_T(i);
        end
      end
    end


    Ts=T3+eta_Pz*Delta_Ts;
    Tpz_mean=T3+eta_Pz*0.5*(Delta_Ts+Delta_T(2));

end %end nn=1
```

Combustion efficiency off:

```
if nn==2
  for i=1:Zones
     Tg(i)=T3+Delta_T(i);
  end
  Ts=T3+Delta_Ts;
  Tpz_mean=T3+0.5*(Delta_Ts+Delta_T(2));

eta_Rz=0;
eta_Pz=0;
eta_Sz=0;
eta_Dz=0;
end
```

Calculation of Theta:

```
phiPz=(Equivalence_Ratio(1)+Equivalence_Ratio(2))/2;

if phiPz < 1
   b=245*(1.39+log(phiPz));
else
   b=170*(2-log(phiPz));
end

theta=(((P3^1.75)*A_ref*(Dref^0.75)*exp(T3/b))/ma)/1000000;

 Tgas=zeros(1,Zones+1);
 Tgas(1)=T3;
 Tgas(2:Zones+1)=Tg(1:Zones);
```

[Emissions]
The following empirical expressions will predict CO within about a factor of 2 for aircraft engines using pressure liquid fuel atomizers [NREC Vol II]

```
EI_CO=10^(13.477-4.5276*log10(T3)); %[g CO/kg fuel]
```

[Hydrocarbons]
  Almost the same comments apply to hydrocarbons as to CO [NREC Vol II]

```
EI_HC=10^(19.730-7.1915*log10(T3));
```

[NO$_x$ Emissions]
  Combustion Volume (Vc): Assume it to be up to the secondary zone

----

```
Vc=0;
for i=1:Number_of_nodes
   if X(i) <= Sz_boundary
      Vc=Vc+((pi*Liner_D(i)^2)/4)*element_th(i);
   end
end

Tmax=max(Tgas);
r_time=0;%(P3*Vc)/(287.5*Tpz_mean*(Airflow_zone(3)/nCans));

%Lefebvre Model
if Nb < 3
   Nox = 0;
else
   Nox=(9e-8)*(P3/1000)^1.25*Vc*exp(0.01*Ts)/((Airflow_zone(3))*Tpz_mean);
end

%Odgers Model
if Nb < 3
   NOx = 0;
else
   NOx=29*(10^(-9410/Tmax))*P3^0.66*(1-exp(-250*r_time));
end
```

[Combustion Efficeincy (Calculated from emission levels)]

```
eta_comb=(1-10^(-3)*(0.24*EI_CO+EI_HC))*100;
```

  --------Combustion Efficeincy (figure 2.2 NREC)--------

```
   if theta < 17
      Comb_eff=(1.8467 - (0.01634*15)+ (0.000104*15*15) - (18.296/15))*100;
   elseif theta > 70
      Comb_eff=(1.8467 - (0.01634*70)+(0.000104*70*70)-(18.296/70))*100;
   else
      Comb_eff=(1.8467-(0.01634*theta)+(0.000104*theta*theta)-18.296/theta)*100;
   end
```

D.6   ELEMENTS

Define function for "elements":

```
function[Momflux,T_GAS,m_annulus,Hyd_D,dp_hot,Reo,Rei,d_AL,d_ACi,ALi,ALo,Aci,Aco,m_internal,
Pattern_Factor,M_inner,Local_AF,Y_max]=Elements(Zones,Length,Tgas,X,Number_of_nodes,Rz_bound
ary,Pz_boundary,Sz_boundary,Total_comb_length,Massflow,ma,Hole_Position,Nb,Fuel_flow,Airflow_no
de,Casing_D,Liner_D,t_L,t_C,P3,R,T3,U_ref,mu_a,mu_g,element_th,Nodes,Tgx,nCans,q_ref,Pressure_dr
op,Dref,Overall_A_F,Liner_Diameter,rho_hole_gas,rho_annulus,V_jet,Cd,Hole_diameter,Com,Number_o
f_holes);
```

Convert units from mm to m:

```
Hole_Position=Hole_Position/1000;
Liner_Diameter=Liner_Diameter/1000;
Hole_diameter=Hole_diameter/1000;
```

Gas temperature at end of each zone:

```
Fuel_flow=ma/Overall_A_F;

for j=1:Zones+1
  if j==1
    T_GAS(j)=(((X(j)-0)/(Tgx(2)-0))*(Tgas(2)-T3))+T3;
  else
    T_GAS((j-1)*Nodes)=Tgas(j);
  end
end
```

Interpolate between main gas temperaure values to obtain gas temp at other nodes:

```
for i=1:Zones
  if i==1
    for j=(i+1):(i*Nodes-1)
    T_GAS(j)=T_GAS(i*Nodes)+((X(j)-X(i*Nodes))/(X(i)-X(i*Nodes)))*(T_GAS(i)-T_GAS(i*Nodes));
    end
  else
    for j=((i-1)*Nodes+1):(i*Nodes-1)
        T_GAS(j)=T_GAS(i*Nodes)+((X(j)-X(i*Nodes))/(X((i-1)*Nodes)-X(i*Nodes)))*(T_GAS((i-
                  1)*Nodes)-T_GAS(i*Nodes));
    end
  end
end
```

Annulus air mass flow rate at each computational node:

```
for i=1:Nb
  if i==1
```

```
      M_inner(i)=Massflow(i);
   else
      M_inner(i)=M_inner(i-1) + Massflow(i);
   end
end

for j=1:Nb
  for i=1:Number_of_nodes
  m_internal(1)=M_inner(1);
  m_annulus(1)=ma-m_internal(1);

        if (Hole_Position(j) < X(i))%(X(i) >= Hole_Position(j)) & (X(i) <= Hole_Position(j+1))
           m_internal(i)=M_inner(j);
           m_annulus(i)=ma-m_internal(i);
        end

   end
end

for i=1:Number_of_nodes
   if m_internal(i) <= 0
      m_internal(i)=ma/1000000;
   end
   if m_annulus(i) <= 0
      m_annulus(i)=ma/1000000;
   end
end

for i=1:Number_of_nodes
   Local_AF(i)=m_internal(i)/Fuel_flow;
end
```

Heat transfer area of each element:

```
for i=1:Number_of_nodes
   d_AL(i)=pi*(Liner_D(i)+(t_L))*element_th(i);%Liner mean area
   d_ACi(i)=pi*(Casing_D(i))*element_th(i);%Casing inside area
   ALi(i)=pi*(Liner_D(i))*element_th(i);
   ALo(i)=pi*(Liner_D(i)+(2*t_L))*element_th(i);
   Aci(i)=pi*(Casing_D(i)*element_th(i));
   Aco(i)=pi*(Casing_D(i)+(2*t_C))*element_th(i);
end
```

Hydroulic diameter of annuls:

```
Average_L_Diam=0;
for i=1:Number_of_nodes
  Annulus_flow_area(i)=(pi/4)*(Casing_D(i)^2-(Liner_D(i)+2*t_L)^2);
  Hyd_D(i)=(4*Annulus_flow_area(i))/(pi*((Liner_D(i)+2*t_L)+Casing_D(i)));
  Liner_flow_area(i)=(pi/4)*(Liner_D(i)^2);
  Average_L_Diam=Average_L_Diam+Liner_D(i);
end
Average_L_Diam=Average_L_Diam/Number_of_nodes;
```

Pressure los due to hot gases:

----
dp_hot=0.5*(P3/(R*T3))*(U_ref^2)*((T_GAS(Number_of_nodes)/T3)-1);

Pattern factor:

Pattern_Factor=1-exp(-(Dref*q_ref)/(0.07*Total_comb_length*Pressure_drop));

Reynolds number in annulus and inside liner:

```
for i=1:Number_of_nodes
    Reo(i)=(m_annulus(i)/Annulus_flow_area(i))*(Hyd_D(i)/mu_a(i));
    Rei(i)=(m_internal(i)/Liner_flow_area(i))*(Liner_D(i)/mu_g(i));
end
```

Gas velocity at hole:

```
for i=1:Nb
    V_g(i)=(M_inner(i))/((Liner_Diameter(i)^2*0.25*pi)*rho_hole_gas(i));
end
```

Momentum flux ratio:

```
for i=1:Nb
    Momflux(i)=(rho_annulus(i)*(V_jet(i)^2))/(rho_hole_gas(i)*(V_g(i)^2));
end
```

Max peneteration:

```
for i=1:Nb
    m_j(i)=Massflow(i)/(Number_of_holes(i));
    d_j(i)=(Cd(i)^0.5)*Hole_diameter(i);
    Y_max(i)=(1.25*d_j(i)*(Momflux(i)^0.5)*((M_inner(i))/((M_inner(i))+m_j(i))))*1000;
end
```

D.7   HEAT TRANSFER

Define function of "Heat Transfer":

```
function[Liner_temp,Casing_temp,New_Tannulus,old_Tannulus,eta_filmcooling,J,distance_downstream_s
lot,e_g,Average_haLo]=Heat_transfer(Zones,Nodes,Number_of_nodes,ma,Overall_A_F,T_GAS,R,Liner_
D,Casing_D,element_th,x,y,Hole_type,Massflow,Number_of_cooling_slots,cooling_slot_height,mu_a,Pz_
boundary,k_g,T_annulus,sigma,k_L,k_C,t_L,t_C,Airflow_node,Nb,X,mu_g,k_a,Hyd_D,m_annulus,d_AL,
d_ACi,T3,Cp_an,bb,Reo,Rei,Pr_air,Pr_gas,Fuel_flow,FAR,P3,Hole_Position,Tamb,ALi,ALo,Aci,Aco,eLi,
eLo,eCi,eCo,Total_comb_length,Radiation_Model,m_internal,Liner_Diameter,nCans,M_inner,Local_AF,h
0,Outside_conv,Outside_rad);
```

Convert units from mm to m:

```
Hole_Position=Hole_Position/1000;
cooling_slot_height=cooling_slot_height/1000;
Liner_Diameter=Liner_Diameter/1000;
```

Assume internal pressure is constant throughout combustion chamber:

```
 for i=1:Number_of_nodes
    Internal_Pressure(i)=P3;
 end
```

Beam length l_b:

```
for i=1:Number_of_nodes
    l_b(i)=(3.4*Total_comb_length*0.25*pi*Liner_D(i)^2)/(pi*Liner_D(i)*Total_comb_length);
    q(i)=1/Local_AF(i);
end
```

Carbon to hydrogen ratio:

```
C_H=15; %Fuel atomic ratio C/H
L=3*(((C_H)-5.5)^0.75);
```

Calculation of cooling slot distance in terms of computational nodes:

```
if bb==1                                              [Wall cooling on]

   for i=1:Number_of_cooling_slots
     slot_lip_thickness(i)=t_L;
   end
```

Massflow through cooling slots:

```
k=0;

    for i=1:Nb

      Holetype=Hole_type(i);
      if Holetype==3                                    [Splash Cooling device]
        j=k+1;
        Cooling_massflow(j)=Massflow(i);
        x_cooling_slot(j)=Hole_Position(i);
        if j < Number_of_cooling_slots
          k=j;
        end
      end

      if Holetype==4                                    [Wiggle strip device]
        j=k+1;
        Cooling_massflow(j)=Massflow(i);
        x_cooling_slot(j)=Hole_Position(i);
        if j < Number_of_cooling_slots
          k=j;
        end
      end

      if Holetype==5                                    [Machined Ring]
        j=k+1;
        Cooling_massflow(j)=Massflow(i);
        x_cooling_slot(j)=Hole_Position(i);
        if j < Number_of_cooling_slots
          k=j;
        end
      end
    end
```

Downstream distance from slot [x] & Reynolds numbers:

```
for j=1:Number_of_cooling_slots
    for i=1:Number_of_nodes
```

Inside convective heat transfer coeff.:

```
        if (X(i) < x_cooling_slot(1))
            eta_filmcooling(i) =0;
            NuLi(i)=0.020*(Rei(i)^0.8)*(Pr_gas(i)^0.33333);
            haLi(i)=NuLi(i)*(k_g(i)/Liner_D(i));
        end
```

Calculate distance from cooling slot j:

```
        if x_cooling_slot(j) <= X(i)
            distance_downstream_slot(i) = X(i) - x_cooling_slot(j);
            if (X(i) - x_cooling_slot(j) <=0.000001)
                distance_downstream_slot(i)=(0.000001);
            end

            if distance_downstream_slot(i) < cooling_slot_height(j)
                distance_downstream_slot(i) = cooling_slot_height(j);
            end
```

Momentum flux ratio:

```
J(i)=(Cooling_massflow(j)/(pi*Liner_D(i)*cooling_slot_height(j)))/(m_internal(i)/(pi*(Liner_D(i)^2)
    *0.25));
```

Slot Reynolds number:

```
Res(i)=(Cooling_massflow(j)/(pi*Liner_D(i)*cooling_slot_height(j)))*(cooling_slot_height(j)/ mu_a(i));
```

Film cooling effieicncy:

```
if J(i) < 1.3

eta_filmcooling(i)=1.1*(J(i)^0.65)*((mu_a(i)/mu_g(i))^0.15)*((distance_downstream_slot(i)/cooling_slot_
height(j))^-0.2)*...
                    ((slot_lip_thickness(j)/cooling_slot_height(j))^-0.2);
                if eta_filmcooling(i) > 1
                    eta_filmcooling(i) = 1;
                end
                NuLi(i)=0.069*((Res(i)*(distance_downstream_slot(i)/cooling_slot_height(j)))^0.7);
                haLi(i)=NuLi(i)*(k_a(i)/distance_downstream_slot(i));

elseif J(i) >= 1.3

eta_filmcooling(i)=1.28*((mu_a(i)/mu_g(i))^0.15)*((distance_downstream_slot(i)/cooling_slot_height(j))^
                    -0.2)*((slot_lip_thickness(j)/cooling_slot_height(j))^-0.2);
                if eta_filmcooling(i) > 1
                    eta_filmcooling(i) = 1;
                end
                NuLi(i)=0.1*(Res(i)^0.8)*((distance_downstream_slot(i)/cooling_slot_height(j))^0.44);
                haLi(i)=NuLi(i)*(k_a(i)/distance_downstream_slot(i));
            end


        end


    end
end
```

Calculate gas temperature near inside liner wall:

```
   for i=1:Number_of_nodes

      Tw_ad(i)=T_GAS(i)-eta_filmcooling(i)*(T_GAS(i)-T_annulus(i));

   End
```

Liner outside heat transfer coeff.:

```
   for i=1:Number_of_nodes

      if Reo(i) <= 2300
         NuLo(i)=3.66;
      else
         NuLo(i)=0.020*(Reo(i)^0.8)*(Pr_air(i)^0.333);
      end

      if Reo(i) <= 2300
         NuCi(i)=3.66;
      else
         NuCi(i)=0.020*(Reo(i)^0.8)*(Pr_air(i)^0.3333);
      end
   end

end                                             [end for film cooled liner]
```

Calculate gas emisivity:

```
for i=1:Number_of_nodes
   e_g(i)=1-exp(-290*(Internal_Pressure(i)/1000)*L*sqrt(q(i)*l_b(i))*(T_GAS(i)^-1.5));
end
```

No film cooling devices used:

```
if bb==2 % Uncooled Liner
   eta_filmcooling=zeros(1,Number_of_nodes);
   J=zeros(1,Number_of_nodes);
   distance_downstream_slot=zeros(1,Number_of_nodes);
   for i=1:Number_of_nodes
      Tw_ad(i)=T_GAS(i)-eta_filmcooling(i)*(T_GAS(i)-T_annulus(i));
      NuLi(i)=0.020*(Rei(i)^0.8)*(Pr_gas(i)^0.33333);
      haLi(i)=NuLi(i)*(k_g(i)/Liner_D(i));

      %Backside heat transfer
      if Reo(i) <= 2300
         NuLo(i)=3.66;
      else
         NuLo(i)=0.020*(Reo(i)^0.8)*(Pr_air(i)^0.333);
      end

      if Reo(i) <= 2300
         NuCi(i)=3.66;
```

```
        else
            NuCi(i)=0.020*(Reo(i)^0.8)*(Pr_air(i)^0.3333);
        end


    end
end
```

```
old_Tannulus=T_annulus;
```


Heat Transfer process:

```
for i=1:Number_of_nodes


  if i==1
      T=T3;
  else
      T=New_Tannulus(i-1);
  end
  converg =1;


    TTR=T_GAS(i);
    TTL=Tamb;
    TwCi=T+10;


    while converg > 0.000001


        TwLi=(TTR+TTL)/2;
```

        [Heat flux to inside liner wall]
```
        QfcLi=haLi(i)*ALi(i)*(Tw_ad(i)-TwLi);
```

```
        if Radiation_Model ==1                                   [Simple Method]
            QradLi=eLi*sigma*ALi(i)*((T_GAS(i)^4)-(TwLi^4));
        elseif Radiation_Model ==2                               [Accurate Method]
            QradLi=0.5*sigma*(1+eLi)*e_g(i)*(T_GAS(i)^1.5)*ALi(i)*((T_GAS(i)^2.5) - (TwLi^2.5));
        elseif Radiation_Model==3
            QradLi=0;
        end
```

```
        QwallL=QfcLi+QradLi;                                     [Total wall heat flux]
```

```
        TwLo=TwLi-(QwallL/(0.5*(ALi(i)+ALo(i))*k_L/t_L));
        if TwLo <= 0
            TwLo = TwLi - 0.00001;
        end
```

[Backside heat transfer]

```
haLo(i)=NuLo(i)*(k_a(i)/Hyd_D(i));
QfcLo=haLo(i)*ALo(i)*(TwLo-T);

QradLo=QwallL-QfcLo;


TwCi=T+10;
tel=0;
while tel < 50
   tel=tel+1;
   term=(eLo*eCi)/(eCi+eLo*(1-eCi)*(ALo(i)/Aci(i)));
   hradLo=term*sigma*(TwLo^2+TwCi^2)*(TwLo+TwCi);
   TwCi=TwLo-QradLo/(hradLo*ALo(i));
   if TwCi < Tamb+0.00001
      TwCi=Tamb+0.00001;
   end
end

haCi(i)=NuCi(i)*(k_a(i)/Hyd_D(i));
QfcCi=haCi(i)*Aci(i)*(T-TwCi);
```

[Heating to annulus air]

```
dQa=QfcLo-QfcCi;
if m_annulus(i) <= 1e-3
   Tao= T;
else
   Tao=T+(dQa/(Cp_an(i)*m_annulus(i)));
end

QradCi=QradLo;

QwallC=QradCi+QfcCi;

TwCo=TwCi-(QwallC/(0.5*(Aci(i)+Aco(i))*(k_C/t_C)));
if TwCo < Tamb+0.000001
   TwCo=Tamb+0.000001;
end


if Outside_conv ==1                              [Default convection on]
   QncCo=Aco(i)*1.24*((TwCo-Tamb)^1.3333);
elseif Outside_conv ==2                          [Define heat transfer coeff]
   QncCo=Aco(i)*h0*(TwCo-Tamb);
elseif Outside_conv ==3
   QncCo=0; % Convection off
end

if Outside_rad==1                                [Radiation on]
   QradCo=eCo*sigma*Aco(i)*(TwCo^4-Tamb^4);
elseif Outside_rad==2
   QradCo=0;
end
```

```
        Qlost=QncCo+QradCo;

        if Outside_rad == 2 & Outside_conv ==3 %    Adiabatic wall
            if QwallC < 0
                TTR=TwLi;
            else
                TTL=TwLi;
            end
            converg=abs(QwallC);
        else
```

[Check for convergence]

```
            if QwallC < Qlost
                TTR=TwLi;
            else
                TTL=TwLi;
            end
            converg=abs(100*(QwallC-Qlost)/QwallL);
        end


    end

  TLi(i)=TwLi;
  TLo(i)=TwLo;
  New_Tannulus(i)=Tao;
  Tci(i)=TwCi;
  Tco(i)=TwCo;

  Liner_temp(i)=(TLi(i)+TLo(i))/2;
  Casing_temp(i)=(Tci(i)+Tco(i))/2;

end

Total_haLo = 0;
for i = 1:Number_of_nodes
  Total_haLo=Total_haLo + haLo(i);
end

Average_haLo=Total_haLo/Number_of_nodes;           [Average Backside heat transfer coeff.]
```

APPENDIX E –

Boundary conditions

TableE.1: Base case boundary conditions

Fluent Inlet Designation	Flow splits [%]	Flow splits [kg/s] 2.37642	Splits to individual holes [kg/s]	Directional vector components			Hydraulic diameter [mm]
				x	y	z	
Injector	0.7448178	0.0177	0.0177	normal to inlet boundary			7.4
shell swirl 1			0.08551	normal to inlet boundary			2.4
shell swirl 2			0.05938	normal to inlet boundary			3.72
shell swirl 1+2	6.0969862	0.14489					
wigg 1 bottom			0.18428	normal to inlet boundary			3.27
wigg 1 top			0.18428	normal to inlet boundary			3.27
wigg 1 total	15.509043	0.36856					
shell2 hole 1			0.016245714	0.63474	-0.73253	0.245984	
shell2 hole 2			0.016245714	0.969274	0	0.245984	
shell2 hole 3			0.016245714	0.63474	0.732528	0.245984	
shell2 hole 4			0.016245714	0.137943	0.959408	0.245984	
shell2 hole 5			0.016245714	-0.63474	0.732528	0.245984	
shell2 hole 6			0.016245714	-0.96927	0	0.245984	
shell2 hole 7			0.016245714	-0.63474	-0.73253	0.245984	
shell 2 hole total	4.7853494	0.11372					6.828
wigg 2 bottom			0.12605	normal to inlet boundary			3.27
wigg 2 top			0.12604	normal to inlet boundary			3.27
wigg 2 total	10.607973	0.25209					
shell3 splash	0.1880981	0.00447	0.00447	normal to inlet boundary			3.63
shell 3 hole 1			0.027606667	0.93863	-0.27561	0.2074	
shell 3 hole 2			0.027606667	-0.13922	0.968299	0.2074	
shell 3 hole 3			0.027606667	-0.93863	-0.27561	0.2074	
shell 3 hole total	3.4850742	0.08282					9.02
wigg 3 bottom			0.13055	normal to inlet boundary			3.27
wigg 3 top			0.13055	normal to inlet boundary			3.27
wigg 3 total	10.987115	0.2611					
shell4 hole 1			0.0389175	0.647886	-0.7477	0.145567	
shell4 hole 2			0.0389175	0.410991	0.899943	0.145567	
shell4 hole 3			0.0389175	-0.41099	0.899943	0.145567	
shell4 hole 4			0.0389175	-0.64789	-0.7477	0.145567	
shell 4 hole total	6.5506097	0.15567					11.254
shell 4 splash 1			0.00977	normal to inlet boundary			3.63
shell 4 splash 2			0.00977	normal to inlet boundary			3.63
shell 4 splash total	0.8222452	0.01954					
wigg 4 bottom			0.1131	normal to inlet boundary			3.27
wigg 4 top			0.11311	normal to inlet boundary			3.27
wigg 4 total	9.5189403	0.22621					
wigg 5 bottom			0.11649	normal to inlet boundary			3.27
wigg 5 top			0.11649	normal to inlet boundary			3.27
wigg 5 total	9.8038226	0.23298					
dilute hole 1			0.063725	0.70639	-0.70639	0.045014	
dilute hole 2			0.063725	0.70639	0.70639	0.045014	
dilute hole 3			0.063725	-0.70639	0.70639	0.045014	
dilute hole 4			0.063725	-0.70639	-0.70639	0.045014	
dilute hole total	10.726218	0.2549					16
dilute hole 5	4.3321467	0.10295	0.10295	0.972876	-0.2307	0.017103	20.2
dilute hole 6	3.2435344	0.07708	0.07708	-0.46946	-0.88293	0.007156	15.86
dilute splash	1.7315963	0.04115	0.04115	normal to inlet boundary			3.63
trans splash	0.8664293	0.02059	0.02059	normal to inlet boundary			3.63
	100	2.37642	2.37642				

Table E.2: Base Case with blocked cooling devices boundary conditions

Fluent Inlet Designation	Flow splits [%]	Flow splits [kg/s] 2.37642	Splits to individual holes [kg/s]	Directional vector components x	y	z	Hydraulic diameter [mm]
Injector	0.750709	0.01784	0.01784	normal to inlet boundary			7.4
shell swirl 1			0.0754	normal to inlet boundary			2.4
shell swirl 2			0.05236	normal to inlet boundary			3.72
shell swirl 1+2	5.376154	0.12776					
wigg 1 bottom			0.185695	normal to inlet boundary			3.27
wigg 1 top			0.185695	normal to inlet boundary			3.27
wigg 1 total	15.62813	0.37139					
shell2 hole 1			0.01637	0.63474	-0.73253	0.245984	
shell2 hole 2			0.01637	0.969274	0	0.245984	
shell2 hole 3			0.01637	0.63474	0.732528	0.245984	
shell2 hole 4			0.01637	0.137943	0.959408	0.245984	
shell2 hole 5			0.01637	-0.63474	0.732528	0.245984	
shell2 hole 6			0.01637	-0.96927	0	0.245984	
shell2 hole 7			0.01637	-0.63474	-0.73253	0.245984	
shell 2 hole total	4.8219591	0.11459					6.828
wigg 2 bottom			0.12701	normal to inlet boundary			3.27
wigg 2 top			0.12701	normal to inlet boundary			3.27
wigg 2 total	10.689188	0.25402					
shell3 splash	0.1897813	0.00451	0.00451	normal to inlet boundary			3.63
shell 3 hole 1			0.02782	0.93863	-0.27561	0.2074	
shell 3 hole 2			0.02782	-0.13922	0.968299	0.2074	
shell 3 hole 3			0.02782	-0.93863	-0.27561	0.2074	
shell 3 hole total	3.5120055	0.08346					9.02
wigg 3 bottom			0.13155	normal to inlet boundary			3.27
wigg 3 top			0.13155	normal to inlet boundary			3.27
wigg 3 total	11.071275	0.2631					
shell4 hole 1			0.0392175	0.647886	-0.7477	0.145567	
shell4 hole 2			0.0392175	0.410991	0.899943	0.145567	
shell4 hole 3			0.0392175	-0.41099	0.899943	0.145567	
shell4 hole 4			0.0392175	-0.64789	-0.7477	0.145567	
shell 4 hole total	6.6011059	0.15687					11.254
shell 4 splash 1			0.009845	normal to inlet boundary			3.63
shell 4 splash 2			0.009845	normal to inlet boundary			3.63
shell 4 splash total	0.8285572	0.01969					
wigg 4 bottom			0.11397	normal to inlet boundary			3.27
wigg 4 top			0.11398	normal to inlet boundary			3.27
wigg 4 total	9.5921596	0.22795					
wigg 5 bottom			0.11738	normal to inlet boundary			3.27
wigg 5 top			0.11738	normal to inlet boundary			3.27
wigg 5 total	9.8787251	0.23476					
dilute hole 1			0.064215	0.70639	-0.70639	0.045014	
dilute hole 2			0.064215	0.70639	0.70639	0.045014	
dilute hole 3			0.064215	-0.70639	0.70639	0.045014	
dilute hole 4			0.064215	-0.70639	-0.70639	0.045014	
dilute hole total	10.808695	0.25686					16
dilute hole 5	4.36539	0.10374	0.10374	0.972876	-0.2307	0.017103	20.2
dilute hole 6	3.2683617	0.07767	0.07767	-0.46946	-0.88293	0.007156	15.86
dilute splash	1.7450619	0.04147	0.04147	normal to inlet boundary			3.63
trans splash	0.8727414	0.02074	0.02074	normal to inlet boundary			3.63
	100	2.37642	2.37642				

Table E.3: Case 1 boundary conditions

Fluent Inlet Designation	Flow splits [%]	Flow splits [kg/s] 2.37642	Splits to individual holes [kg/s]	Directional vector components x	y	z	Hydraulic diameter [mm]
Injector	0.7448178	0.0177	0.0177	normal to inlet boundary			7.4
sw1			0.013171848	-0.52258	-0.15344	0.83867	4.0166
sw2			0.013171848	-0.35666	-0.41161	0.83867	4.0166
sw3			0.013171848	-0.07751	-0.5391	0.83867	4.0166
sw4			0.013171848	0.22625	-0.49542	0.83867	4.0166
sw5			0.013171848	0.45818	-0.29445	0.83867	4.0166
sw6			0.013171848	0.54464	0	0.83867	4.0166
sw7			0.013171848	0.45818	0.29445	0.83867	4.0166
sw8			0.013171848	0.22625	0.49542	0.83867	4.0166
sw9			0.013171848	-0.07751	0.5391	0.83867	4.0166
sw10			0.013171848	-0.35666	0.41161	0.83867	4.0166
sw11			0.013171848	-0.52258	0.15344	0.83867	4.0166
TOTAL SWIRLER	6.097	0.144890327					
wigg 1 bottom			0.18428	normal to inlet boundary			3.27
wigg 1 top			0.18428	normal to inlet boundary			3.27
wigg 1 total	15.509043	0.36856					
shell2 hole 1			0.016245714	0.63474	-0.73253	0.245984	
shell2 hole 2			0.016245714	0.969274	0	0.245984	
shell2 hole 3			0.016245714	0.63474	0.732528	0.245984	
shell2 hole 4			0.016245714	0.137943	0.959408	0.245984	
shell2 hole 5			0.016245714	-0.63474	0.732528	0.245984	
shell2 hole 6			0.016245714	-0.969274	0	0.245984	
shell2 hole 7			0.016245714	-0.63474	-0.73253	0.245984	
shell 2 hole total	4.7853494	0.11372					6.828
wigg 2 bottom			0.12605	normal to inlet boundary			3.27
wigg 2 top			0.12604	normal to inlet boundary			3.27
wigg 2 total	10.607973	0.25209					
shell3 splash	0.1880981	0.00447	0.00447	normal to inlet boundary			3.63
shell 3 hole 1			0.027606667	0.93863	-0.27561	0.2074	
shell 3 hole 2			0.027606667	-0.139222	0.968299	0.2074	
shell 3 hole 3			0.027606667	-0.93863	-0.27561	0.2074	
shell 3 hole total	3.4850742	0.08282					9.02
wigg 3 bottom			0.13055	normal to inlet boundary			3.27
wigg 3 top			0.13055	normal to inlet boundary			3.27
wigg 3 total	10.987115	0.2611					
shell4 hole 1			0.0389175	0.647886	-0.7477	0.145567	
shell4 hole 2			0.0389175	0.410991	0.899943	0.145567	
shell4 hole 3			0.0389175	-0.410991	0.899943	0.145567	
shell4 hole 4			0.0389175	-0.647886	-0.7477	0.145567	
shell 4 hole total	6.5506097	0.15567					11.254
shell 4 splash 1			0.00977	normal to inlet boundary			3.63
shell 4 splash 2			0.00977	normal to inlet boundary			3.63
shell 4 splash total	0.8222452	0.01954					
wigg 4 bottom			0.1131	normal to inlet boundary			3.27
wigg 4 top			0.11311	normal to inlet boundary			3.27
wigg 4 total	9.5189403	0.22621					
wigg 5 bottom			0.11649	normal to inlet boundary			3.27
wigg 5 top			0.11649	normal to inlet boundary			3.27
wigg 5 total	9.8038226	0.23298					
dilute hole 1			0.063725	0.70639	-0.70639	0.045014	
dilute hole 2			0.063725	0.70639	0.70639	0.045014	
dilute hole 3			0.063725	-0.70639	0.70639	0.045014	
dilute hole 4			0.063725	-0.70639	-0.70639	0.045014	
dilute hole total	10.726218	0.2549					16

dilute hole 5	**4.3321467**	0.10295	0.10295	0.972876	-0.2307	0.017103	20.2
dilute hole 6	**3.2435344**	0.07708	0.07708	-0.46946	-0.88293	0.007156	15.86
dilute splash	**1.7315963**	0.04115	0.04115	normal to inlet boundary			3.63
trans splash	**0.8664293**	0.02059	0.02059	normal to inlet boundary			3.63
	100.00001	2.376420327	2.376420327				

Table E.4: Case 2 boundary conditions

Fluent Inlet Designation	Flow splits [%]	Flow splits [kg/s] 2.37642	Splits to individual holes [kg/s]	Directional vector components			Hydraulic diameter [mm]
				x	y	z	
Injector	**0.7448178**	0.0177	0.0177	normal to inlet boundary			7.4
sw1			0.014489033	-0.61133	-0.19863	0.76604	4.38343
sw2			0.014489033	-0.37782	-0.52003	0.76604	4.38343
sw3			0.014489033	0	-0.64279	0.76604	4.38343
sw4			0.014489033	0.37782	-0.52003	0.76604	4.38343
sw5			0.014489033	0.61133	-0.19863	0.76604	4.38343
sw6			0.014489033	0.61133	0.19863	0.76604	4.38343
sw7			0.014489033	0.37782	0.52003	0.76604	4.38343
sw8			0.014489033	0	0.64279	0.76604	4.38343
sw9			0.014489033	-0.37782	0.52003	0.76604	4.38343
sw10			0.014489033	-0.61133	0.19863	0.76604	4.38343
TOTAL SWIRLER	**6.097**	0.144890327					
wigg 1 bottom			0.18428	normal to inlet boundary			3.27
wigg 1 top			0.18428	normal to inlet boundary			3.27
wigg 1 total	**15.509043**	0.36856					
shell2 hole 1			0.016245714	0.63474	-0.73253	0.245984	
shell2 hole 2			0.016245714	0.969274	0	0.245984	
shell2 hole 3			0.016245714	0.63474	0.732528	0.245984	
shell2 hole 4			0.016245714	0.137943	0.959408	0.245984	
shell2 hole 5			0.016245714	-0.63474	0.732528	0.245984	
shell2 hole 6			0.016245714	-0.96927	0	0.245984	
shell2 hole 7			0.016245714	-0.63474	-0.73253	0.245984	
shell 2 hole total	**4.7853494**	0.11372					6.828
wigg 2 bottom			0.12605	normal to inlet boundary			3.27
wigg 2 top			0.12604	normal to inlet boundary			3.27
wigg 2 total	**10.607973**	0.25209					
shell3 splash	**0.1880981**	0.00447	0.00447	normal to inlet boundary			3.63
shell 3 hole 1			0.027606667	0.93863	-0.27561	0.2074	
shell 3 hole 2			0.027606667	-0.13922	0.968299	0.2074	
shell 3 hole 3			0.027606667	-0.93863	-0.27561	0.2074	
shell 3 hole total	**3.4850742**	0.08282					9.02
wigg 3 bottom			0.13055	normal to inlet boundary			3.27
wigg 3 top			0.13055	normal to inlet boundary			3.27
wigg 3 total	**10.987115**	0.2611					
shell4 hole 1			0.0389175	0.647886	-0.7477	0.145567	
shell4 hole 2			0.0389175	0.410991	0.899943	0.145567	
shell4 hole 3			0.0389175	-0.41099	0.899943	0.145567	
shell4 hole 4			0.0389175	-0.64789	-0.7477	0.145567	
shell 4 hole total	**6.5506097**	0.15567					11.254
shell 4 splash 1			0.00977	normal to inlet boundary			3.63
shell 4 splash 2			0.00977	normal to inlet boundary			3.63
shell 4 splash total	**0.8222452**	0.01954					
wigg 4 bottom			0.1131	normal to inlet boundary			3.27
wigg 4 top			0.11311	normal to inlet boundary			3.27
wigg 4 total	**9.5189403**	0.22621					
wigg 5 bottom			0.11649	normal to inlet boundary			3.27

wigg 5 top			0.11649	normal to inlet boundary			3.27
wigg 5 total	**9.8038226**	0.23298					
dilute hole 1			0.063725	0.70639	-0.70639	0.045014	
dilute hole 2			0.063725	0.70639	0.70639	0.045014	
dilute hole 3			0.063725	-0.70639	0.70639	0.045014	
dilute hole 4			0.063725	-0.70639	-0.70639	0.045014	
dilute hole total	**10.726218**	0.2549					16
dilute hole 5	**4.3321467**	0.10295	0.10295	0.972876	-0.2307	0.017103	20.2
dilute hole 6	**3.2435344**	0.07708	0.07708	-0.46946	-0.88293	0.007156	15.86
dilute splash	**1.7315963**	0.04115	0.04115	normal to inlet boundary			3.63
trans splash	**0.8664293**	0.02059	0.02059	normal to inlet boundary			3.63
	100.00001	2.376420327	2.376420327				

Table E.5: Case 3 boundary conditions

Fluent Inlet Designation	Flow splits [%]	Flow splits [kg/s] 2.37642	Splits to individual holes [kg/s]	Directional vector components			Hydraulic diameter [mm]
				x	y	z	
Injector	**0.7448178**	0.0177	0.0177	normal to inlet boundary			7.4
sw1			0.018111291	-0.70773	-0.29315	0.64279	5.213
sw2			0.018111291	-0.29315	-0.70773	0.64279	5.213
sw3			0.018111291	0.29315	-0.70773	0.64279	5.213
sw4			0.018111291	0.70773	-0.29315	0.64279	5.213
sw5			0.018111291	0.70773	0.29315	0.64279	5.213
sw6			0.018111291	0.29315	0.70773	0.64279	5.213
sw7			0.018111291	-0.29315	0.70773	0.64279	5.213
sw8			0.018111291	-0.70773	0.29315	0.64279	5.213
TOTAL SWIRLER	**6.097**	0.144890327					
wigg 1 bottom			0.18428	normal to inlet boundary			3.27
wigg 1 top			0.18428	normal to inlet boundary			3.27
wigg 1 total	**15.509043**	0.36856					
shell2 hole 1			0.016245714	0.63474	-0.73253	0.245984	
shell2 hole 2			0.016245714	0.969274	0	0.245984	
shell2 hole 3			0.016245714	0.63474	0.732528	0.245984	
shell2 hole 4			0.016245714	0.137943	0.959408	0.245984	
shell2 hole 5			0.016245714	-0.63474	0.732528	0.245984	
shell2 hole 6			0.016245714	-0.969274	0	0.245984	
shell2 hole 7			0.016245714	-0.63474	-0.73253	0.245984	
shell 2 hole total	**4.7853494**	0.11372					6.828
wigg 2 bottom			0.12605	normal to inlet boundary			3.27
wigg 2 top			0.12604	normal to inlet boundary			3.27
wigg 2 total	**10.607973**	0.25209					
shell3 splash	**0.1880981**	0.00447	0.00447	normal to inlet boundary			3.63
shell 3 hole 1			0.027606667	0.93863	-0.27561	0.2074	
shell 3 hole 2			0.027606667	-0.139222	0.968299	0.2074	
shell 3 hole 3			0.027606667	-0.93863	-0.27561	0.2074	
shell 3 hole total	**3.4850742**	0.08282					9.02
wigg 3 bottom			0.13055	normal to inlet boundary			3.27
wigg 3 top			0.13055	normal to inlet boundary			3.27
wigg 3 total	**10.987115**	0.2611					
shell4 hole 1			0.0389175	0.647886	-0.7477	0.145567	
shell4 hole 2			0.0389175	0.410991	0.899943	0.145567	
shell4 hole 3			0.0389175	-0.410991	0.899943	0.145567	
shell4 hole 4			0.0389175	-0.647886	-0.7477	0.145567	
shell 4 hole total	**6.5506097**	0.15567					11.254
shell 4 splash 1			0.00977	normal to inlet boundary			3.63
shell 4 splash 2			0.00977	normal to inlet boundary			3.63
shell 4 splash	**0.8222452**	0.01954					

total							
wigg 4 bottom			0.1131	normal to inlet boundary			3.27
wigg 4 top			0.11311	normal to inlet boundary			3.27
wigg 4 total	**9.5189403**	0.22621					
wigg 5 bottom			0.11649	normal to inlet boundary			3.27
wigg 5 top			0.11649	normal to inlet boundary			3.27
wigg 5 total	**9.8038226**	0.23298					
dilute hole 1			0.063725	0.70639	-0.70639	0.045014	
dilute hole 2			0.063725	0.70639	0.70639	0.045014	
dilute hole 3			0.063725	-0.70639	0.70639	0.045014	
dilute hole 4			0.063725	-0.70639	-0.70639	0.045014	
dilute hole total	**10.726218**	0.2549					16
dilute hole 5	**4.3321467**	0.10295	0.10295	0.972876	-0.2307	0.017103	20.2
dilute hole 6	**3.2435344**	0.07708	0.07708	-0.46946	-0.88293	0.007156	15.86
dilute splash	**1.7315963**	0.04115	0.04115	normal to inlet boundary			3.63
trans splash	**0.8664293**	0.02059	0.02059	normal to inlet boundary			3.63
	100.00001	2.376420327	2.376420327				

Table E.6: Case 4 boundary conditions

Fluent Inlet Designation	Flow splits [%]	Flow splits [kg/s] 2.37642	Splits to individual holes [kg/s]	Directional vector components			Hydraulic diameter [mm]
				x	y	z	
Injector	**0.746501**	0.01774	0.01774	normal to inlet boundary			7.4
sw1			0.029589091	-0.52258	-0.15344	0.83867	7.4728
sw2			0.029589091	-0.35666	-0.41161	0.83867	7.4728
sw3			0.029589091	-0.07751	-0.5391	0.83867	7.4728
sw4			0.029589091	0.22625	-0.49542	0.83867	7.4728
sw5			0.029589091	0.45818	-0.29445	0.83867	7.4728
sw6			0.029589091	0.54464	0	0.83867	7.4728
sw7			0.029589091	0.45818	0.29445	0.83867	7.4728
sw8			0.029589091	0.22625	0.49542	0.83867	7.4728
sw9			0.029589091	-0.07751	0.5391	0.83867	7.4728
sw10			0.029589091	-0.35666	0.41161	0.83867	7.4728
sw11			0.029589091	-0.52258	0.15344	0.83867	7.4728
TOTAL SWIRLER	**13.696232**	0.32548					
wigg 1 bottom			0.18462	normal to inlet boundary			3.27
wigg 1 top			0	normal to inlet boundary			3.27
wigg 1 total	**7.7688287**	0.18462					
shell2 hole 1			0.016274286	0.63474	-0.73253	0.245984	
shell2 hole 2			0.016274286	0.969274	0	0.245984	
shell2 hole 3			0.016274286	0.63474	0.732528	0.245984	
shell2 hole 4			0.016274286	0.137943	0.959408	0.245984	
shell2 hole 5			0.016274286	-0.63474	0.732528	0.245984	
shell2 hole 6			0.016274286	-0.969274	0	0.245984	
shell2 hole 7			0.016274286	-0.63474	-0.73253	0.245984	
shell 2 hole total	**4.7937654**	0.11392					6.828
wigg 2 bottom			0.12627	normal to inlet boundary			3.27
wigg 2 top			0.12627	normal to inlet boundary			3.27
wigg 2 total	**10.626909**	0.25254					
shell3 splash	**0.1880981**	0.00447	0.00448	normal to inlet boundary			3.63
shell 3 hole 1			0.027656667	0.93863	-0.27561	0.2074	
shell 3 hole 2			0.027656667	-0.139222	0.968299	0.2074	
shell 3 hole 3			0.027656667	-0.93863	-0.27561	0.2074	
shell 3 hole total	**3.4913862**	0.08297					9.02
wigg 3 bottom			0.13078	normal to inlet boundary			3.27
wigg 3 top			0.13078	normal to inlet boundary			3.27
wigg 3 total	**11.006472**	0.26156					
shell4 hole 1			0.0389875	0.647886	-0.7477	0.145567	

	Flow splits	Flow splits [kg/s]	Splits to individual	Directional vector components			Hydraulic
shell4 hole 2			0.0389875	0.410991	0.899943	0.145567	
shell4 hole 3			0.0389875	-0.410991	0.899943	0.145567	
shell4 hole 4			0.0389875	-0.647886	-0.7477	0.145567	
shell 4 hole total	**6.5623922**	**0.15595**					11.254
shell 4 splash 1			0.00979	normal to inlet boundary			3.63
shell 4 splash 2			0.00979	normal to inlet boundary			3.63
shell 4 splash total	**0.8239284**	**0.01958**					
wigg 4 bottom			0.11331	normal to inlet boundary			3.27
wigg 4 top			0.11331	normal to inlet boundary			3.27
wigg 4 total	**9.5361931**	**0.22662**					
wigg 5 bottom			0.1167	normal to inlet boundary			3.27
wigg 5 top			0.1167	normal to inlet boundary			3.27
wigg 5 total	**9.8214962**	**0.2334**					
dilute hole 1			0.06384	0.70639	-0.70639	0.045014	
dilute hole 2			0.06384	0.70639	0.70639	0.045014	
dilute hole 3			0.06384	-0.70639	0.70639	0.045014	
dilute hole 4			0.06384	-0.70639	-0.70639	0.045014	
dilute hole total	**10.745575**	**0.25536**					16
dilute hole 5	**4.3397211**	**0.10313**	0.10313	0.972876	-0.2307	0.017103	20.2
dilute hole 6	**3.2494256**	**0.07722**	0.07722	-0.46946	-0.88293	0.007156	15.86
dilute splash	**1.7349627**	**0.04123**	0.04123	normal to inlet boundary			3.63
trans splash	**0.8676917**	**0.02062**	0.02062	normal to inlet boundary			3.63
	99.999579	2.37641	2.37642				

Table E.7: Case 5 boundary conditions

Fluent Inlet	Flow splits	Flow splits [kg/s]	Splits to individual	Directional vector components			Hydraulic
Designation	**[%]**	**2.37642**	**holes [kg/s]**	**x**	**y**	**z**	**diameter [mm]**
Injector	**0.7452386**	**0.01771**	0.01771	normal to inlet boundary			7.4
sw1			0.029533636	-0.52258	-0.15344	0.83867	7.4728
sw2			0.029533636	-0.35666	-0.41161	0.83867	7.4728
sw3			0.029533636	-0.07751	-0.5391	0.83867	7.4728
sw4			0.029533636	0.22625	-0.49542	0.83867	7.4728
sw5			0.029533636	0.45818	-0.29445	0.83867	7.4728
sw6			0.029533636	0.54464	0	0.83867	7.4728
sw7			0.029533636	0.45818	0.29445	0.83867	7.4728
sw8			0.029533636	0.22625	0.49542	0.83867	7.4728
sw9			0.029533636	-0.07751	0.5391	0.83867	7.4728
sw10			0.029533636	-0.35666	0.41161	0.83867	7.4728
sw11			0.029533636	-0.52258	0.15344	0.83867	7.4728
TOTAL SWIRLER	**13.670563**	**0.32487**					
wigg 1 bottom			0.18428	normal to inlet boundary			3.27
wigg 1 top			0.18428	normal to inlet boundary			3.27
wigg 1 total	**15.509043**	**0.36856**					
shell2 hole 1			0.016245714	0.63474	-0.73253	0.245984	
shell2 hole 2			0.016245714	0.969274	0	0.245984	
shell2 hole 3			0.016245714	0.63474	0.732528	0.245984	
shell2 hole 4			0.016245714	0.137943	0.959408	0.245984	
shell2 hole 5			0.016245714	-0.63474	0.732528	0.245984	
shell2 hole 6			0.016245714	-0.969274	0	0.245984	
shell2 hole 7			0.016245714	-0.63474	-0.73253	0.245984	
shell 2 hole total	**4.7853494**	**0.11372**					6.828
wigg 2 bottom			0.12605	normal to inlet boundary			3.27
wigg 2 top			0.12605	normal to inlet boundary			3.27
wigg 2 total	**10.608394**	**0.2521**					
shell3 splash	**0.1880981**	**0.00447**	0.00447	normal to inlet boundary			3.63
shell 3 hole 1			0.027606667	0.93863	-0.27561	0.2074	

shell 3 hole 2			0.027606667	-0.139222	0.968299	0.2074	
shell 3 hole 3			0.027606667	-0.93863	-0.27561	0.2074	
shell 3 hole total	**3.4850742**	0.08282					9.02
wigg 3 bottom			0.13055	normal to inlet boundary			3.27
wigg 3 top			0.13055	normal to inlet boundary			3.27
wigg 3 total	**10.987115**	0.2611					
shell4 hole 1			0.03892	0.647886	-0.7477	0.145567	
shell4 hole 2			0.03892	0.410991	0.899943	0.145567	
shell4 hole 3			0.03892	-0.410991	0.899943	0.145567	
shell4 hole 4			0.03892	-0.647886	-0.7477	0.145567	
shell 4 hole total	**6.5510305**	0.15568					11.254
shell 4 splash 1			0.009775	normal to inlet boundary			3.63
shell 4 splash 2			0.009775	normal to inlet boundary			3.63
shell 4 splash total	**0.822666**	0.01955					
wigg 4 bottom			0.11311	normal to inlet boundary			3.27
wigg 4 top			0.11311	normal to inlet boundary			3.27
wigg 4 total	**9.5193611**	0.22622					
wigg 5 bottom			0.11649	normal to inlet boundary			3.27
wigg 5 top			0.11649	normal to inlet boundary			3.27
wigg 5 total	**9.8038226**	0.23298					
dilute hole 1			0.06373	0.70639	-0.70639	0.045014	
dilute hole 2			0.06373	0.70639	0.70639	0.045014	
dilute hole 3			0.06373	-0.70639	0.70639	0.045014	
dilute hole 4			0.06373	-0.70639	-0.70639	0.045014	
dilute hole total	**10.72706**	0.25492					16
dilute hole 5	**0**	0	0	0.972876	-0.2307	0.017103	20.2
dilute hole 6	**0**	0	0	-0.46946	-0.88293	0.007156	15.86
dilute splash	**1.7320171**	0.04116	0.04116	normal to inlet boundary			3.63
trans splash	**0.8664293**	0.02059	0.02059	normal to inlet boundary			3.63
	100.00126	2.37645	2.37645				